AD NUMBER
AD829084
LIMITATION CHANGES
TO: **Approved for public release; distribution is unlimited. Available only to DTIC users. U.S. Government or Federal Purpose Rights License.**
FROM: **Distribution authorized to U.S. Gov't. agencies and their contractors; Critical Technology; AUG 1967. Other requests shall be referred to Air Force Office of Scientific Research, Attn: SRGO, 1400 Wilson Blvd., Arlington, VA 22209. This document contains export-controlled technical data.**
AUTHORITY
afosr, ltr, 12 nov 1971

OSR 68-0243

AD829084

University of Utah

Department of Chemical Engineering

Salt Lake City, Utah

[redacted]

280

Qualified requestors may obtain additional copies from the Defense Documentation Center.

Conditions of Reproduction

UNIVERSITY OF UTAH

DEPARTMENT OF CHEMICAL ENGINEERING

Technical Report

on

THERMAL EFFECTS OF COMPOSITE-PROPELLANT REACTIONS

Under Air Force Grants AFOSR 40-66 and 40-67

August 1, 1967

This research under Grants AF AFOSR 40-66 and 40-67, Project Task No. 9711-01, for the period June, 1966, through July, 1967, was sponsored by the Air Force Office of Scientific Research, Office of Aerospace Research, United States Air Force.

The Technical Supervisor for this program is Dr. Bernard T. Wolfson, Project Scientist, Propulsion Division, Directorate of Engineering Sciences, Air Force Office of Scientific Research.

This report was prepared by J. C. Cheng, Alva D. Baer, and Norman W. Ryan.

Report approved by

Norman W. Ryan

Norman W. Ryan
Principal Investigator

TABLE OF CONTENTS

LIST OF FIGURES

Figure | Page

Figure | Page

Figure | Page

LIST OF TABLES

ABSTRACT

The decomposition reactions of epoxy-cured polybutadiene-acrylic acid copolymer (PBAA) were studied at heating rates from 50 to 150°C per second. Blackened films of material 100 microns thick were bonded to a copper disk, 325 microns thick, which served as a thermojunction to measure the temperature of the film-copper interface, and the free surface was exposed to black body radiation in a tube furnace. Special techniques were developed for mixing, curing and cutting the films, and for mounting them with negligible thermal resistance.

The interface temperature and the response of a photocell viewing the polymer surface were recorded, then interpreted to determine the events occurring at the heated surface. Weight loss measurements were also made. Both simple polymer and polymer mixed with burning rate catalysts, ammonium perchlorate (AP), and glass beads were studied. The ranges of experimental conditions were: furnace temperature, 800 to 1100°C; gaseous environment, oxygen and nitrogen; pressure, vacuum to 5 atmospheres.

Specimens heated in vacuum indicated an endotherm at about 600°K, the reaction having an activation energy of about 43 kcal. per gm.mole. Under nitrogen pressure, the endotherm was found to be pressure dependent, having some of attributes of equilbrium vaporization, with a heat of vaporization of 32 kcal. per gm.mole, but with very little weight loss. A later reaction, signaled by the photocell and corresponding to a significant rate of weight loss, appeared to be equilibrium vaporization with a heat of vaporization of 16 kcal. per gm.mole. A two-stage

pyrolysis mechanism, the second stage being simple vaporization, is postulated.

Corresponding tests in oxygen were characterized by an exotherm followed by ignition. The expected increase in exotherm temperature with heating rate was not found, leading to the inference that the oxygen temperature had a significant effect. As the exotherm temperature is lower than the endotherm temperature (observed with nitrogen pressure), it is concluded that heterogeneous oxygen-polymer reaction precedes pyrolysis; and further, that simple thermal decomposition of the polymer is not a contributing process when hot oxygen is present at atmospheric and higher pressures.

When samples containing 5 to 10 weight per cent AP were heated at 0.85 atm under nitrogen, the endotherm temperature was lowered, an exotherm followed, and rapid gas evolution occurred still later. As the AP loading was increased, the endotherm disappeared as the exotherm temperature dropped lower and the rapid weight loss temperature dropped also. The AP polymer interaction dominated, and again simple polymer pyrolysis no longer played a role.

Corresponding tests in oxygen indicated that at low AP levels, the oxygen-polymer exotherm was the initial process, followed closely by AP participation and ignition. As AP concentration was increased, the effect of oxygen was less pronounced. Extraporation of the results to AP levels typical of composite propellants indicates that the reaction between polymer and AP (or its decomposition products) is the initial and dominant process in polymer decomposition.

Experiments with burning rate catalysts indicated that copper chromite expedites the thermal decomposition of PBAA, lowering the observed reaction temperatures by about 40°C. Iron oxide did not have an effect. When glass beads were incorporated in the polymer and samples were heated in oxygen, the estimated reaction rate indicated roughly a second order dependence on available polymer surface.

Careful weight loss tests performed by use of an alternative technique, which employed an imaging furnace, showed that, for the same exposure, ammonium perchlorate-containing samples had a much higher weight loss than samples of PBAA alone. The analysis of liquid decomposition products also showed a result of interaction between the oxidizer and fuel-binder. These results complement the thin-film data in indicating the probable importance of heterogeneous reaction between polymer and ammonium perchlorate (or its decomposition products).

CHAPTER I

INTRODUCTION

No one knows exactly when or by whom rockets were invented. Some historians of rocketry believe that the first man ever to use rocket power in war was the Chinese conqueror Ogdai, the son of Ghengis Khan, about 1230 AD. The rockets used then were probably propelled by a mixture of slow burning saltpetre and an excess of charcoal or sulphur (the black powder which was invented about 200 years earlier). These missiles were essentially arrows, a fact which explains why the Chinese word for rocket is "huo-chien" which means "fire arrow".

Later in the 13th Century rockets appeared in Europe. There is indication that the first use was by the Tartars against the Polish in the year 1241 AD. Later, as guns developed, the use of rockets as war weapons died out in Europe until early in the 19th Century when the British used Congreve's rockets against France and Denmark.

It is believed that the only propellant used through all these years was black powder which, especially for modern uses, has several deficiencies. It has poor mechanical properties, it does not burn cleanly, and it absorbs moisture. In the year 1888 AD Alfred Nobel, a Swedish Chemist, discovered the solvent and colloiding actions of nitroglycerin on nitrocellulose and combined them into a more powerful propellant, called

double-base propellant. Robert Goddard, an American physicist and rocket expert, employed the double-base propellant and developed useful weapons by 1918.

Composite propellants which consist of oxidizing salts and burning rate modifiers distributed in an elastomeric matrix of organic polymer were introduced in tha 1940's. These propellants are considered superior to double-base propellants with respect to (a) safety in processing and handling, and (b) mechanical properties. They have, therefore, displaced double-base propellants in many applications, especially in large rocket engines. One of the areas of fundamental research has been an attempt to understand the behavior of these composite solid propellants during the ignition and burning processes. The work discussed here is concerned with the reaction characteristics of the polymer fuels in these propellants.

Rocket performance clearly depends on the combustion characteristics of propellants. Much rasearch on propellants is premised on the basic assumption that knowledge of the decomposition chemistry of each of the several ingredients of propellants is necessary to the rational development of improved propellants. Black powder and double-base propellants contain only a limited number of ingredients. Since these materials have been used for a long time, their chemistries, separately and together, have been extensively studied [20, 22, 44, 52]. There are only a few oxidizing salts, ammonium nitrate, ammonium perchlorate (AP), potassium perchlorata etc., which are used in the composite propellants. They too have been extensively studied [2, 30, 42, 43]. Useful studies of decomposition chemistry of polymers have lagged behind for several reasons, (a) many kinds of polymers are used, and they behave differently, (b) decomposition

processes are usually very complex, and (c) as discussed later in Chapter II, suitable techniques have not been always used.

The assumption that the ingredients of typical composite propellants decompose independently in the precombustion phases of the reactions has been the premise of some fruitful research. It is not, however, compatible with certain experimental observations. For example, char forms on the surface of some polymers when they are heated at flux levels typical of propellant combustion, yet no char is seen on the polymer surface of extinguished propellant. Both the mode and the rate of gasification of the polymer are apparently altered by the oxidizer or its decomposition products.

Another assumption commonly made is that the decomposition reactions observed at the lowest temperature where pyrolysis rates are appreciable are the same as those that occur at higher temperatures. It is probably, though it has not been demonstrated for polymers as it has for some other organic compounds, that the relative rates of competing pyrolysis mechanisms are reversed as temperature is increased. Heating rates less than 100° C per min. are typical of pyrolysis studies. In propellant combustion, on the other hand, the polymer is heated at the rates of thousands of degrees per second. Very high temperatures are obtained before low-temperature pyrolysis reactions proceed to a significant extent, and the high-temperature mechanisms are therefore dominant.

In the study reported here, neither of the two assumptions is made. Not only pure polymer but also polymers containing small amounts of ammonium perchlorate and burning rate catalysts were pyrolyzed. Furthermore, heating rates considerably greater than those of most pyrolysis

studies were employed. The experimentsl complications attending these aspects of the study precluded a comprehensive examination of many polymers. Only one polymer, a copolymer of polybutadiene and acrylic acid (PBAA), was studied.

In Chapter II of this paper, relevant research performed by previous workers is discussed. In the following chapter (Chapter III) the current theories concerning the mechanisms of polymer decomposition in inert and chemically reactive gases will be discussed. The composition of various test samples and the method of preparation are presented in Chapter IV. In Chapter V, the details of experimental apparatus and procedures are discussed. In Chapters VI, VII, and VIII, the results of the experiments are presented, along with an analysis of the data and a discussion of their significance. Chapter IX contains an attempt to combine all experimental facts which have been found and from them to draw significant concluaions which, hopefully, will further help understand ignition and combustion mechanisms.

Appendices include a table of nomenclature, a discussion of the methods for measuring the physical properties of various polymers, a presentation of the calibration techniques for the apparatus used in this study, a series of tables summarizing the experimental data and finally the FORTRAN programs used for the numerical solution to the transient-heat-conduction equations.

CHAPTER II

PAST STUDIES OF POLYMER DECOMPOSITION

The thermal breakdown of rubber to isoprene, dipentene and other relatively simple and obviously related molecules was first described over a century ago. It was also noted that monomeric styrene could be recovered in high yield from the products of pyrolysis of the hard glass-like material formed when polystyrene is exposed to gentle heating. Little progress was made in the understanding of these decomposition reactions, however, until the 1920's, when the importance and nature of chain reactions was appreciated, and it was proposed that polymers are composed essentially of thread-like molecules built up from simple molecule units joined together by primary valence forces.

By the early 1930's a good deal of information about the decomposition of natural polymers had accumulated as a result of investigations into the details of polymeric structure. The rapid development of the synthetic plastics industry, some years later, stimulated studies of the thermal decomposition of polymers. A wide range of problems associated with the stability of large molecules, both natural and synthetic, was encountered. In pyrolysis studies, however, polymers were subject to only moderate environmental conditions.

Since 1945, new uses for natural and synthetic polymers have multiplied. In a large number of such applications, high temperatures and large heating rates are encountered.

Conventional Bulk Degradation

Because of the usual complexity of polymer decomposition reactions, the degradation of solid polymers is conventionally carried out at a constant heating rate low enough that the temperature is nearly uniform throughout the test specimen. These studies of thermal degradation can be divided into two principal categories. One category aims at finding (a) the thermal stability, that is, the temperatures for significant rates of polymer decomposition, and (b) the compositions of the degradation products, including the residue, as a function of temperature and pressure. The second category deals with measurements of rates of thermal degradation to determine activation energies and the mechanisms of decomposition.

For studies in the first category, the most frequently used experimental device is an insulated vacuum chamber [34] which is heated electrically. The decomposition products are analyzed by use of gas chromstography and mass spectrometry. For experiments in the second category, the measurements involve use of a similar chamber and usually one of three other techniques:

(a) Differential Thermal Analysis (DTA), originated by Le Chatelier in the 1870's, in which a comparison of the temperatures in two samples is continuously made, one sample being inert and the second the material under study, while both are heated at a uniform rate.

(b) Thermogravimetric Analysis (TGA), in which weight loss is measured as a function of temperature.

(c) Differential Scanning Calorimetry (DSC), in which samples are subjected to a programmed temperature history and the rate of energy input is measured.

Bulk Pyrolysis of Polystyrene

Polystyrene (PS) is probably the most thoroughly studied organic polymer. The results provide a guide to an understanding of other materials. The pyrolysis of polystyrene was carried out separately by Jellinek [25, 26], Madorsky and coworkers [32, 33] and Grassie and Kerr [16, 17] at temperatures from 280° C to 360° C. Their results were in fairly good agreement despite the great difference in the molecular weights and purities of the polystyrene samples used. In all casea the molecular weight dropped abruptly during the first few per cent loss of weight of sample to about 80,000. Beyond this the drop was gradual.

A plausible mechanism of the thermal degradation of this polymer, which is in agreement with the experimental results, is as follows [33]. As the polymer undergoes pyrolysis its molecular weight drops rapidly during the first 5-10% loss of weight and slowly thereafter. The range in which the slow drop occurs seems to be independent of the initial molecular weight or of the molecular weight distribution in the polymer species, provided the initial molecular weight is not below this range. The initisl drop in molecular weight may be due partially to scission at weak bonds (for example, linkages formed by oxygen contsminstion and carbon-carbou bonds adjacent to tertiary or quaternary csrbons) in the polymers, but is mainly caused by random thermal scission in the chain.

This continues to a point where the drop in molecular weight caused by scission is nearly counterbalanced by the disappearance of smaller chains through unzipping, mainly into monomers.

The effect of pressure on the pyrolysis of polystyrene was studied by Straus and Madorsky [48]. The results are summarized in Tables I and II. A comparison of the data in Tables I and II indicates, though not unambiguously, that an increase in pressure tends to increase the amount of heavier products vaporized.

It has been found that for polystyrene [48], the decomposition products of pyrolysis at 500° C do not differ essentially from those obtained at lower pyrolysis temperatures. However, the results obtained at 800° C and 1200° C show a difference in product distribution from those obtained at or below 500° C. This difference consists mainly in the appearance of more hydrogen and light hydrocarbons in the more volatile fraction for higher pyrolysis temperatures.

The rate of thermal degradation of polystyrene was studied by Jellinek [26], Madorsky [32, 33], Grassie and Kerr [16, 17]. The curves of rate of degradation versus per cent of degradation ordinarily exhibit maxima. However, these maxima broaden into plateaus with lowering of the temperature of pyrolysis.

Madorsky [33] explains the maxima and plateaus as a balance of free radical formation by scission and free radical disappearance by unzipping. His explanation fails, however, to account for the increasing concentration of free radicals needed to maintain the rate in the diminishing supply of reactant, especially as the scission process, which generates the free radicals, is slowing down. Also he erroneously assumes that

TABLE I

PYROLYSIS OF POLYSTYRENE IN A VACUUM AT ELEVATED TEMPERATURES

(Straus and Madorsky [48])

Temp. °C	Volatilization per cent	Mass % Based on Total Volatilized V^1_{pyr}	V^2_{25}	V^3_{-190}
500	100.0	36.5	63.5	----
800	99.7	28.2	71.8	----
1200	98.0	34.4	65.0	0.6

TABLE II

PYROLYSIS OF POLYSTYRENE IN 1 ATM HELIUM AT ELEVATED TEMPERATURES

(Straus and Madorsky [48])

Temp. °C	Volatilization per cent	Mass % Based on Total Volatilized V^1_{pyr}	V^2_{25}	V^3_{-190}
500	100.0	35.2	64.8	----
800	98.5	40.0	60.0	----
1200	95.3	74.6	25.4	----

1 Material volatile at the temperature of pyrolysis but not at room temperature.

2 Material volatile at room temperature but not at -190° C.

3 Material volatile at -190° C.

constant mass rate of volatilization implies a reaction zero-order with respect to polymer. Using maximum and plateau rates, he calculates an activation energy of 55 kcal/gmole. What process, if any, this figure can be attributed to is not clear.

Bulk Pyrolysis of Other Polymers

Polybutadiene is related to the fuel-binder investigated in this work. Its pyrolysis by a slow process was carried out by Straus and Madorsky et al. [35, 47] in insulated apparatus in the temperature region of 325° C to 425° C. The effect of temperature on the pyrolysis products distribution noted in the pyrolysis of polystrene was also observed. The fraction V_{25} (volatile at 25° C), was too complex and V_{-80} (volatile at -80° C) was separated from it. The analysis of V_{-80} portion by use of mass spectrometer showed that the monomer, 1, 3-butadiene, increased from 28.2 per cent to 58.9 per cent by weight of V_{-80} as the decomposition temperature decreased from 400° C to 325° C. Fraction V_{pyr}, wax-like in appearance, was tested for average molecular weight by microcryoscopy in benzene solution. An average value of 739 was obtained.

The rate of thermal degradation of polybutadiene in vacuum was investigated by means of the tungsten-spring balance [47]. Initial rates were high, diminishing sharply up to about 30 per cent volatilized, and slowly thereafter. From the slower rates observed for temperatures from 380° C to 395° C, the overall activation energy was calculated to be 62 kcal/gmole.

Straus and Madorsky et al. also studied the thermal behavior of styrene-butadiene rubber (SBR, 75% butadiene and 25% styrene) and

butadiene-acrylonitrile copolymer (NBR, 70% butadiene and 30% acrylonitrile) [47]. The general conclusions from these tests are similar to those from polybutadiene tests. The fraction V_{25} for SBR in vacuum and 30 min of pyrolysis at temperatures from 320° C - 400° C consisted of 11.8 per cent of total volatiles as compared with 14.1 for polybutadiene. For NBR the value was 14.5 per cent. Microcryoscopic analysis of the wax-like fraction V_{pyr} from SBR in benezene solution showed an average molecular weight of 712. For NBR the value was 401 obtained by microcryoscopic analysis in diphenylamine. Rates of degradation of SBR and NBR were also studied by means of a tungsten-balance. No definite conclusions can be drawn as to the initial reaction rates and activation energies.

The pyrolysis and ignition behavior of PBAA (polybutadiene-acrylic acid copolymer) in gases in a heated stainless steel tube has been studied by Meek and Thompson [39]. This was essentially the aame polymer used in this work. Pyrolysis rates calculated as weight loss per unit time below ignition temperatures were found higher in nitrogen than in oxygen. The data cannot be fit to a simple rate law, probably because of competing reactions. An activation energy of 25 to 30 kcal/gmole was calculated for the initial pyrolysis reaction in nitrogen. Samples pyrolyzed in nitrogen changed from a golden color to a dark brown and from a rubber-like material to a tough plastic. Apparently thermal polymerization occurred. Samples pyrolyzed in oxygen became brittle and were a glossy black. Apparently cross-linking involving absorbed oxygen occurred. In all cases, the sample size was not diminished by the loss of material, and pyrolysis occurred uniformly throughout the sample. Most evolved polymer fragments were quite large and could be condensed at

room temperature. Ignition in oxygen showed a dependence of minimum ignition temperature on oxygen pressure, from 285° C at 1.53 atms to 245° C at 10.4 atms. Several relevant conclusions can be drawn from these tests:

(1) PBAA polymer decomposes at significant rates in the temperature range of 250° C to 350° C by homogeneous decomposition. Reactions in this temperature range are important in composite propellant ignition. The character of the residue after being heated in an inert environment suggests that further polymerization has occurred.

(2) There are evidences of oxygen-polymer reactions. The lower rate of weight loss of PBAA in oxygen than in nitrogen indicates absorption of oxygen in the polymer. The change in the physical properties of the residue indicates that polymerization and cross-linking have occurred. The data do not allow one to infer other possible effects of oxygen, for example increased evolution rates of hydrogen and carbon species as a result of oxygen attack on surface molecules.

(3) Most of the evidence would support a gas-phase ignition mechanism. The temperature and pressure range for ignition corresponds to the range normally required for the homogeneous ignition of gaseous hydrocarbon-oxygen mixtures.

(4) There is no evidence of significant further polymerization or cross-linking of polymer during burning of PBAA composite propellants though oxygen-bearing species from oxidant

decomposition are surely present. It is clear, therefore, that the work of Meek and Thompson makes only a limited contribution to understanding the burning process. If polymer pyrolysis experiments are to be relevant to ignition and burning, they must employ the same time scale of those processes.

An important result relating to the effect of pressure on polymer pyrolysis is illustrated by Lewis and Naylor's work on polytetrafluoroethylene [31]. At pressure of a few millimeters, yields of the monomer (C_2F_4) from polytetrafluoroethylene approach one hundred per cent. As the pressure is increased, increasing amounts of dimer and a compound with the formula C_3F_6 appear, until at atmospheric pressure these compounds comprise 84 per cent of the volatile products of pyrolysis. A possible explanation of this pressure effect is that apparently while the monomer is usually the primary product of the decomposition reaction, increasing external pressure results in this monomer remaining within the hot polymer for longer periods so that the probability of its taking part in subsequent reactions is increased. Whatever the explanation is, that there is a pressure effect on the decomposition of many polymers is very clear.

Linear Pyrolysis

Another technique for the study of thermal decomposition of polymeric materials involves the measurement of the linear regression rate of the heated surface of polymers. Experimental devices for heating the surface are hot plates [2], flat diffusion flames [42] and

porous plugs [38]. Such experiments are mostly performed in an attempt to explain steady-state burning of solid propellants and are found to be most suited for the study of the oxidizer crystal pyrolysis.

Andersen et al. [2], using a hot plate, studied the linear pyrolysis rate of linear polymethylmethacrylate (PMM) and PMM cross-linked with 2% and 5%, respectively, of ethylene glycol diacrylate. It was found that for a plate temperature in a range of 440° C to 575° C, the effect of increasing the extent of cross-linking was to decrease the pyrolysis rate at a given temperature; however, the apparent activation energy (18.2 kcal/mole) appears to remain unchanged. They also found that the chamber pressure up to 70 atms had no detectable influence in the linear pyrolysis rates of pure PMM. However, since in this experiment the polymer strand was pressed against the hot plate by an external force, the effective pressure at the decomposing surface is not known.

In their study of linear pyrolysis rates for both linear and cross-linked polymethylmethacrylate (PMM), Cnaiken et al. [12] found that at a high surface heating rate the pyrolysis rate of PMM possessed a lower activation energy than that which was reported for the bulk degradation. At hot plate temperatures larger than 700° K, the activation energy obtained from the slope of a semi-log rate plot approaches a limiting value of 11.2 kcal/gmole which is too low to suggest formation of monomer by chain rupture as the rate controlling mechanism. Rather, it is more consistent with a surface process of monomer desorption. The heat of vaporization of liquid monomer at 100° C has been estimated from vapor pressure data to be 9.2 kcal/g-mole.

Chaiken et al. proposed the reaction scheme of PMM pyrolysis as follows. The duality of rate processes is probably associated with the surface heating rate. At high temperatures the polymer surface is saturated with monomer, and desorption of monomer is the rate-controlling step in the pyrolysis process. At lower temperatures, the polymer surface is not saturated with monomer, so the monomer formation may be rate-controlling.

There have been questions concerning the validity of the hot plate technique for pyrolysis measurements. Cantrell [10], analyzing his experimental data on dry ice, concluded that the gas film thermal resistance has an important effect on the linear pyrolysis of solids. In agreement with Cantrell's conclusion, Nachbar and Williams [40] showed by a one-dimensional, steady-state analysis that there should be a significant difference between the plate temperature and the solid surface temperature. They also suggested the use of a porous hot plate, and data were obtained by Coates [13] for linear pyrolysis of AP by a porous hot plate. Because the residual product of polymer decomposition tends to plug the porous plate, the device is not useful for polymer studies.

Only limited work has been done on the effect of a chemically reactive environment on the linear pyrolysis of polymeric materials. In one such study, McAlevy [38] used a technique which permitted experimental variation of the test gas concentration at the heated, regressing surface. He found that for conditions typical of propulsion applications, O_2 and even ClO_3F do not have a sufficiently fast rate of surface reaction with either polystyrene (PS) or PMM to accelerate noticeably their thermal

degradstion rates. Neither Cl_2 nor NO_2 alter the degradation rate of PMMA. PS, however, is sttscked by Cl_2 and NO_2 at a rate sufficiently large to produce a noticeable increase in its degradation rate. These findings show that reaction between oxidizing gases and polymer surfaces probably cannot be described by convenient generalizations.

High Flux Pyrolysis

Considerable interest exists in the surface pyrolysis of polymeric materials when they are exposed to high surface fluxes, both because of the use of such materials in propellants and because of their application as sblative thermal barriers. More satisfactory than the hot plate for providing the desired high level of energy flux are radiant source imaging furnaces, Xenon flash tubes, electrically heated radiation furnaces, gaseous combustion products or shock-heated gas.

Carbon-arc imaging furnaces, which can produce a heat flux greater than 150 cal/(sec)(cm)^2 for a considerable period, are used extensively for high temperature research. However, there are several serious drawbacks to these devices; for example, at the image point a non-uniform spatial heat flux distribution exists and serious fluctuation of the local heat flux with time occurs. These shortcomings discourage the use of the carbon-arc furnace for any serious quantitative studies. Naglar [41] used a carbon-arc imaging furnace to produce steady regression of polymeric materials at a variety of heating rates and at reduced pressures. All the craters formed after exposure showed the effect of the non-uniform heat flux distribution. Also the character of the degradation products he collected is at variance with that reported by

experimenters using other techniques. The discrepancy is supposedly due to the different heating rates at different points on the surface. The machanism of pyrolysis is determined by the temperature of the surface and its thermal history, and these are influenced by the heating rate.

Ignition Studies

Research on the ignition of polymers and propellants throws interesting light on the polymer decomposition aspects of propellant combustion.

The simplest adequate description of the ignition of polymers in contact with a reactive gas (except those that, like nitrate esters, decompose exothermically) considers the surface heated by an external source. Part of the heat is conducted into the body, part is conducted out into the gaa phase, and part accumulates in the polymer surface. If the external flux is great enough, the surface temperature will reach a level where significant decomposition occurs. Fuel vapors diffuse into the gas phase where, when temperature and composition are right, they eventually burn with oxygen in the ambient gas. Energy feed-back from the flame sustains the process, and the external flux can be cut off.

This description was qualitstively confirmed by Alvares [1], who studied the ignition of alpha-cellulose using a Mitchell carbon arc [7] with refracting optics. He found that the time to ignition decreased as the total stmospheric pressure of dry air increased. Ignition would not occur below 0.15 atmospheres. He also observed that the

thermal conductivity of diluent gas in an oxygen-diluent gas mixture which was kept at a constant total pressure affects the time to ignition. Helium, which has a conductivity almost a factor of 10 larger than nitrogen, always resulted in a greater time to ignition than nitrogen while carbon dioxide which is approximately 10% lower in thermal conductivity, resulted in a smaller time to ignition. At the same total pressure, the ignition time was found to decrease smoothly with increasing oxygen concentration.

The description is also a statement of the theory proposed by McAlevy, Cowan, and Summerfield [37] for ignition of ammonium perchlorate-polymer composite propellants. They asserted that the oxidizer did not participate in combustion until after tha gasified polymer-ambient oxygen flame was established. They supported their theory by showing the oxygen concentration dependence of ignition time. Baer, Ryan [4, 45] and Keller [28] showed the inadequacy of the theory by demonstrating that propellauts with non-volatile, non-decomposable fuels (carbon black and graphite) ignited in the same way as those with polymer fuels. Keller showed further (1) that if the exposed propellant surface is smooth, the oxygen concentration of the ambient gas has no effect on ignition time, and (2) that the key reaction in propellant ignition by thermal stimulus is ammonium perchlorate decomposition.

Clearly the theory is not generally applicable to propellant ignition, and the question arises regarding its applicability to ignition of pure polymers. Martin [36] introduced one complication by noting that ignition in air of alpha-cellulose heated in an arc-imaging furnace occurs at about the time hydrogen and light hydrocarbons first appear in

the evolving products of decomposition. Apparently the mechanism or the degree of pyrolysis is a factor to be considered.

Anderson et al. [3] suggested an alternate description of ignition in oxygen. Taking a cue from their experiments with hypergolic ignition, they proposed that a heterogeneous reaction of the oxygen with the polymer is the critical step. The heterogeneous reactions may well be a very important feature of propellant ignition and burning, though Keller's results indicate that they are probably not rate controlling in thermal ignition [28]. They may be important also in polymer decomposition in a reactive environment.

Summary

In summary, although the results of bulk decomposition studies provide a good guide to understanding the parameters which might affect polymer decomposition reactions, for example, pyrolysis temperatures, external pressures, chemical environments, they need critical interpretation when applied to the understanding of ignition and burning processes, because:

(1) The pyrolysis products are so complicated that relisble information about reaction mechanisms has not been produced.

(2) For ignition, normally initial products are important, and bulk decomposition experimenters ususlly neglect the study of them.

(3) In the bulk decomposition, many competing reactions are possible because of prolonged reaction time, while in the ignition process probsbly only a few initial resctions predominate.

Linear pyrolysis data are hard to interpret with respect to the ignition process. A survey of previous work shows that the regression rate in pyrolysis may be either kinetically or flux controlled, and reactive gases may or may not be important. In some work there is evidence that pyrolysis rates may be function of surface temperature, total pressure, and rate of heating. Ignition may be the result of homogeneous gas phase reaction, or the result of heterogeneous hypergolic reaction. In all cases, ignition probably proceeds through reaction steps involving free-radicals or reactive intermediates.

CHAPTER III

THEORY AND MECHANISM

The most useful theoretical treatments of thermal decomposition of polymers treat two mechanisms: scission of bonds and chain unzipping. Scission of bonds can be further divided into random scission and scission of weak links. Chain unzipping can also be further divided according to kind of initiation, whether randomly along the chain or at the end. Since the random scission and random initiation of unzipping are probably the most common degradation processes, at least according to the theoreticians' emphasis, they will be discussed in some detail.

Random Scission

The fundamental assumptions of the theory of random breaking of links are as follows:

(1) The polymer sample under consideration is initially homogeneous; that is, chains of one length only are present. (The results can be generalized to eliminate the restriction imposed by this assumption.)

(2) All links between the monomer units in the chain molecules are of equal strength and equal accessibility, regardless

of their positions in the chains and regardless of the length of the chains.

(3) The rate of breaking links is proportional to the number of links present in the reaction system.

According to these three assumptions, the rate equations for the random degradation process are as follows:

$$\frac{dN_{p_o}}{dt} = -(p_o - 1)kN_{p_o} , \qquad \text{(III-1)}$$

$$\frac{dN_p}{dt} = 2k \sum_{i=p+1}^{p_o} N_i - (p-1)kN_p , \text{ for } p < p_o . \qquad \text{(III-2)}$$

In this set of differential equations p_o and p are original chain length and chain length of intermediates respectively. N_{p_o} and N_p are the number of chains of length p_o and p respectively. k is the rate constant for the breaking of links.

The solution to Eq. (III-1) is a straightforward integration. Letting N_o be the original number of chains of length p_o, we have

$$N_{p_o} = N_o e^{-(p_o-1)kt} . \qquad \text{(III-3)}$$

Eq. (III-2) can be solved by a method of mathematical induction. The final result is given by

$$N_p = N_o \left[(p_o-p-1)e^{-(p+1)kt} - 2(p_o-p)e^{-pkt} - (p_o-p+1)e^{-(p-1)kt} \right] . \qquad \text{(III-4)}$$

Eqs. (III-3) and (III-4) constitute the mathematical expressions for the size distribution as a function of time of degradation by random scission. These two equations check with the results obtained by Simha [46] for the same degradation process.

If the pyrolyzed polymer fragments with chain length p equal to or less than m are volatile and leave the pyrolyzing polymer, the number average molecular weight of residue in monomer units can be calculated by

$$M_n = \frac{\sum_{p=m+1}^{p_o} pN_p}{\sum_{p=m+1}^{p_o} N_p} , \qquad \text{(III-5)}$$

and the fraction of weight loss by

$$w_f = \frac{1}{p_o N_o} \sum_{p=1}^{m} pN_p . \qquad \text{(III-6)}$$

Using Eqs. (III-3) and (III-4) in Eq. (III-5), we have

$$M_n = \frac{p_o + m(p_o - m - 1)(1 - e^{-kt})}{1 + (p_o - m - 1)(1 - e^{-kt})} ,$$

or, if $p_o >> m + 1$

$$M_n \doteq \frac{p_o + mp_o(1 - e^{-kt})}{1 + p_o(1 - e^{-kt})} . \qquad \text{(III-7)}$$

Using Eqs. (III-3) and (III-4) in Eq. (III-6), we have

$$w_f = 1 - (m+1)\frac{p_o^{-m}}{p_o} e^{-mkt} + m\frac{p_o^{-m-1}}{p_o} e^{-(m+1)kt} ,$$

or, if $p_o >> m+1$

$$w_f \doteq 1 - (m+1)e^{-mkt} + me^{-(m+1)kt} . \qquad \text{(III-8)}$$

If we differentiate Eq. (III-8), the rate of weight loss is found to be

$$\frac{\dot{w}_f}{k} = m(m+1)(e^{-mkt} - e^{-(m+1)kt}) . \qquad \text{(III-9)}$$

Random Initiation Followed by Unzipping

At the other mechanistic extreme, it is assumed that, as before, there is first-order bond attack with rate constant k, but with each attack followed immediately by complete unzipping to volatile fragments. Eqs. (III-1) and (III-3) are still valid, and we find

$$M_n = p_o , \qquad \text{(III-10)}$$

$$w_f = 1 - e^{-(p_o-1)kt} , \qquad \text{(III-11)}$$

$$\frac{\dot{w}_f}{k} = (p_o-1)e^{-(p_o-1)kt} \qquad \text{(III-12)}$$

Random Scission With Some Unzipping

The intermediate cases of random scission with partial unzipping or complete unzipping for only a part of the scissions are generally too complicated to formulate concisely. There is, however, one special case that is tractable, namely random scission with half the scissions followed by rapid and complete unzipping. This case is equivalent to random scission with one of the two fragments formed unzipping.

Eqs. (III-1) and III-3) are valid as before. Eq. (III-2) is replaced by

$$\frac{dN_p}{dt} = k \sum_{i=p+1}^{p_o} N_i - (p-1)kN_p \text{ , for } 1 < p < p_o \text{ ,} \qquad \text{(III-13)}$$

and

$$\frac{dN_1}{dt} = kN_o e^{-kt} + \frac{1}{2} k \sum_{p=2}^{p_o} (p-1)pN_p \text{ .} \qquad \text{(III-14)}$$

Integration gives

$$N_1 = N_o(p_o - \frac{2e^{-kt} - e^{-2kt} - e^{-p_o kt}}{1 - e^{-kt}}) \text{ ,} \qquad \text{(III-15)}$$

and

$$N_p = N_o(e^{-(p-1)kt} - e^{-pkt}) \text{ , for } 1 < p < p_o \text{ .} \qquad \text{(III-16)}$$

If Eqs. (III-3), (III-15) and (III-16) are used in Eqs. (III-5) and (III-6), we have

$$M_n = \frac{m+1 - me^{-kt} - e^{-(p_o-m)kt}}{1 - e^{-kt}} , \qquad \text{(III-17)}$$

$$w_f = 1 - \frac{1}{p_o} \frac{(m+1)e^{-mkt} - me^{-(m+1)kt} - e^{-p_o kt}}{1 - e^{-kt}} , \qquad \text{(III-18)}$$

$$\frac{\dot{w}_f}{k} = - \frac{1}{p_o(1-e^{-kt})} \left[m(m+1)e^{-(m+1)kt} - m(m+1)e^{-mkt} + p_o e^{-p_o kt} \right]$$

$$+ \frac{1}{p_o(1-e^{kt})^2} \left[(m+1)e^{-(m+1)kt} - me^{-(m+2)kt} - e^{-(p_o+1)kt} \right] . \qquad \text{(III-19)}$$

Comparison of Cases

The differences found for the three cases of the dependencies of residue molecular weight, weight loss, and rate of weight loss on time, initial chain length (p_o), and the least size of molecule in the residue (m+1) make a graphical comparison very difficult. We attempt it nevertheless in Figs. 1, 2, and 3, where values of 1000 are assumed for p_o, and 5 for m. For obtaining better comparison, Fig. 2 uses two time scales, and Fig. 3 different scales for the rate of weight loss. The symbol θ represents the fraction of scissions followed by unzipping.

Fig. 1 shows molecular weight as a function of time in units of average bond life with respect to scission. The interesting feature is that the simple scission and the scission-half-unzipping cases are virtually indistinguishable. The molecular weight for the case of total unzipping stays constant as expected.

On the other hand, Fig. 2, giving fraction weight loss as a function of time, makes the total and the half-unzipping cases appear

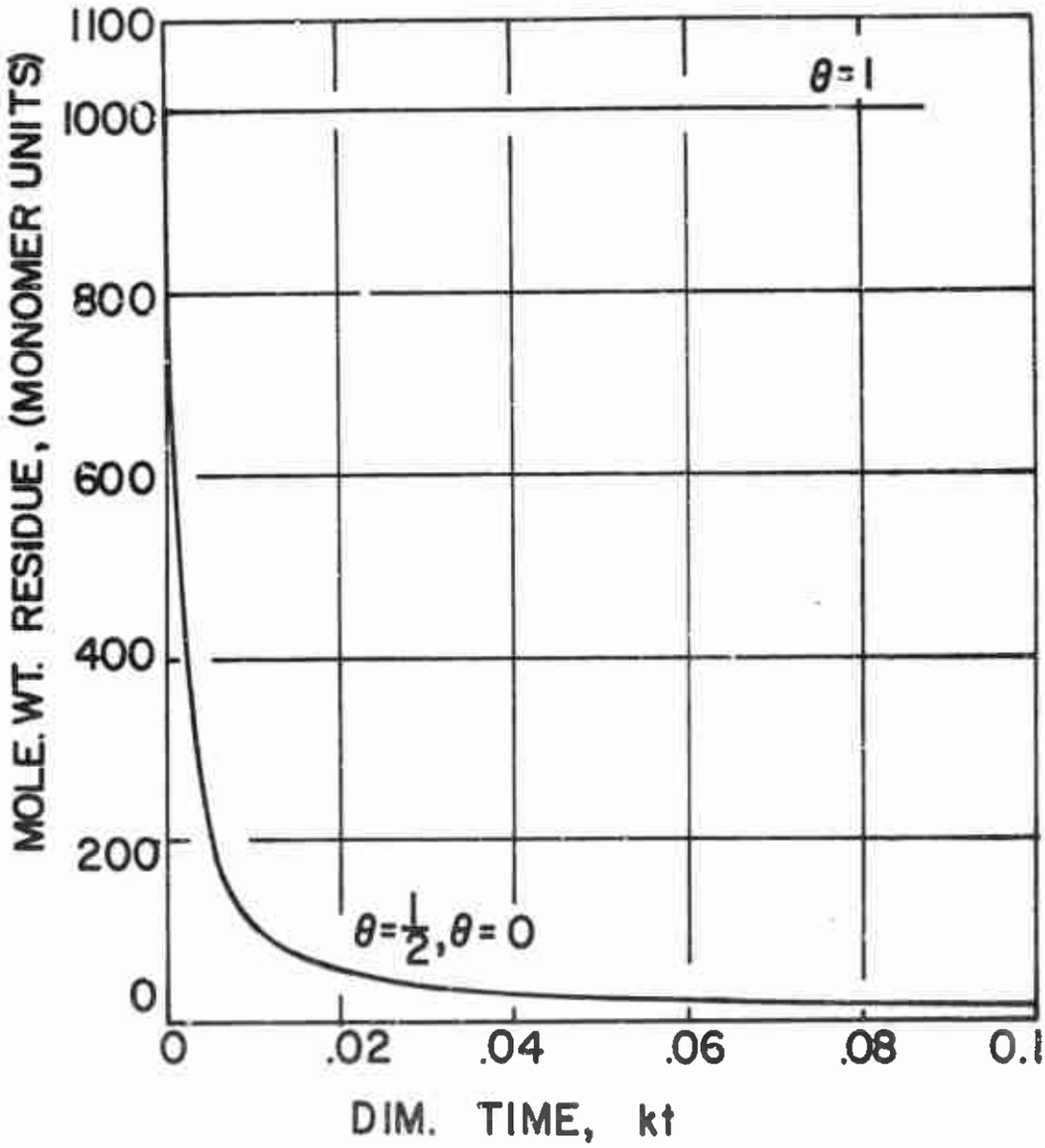

Fig. 1. -- Number average molecular weight of a pyrolyzing polymer as a function of time for different decomposition mechanisms. θ is the fraction of scissions followed by unzipping. In this plot m is 5, and p_o is 1000. For $\theta = 1$ and $\theta = 1/2$ the values are so close that only one curve is shown.

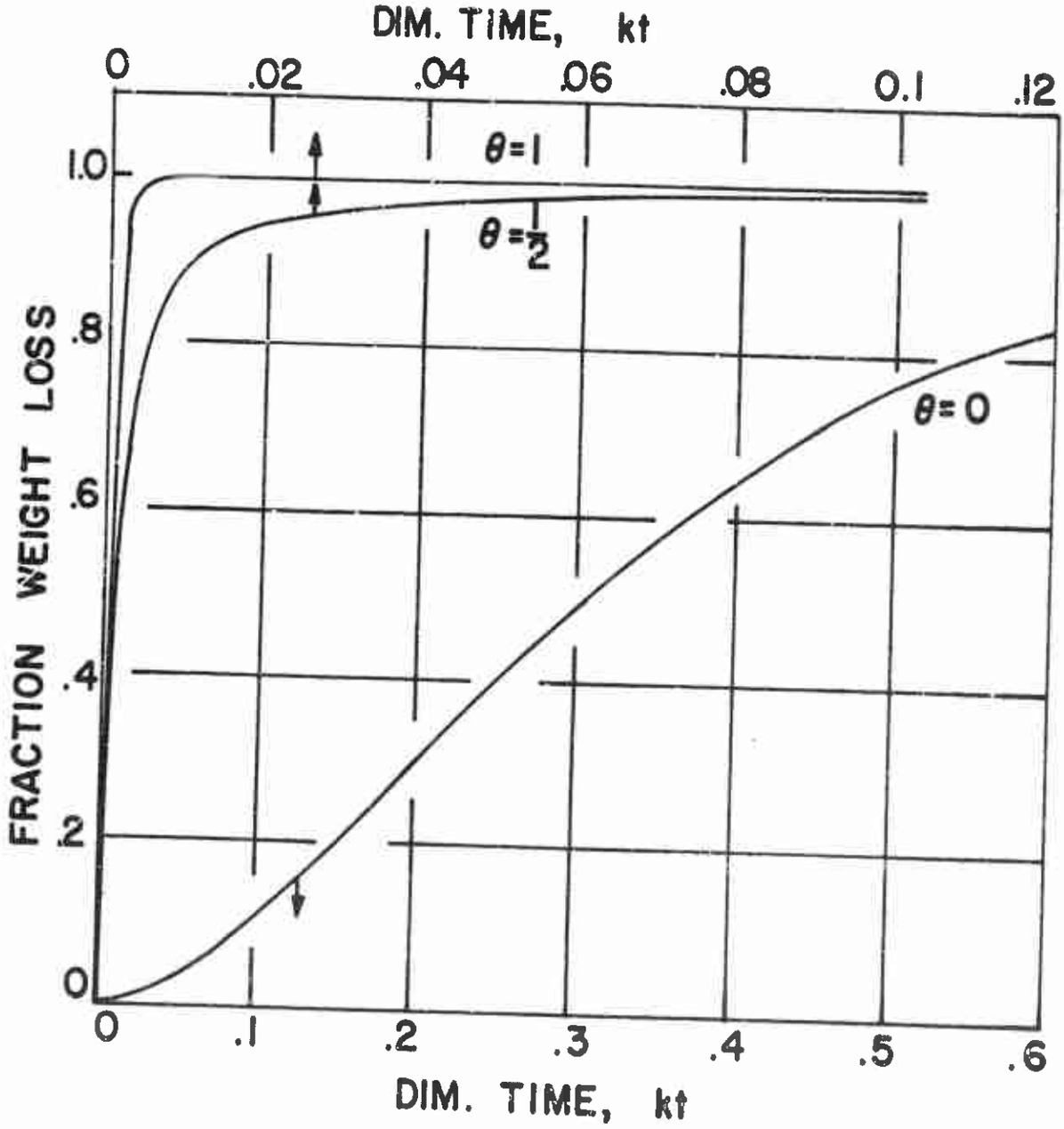

Fig. 2. -- Loss-in-weight for a pyrolyzing polymer as a function of time for different decomposition mechanisms. θ is the fraction of scissions followed by unzipping. In this plot m is 5, and p_o is 1000.

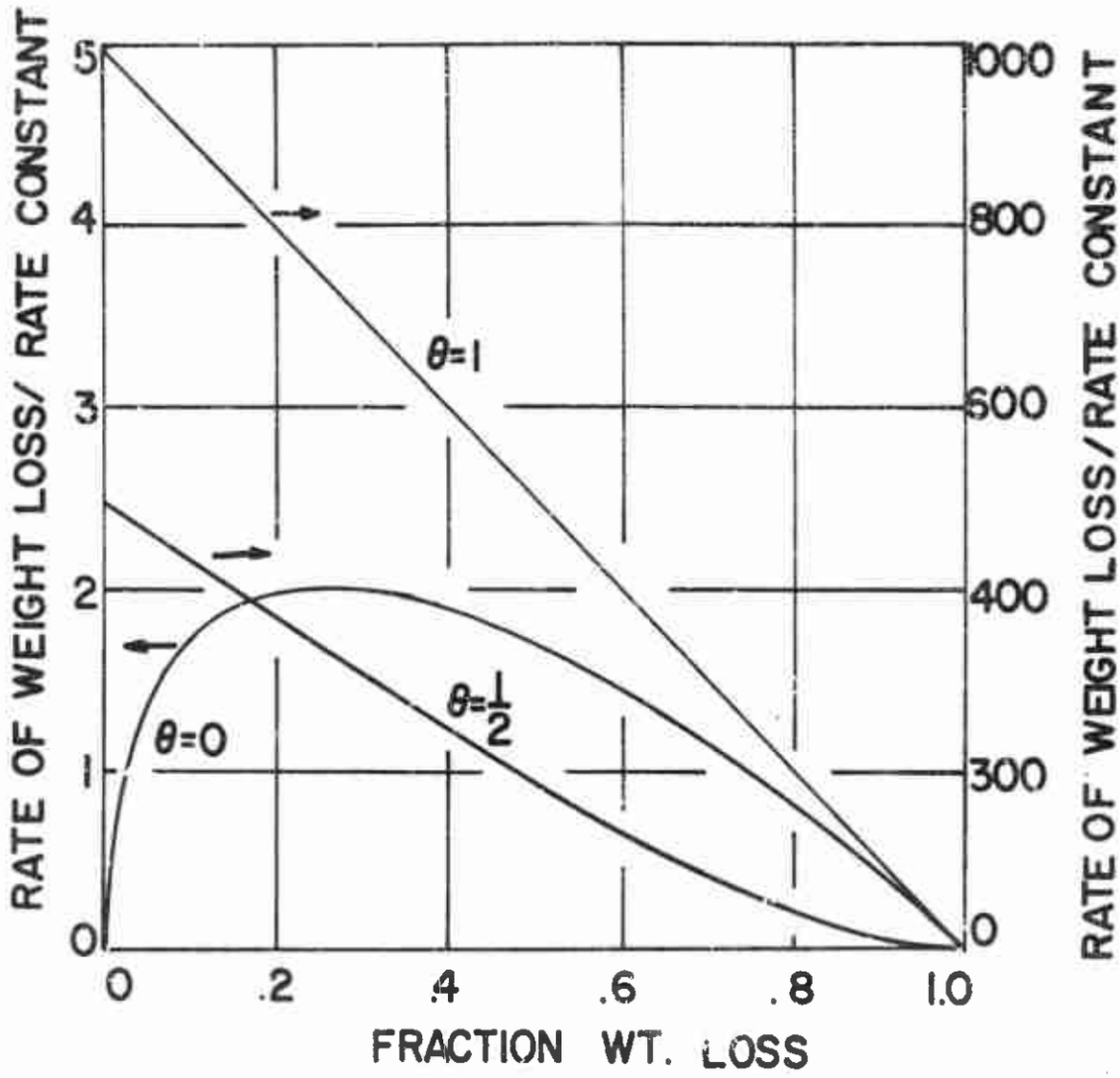

Fig. 3. -- Rate of volatilization for a pyrolyzing polymer as a function of fraction weight loss for different decomposition mechanisms. θ is the fraction of scissions followed by unzipping. In this plot m is 5, and p_o, 1000.

very similar. Maximum rates are at zero time and the half-unzipping case also has a rate decaying very rapidly in time except very late in the process. In contrast, simple scission gives a very small initial rate of weight loss and a maximum rate at about 30 per cent weight loss. Another interesting feature of simple scission is that the rate of weight loss is nearly constant from about 15 per cent to about 45 per cent loss. Some experimenters have erroneously interpreted this nearly constant rate as signifying zero-order reaction.

Fig. 3, representing a common way to present experimental results, shows rate of weight loss versus weight loss. For total unzipping the rate of weight loss is the highest at the beginning, and decreases linearly with the fraction volatilized until complete vaporization. The rate of weight loss for half-unzipping case also gives the highest value at the beginning, and decreases almost linearly with the fraction volatilized until very late in the process. The rate of weight loss at the start is about half as big as that of total unzipping. The interesting feature of the simple scission case, a maximum in rate of weight loss, has been mentioned.

Theoretically, the activation energy of bond breaking can be evaluated from the measurement of rate of weight loss at different pyrolysis temperatures. The method is not always simple. Take $\theta = \frac{1}{2}$ for instance. Eq. (III-19) suggests that there is no simple way to calculate the activation energy from the data for rate of weight loss. However, for $\theta = 1$ and $\theta = 0$ simple methods can be found. When time is equal to zero Eq. (III-12) becomes

$$\dot{w}_f = (p_o-1)k = (p_o-1)Ae^{-E/RT} \quad . \qquad \text{(III-20)}$$

Hence for $\theta = 1$ the activation energy can be calculated by plotting the logarithm of initial rate of production of volatiles versus reciprocal pyrolysis temperature. The difficulty comes in determining the initial rates. Alternatively, for $\theta = 1$, we can write

$$\frac{\dot{w}_f}{1 - w_f} = -(p_o-1)k = -(p_o-1)Ae^{-E/RT} \quad . \qquad \text{(III-21)}$$

Then the logarithms of slopes of $\dot{w}_f$ versus $1-w_f$ lines for different temperatures may be plotted against reciprocal pyrolysis temperatures to give a line whose slope is the activation energy.

For pure random scission or $\theta = 0$ the activation energy can be evaluated from the measurement of the maximum rates of production of volatiles. This maximum rate of volatilization is found to be

$$\dot{w}_{f\ max} = m\left(\frac{m}{m+1}\right)^m k = m\left(\frac{m}{m+1}\right)^m Ae^{-E/RT} \quad . \qquad \text{(III-22)}$$

The activation energy is obtained by plotting logarithm of $\dot{w}_{f\ max}$ versus $\frac{1}{T}$. As temperature increases, larger fragments become volatile, that is, m is increased. However, the temperature dependence of the function of m (also that of the factor A) is weak compared to that of the exponential factor.

Generalization to Eliminate First Assumption

It was mentioned that the assumption of uniform p_o was unnecessary. The number of chains of length p has been derived on the basis of N_o number of original chains of length p_o. (See Eq. (III-4).) If the total number of chains of chain length less than p_o is represented by N_{p_o}, the original number of chains of size p_o is found to be

$$\frac{dN_{p_o}}{dp_o} ,$$

and the mass of these chains in monomer units is found to be

$$p_o \frac{dN_{p_o}}{dp_o} .$$

Hence the number average molecular weight of virgin polymer in monomer units is given by

$$M_n(0) = \frac{\int_0^\infty p_o \frac{dN_{p_o}}{dp_o} dp_o}{\int_0^\infty \frac{dN_{p_o}}{dp_o} dp_o} \qquad \text{(III-23)}$$

As the degradation reaction goes on, the total number of chains produced from one original chain of particular length p_o is

$$\sum_{p=m+1}^{\infty} n_p(p,p_o,t) ,$$

where $n_p = \frac{N_p}{N_o}$.

The total mass of residue from one original chain of particular length p_o is

$$\sum_{p=m+1}^{\infty} p n_p(p,p_o,t) \quad .$$

Hence the number average molecular weight of residue at later time is given by

$$M_n(t) = \frac{\int_o^{\infty} \frac{dN_{p_o}}{dp_o} \left\{ \sum_{p=m+1}^{\infty} p n_p(p,p_o,t) \right\} dp_o}{\int_o^{\infty} \frac{dN_{p_o}}{dp_o} \left\{ \sum_{p=m+1}^{\infty} n_p(p,p_o,t) \right\} dp_o} \quad . \qquad \text{(III-24)}$$

The mass of polymer fragments volatilized in monomer units from one original chain of length p_o is

$$p_o w_f(p_o,m,t) \quad .$$

The total weight loss summed over all values of p_o is

$$\int_o^{\infty} p_o w_f(p_o,m,t) \frac{dN_{p_o}}{dp_o} \, dp_o \quad .$$

Hence the total weight fraction volatilized is given by

$$w_f(t) = \frac{\int_0^\infty p_o w_f(p_o,m,t) \frac{dN_{p_o}}{dp_o} \, dp_o}{\int_0^\infty p_o \frac{dN_{p_o}}{dp_o} \, dp_o} \quad . \qquad \text{(III-25)}$$

Other Theoretical Considerations

Experiments on the degradation of long-chain molecules lead in some cases to the conclusion that weak links are distributed in the polymer chains. These weak links are ruptured more easily than the normal links or may even be, under certain conditions, the only links which are broken. One case of depolymerization of random breaking of weak links which are distributed at random over each chain has been discussed theoretically by Jellinek [24]. A detailed discussion of weak link theory will not be presented here. It sufficies to mention that weak-link scission can be treated as a process like the concomitant random scission between monomer units but with a much larger rate constant. The first phase of the combined process is therefore one in which there is a rapid reduction in residue molecular weight accompanied by little weight loss, weak-link scission giving, for the most part, non-volatile fragments. In the second phase, weak-link scission is virtually complete, and the slower processes already described come into play, but with p_o taking the value characteristic of the molecules left after weak-link scission.

There are also polymers which decompose by initiation at the chain ends followed by unzipping. If the average kinetic chain length (which is the number of monomer units which are split off on the average

from one activated chain end) is bigger than the number of monomer units in the original polymer, then once a chain is activated, it unzips completely into monomer units. In this case the number average molecular weight of residue will not change with time. For simplicity only the kinetics of initial stages of degradation will be considered. Assuming that the unzipping reaction is very fast compared with the initiation reaction, we have

initiation $$\frac{dN^*_{p_o}}{dt} = k_o N_{p_o} ,$$

rate of production of monomers

$$\frac{dm_1}{dt} = P_o \frac{dN^*_{p_o}}{dt} = k_o N_{p_o} P_o .$$

As $N_{p_o} = \frac{m_o}{P_o}$, we have

$$\frac{dm_1}{dt} = k_o m_o . \qquad \text{(III-26)}$$

In these equations $N^*_{p_o}$ is the number of activated radicals by breaking off one monomeric radical at the chain ends, m_1 is monomer, k_o is the rate constant for initiation, and m_o is total number of monomer units in the polymer sample. Eq. (III-26) shows that for chain end initiation and unzipping the initial rate of monomer formation is independent of the initial chain length but proportional to the amount of polymer.

Application of Theory to Past Work

The theories of thermal decomposition of polymers discussed on these pages have been found satisfactory in explaining the experimental results of some of the earlier works. The pyrolysis of polymethylmethacrylate has been explained by a chain-end initiation followed by a complete unzipping with a slight amount of random scission, because for this polymer the molecular weight of residue changes only slightly over the first 10 to 20 % conversion, and the rate of volatilization versus per cent conversion decreases monotonously [18, 49]. Poly - α - methylstyrene has a similar pyrolysis mechanism, but the unzipping is not complete; a continued drop of molecular weight of residue with time is observed [9]. The thermal decomposition of linear polyethylene is very close to simple random scission; the number average molecular weight of residue drops by a factor of about 1000 within 2 % conversion [49], and the plot of rate of weight loss versus time shows a maximum [50].

The pyrolysis mechanism of polystyrene is an example of an intermediate type [34]. For this polymer there is evidence of the further complication that for the larger molecules, unzipping is not complete after initiation. Random scission is suspected to be responsible for the decrease of molecular weight of residue.

In some polymers there are linkages which are weaker than the regularly-spaced bonds where simple random scission occurs, for example, sites where contsminating oxygen is attached or chain branching exists. These weak links are more likely to rupture in the initial stage of degradation.

Application of Theory to Present Work

As just discussed, the theories of thermal decomposition have found application in explaining the pyrolysis of some polymers. They are, however, found not adequate to explain the results of this work. In this work it appears that the decomposition reaction (corresponding to the endotherm in the temperature history of pyrolysis, to be discussed later) requires a reversible formation of volatiles, and that a significant vaporization process occurs later; both are pressure dependent. Despite these additional complications, some fundamental mechanisms of polymer decomposition, like random scission, random initiation and unzipping, scission of weak links etc., are active during one or other stages of degradation.

When there are chemically reactive agents in the environment, for example oxygen, a multitude of reactions may occur. The most important ones are perhaps:

(1) The reactive agent may help initiate the polymer decomposition reaction.

(2) The intermediate steps may be accelerated.

(3) The reactive agents may react exothermically with gaseous products of decomposition.

That the reactive agent has entered into the initiation step of decomposition reaction can be illustrated by the oxidation of polystyrene. The mechanism of oxidation is likely that hydroperoxides are formed first on the tertiary carbon atoms. These hydroperoxides provide scission sites, and also decay to free radicals which initiate chain reactions. The reaction between the chemically reactive agent and gaseous products

of decomposition is a spontaneous combustion reaction. The energy fed back to the polymer surface contributes to the further degradation of polymers.

When there is solid oxidizer, for example ammonium perchlorate, in the polymer, several effects are possible. First the initiation reaction may become easier because of the increase of the number of weak links from the formation of oxygen linkages. Second, the oxidizing species produced by decomposing oxidizers may accelerate the degradation reaction of polymers by affecting the intermediate reaction steps. Third, the decomposed oxidizing species may react exothermically with the gaseous products of degradation of polymer. As a result of these possible reactions it is anticipated that both oxygen and ammonium perchlorate enter into the pyrolysis reactions.

CHAPTER IV

TEST SAMPLES AND THEIR PREPARATION

A totsl of nineteen formulations of PBAA polymer with and without dispersed solids were used in this study. See Table X for complete compositions, Table XI for thermal properties and Appendix A for the measurements and estimates of thermal properties. For convenience they are classified into four categories as follows: (a) straight polymers, (b) polymers with combustion catalyst, (c) polymers containing glass beads, and (d) polymers containing ammonium perchlorate.

The method for preparing these polymeric and propellant-like msterials were the same. First, all the ingredients were carefully weighed, then mixed to make a sample of total weight equal to 25 to 30 grams. The mixture was then blended in a beaker until all the constituents appesred homogeneous to the eye. This mixing required 15 minutes to half an hour depending upon the quantity of solids to be dispersed. Becsuse close examination revealed that some agglomerates were still undispersed, a second stage of mixing was required.

Because of the small quantity of the mixture, none of the conventional mixers could be employed. Satisfactory dispersion required a special technique. A thick glass plate, 18 inches square, was used as a platen. Four to five grams of the mixture were poured on the plste

and repeatedly smeared with a smooth cylindrical bar of stainless steel. This was a time-consuming (15 to 20 minutes) but very effective procedure.

The homogeneous mixtures were carefully poured into special aluminum molds. The mold, an aluminum disk 2 inches in diameter and one quarter inch thick, had a shallow crater milled in one flat surface. This shallow crater was 1.5 inches diameter and 0.06 inches deep. The inner face of the hole was polished and sprayed with a thin layer of Rulon Spray, a mold release compound. The durability and performance of this mold release agent were much improved by heating the coated mold to 500° F for half an hour after coating.

Except for the PO polymer, three parts carbon black per hundred of the rest of the formulation was always compounded into these materials to render the test sample opaque to thermal radiation. The quantity of carbon black added was selected on the basis of a series of tests in which 1, 2, 3, 4, and 5 per cent of carbon black was mixed with the polymer. After the carbon black particles were completely dispersed, the polymer mixture was examined for transparency by spreading a thin layer of the mixture between two thin glass plates. Three per cent was selected because the samples were opaque and black enough for the purpose of the experiments performed.

The mixing process introduced fine bubbles of air into the mixture. Deaeration was necessary prior to polymerization. The deaeration was accomplished by placing the aluminum mold containing the uncured but viscous polymer inside a bell type vacuum chamber [51] which could be evacuated to 20 microns Hg. Satisfactory deaeration could be obtained

by intermittently applying gentle radistion heat to the surface of the polymer. Three to five hours were needed for complete deaeration.

The mold was then transfered to a thermostatted, sealed oven. The sealed furnace was needed because the curing process in the presence of air always leads to contamination with oxygen which must be avoided for reliable experiments. The polymerization reaction took place in helium at atmospheric pressure and at 80 $\pm$ 1° C for seven full days.

The approximately 0.15 cm thick sheets of cured polymers and propellant-like materials were quite flexible. Once removed from the aluminum molds, these sheets were placed in numbered aluminum dishes and stored in a silica-gel containing desiccator to avoid absorption of moisture from the air.

CHAPTER V

APPARATUS AND EXPERIMENTAL PROCEDURES

Radiation Furnace and Auxiliary Devices

The radiation furnace discussed here was originally constructed to measure the ignition characteristics of solid propellants in a gaseous environment of controlled composition and pressure. This furnace is an electricslly heated tube furnace; Fig. 4 is a side section of the furnace, and Fig. 5 shows two photographic views. The heated tubular core is an alumina tube 18-inches long and 2-inchea inside diameter with a helicsl groove on the outside in which a 96-foot length of 18-gage Nichrome wire is wound. The alumina core is supported on annular disks of Johns-Manville "J-M" Superex insulsting block. The core and insulating block were housed in a 6-inch achedule 40 pipe to which 300-pound flanges were welded. Modified 14 mm spark plugs are used to make electrical connection to the Nichrome wire heating element. The temperature inside the core is measured by a Chromel-Alumel thermocouple; the control of the furnace tempersture is achieved by a aimple "high-low" control system which includes an ON-OFF controller, a relay and a rheostat. Because of the temperature limitation of the heating wire, the maximum practical operating temperature of the furnace is 1150° C.

In one end of the furnace a system is used to introduce oxygen and nitrogen and to accommodate the test sample injection rod. The test

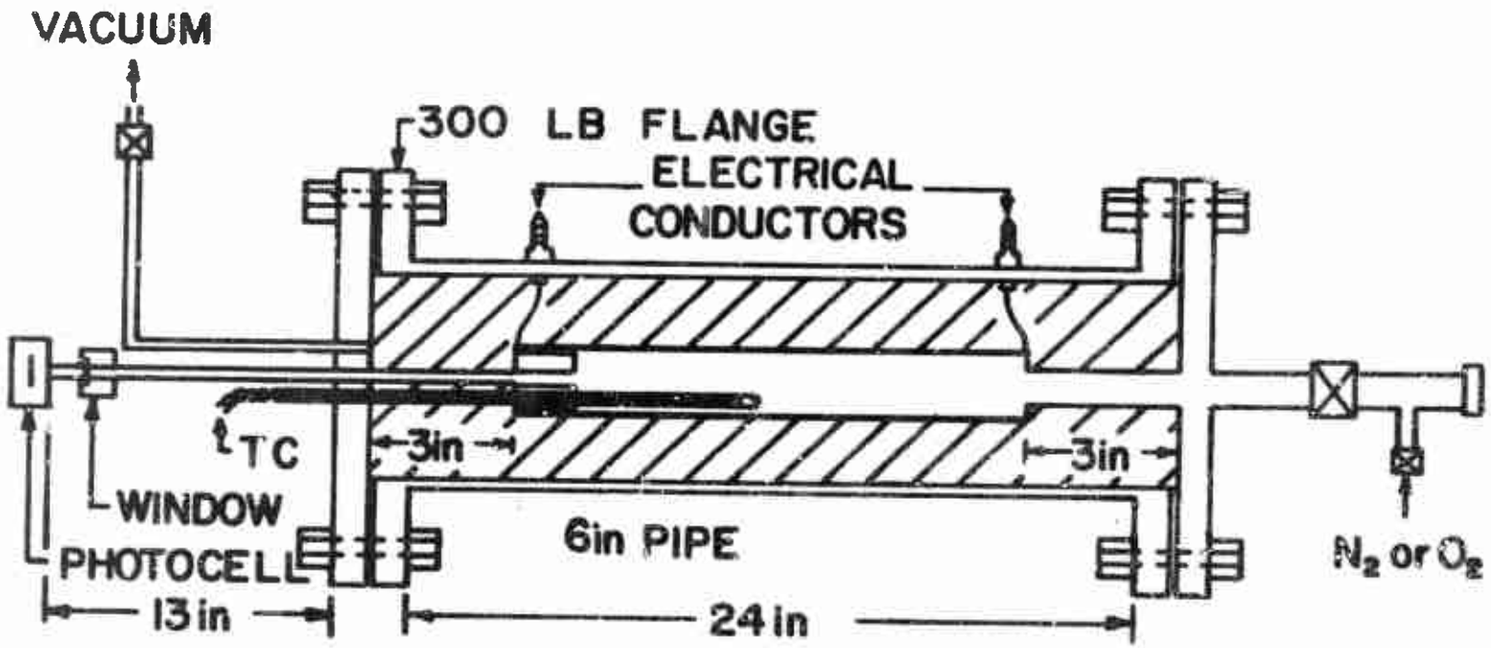

Fig. 4. — Sectional view through the center of radiation furnace. All essential accessories like thermocouple, window, photodiode etc., are also shown.

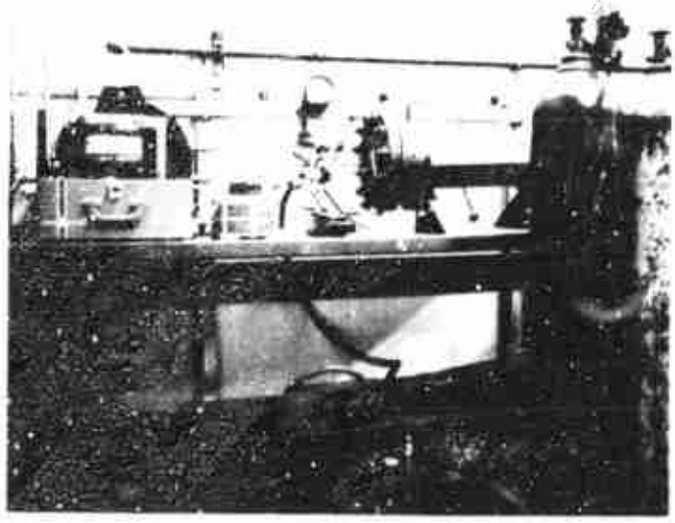

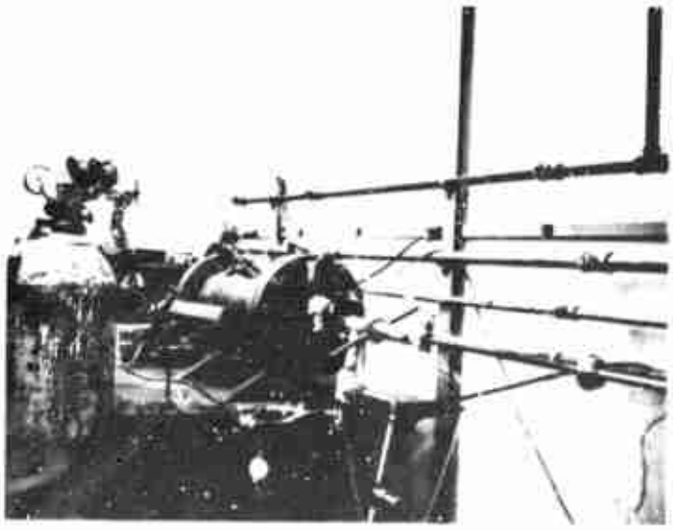

Fig. 5. -- Two photographic views of the radiation furnace and its accessories. The picture on the top shows the photocell observation end of the furnace. The temperature controlling system can be seen. The picture on the bottom shows the sample injection end of the furnace with the injection rod in the waiting position.

sample holder and injection rod are housed in a 1 1/4-inch pipe which is connected to the furnace flange. Water cooled copper coils are wrapped around that part of the pipe where the test sample was held before it was thrust into the furnace. A gate valve with a small hole in the center is also installed in the mounting pipe between the sample rest position and the furnace core.

On the opposite end of the furnace another system is installed to permit (a) connecting the radiation furnace to a vacuum pump, (b) mounting a photodiode, (c) mounting a thermocouple and (d) installing an exhaust valve. A RCA 1P40 gas photodiode, which mounted in a tube at the end of the furnace, had a narrow angle of view down the axis of the core. A two-inch diameter cylindrical insulating brick plug was inserted in the furnace core near the photocell end of the furnace; the plug has a 1/4 inch diameter hole in its center to give the photocell a view along the center line of the core. With the exception of this hole, a test sample thrust into the furnace is in view of only isothermal radiation. The furnace can be operated at pressures from vacuum to 10 atmospheres.

The sample injection rod is constructed from a 1/2 inch o.d. stainless steel tube, 38 inches long. Fig. 6 shows a sketch of the injection rod and its accessories. The rod can move freely along the axis of the 1 1/4 inch o.d. pipe. The injection rod is aligned and the furnace sealed from the atmosphere by O-ring seals around the rod. A normally open switch is attached on the end of the pipe. A 2 inch o.d. annular ring, connected to the injection rod 6 inches from one

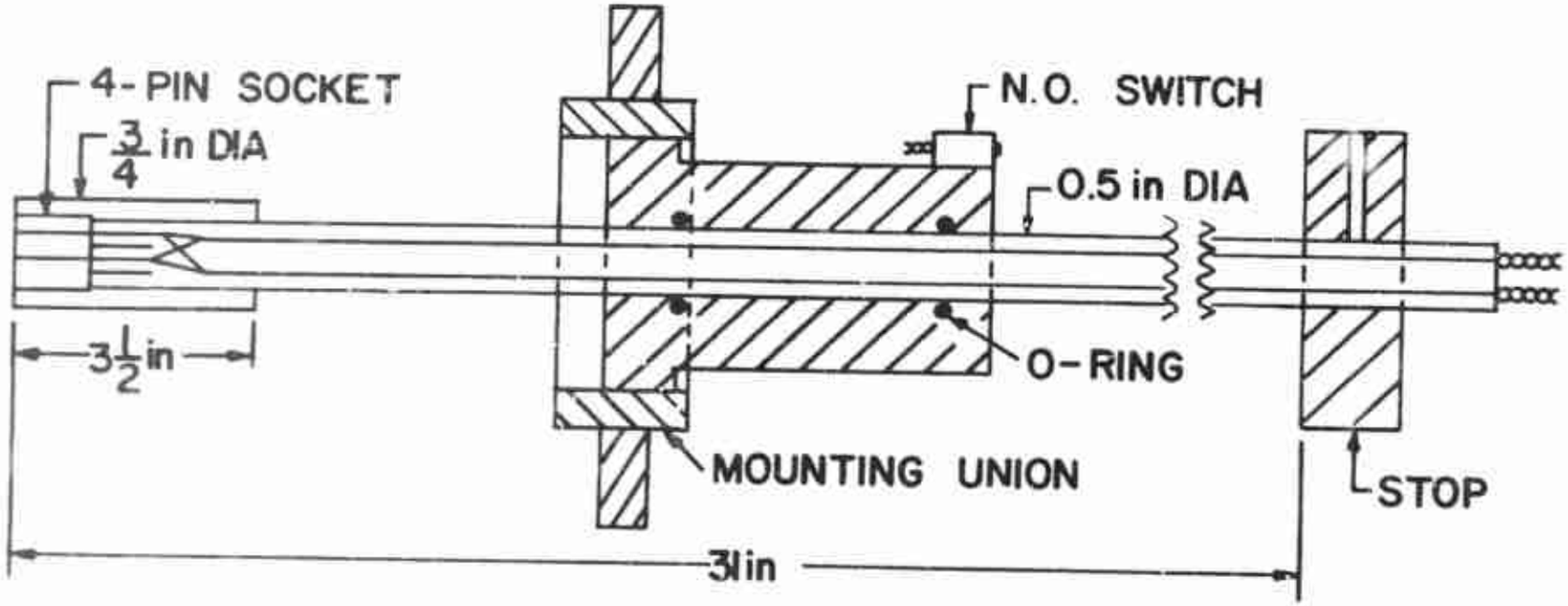

Fig. 6. -- Sectional view through the center of sample injection rod and its accessories. The 4-prong socket is to receive the male plug on the sample holder. The injection rod can move freely along an O-ring sealed guide pipe. During experiment the whole assembly is connected to radiation furnace by the mounting union.

end, closes the switch when the injection rod is inserted into the furnace and the sample is in test position. Four electrical leads were placed inside the injection rod; two were connected to a galvanometer in the Visicorder; the others to an oscilloscope. The other ends of the four leads were soldered to a 4-prong socket which was to receive a copper disk sample support.

Fig. 7 shows a detailed sketch of the copper disk sample support, which also served as a calorimeter. Also shown in the figure is a protective shield for the calorimeter. The copper disk was made of pure copper metal. 0.0325 cm thick (for tests in the vacuum the thickness was 0.09 cm), 1.3 cm diameter with the surface flat and smoothly polished. On the back face two tiny holes were drilled, one in the center, one half-way between the center and edge. Into the center hole a 0.025-cm diameter constantan wire was silver-soldered. Into the other hole a copper wire of the same gage was soldered. Thus the disk was one junction of a copper-constantan thermocouple. The other ends of the thermocouple wires were soldered to a 4-prong plug. The wires between the disk and the plug were carefully wrapped first with tape then a layer of aluminum foil to strengthen the assembly and to reduce heat transfer between the wires and the protective shield. During the experiment the copper disk was housed in a fired pyrophyllite ring. The pyrophyllite ring was also covered with aluminum foil. A hole in this foil exposed the central section of the test sample to radiation. Four sizes of holes were employed in this work, i.e., 1.11, 1.19, 1.25, and 1.31 cm diameter. Since aluminum has a high reflectivity, the temperature of the pyrophyllite ring was close to room temperature during the short time of an experimental test.

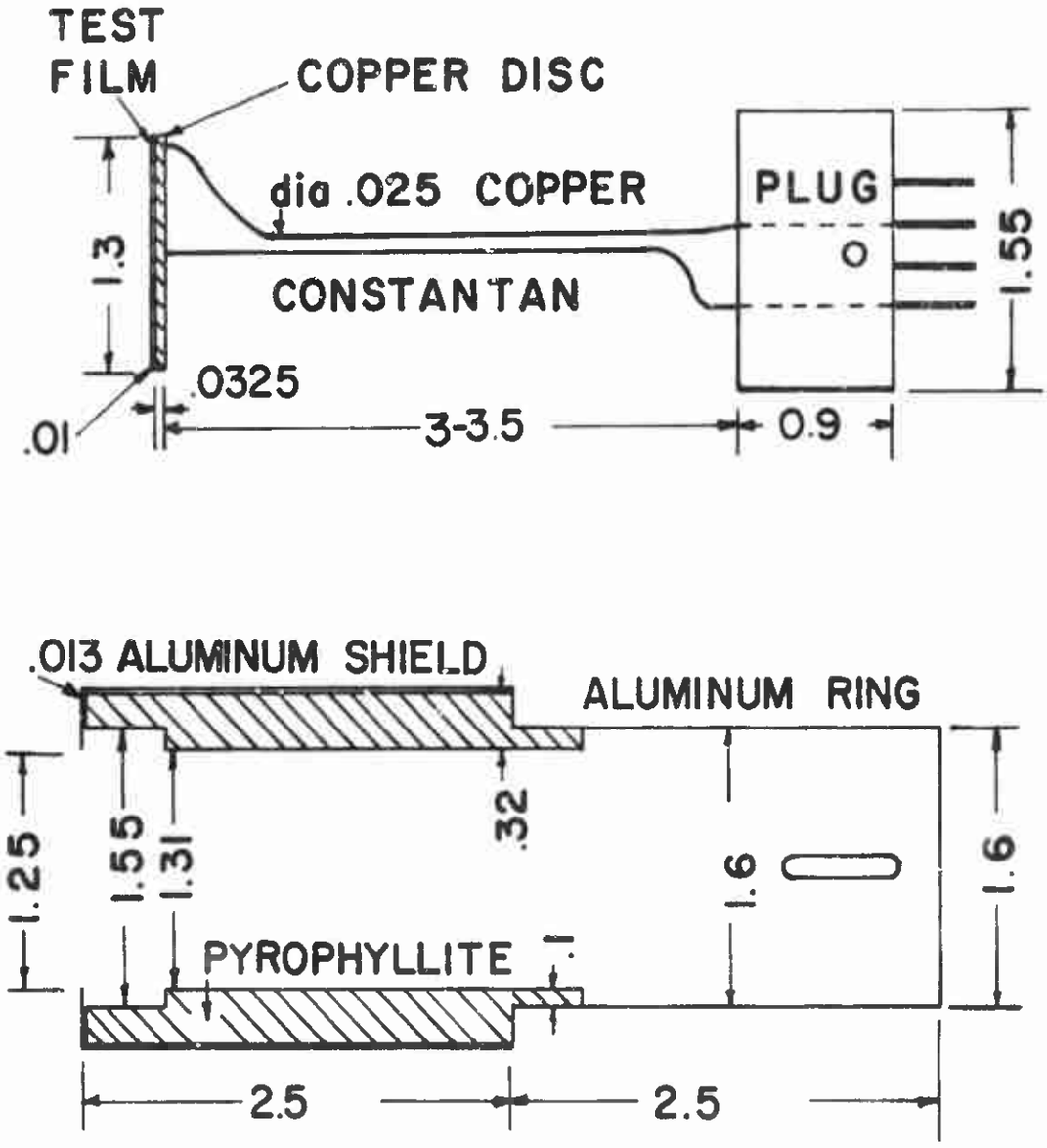

Fig. 7. -- These sketches are side sections of the test-film ssmple holder (top) and shield (bottom) used in the polymer decomposition study. The sample holder was held inside the shield by use of a small screw through the slot shown on the right. The male plug on the sample holder connected with a matching socket, which wss attsched to a long injection rod, which was, in turn, mounted in guides. The test-film sample holder and shield were then thrust into the interior of the sealed radiation furnace. All dimensions are in centimeters.

Two types of recording instruments were used in this work. One was a Direct Recording Visicorder Oscillograph, Model 906B, manufactured by the Honeywell Company. Three galvanometers were used simultaneously for recording. One of them was of the electromagnetically damped type, No. M-100-350, which was very sensitive and used directly for recording the emf output of the thermocouple. The other two were of the fluid damped type, No. M-1000, and were used to indicate the time when the injection rod reached its stop position and to trigger the oscilloscope.

The sensitivity of these galvanometers depends upon the series and parallel resistances connected with them. The sensitivity for each of six circuit combinations was calibrated using a copper disk gage, a thermometer and a potentiometer, and the results are shown in Table XVI. The calibration procedure is discussed in Appendix E.

The second recording device was a Tektronix Model 502 Oscilloscope. One channel in the oscilloscope was used in parallel with the Visicorder to record the emf developed by the copper disk thermocouple during each experimental run. The other channel was used to record the signal from the photocell. At high sensitivity, a careful grounding was necessary to eliminate 60-cycle AC interference. The vertical sensitivity of the oscilloscope was calibrated against an external precision potentiometer after every five to six tests. A Polaroid camera was used to record the oscilloscope traces.

Preparation of Thin Polymer Film Test Samples

Satisfactory techniques for preparing uniform and reproducible polymer films, and for mounting them on the copper disks were developed

only after a long, systematic effort. Techniques based on painting and spraying of the films were tried and rejected. One of the aerious problems with the painting technique is that tiny air bubbles which atrongly resisted elimination were introduced into the films. When films were sprayed, the uncured, viscous polymers tended to coagulate and form wave-like and uneven surfaces. Both painting and spraying produced thin films with convex surfaces after cure. Also it was difficult to control and measure the thickness of the film.

The technique for producing and mounting thin films which proved successful and was used throughout this work will be discussed next in more detail. The preparation of cured polymers and propellant-like sheets has alresdy been discussed in Chapter IV. These sheets were cut into small disks of 1.5 cm diameter (slightly bigger than 1.3 cm of the diameter of copper disk). The final test films were cut from these disks. The slicing process was performed by a manually operated microtome (AO Spencer Table Microtome). Fig. 8 shows the microtome, microtome knife, and CO_2 cylinder.

According to the apecification of the manufacturer, the device is capable of cutting thin films of 5 to 500 microns in thickness, if the material to be cut has a proper degree of hardness and resistance. The polymera and propellant-like materials studied in thia work were all rubber-like, and freezing was necessary to produce a material of proper hardness for smooth cutting. This freezing was done by expansion of carbon dioxide from a pressure bottle to produce a cold gas to chill the pol· .r disks. The material to be aliced was placed on the top of

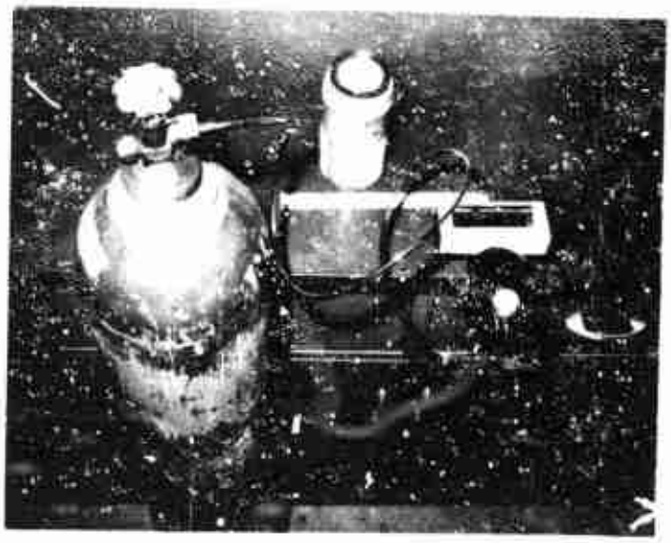

Fig. 8. -- This picture shows the equipment for slicing thin test film. They are microtome, microtome knife, knife chilling bottle and CO_2 cylinder.

freezing attachment which was wet with water. The disk was then frozen in place. The thickness of film to be cut was determined by a feed screw at the bottom of the microtome. For a successful cut, the microtome knife was chilled beforehand in ice-water. The cutting of materials highly loaded with solids was fairly simple; however, cutting polymer-rich materials required the cooperation of two persons, with one operating the microtome knife and the other holding a tweezer to keep the film from sticking to itself. This precaution waa necessary because the unloaded polymer was quite tacky and the film tended to curl when the film thickness was less than 200 microns. Except where noted, the thickness of the test film was always 100 microns.

The mounting of the thin test films onto the copper disks required several steps. First a very thin bonding layer of uncured polymer, PO (see Table X), wss applied on the surface of the copper disk which had already been carefully cleaned with analytical grsde benezene. The test film was then placed on the disk and smoothed out cautiously with a tiny nylon roller to eliminate as much of the trapped air as possible. The trapped air at the interface, even in a very small quantity, was highly undesirable. Complete elimination of small bubbles of air at the film-disk interface was accomplished in a vacuum bell jar [51]. The test samples were placed in the jar, and the surface of the film was rolled by a nylon roller which could be manipulated from outside the jar. This operation was conducted under vacuum. An hour or two were required for this process. The test samples were then put inside a sealed oven and

the bonding layer was cured under 0.85 atm helium at 80 ± 1°C for three full days. The mounted test films were then placed inside a desiccator until used. A sketch of the copper disk gage and the pyrophyllite shield have been shown in Fig. 7. Fig. 9 shows pictures of the finished test sample and shield.

Experimental Procedures, Radiation Furnace Tests

Experiments in the radiation furnace formed the major part of this work. Before any test, the furnace was turned on and kept at the planned temperature for more than four hours until a steady condition was attained. All recording instruments were turned on one hour before use. The test procedures are summarized below:

(1) The copper disk mounted sample was removed from the desiccator and weighed carefully, if the knowledge of weight change was desired.

(2) The 4-prong plug of the copper disk gage was inserted into the socket at the front end of the injection rod.

(3) The aluminum-foil-wrapped pyrophyllite shield was positioned and the whole assembly was wrapped with several layers of thin aluminum foil.

(4) The injection rod holder was attached to the end of the radiation furnace.

(5) The furnace was evacuated, then filled to the desired pressure with either N_2 or O_2.

(6) The temperature reading of the furnace was closely observed. The condition was close to readiness when the on and the off

Fig. 9. - Copper disk test sample and pyrophyllite protective ıng. On the far left is a copper disk holder with polymer test sample. On the far right is a pyrophyllite protective ring wrapped with a layer of aluminum foil. In the middle are a coppper disk gage without polymer film and a copper disk test sample inside a protective shield.

parts of the relay opersting cycle were about equal in time. "Go" time was one-half minute after the relay switched to off in any subsequent on-off cycle.

(7) The paper drive motor of the Visicorder was turned on, and a switch was closed to leave a mark on the recording paper and at the same time to trigger the oscilloscope. Finally the gate valve was opened and the injection rod thrust into the furnace as quickly as possible. The final act could be completed in 0.1 to 0.15 sec. When the injection rod reached the stop position, it contacted a normally open switch which resulted in the placing of another mark on the recording paper. The temperature history of the copper disk was recorded simultaneously by the Visicorder and the oscilloscope. Radiation from or near the surface of the sample was detected by the photocell and recorded by the oscilloscope camera.

(8) When the temperature of the copper disk gage reached the maximum permissible temperature, the injection rod was quickly withdrawn from the furnace. The Visicorder paper feeding motor was turned off. When the assembly was cool, the copper disk gage was detached from the injection rod and put inside the desiccator. After several hours the exposed copper disk gage was weighed, if the knowledge of weight change was desired.

Normally the complete experimental cycle for a test required 20 to 30 minutes.

Imaging Furnace and Auxiliary Devices

The imaging furnace used in this work was originally conatructed by L. S. Bouck for a study of solid propellant ignition [6]. It was modified for the purpose of this work. Fig. 10 ahows a sketch of the optical system. Figs. 11 and 12 show photographs of the furnace. The reflectors are Heyer-Shultz metal reflectors Model 1650 with standard rhodium finish. They have a diameter of 16 inches, a primary focus of 6 7/16 inches and a secondary focus of 35 inches. A 1200 W projection lamp (G.E. CYS) with a small built-in reflector was used as the energy source. The lamp was placed at the focus of the source reflector and the image accordingly appeared at the primary focus of the image reflector.

A 3-inch diameter shutter from an aircraft camera was modified and installed at the common secondary focus of the two reflectors. The shutter could be opened and closed in 3-5 milliseconds by DC solenoids. The durstion of the opening was controlled by a timer. A sample testing chamber (see Figs. 13 and 14) was placed at the focus of the image reflector. This testing chamber was built to be operated at pressures from vacuum to 10 atmospheres. A gas sampling system was also installed to collect gas products in s stainless steel chamber for anslysis. Liquid products were collected on a thin glass plate which was placed in front of the test sample. (See Fig. 13)

Calorimeter for Heat Flux Measurements

Fig. 15 shows pictures of the cslorimeter used to cslibrste this furnace. The calorimeter design was an sdsptstion of one described by Broido and Willoughby [8]. The receiver was constructed from s copper

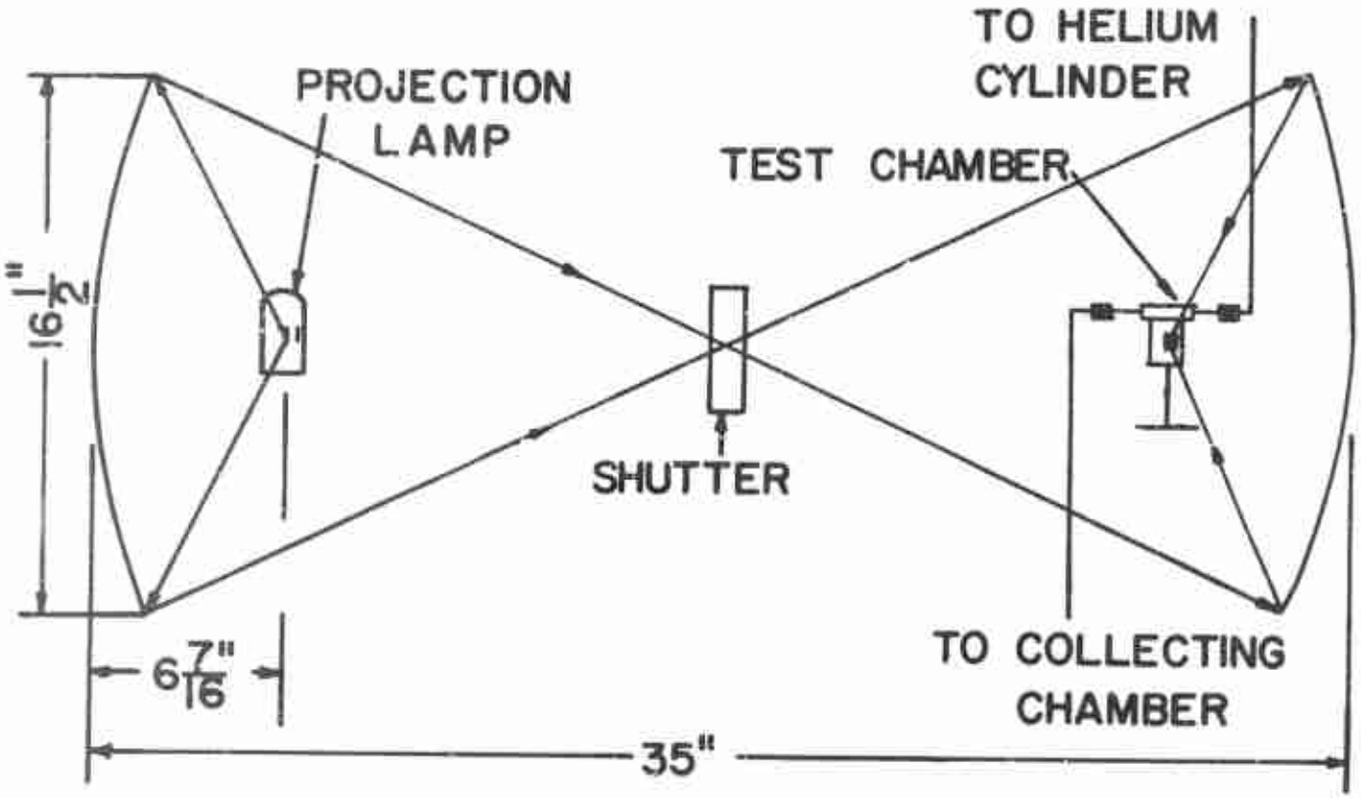

Fig. 10. -- This is a sketch of ellipsoidal imaging furnace optical system. Also shown in the sketch are projection lamp energy source (left), shutter (center) and test chamber (right).

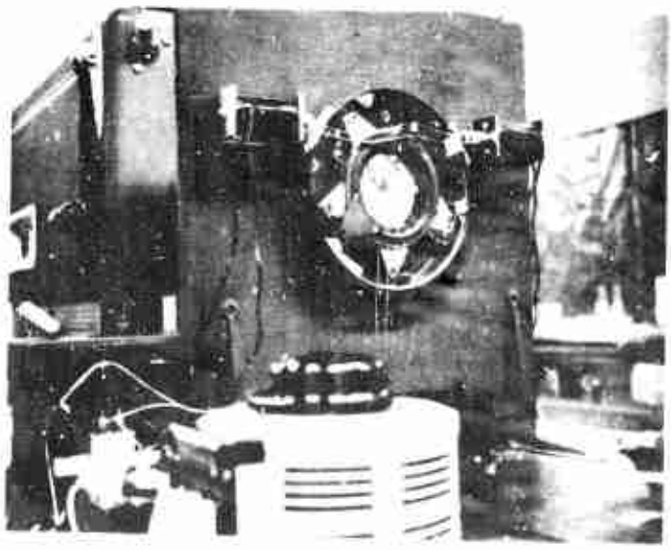

Fig. 11. -- Two photographic views of imaging furnace. The picture on the top shows the complete assembly snd instruments. The shutter and two DC solenoids are seen in the picture on the bottom.

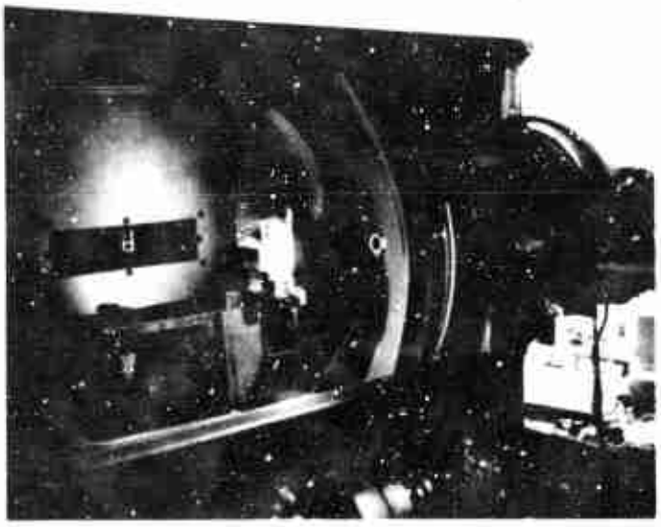

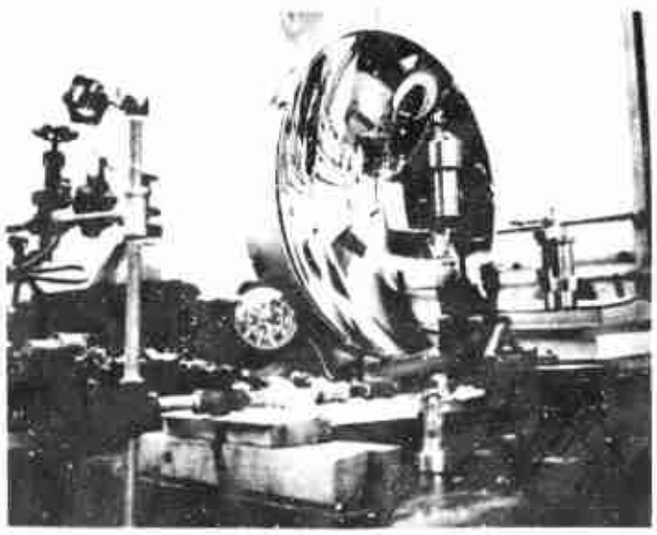

Fig. 12. -- Viewa of imaging furnace. The picture on the top ahowa aource reflector and projection lamp inaide the lamphouae. The picture on the bottom ahowa image reflector, teat chamber and gaa sample collecting chamber.

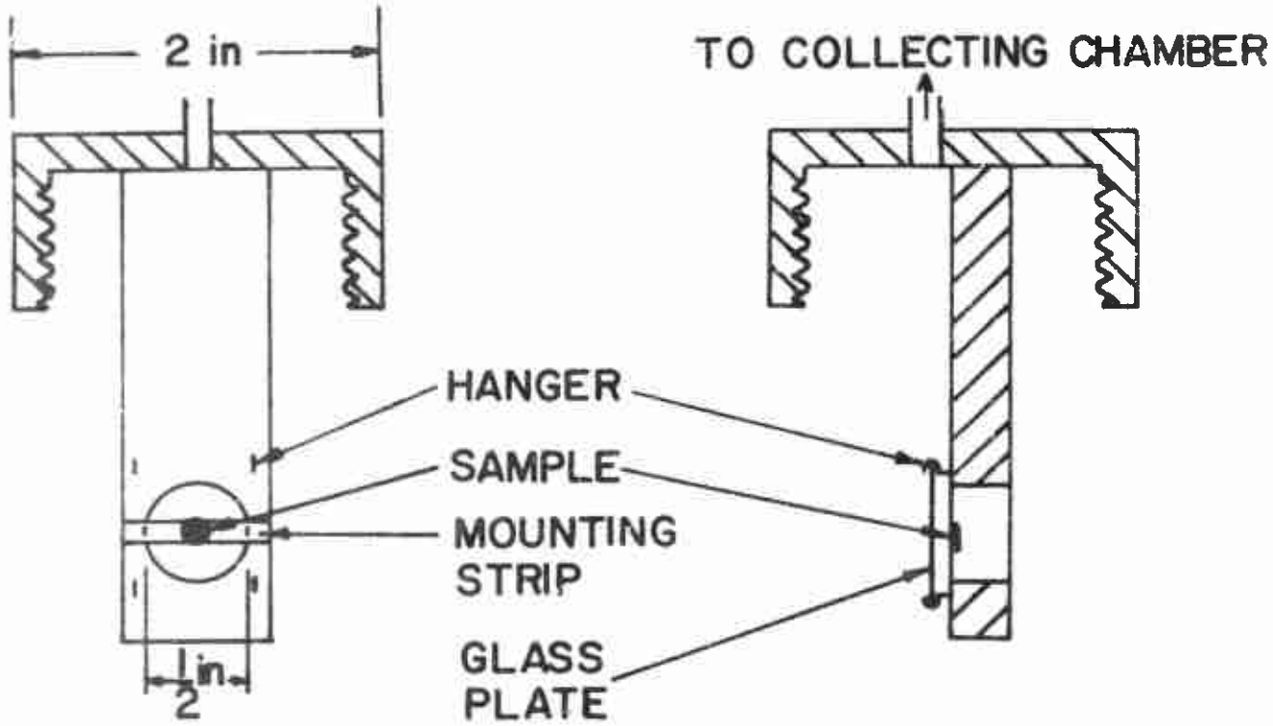

Fig. 13. -- Two sectional views of test sample holder. The black spot shows the position where the test sample is supposed to be placed. On the right view the glass plate to collect liquid products can be seen held by hangers.

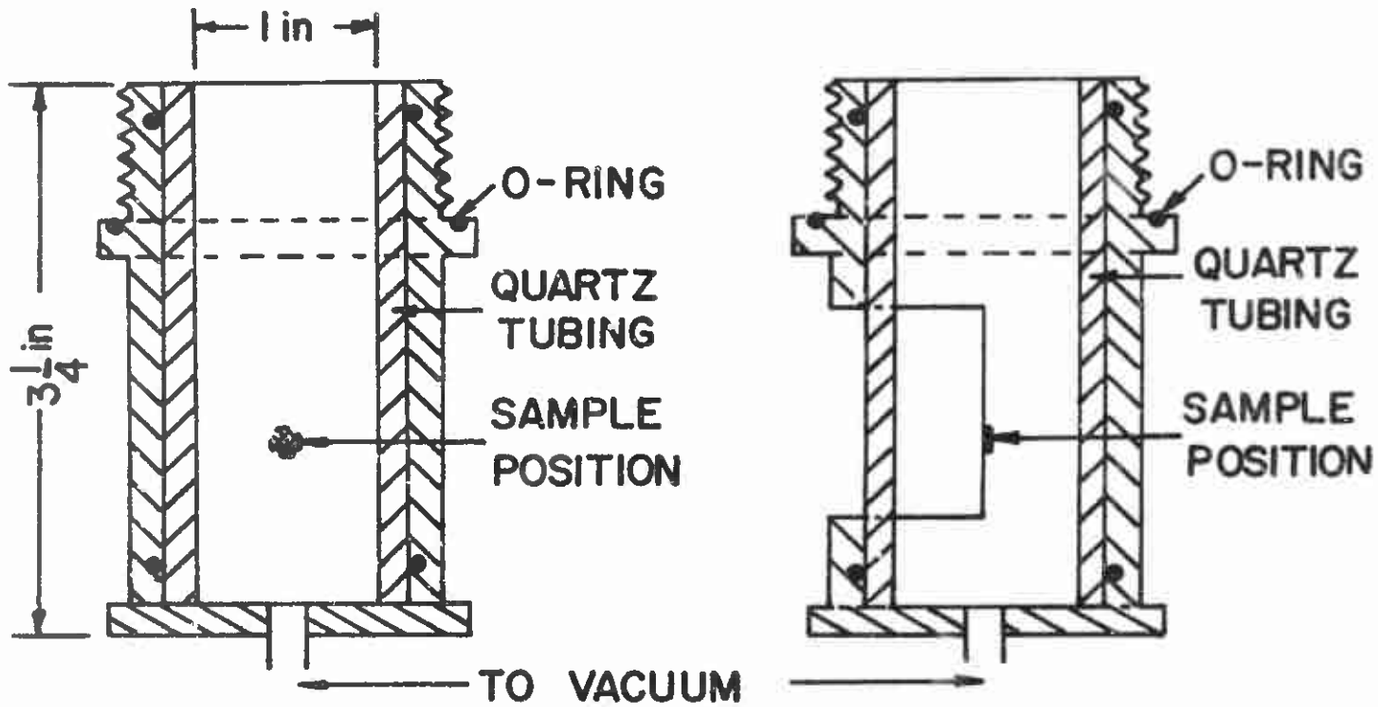

Fig. 14. -- Two sectional views of teat chamber outer case and window. Shaded spot shows the sample position.

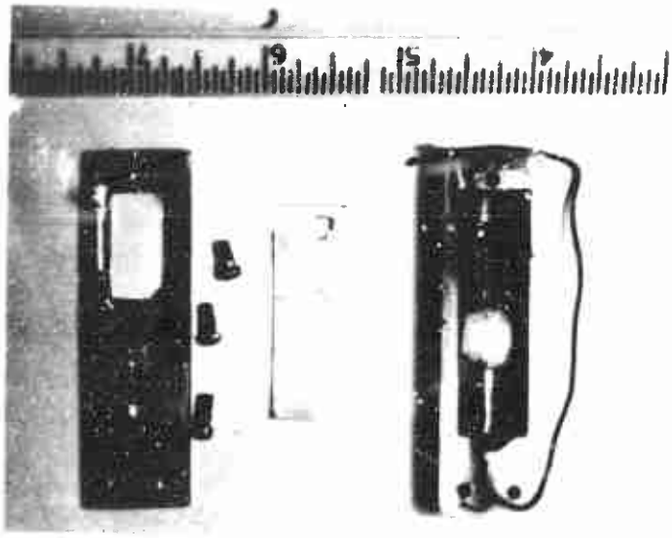

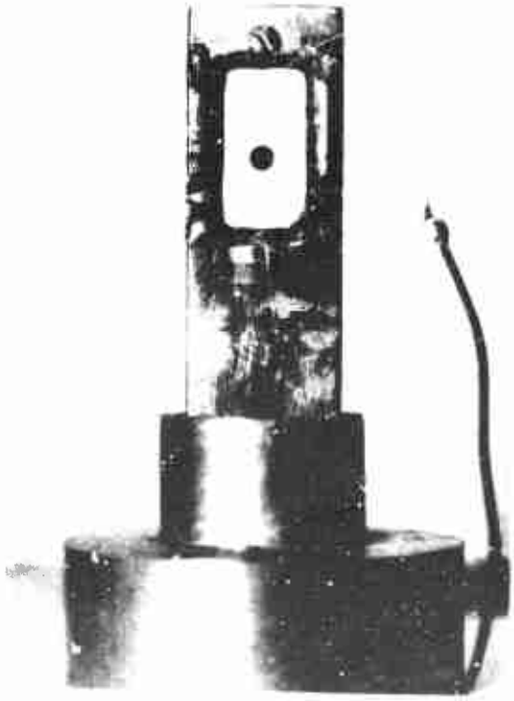

Fig. 15. -- Calorimeter and its components. The picture on the top shows steel cover (left), aluminum foil shield (center) and blackened copper receiver inside the holder (right). The picture on the bottom shows the assembled calorimeter.

disk, 0.0508 cm thick, which was pressed into a spherical segment with an inner radius of 0.53 cm and an inner height of 0.25 cm. Initially the inner surface was blackened with electro-deposited platinum black. This platinum black became ineffective after some use and occasional over heating, and was later replaced by a coating of optical black lacquer manufactured by Thos. Parsona & Sons Ltd. The manufacturer recommends the use of a layer of undercoat before applying the top black lacquer to improve the lacquer-metal bond. However, to reduce the weight of the applied film only a final coat was applied. The resulting aurface was very black, yet the weight increase was only about 0.8 per cent of the receiver weight. A plane aluminum foil shield, 0.127 cm thick, with an aperture of 0.151 cm radius was placed in front of the concave surface to limit the area of the beam intercepted by the calorimeter. The shield was placed approximately 0.05 cm from the rim of the receiver with the center of the aperture on the optical axis of the system. A 0.025 cm diameter copper-constantan thermocouple was silver-soldered (prior to aurface blackening) to the back side of the receiver 0.1 cm from the rim. The two thermocouple wires were separated by 120° to avoid contact with each other. The receiver was supported only on the two wires t reduce the heat transfer between the copper receiver and its environment.

The physical constants of the receiver were:

k_c = thermal conductivity, 0.91 cal/(cm)(°C)(sec).

ρ_c = density, 8.92 g/cm^3.

c_c = specific heat, 0.093 cal/(°C)(g).

δ = thickness, 0.0508 cm.

m_r = mass, 0.5547 g.

α_r = thermal diffusivity, 1.095 cm^2/sec.

Beyer, McCulley and Evans [5] designed a similar calorimeter and demonstrated mathematically that the measurement of temperature at the edge of the calorimeter gives a good approximation to the average temperature of the whole receiver. Thus the average heat flux, f, at the plane of the aperture and over the aperture area may be calculated as:

$$f = \frac{m_r c_c \Delta T}{a_r A_a \Delta t}$$

where

f = average heat flux, cal/(sec)$(cm)^2$.

ΔT = temperature rise, °C.

a_r = absorptivity of receiver, 0.95 by assumption.

A_a = aperture area, cm^2.

Δt = exposure time, sec.

Measurement of Heat Flux Density Distribution in the Focus Volume

The calorimeter discussed in the last paragraph was used to measure the heat flux distribution in the focus volume of the imaging furnace. The heat flux distribution was measured along three directions at a projection lamp output of 1065 W. Tables XII, XIII, and XIV give the result of the heat flux distribution tests for longitudinal (axial), vertical and horizontal (transverse) traverses. These data are plotted

in a normalized form in Figs. 16, 17, and 18. From these figures it can be seen that the energy fluxes were essentially constant over a square area of 0.75 cm x 0.75 cm.

In the earlier stages of study, a regular projection lamp, G.E. 1000 W DFD, was employed. It was discovered that an exact image, only smaller, of the lamp filament was formed on the focus plane. The TYPE CYS lamp, which has a built-in reflector, effectively smeared the filament image and gave a uniform flux field. A weak filament effect was, however, still observed on the plane of maximum heat flux density. The most satisfactory working position was found at 0.16 cm from the position of maximum heat flux in the direction of the center of the optical system.

Samples for Imaging Furnace

The preparation of test specimens for the imaging furnace was much simpler than for the radiation furnace tests. The first step was to cut off a few thin layers of polymers from both sides of the originally prepared thick polymer samples, so that the surface was smooth but not shiny. A No. 2 cork bore was used to cut out small cylinders of polymers 0.45 cm in diameter. The thickness of these cylinders was 0.14 $\pm$ 0.01 cm. The final step of preparation was to attach the cylindrical sample of polymer on a copper strip with a bit of rubber cement. The finished samples were kept inside a desiccator waiting for experiment. Fig. 19 shows a picture of test samples and their holders before and after test.

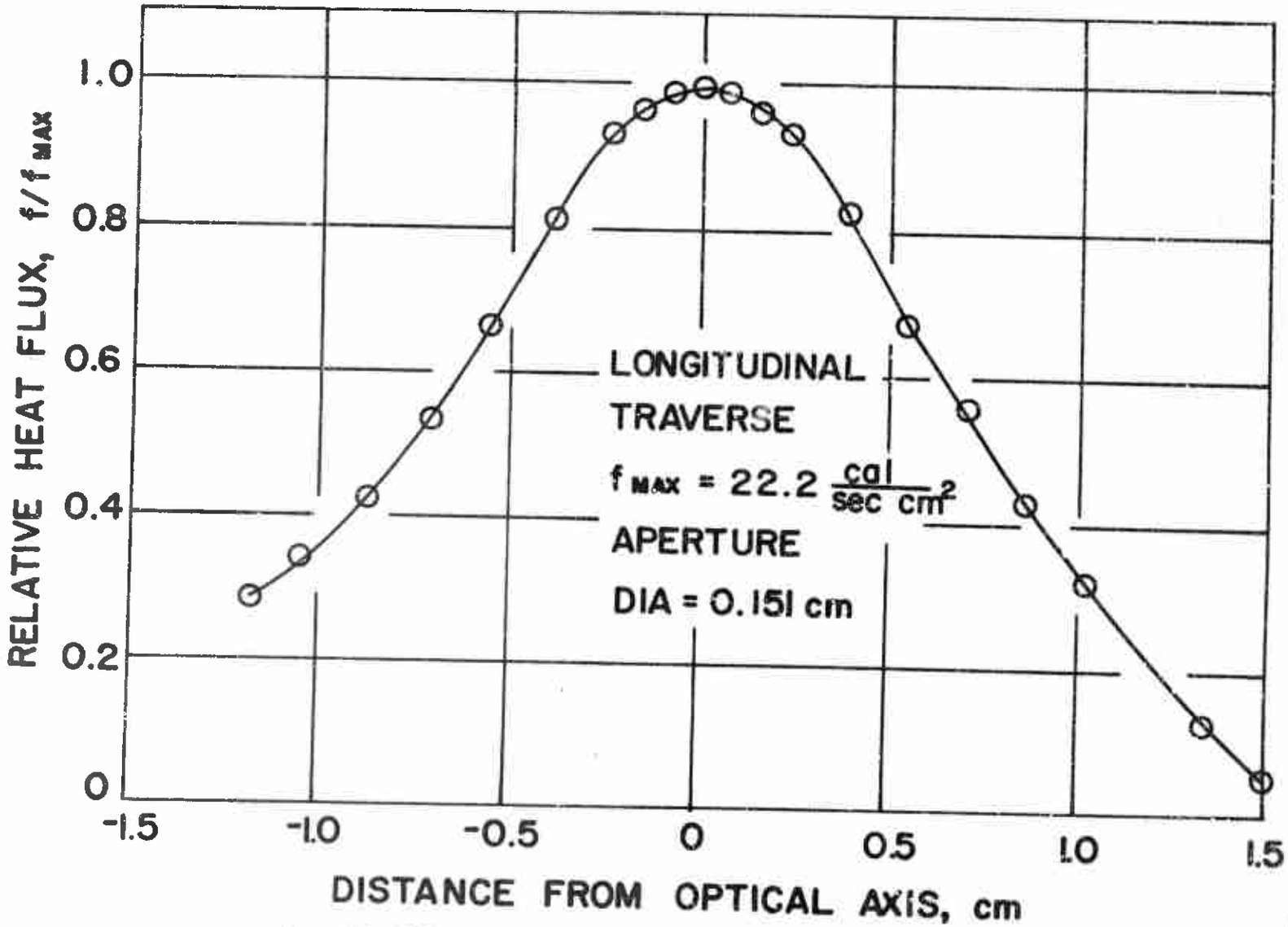

Fig. 16. -- Normalized longitudinal (axial) heat flux distribution within the focus volume of imaging furnace.

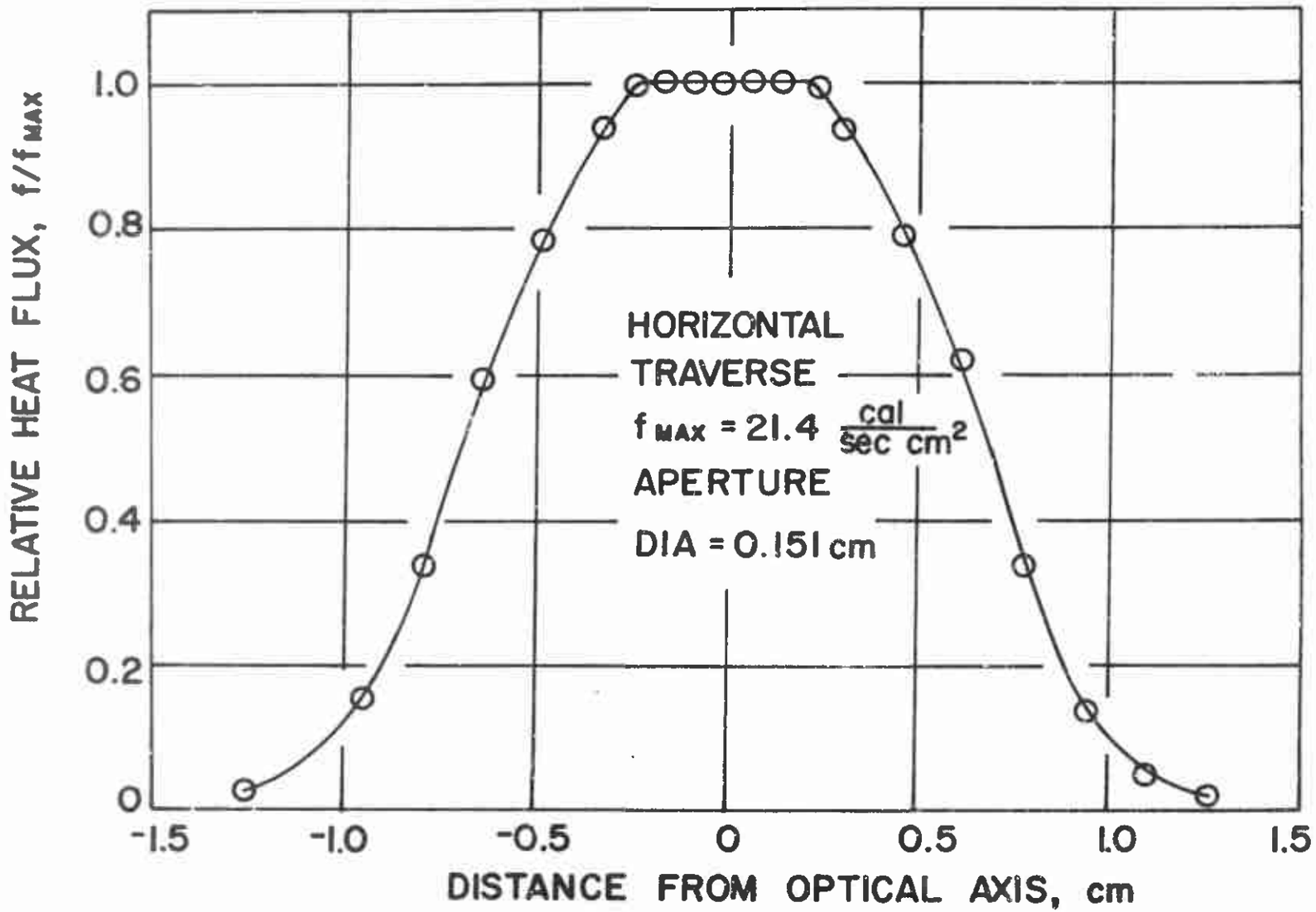

Fig. 17. -- Normalized horizontal heat flux distribution within the focus volume at longitudinal position one turn from maximum heat flux in the direction of source reflector.

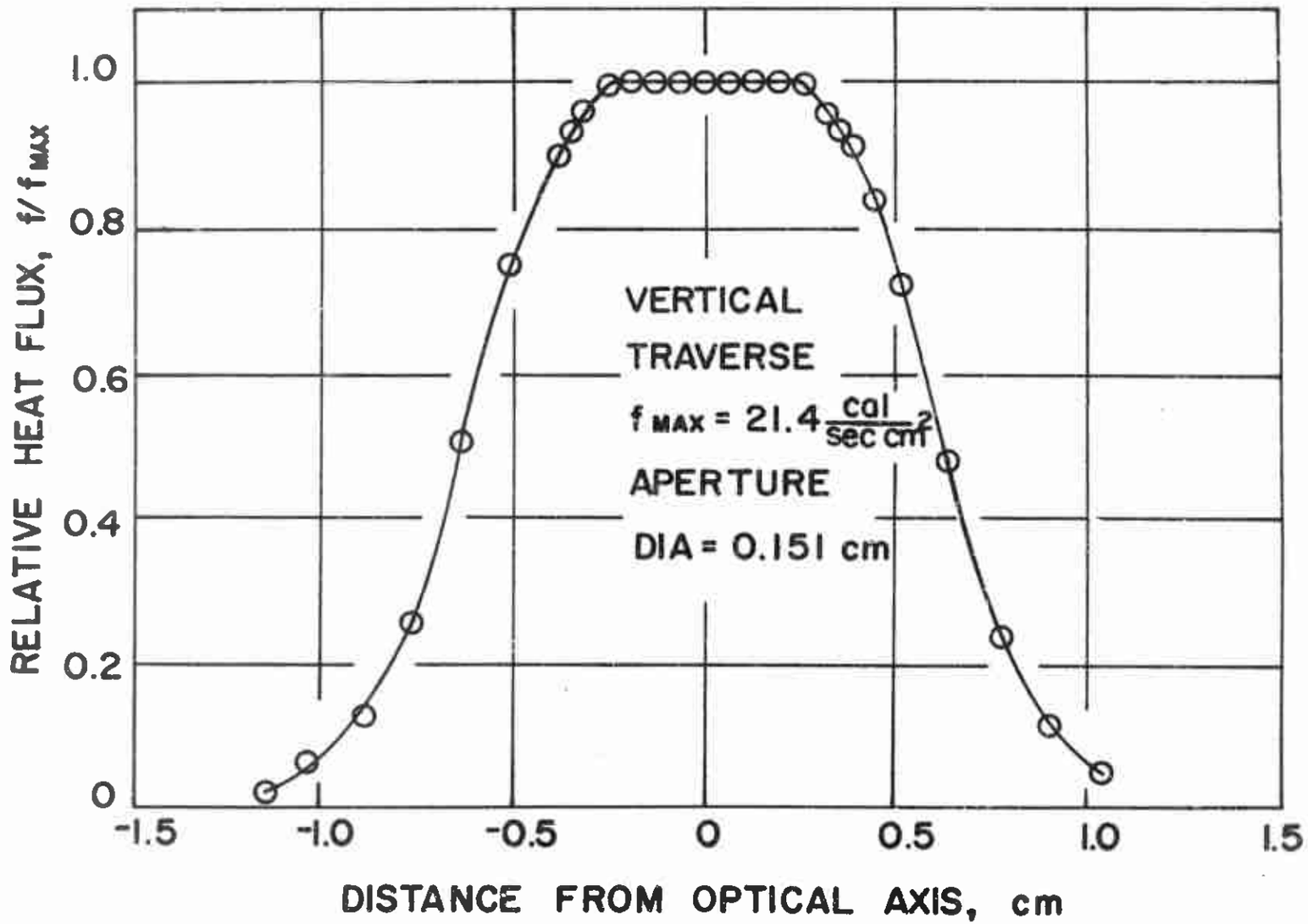

Fig. 18. -- Normalized vertical heat flux distribution within the focus volume at longitudinal position one turn from maximum heat flux in the direction of source reflector.

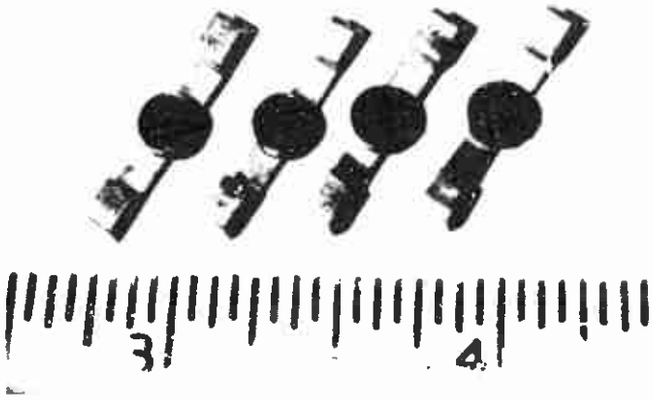

Fig. 19. - Polymer sample on copper strip for imaging furnace test. Two on the right are samples before test, and two on the left are after test. Uniform regression of surface can be seen from the two tested samples on the left.

Procedures for Image Furnace Tests

Two types of experiments were performed in the imaging furnace. Weight loss versus energy input was determined and the gas and liquid products were collected for snalysis. The general procedures were the same, and they are described below:

(1) The small cylindrical sample and its copper strip were removed from the desiccator and weighed five times. The samples were handled with tweezers.

(2) The copper strip was inserted into the sample holder by use of the tweezers, then the polymer was covered with a perforated aluminum shield to protect the edge of the plane surface and the curved surface of the cylindrical sample from the radiation.

(3) The sample holder was turned and locked to the test chamber, then the vacuum pump was started to evacuate the test chamber. The sample was held under vacuum or the chamber was pressurized with helium, depending upon desired experimental conditions.

(4) The shutter timer was set for the desired exposure time, and the DC generator which powered the shutter solenoids was turned on. The oscilloscope and camera were readied.

(5) The power to the projection lamp, which was constantly cooled by two blowers, was turned on and the voltage on the lamp was adjusted to the desired value.

(6) The oscilloscope was triggered by pushing a normally open switch. The manually operated lamphouse douser was opened

immediately and a button pushed to actuate the solenoids. The shutter was opened and closed by the pull and push action of the solenoids according to the time set by the timer.

(7) If gaseous products were desired, the test chamber was pressurized, and after five minutes the gaseous products were collected in the pre-evacuated stainless steel sample chamber.

(8) The sample holder was unscrewed, the copper strip was detached, weighed both right after the test and again after five hours in the desiccator. The latter weighing was repeated five times and the results averaged.

The liquid products were collected on a thin cover glass, 2.2 x 2.2 cm to a side, placed at 0.5 cm from the surface of the test polymer. Test showed that the presence of the cover glass in front of the sample reduced the heat flux by 10.6 per cent. For most of the loss-in-weight experiments no cover glass was used. Before each series of tests the oscilloscope was calibrated and the heat flux was measured. Weighing was done on a Heusser Model SM120 balance to a precision of $\pm$ 0.01 mg.

CHAPTER VI

RADIATION FURNACE EXPERIMENTS: INERT ATMOSPHERE

In this chapter and the following two chapters, the results of experiments employing the radiation furnace will be presented and discussed. For the convenience of presentation, the procedure of data analysis which involves the application of heat transfer theory to the physical system used in this work will be discussed first. The procedure described applies, in general, to all pyrolysis and ignition experiments in the radiation furnace.

The Technique of Data Analysis

The copper disk temperature measuring gage and the finished test sample can be depicted in terms of a simplified model shown in Fig. 20. No surface regression will be considered in this model, for insofar as data can be analyzed with confidence, only the events occurring before appreciable surface regression are pertinent. The circumferential area of the test film and copper disk are so small compared with planar surface areas that heat losses from the curved areas are neglected. Since the temperature gradient through the copper disk is negligible, the temperature measured by the thermocouple on the back face of copper disk can be taken as the temperature at the interface. This can be justified from the following consideration. The characteristic thermal equilibration

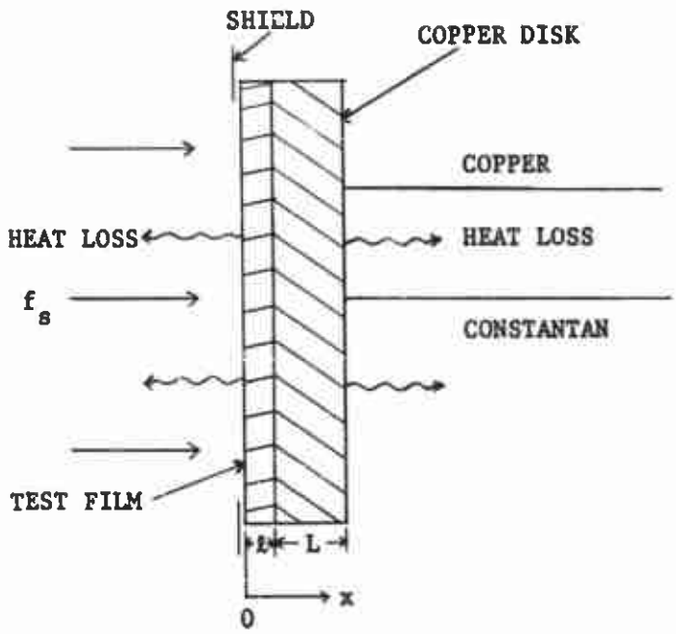

Fig. 20. -- A sketch of experimental model used in this work.

time for heating a body by surface flux is ℓ^2/α , where ℓ is distance below the surface and α is thermal diffusivity. For the copper disk used here, ℓ^2/α is about 10^{-3} sec. The least time interval which is to be discriminated in the experiment is about 0.1 sec. For the purpose of thia work it is therefore safe to assume that any energy reaching the copper is instantaneously and uniformly distributed in it.

For application to the polymer film, the one dimensional, transient heat transfer equation assumed to describe temperature as a function of time, position and chemical parameters is:

for $\quad 0 < x < \ell$

$$\rho c \frac{\partial T}{\partial t} = k_s \frac{\partial^2 T}{\partial x^2} + Ae^{-E_a/RT} \quad . \qquad \text{(VI-1)}$$

The boundary conditions are

(a) $t = 0, \quad T = T_o$; (VI-2)

(b) $x = 0, \quad -k_s \frac{\partial T}{\partial x} = \varepsilon f_s + Be^{-E_b/RT} + Ce^{-E_c/RT} - L_{rs} + G_c$; (VI-3)

(c) $x = \ell, \quad -a_e k_s \frac{\partial T}{\partial x} = aL\rho' c' \left(\frac{dT}{dt}\right)_{x=\ell} + (L_v + L_d + L_{rb})$. (VI-4)

Where

x = distance from the surface of test film, cm.

A, B, C = pre-exponential factors of condensed phase reac ion and surface reactions, $\frac{\text{cal}}{(\text{sec})(\text{cm})^3}$ for A, $\frac{\text{cal}}{(\text{sec})(\text{cm})^2}$ for B and C.

E_a, E_b, E_c = activation energies of condensed phase reaction and surface reactions, cal/g-mole.

ε = surface emissivity, 0.90 by assumption.

a_e = area of exposure, cm^2.

a = area of copper disk gage, cm^2.

k_s = thermal conductivity of test sample, cal/(°C)(sec)(cm).

ℓ = thickness of test film, cm.

L = thickness of copper disk, cm.

ρ, ρ' = densities of test film and copper disk, $g/(cm)^3$.

c, c' = heat capacities of test film and copper disk, cal/(g)(°C).

L_{rs}, L_{rb} = radiation losses from the surface of test film and back face of copper disk, $cal/(sec)(cm)^2$ for L_{rs}, cal/sec for L_{rb}.

L_d, L_v = conduction loss and convection loss, cal/sec.

G_c = energy gain through convection, $cal/(sec)(cm)^2$.

The energy gain and loss by convection have been evaluated experimentally as a function of pressure and temperature, as discussed in Appendix B. The radiation losses were estimated from the Stefan-Boltzmann law by assigning a surface emissivity of 0.9 at the film surface and 0.6 at the back face of copper disk. The conduction losses were evaluated by considering the thermocouple wires as two semi-infinite bodies.

Eq. (VI-1) is a non-linear partial differential equation, for which no analytical solution is known. In addition, the boundary conditions are so cumbersome that the solution to this equation must be handled numerically. The method and procedure of numerical solutions are presented in Appendix B.

The prudent application of the results of numerical solutions require some known and relisble method to confirm the accuracy of the numerical solutions. In this case, the solutions were to be checked against linearized forms of Eq. (VI-1), i.e., equations formed by excluding only the reaction and heat loss terms. Eq. (VI-1) and its boundary conditions now become

for $0 < x < \ell$

$$\rho c \frac{\partial T}{\partial t} = k_s \frac{\partial^2 T}{\partial x^2} \quad . \tag{VI-5}$$

The boundary conditions are

$$\text{(a)} \quad t = 0,\ T = T_o \ ; \tag{VI-6}$$

$$\text{(b)} \quad x = 0,\ -k_s \frac{\partial T}{\partial x} = \epsilon \sigma_s = F \tag{VI-7}$$

$$\text{(c)} \quad x = \ell,\ -k_s \frac{\partial T}{\partial x} = L\rho' c' \left(\frac{dT}{dt}\right)_{x=\ell} \tag{VI-8}$$

Eqs. (VI-5) to (VI-8) can be solved by the method of Laplace transformation. The detailed procedure of the solution appears in Appendix C. Only the final answers are shown here. The temperature as a function of time and depth is given as

$$T-T_o = \frac{F}{k_s}\left[\frac{\alpha t}{\ell+\xi} + \frac{\frac{1}{2}(\ell-x)^2+\xi(\ell-x)}{\ell+\xi} - \frac{\frac{\ell^2}{6}(\ell+3\xi)}{(\ell+\xi)^2}\right.$$

$$\left. -2\ell \sum_{\beta_s} \frac{\left\{\cos\beta_s(1-\frac{x}{\ell}) - \frac{\xi}{\ell}\beta_s \sin\beta_s(1-\frac{x}{\ell})\right\}\exp(-\frac{\alpha\beta_s^2}{\ell^2}t)}{\beta_s^2\cos\beta_s(1+\frac{\xi}{\ell}+\frac{\beta_s^2\xi^2}{\ell^2})}\right], \quad \text{(VI-9)}$$

where β_s's are roots of the equation

$$\tan\beta_s = -\left(\frac{\xi}{\ell}\right)\beta_s \; ; \quad \text{(VI-10)}$$

$$\xi = \frac{L\rho'c'}{\rho c} \; . \quad \text{(VI-11)}$$

At the interface, $x = \ell$; and

$$T_i-T_o = \frac{F}{k_s}\left[\frac{\alpha t}{\ell+\xi} - \frac{\frac{\ell^2}{6}(\ell+3\xi)}{(\ell+\xi)^2} - 2\ell\sum_{\beta_s}\frac{\exp(-\frac{\alpha\beta_s^2 t}{\ell^2})}{\beta_s^2\cos\beta_s(1+\frac{\xi}{\ell}+\frac{\beta_s^2\xi^2}{\ell^2})}\right] . \quad \text{(VI-12)}$$

At the surface, $x = 0$; and

$$T_s - T_o = \frac{F}{k_s}\left[\frac{\alpha t}{\ell+\xi} + \frac{\frac{1}{2}(\ell+2\xi)}{\ell+\xi} - \frac{\ell^2(\ell+3\xi)}{6(\ell+\xi)^2}\right.$$

$$\left. -2\ell \sum_{\beta_s} \frac{(\cos\beta_s - \frac{\xi\beta_s}{\ell}\sin\beta_s)\exp(-\frac{\alpha\beta_s^2}{\ell^2}t)}{\beta_s^2\cos\beta_s\,(1+\frac{\xi}{\ell}+\frac{\beta_s^2\xi^2}{\ell^2})}\right]. \qquad \text{(VI-13)}$$

The FORTRAN programs assembled for the solution of Eqs. (VI-9) to (VI-13) are shown in Table XXXVII. A comparison of the numerical solution of Eq. (VI-5) to the analytical solutions, Eqs. (VI-9) to (VI-13), showed agreement within 0.03 per cent. The numerical computational procedure as applied to the linear equations is thus verified, and confidence established in applying it to solutions of Eqs. (VI-1) to (VI-4).

The temperature history measured by the copper disk is actually the tempersture history of the test film-copper interface, wheraas the events of interest occur on the exposed surface of the sample. Since there is a significant temperature drop across the film and the chemical reaction rates are strcng functions of temperature, the interestiug history of the exposed surfaca must be inferred from the cbserved history of the interface. From the known thermal properties of the film, the equations just presented can be employed to calculate the surface temperature-time relationship from the measured copper disk temperature, at least up to the time when significant reactions occur. The technique involved is essentially one of trial and error. An example is discussed in the following paragraphs to illustrate the general procedure.

Shown in Fig. 21 are the "raw" data from s pyrolysis test of PCC polymer at 1100°C and 0.85 atm nitrogen. Galvanometer sensitivities and thermocouple characteristics are used to convert the "inches history" of a test record into a temperature history. The numerical solution to Eq. (VI-1) can now be employed to convert this measured copper-polymer interface temperature history into a surface temperature history. The procedure is to select parameters which will give an interface temperature history which will match the measured one. Either surface or condensed phase reactions were considered for a single run, sometimes both.

In the analysis of the data of Fig. 21, three sets of kinetic parameters were assumed for the Arrhenius expression, $A\exp\left(-\frac{E_a}{RT}\right)$:

Set	A cal/(sec)(cm)^3	E_a kcal/g-mole
I	2×10^{13}	30
II	7×10^{18}	40
III	2.5×10^{24}	60

Reasonable values of E_a were assigned, and values of A taken such that the calculated interface temperature agreed with the experimental value at the time the onset of reaction was perceived.

From a plot of the calculated results it was found that the measured interface history fell between the results calculated from the first two sets of kinetic parameters. The values 6×10^{15} cal/(sec)(cm)^3 and 37 kcal/g-mole for A and E_a respectively were found to produce the

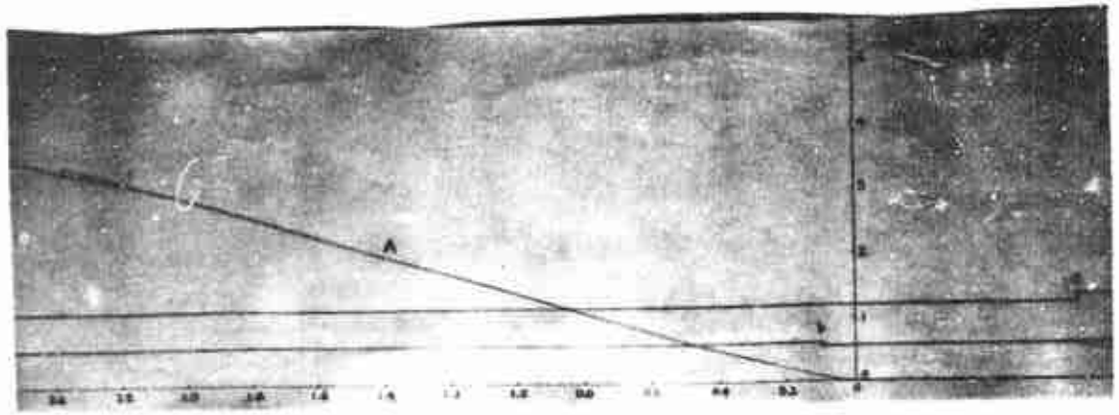

Fig. 21. -- This picture shows the actual record of experimental run on Visicorder sheet (Run No. 32-1-3). Curve A is the interface temperature history. "a" indicates the trigger time, "b", the time when injection rod reaches the test position, and "c", the start of endotherm. The dash line near "c" is the temperature history when there is no endotherm. The numbers in ordinate are in inches, and those in abscissa are in seconds.

best-fit to the interface temperature history. The activation energy determines the sharpness of the break in the temperature-history curve; and since the matching of this "sharpness" is not precise, the activation energies are approximate. Once the interface temperature history was matched, the surface temperature history and temperature gradient across the polymer film could also be calculated.

Since the interface temperature was measured by the copper disk at a position 100 microns behind the exposed face, a time lag existed between the events occurring at the test film surface and the subsequent detection at the interface. In Fig. 22, where the experimental interface temperature (data of Fig. 21) is compared to the calculated surface temperature, one can clearly see the time delay between the occurrence of endothermic reaction at the surface and the detection of the reaction at the interface. The time delay for this experiment was about 0.1 sec, which is close to the value estimated from the characteristic thermal equilibration time, ℓ^2/α . The existence of this delay was also noted in the case of an oxidative reaction when high pressure oxygen was the ambient gas. The photocell light signal denoting a diffusion flame occurred instantly when the event was detected, therefore the corresponding surface temperature must be calculated by adding to the interface temperature the total temperature drop across the polymer film at the time of the event. By this method, the surface temperatures occurring at the start of endothermic reaction, exothermic reaction and photocell response were calculated.

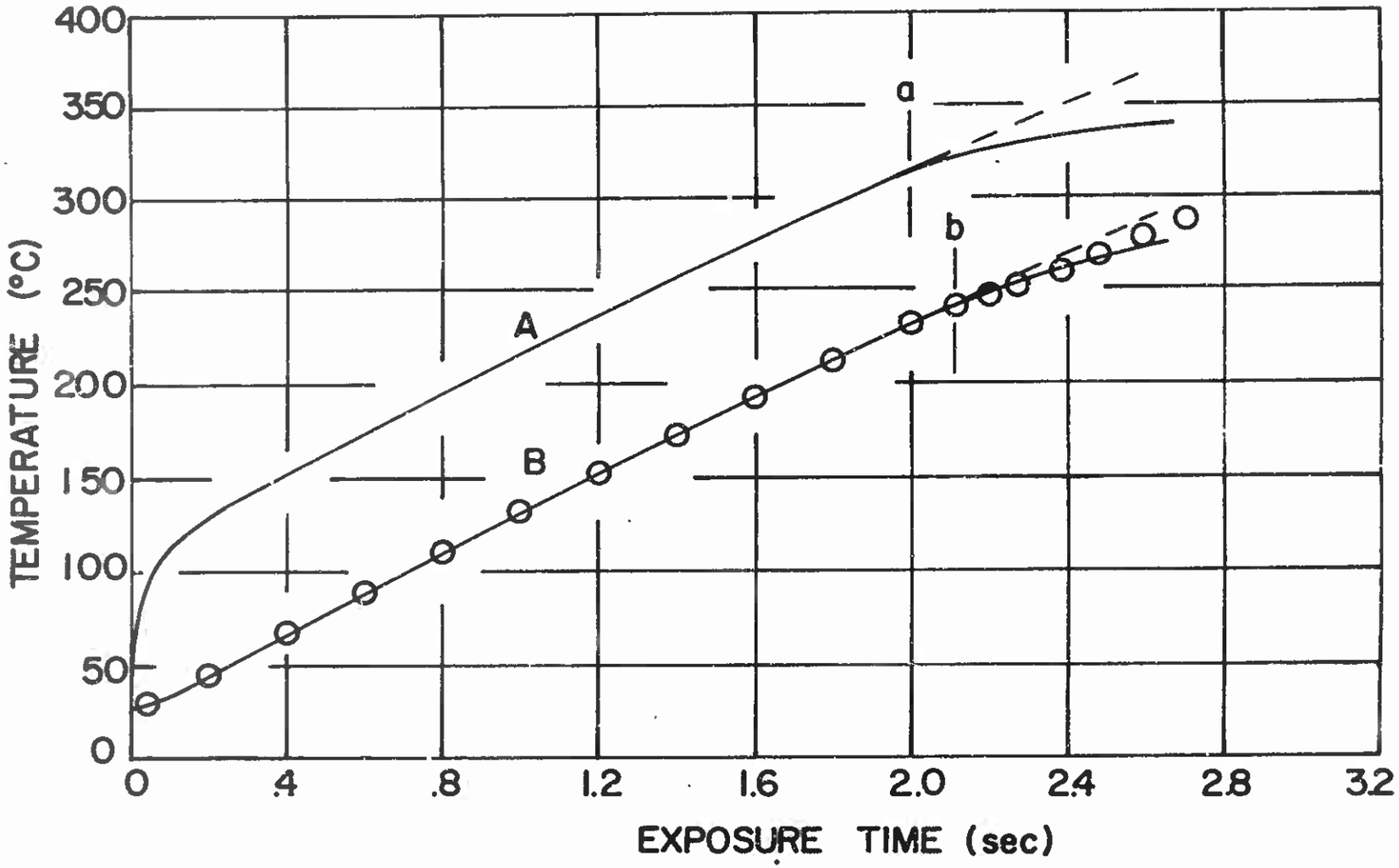

Fig. 22. -- This figure shows the time lag between the appearance of endotherm at the polymer film surface, "a", and the detection of the event at the interface, "b". Curves A and B are calculated surface and interface temperatures versus time. "O" on curve B is from data point in Fig. 21. Dash lines on curves A and B show the temperature histories of surface and interface if there is no endothermic reaction.

Pyrolysis Tests Under Vacuum

Although the results of the pyrolysis tests conducted under vacuum have little direct practical significance, in this work such tests yielded information concerning the nature of the kinetic limitations on the processes since, presumably, rapid vaporization occurred and there could be no accumulation of decomposition products at the very low pressure. Slow pyrolysis under high vacuum is also used to obtain information on the molecular structure and bonding strength of polymers and the result of the fast vacuum tests may be related to auch information.

Reproducibility of the vacuum pyrolysis tests was not as good as in the case of tests at higher pressures. It was necessary to make a large number of runs at given conditions and to average the results to obtain reliable information. The variability was, possibly, caused by expansion at the disk interface of minute bubbles of gas which affected the thermal resiatance at the interface. Also, the assumption that variations in pressure at a total pressure less than 200 mm Hg would not affect the process may be invalid. No provision was made to accurately measure these low pressures. Since the thickness of copper disk used in these vacuum tests was 0.09 cm which was about three times as big as that used in other experiments discussed later, sensitivity was also low.

Fig. 23 shows typical data for PC polymer (see Table X for identification of polymers) pyrolysis in vacuum, reproduced from the Visicorder record. The data are summarized in Table XIX. The temperature trace starts to deflect at an interface temperature of 269 $\pm$ 15°C, 349°C at the surface, a temperature at which endothermic decomposition of polymer

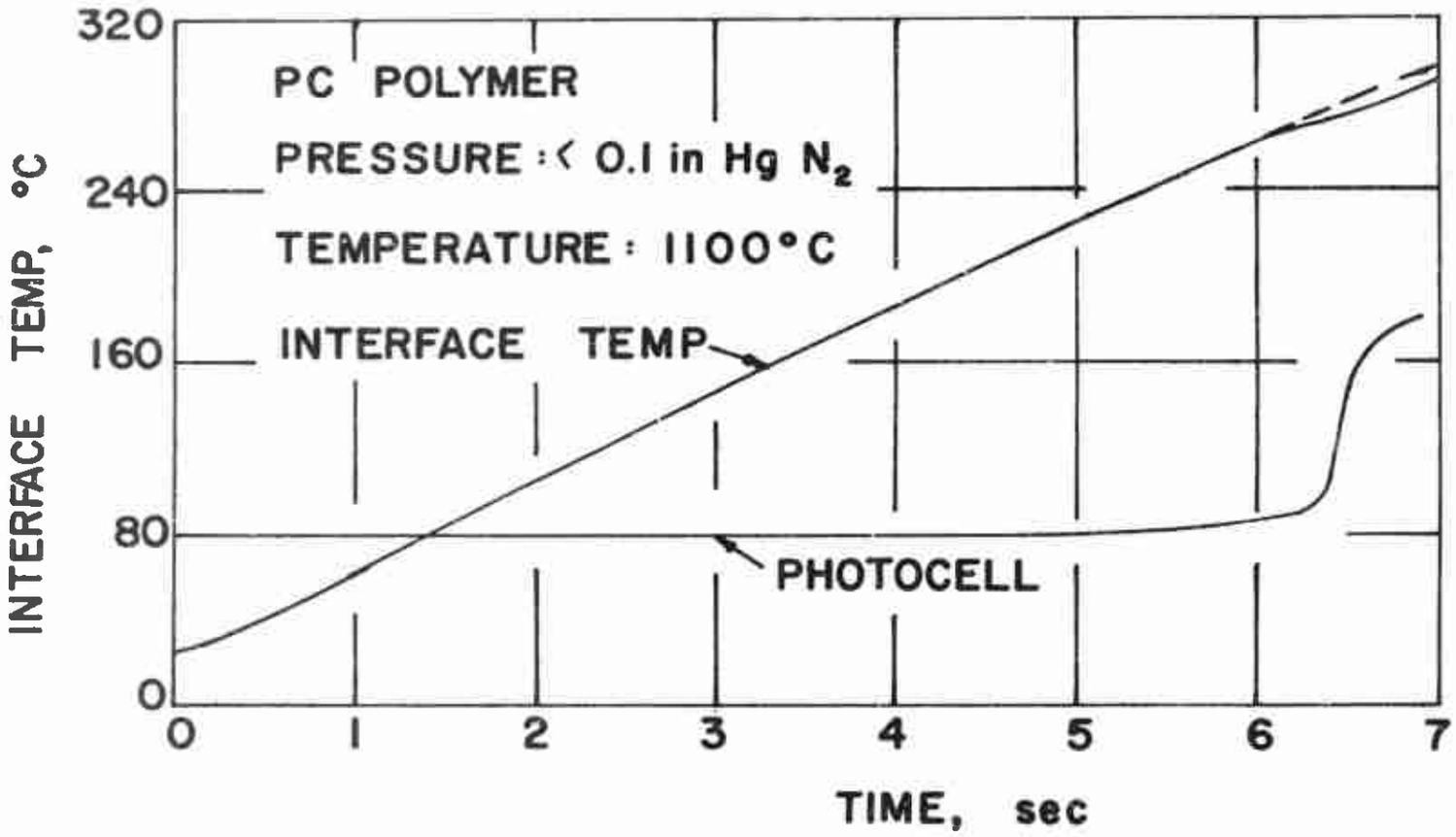

Fig. 23. -- Data for PC polymer pyrolysis in vacuum, reproduced from Visicorder recording sheet and oscillograph. Run No. 25-0-13.

attains an appreciable rate. Part of the scattering of data may be attributable to the external residual presaure, which was not accurstely measured. Since external pressure tends to increase the endotherm temperature (discussed lster), the endotherm temperature in high vacuum is probably best represented by the lower limit of the reaction temperature shown in Table XIX, which is about 600°K. After the endotherm the temperature resumed the previous rate of increase in about one-half second, since the regression of polymer surface quickly starts and the regression coupled with the condensed phase reaction depletes the available reactive polymer.

The aignal detected by the photocell is intereating. A slow rise of the signal is seen at an interface temperature of 230°C, before appreciable endothermic reaction occurs at the expoaed surface. This rise may be caused by the effusion of very light components which were loosely bonded to the main polymer chain, or the change of surface emissivity as the result of the melting of the solid. A ateep rise in the photocell signal, supposedly corresponding to an appreciable gaaification process (this point is discussed later) occurred after the endothermic reaction waa detected by the copper disk gage, indicating a time delay between the first significant decomposition and the production of appreciable volatile products.

Fig. 24 showa data for a "copper chromite" containing polymer, PCC at 1100°C. The data are aummarized in Table XX. While the results shown in Fig. 24 are similar to those for the uncatalyzed polymers, there are at least two diatinct differencea:

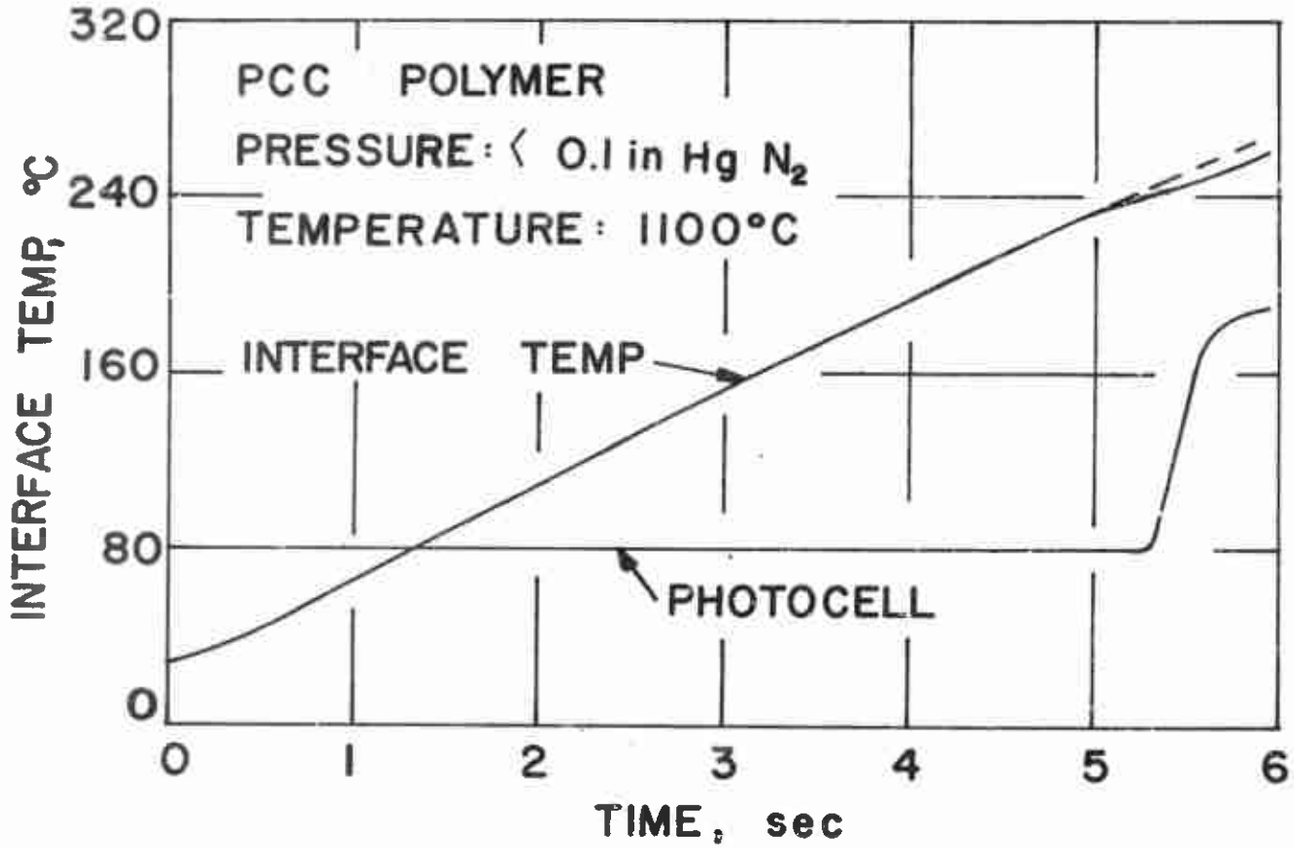

Fig. 24. -- Data for PCC polymer pyrolysis in vacuum, reproduced from Visicorder recording sheet and oscillograph. Run No. 32-0-10.

(1) On the average, the endotherm temperature at the interface is 42°C lower (50°C lower at the surface) in the presence of the catalyst. For catalyzed (PCC) polymer the interface temperature is 227 ± 16°C, 299°C at the surface.

(2) There are no detectable changes in the photocell trace before endothermic reaction. While a slight but obvious change is always observed for uncatalyzed (PC) polymer, it is seen only at temperatures greater than the PCC endotherm temperature.

The effect of copper chromite can be expressed in terms of the activation energies and pre-exponential factors for the pyrolysis of these two polymers, calculated by the trial-and-error procedure previously described. Table III summarizes the results of these calculations.

TABLE III

ACTIVATION ENERGIES AND PRE-EXPONENTIAL FACTORS FOR CATALYZED AND UNCATALYZED PBAA POLYMERS IN VACUUM

Heat Flux cal/(sec)(cm)^2	Catalyzed (Copper Chromite)		Uncatalyzed	
	E_a kcal/g-mole	A cal/(sec)(cm)^3	E_a kcal/g-mole	A cal/(sec)(cm)^3
4.82	37	15×10^{15}	43	3×10^{17}
3.035	37	25×10^{15}	43	5×10^{17}
1.798	37	25×10^{15}	43	5×10^{17}

Although values of the kinetic psrameters are probsbly not exact, it is evident thst the burning rate cstalyst has a pronounced effect on the pyrolysis of PBAA.

The heating rate hss the expected effect on the pyrolysis resction. A decrease in heating rate decresses the surface temperature at which the significant endothermic reaction is observed. These results are summarized in Table IV.

TABLE IV

SIGNIFICANT ENDOTHERMIC REACTION TEMPERATURES FOR POLYMERS IN VACUUM

	PC		PCC	
Surface Heat Flux	Interface	Surface	Interface	Surface
cal/(sec)(cm)^2	°C	°C	°C	°C
4.82	269	349	227	299
3.035	284	335	233	280
1.798	294	324	248	276

This effect of heating rate is predicted by the calculations employing an average of the parameters E_s and A from Table IV. Quantitative agreement is within the experimental error.

Pyrolysis of PC Polymer in Nitrogen

The pyrolysis data obtained when the radiation furnace contained inert gas at high pressures were much more reproducible than were the vacuum data. Three to five tests for each condition were sufficient to obtain an accurate representation of the temperature history of the copper disk for a film of a particular polymer or propellant-like material. Three heating rates were employed, i.e., 4.82, 3.035, 1.987 cal/(sec)(cm)^2, corresponding to furnace temperatures of 1100°C, 950°C, and 800°C respectively. Four to five pressures were used at the highest heating rate to determine the pressure effect. Except where noted all polymers and propellant-like materials were investigated under an inert gas (nitrogen) environment.

Heat transfer by natural convection supplements the radiation flux. The effect on the rate of interface temperature rise was estimated to be only one degree centigrade per sec at 0.85 atmospheres. Even at the highest pressure used (5 atm), the increase in the rate of temperature rise as a result of convection was less than 4°C per sec. The data in Table XXI would indicate that such a small increase in heating rate would produce no significant increase in the temperature at which reaction is observed.

At 0.85 atm N_2, the surface temperature at which the endothermic reaction was first dete ted for PC (carbon blackened PBAA) polymer was on the average 21°C above that for vacuum conditions at the same furnace temperature. The difference was even greater at higher pressures. This

pressure effect is one of the most important experimental findings of this work, as will be discussed later. The increase in the aurface endotherm temperature from 0.85 atm to 5 atm was about 50°C.

Fig. 25 shows five typical oscillograms for pyrolysis of PC polymer under different external pressures. A comparison of these traces shows that the endotherm temperature (at the interface) and the time lag between the appearance of the endothermic reaction and the sharp break of photocell trace increases as the total pressure is raised. These effects are explsined by postulating that the PC polymer decomposes by a two-stage process. In the first stage, most energy absorbed ia for the initial decomposition of polymer and only a small portion of pyrolyzed products escape from the surface. As the temperature is further increased polymer fragments evaporate from the surface carrying the carbon black particles with them. Radiation from the heated carbon produces a response from the photocell. Additional evidence supporting this explanation is presented below. A more detailed mechanism of pyrolysis will be discussed later in the chapter.

A series of experiments was conducted to determine the magnitude of the weight loss and to observe the surface changes. All the test samples were carefully weighed prior to insertion into the furnace. The time the test sample was to remain inside the furnace was selected so that the maximum temperature at the interface was in the vicinity of the endotherm temperature as observed there. The test sample, quickly removed from the furnace and cooled, was carefully weighed again and the polymer surface examined.

a. Run No. 25-1-2
P_f: 0.85 atm nitrogen
T_f: 1100°C

b. Run No. 25-1-8
P_f: 1.48 atm nitrogen
T_f: 1100°C

c. Run No. 25-1-13
P_f: 2.89 atm nitrogen
T_f: 1100°C

d. Run No. 25-1-19
P_f: 5.0 atm nitrogen
T_f: 1100°C

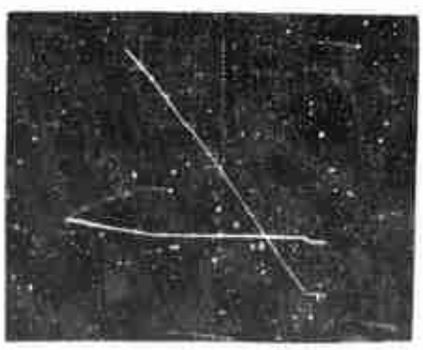

e. Run No. 25-2-3
P_f: 0.85 atm nitrogen
T_f: 950°C

Fig. 25. -- Typical oscillograms of interface temperature histories (diagonal trace) and photocell traces for PC polymer in nitrogen. Time base (right to left) is 0.5 sec/(div.) for a, b and c, and 1 sec/(div.) for d and e. Vertical scale is 2.5 mv/(div.) for a, b, c and e, and 3.6 mv/(div.) for d.

Table V and Fig. 26 summarize the results of these experiments. Since some weight loss probably occurred after the sample was removed from the furnace and before the sample cooled, the data in Table V probably exaggerate the weight loss at the indicated interface temperature.

TABLE V

WEIGHT LOSSES AND SURFACE CONDITIONS OF PC POLYMER FOR THE SURFACE TEMPERATURES IN THE VICINITY OF ENDOTHERMIC TEMPERATURE.
Pressure, 0.85 atm N_2. Original film weight ≈ 13 mg

At Instant of Sample Removal Time	Interface Temperature	Calculated Surface Temperature	Weight Loss	Visible Surface Change
sec	°C	°C	mg	
2.44	279	361	0.21	no change
2.59	285	367	0.22	no change
2.69	298	280	0.25	a little bit shiny
2.92	311	393	0.45	stays shiny
3.16	342	424	0.76	oily look
3.25	348	430	1.92	regressed a little bit
3.42	369	451	6.34	uneven and harder than original polymer

Also plotted on Fig. 26, for reference, are the interface temperature and photocell trace from an experiment in which the sample was not

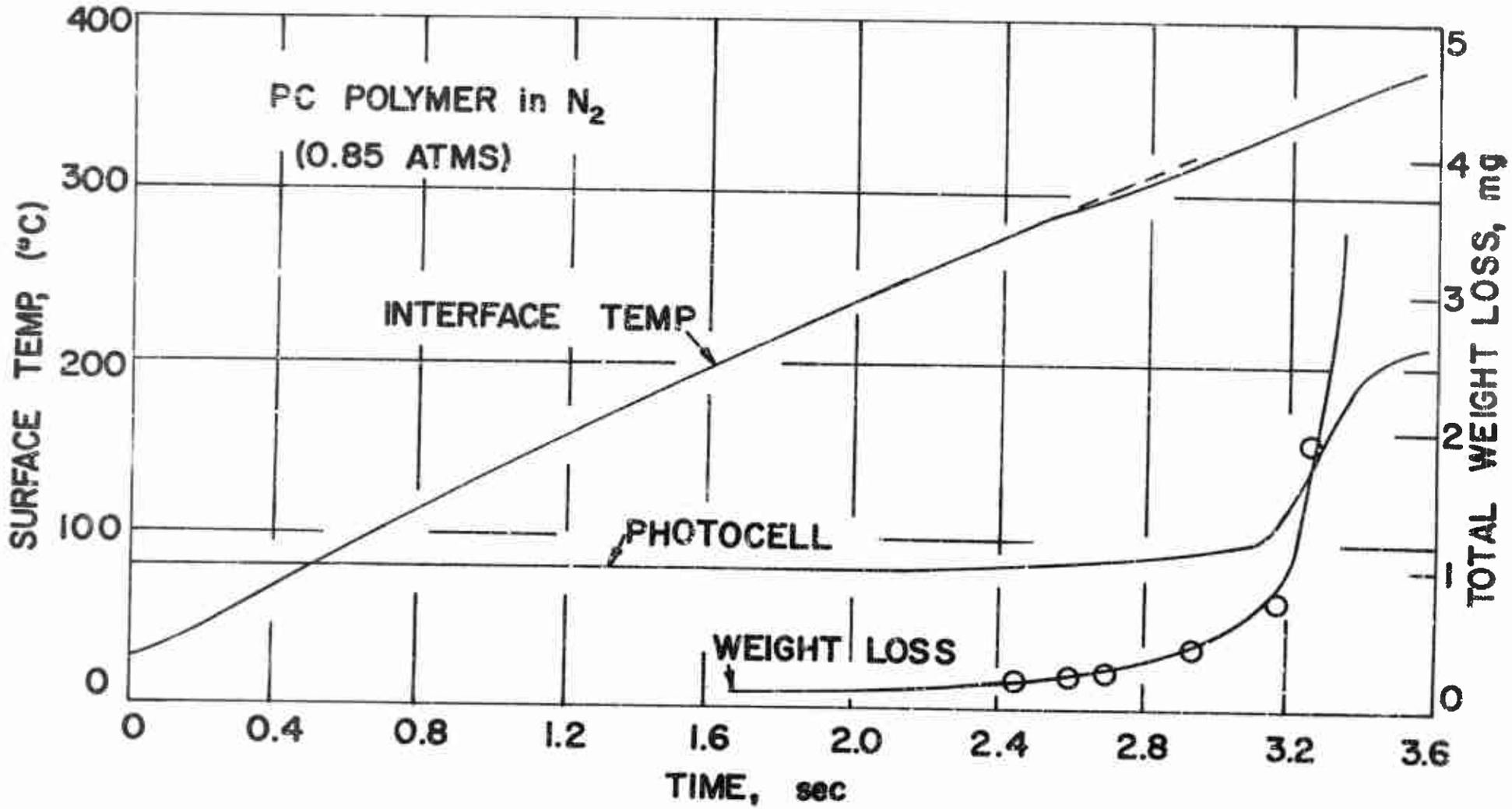

Fig. 26. -- Cumulative weight loss of PC polymers before, during and after significant endothermic reaction at 1100°C and 0.85 atm N_2. Also plotted in this figure is a record of PC polymer pyrolysis at the same furnace condition. Run No. 25-1-2.

removed from the furnace. The figure indicates that the weight loss is almost negligible at the time of the endotherm detected at the interface (0.1 second after the endothermic reaction at the surface) and increases rapidly only after another 40°C or so temperature rise. The resemblance of the weight loss curve to the photocell signal trace is interpreted as indicating that the photocell saw radiation from pyrolysis products in the vapor phase. In particular it saw radiation from carbon black particles carried by vapor from the film surface as significant regression started. Although these loss-in-weight experiments were performed for PC polymer only, at 0.85 atm N_2 and 1100°C furnace temperature, the conclusion is presumed to apply to all conditions and polymers used.

The temperature of both the endotherm indication and the point where the photocell signal indicates vaporization are pressure dependent. When one plots the logarithm of the external pressure against the reciprocal of the surface temperature, at the endothermic reaction and for the ensuing vaporization process, two straight lines result. Fig. 27 shows these plots. Mathematically these two lines can be expressed as

$$\log P_e = -\frac{C_1}{T} + C_2 \quad . \qquad \text{(VI-14)}$$

Where P_e is total external pressure, C_1, C_2 are two constants.

Eq. (VI-14) has the same form as the integrated form of the Clapeyron-Clausius equation,

$$\log P_e = -\frac{\Delta H_\lambda}{RT} + C_2 \quad , \qquad \text{(VI-15)}$$

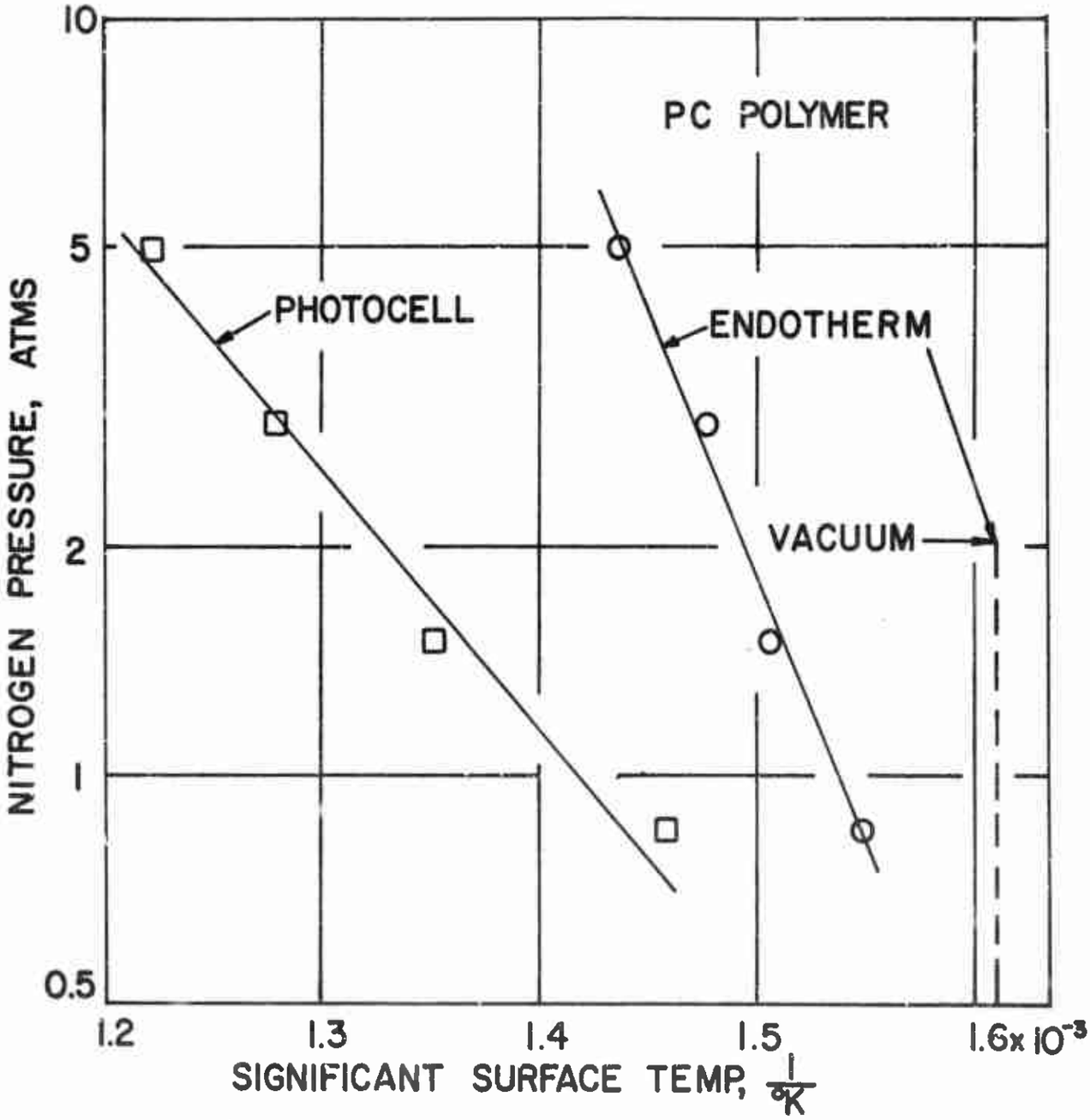

Fig. 27. -- Plots of logarithms of total pressures of nitrogen versus reciprocal surface temperatures of endotherm and significant vaporization for PC polymer at a furnace temperature of 1100°C.

where ΔH_λ is the enthalpy of vaporization. This coincidence leads to the supposition that equilibrium vaporization processes may be occurring in the pyrolysis of this polymer.

Additional suggestion that the quick photocell rise corresponds to the significant equilibrium vaporization of pyrolyzed compounds comes from the results of pyrolysis experiments at different furnace temperatures. Thermodynamically the temperature of equilibrium vaporization is a function of only external pressure. For the pyrolysis of PC polymer at two different furnace temperatures, 1100°C and 950°C, the difference in surface temperatures at the sharp photocell rise was only about 4°C, well within error of measurement.

From the data of Fig. 27 and the Clapeyron-Clausius equation one can calculate the apparent enthalpies of vaporization. For the endotherm process, the enthalpy is 32.4 $\pm$ 3 kcal/g-mole, and for the process at the photocell signal, 15.7 $\pm$ 1.3 kcal/g-mole.

The latter process has the attributes of simple vaporization. Employing the temperature of the sharp photocell signal rise at 1 atm as the boiling point in the rules of Trouton and Kistyakowsky, one obtains a heat of vaporization of about 15 kcal/g-mole. Presumably, after the endotherm the degradation process produces fragments which, in large part, have a boiling point near the temperature of the photocell signal rise. That a second endotherm is not indicated by the calorimeter temperature is a result of surface regression; the effect of reduced rate of surface temperature rise is offset by the reduced resistance to heat transfer through the film.

As the character of the fragments vaporized is not known, one cannot estimate the molecular weight from the heat of vaporization. It can be stated, however, that if the material evolved at the endotherm is of the aame molecular type aa that evolved later, its molecular weight should be lesa and its molal heat of vaporization less. That the apparent heat of vaporization is much greater indicates either that the material is different in kind, or that the endotherm process is not simple vaproization. Probably both statements are true.

When PC polymer was heated in vacuum, the reaction

$$P(s) \longrightarrow M(s) + N(g)$$

is postulated to have occurred. Here P represents the original polymer, M and N represent pyrolysis fragments. The activation energy of 43 kcal is greater than the observed reaction enthalpy of 32.4 kcal, as expected. Under presaure, however, the process is presumed to occur according to the following reactions:

$$P(s) \longrightarrow M(s) + N(s)$$

$$N(a) \rightleftharpoons N(g)$$

$$N(a) + M(s) \longrightarrow P'(s)$$

The volatile N(s) is formed as the endotherm is approached. Prior to vaporization, the N(s) formed ia probably diasolved in the polymer aubstrate, its vapor pressure being proportional to its mole fraction in the substrate. As the endotherm temperature is reached, the vapor

pressure developed by N(s) becomes large enough to offset external pressure and N(s) vaporizes. Therefore the endotherm temperature is the boiling or sublimation temperature of N(s) at its activity in the heavier residue.

The final reaction, recombination of N(s) to high molecular weight material, P' (probably not the same as the original polymer), is needed in the postulated mechanism. Because the observed heat effect is greater than the heat of vaporization of N(s), presumed to be less than 15 kcal/g-mole, the postulated mechanism must provide (1) that the first reaction be fast, yet (2) that the amount of N(s) accumulated before the vaporization temperature is reached is only a small fraction of the total evolved when that temperature is reached. The heat effect observed is, therefore, the sum of the first two reactions. If the heat of vaporization is less than 15 kcal, the heat of the first reaction is greater than 17, probably 20 to 25 kcal/g-mole.

With respect to the endothermic process, it is noted that, according to the weight loss curve of Fig. 26, very little mass is evolved. Presumably weak links in the polymer chains and networks are most vulnerable. They may be associated with the carboxyl appendages on the chains or the ether linkages introduced by the epoxy curing agent.

As the decomposition reactions go on, vigorous random scission along the main polymer chain is presumed to occur, and the pyrolysis products heavier than N(s) are produced rapidly and accumulated on the polymer surface. As surface temperature continues to rise, the vapor pressure developed by these heavier products (undergoing further pyrolysis)

becomes big enough to offset the external pressure, followed by a significant vaporization which then produces the response seen in the photocell trace.

Pyrolysis of PCC Polymer in Nitrogen

PCC polymer is copper chromite catalyzed PC polymer with a proportion of one part of catalyst in nine parts of PBAA polymer. Pyrolysis of this polymer was investigated at five furnace pressures from 0.85 atm to 5 atm nitrogen at a furnace temperature of 1100°C.

Fig. 28 shows five oscillograms of the experimental results. The data are summarized in Table XXII. It is observed that both surface endotherm temperature and significant vaporization surface temperature are about 50°C below the values for PC polymer. These temperature reductions are further manifestations of the catalystic effect of copper chromite.

As with PC polymer, a pressure effect is also observed with PCC polymer. When one makes the same plot as Fig. 27, two straight lines again result (see Fig. 29). Application of Eq. (VI-15) gives ΔH_λ values of 27.6 $\pm$ 2.3 kcal/g-mole and 14.1 $\pm$ 1.5 kcal/g-mole for the endotherm and significant vaporization respectively. Although the mean values are lower than those for PC polymer, the uncertainties are greater than the differences.

The mechanism proposed for PC polymer can also be applied here. The addition of copper chromite catalyst presumably accelerates the first decomposition reaction. At a given temperature more N(s) is produced

a. Run No. 32-1-4

P_f: 0.85 atm nitrogen

b. Run No. 32-1-7

P_f: 1.48 atm nitrogen

c. Run No. 32-1-13

P_f: 2.20 atm nitrogen

d. Run No. 32-1-16

P_f: 3.04 atm nitrogen

e. Run No. 32-1-24

P_f: 4.86 atm nitrogen

Fig. 28. -- Typical oscillograms of interface temperature (diagonal trace) and photocell traces for PCC polymer at 1100°C furnace temperature and several external nitrogen pressures. Time base (right to left) is 0.5 sec/(div.) for a, b, c and d, and 1 sec/(div.) for e. Vertical scale is 2.0 mv/(div.) for a, b, d and e, and 2.2 mv/(div.) for c.

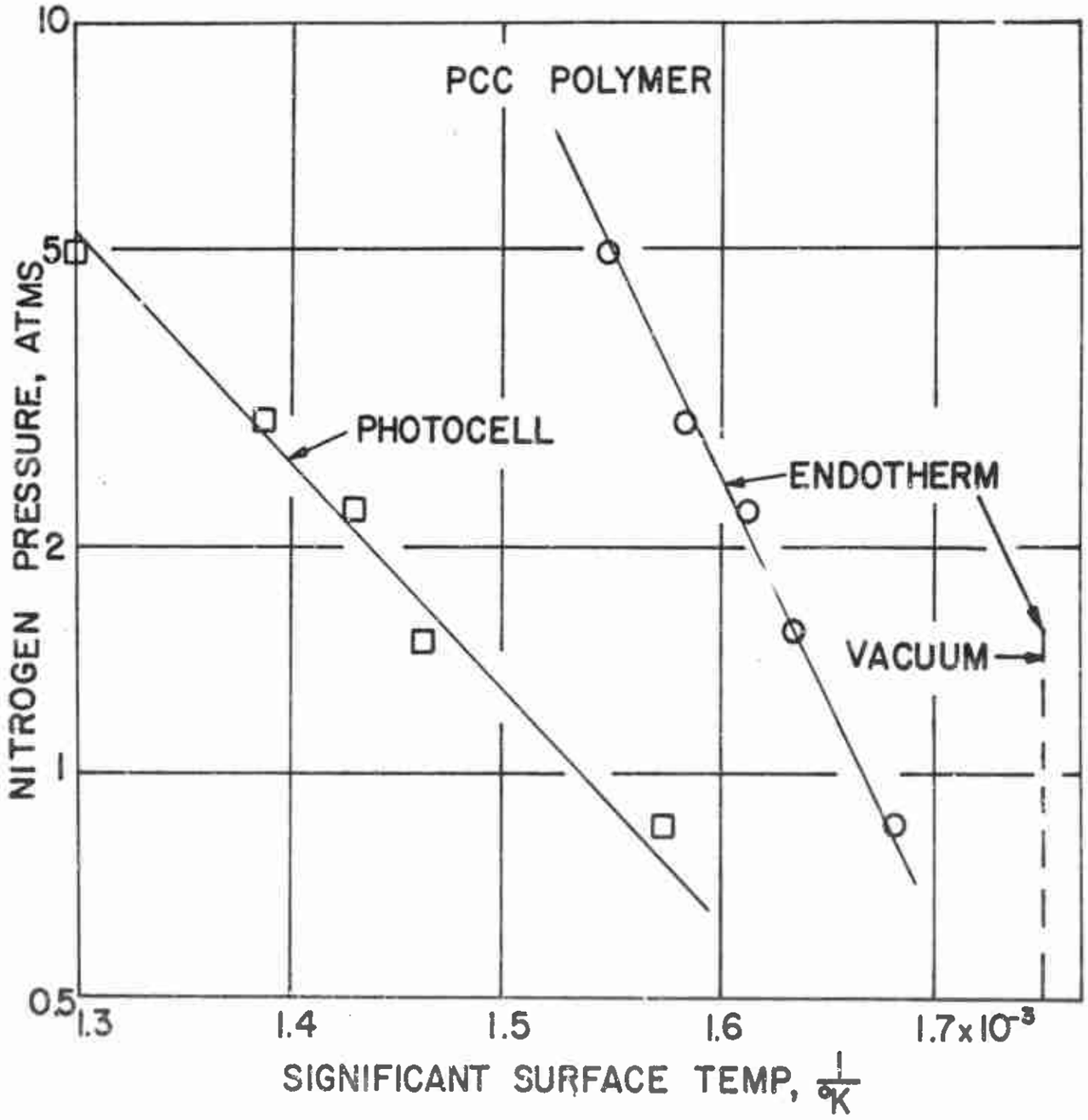

Fig. 29. -- Plots of logarithms of total nitrogen pressures versus reciprocal surface temperatures of endotherm and significant vaporization for PCC polymer at a furnace temperature of 1100°C.

when catalyst is preseut, and the vapor pressure developed by the dissolved N(s) reaches external pressure earlier at a lower temperature. The copper chromite catalyst presumably does not affect the recombination reaction.

Pyrolysis of P12 Polymer in Nitrogen

This polymer contains 10 parts of Fe_2O_3 in 90 parts of PBAA binder, blackened by three per cent of carbon black. Pyrolysis experiments were carried out at the highest available heating rate, 4.82 cal/(sec)(cm)^2 and four different pressures. Fig. 30 shows four typical results of these tests. The data are summarized in Table XXIII. As with the two polymers discussed previously, a pressure effect on the pyrolysis reaction is noted. A plot of logarithm of external pressure versus reciprocal surface temperature of the endotherm and significant vaporization also turns out to be two straight lines, Fig. 31.

As before the Clapeyron-Clausius equation is applied to evaluate the heats of vaporization, ΔH_λ . They are found to be 33.6 $\pm$ 3.6 kcal/g-mole and 17.3 $\pm$ 1 kcal/g-mole for the endotherm and significant vaporization respectively. These values are very close to those for the uncatalyzed polymer, PC, which indicates that the Fe_2O_3 does not affect the decomposition of PBAA binder. The pre-exponential factors are also the same. Actually the decomposition temperature is about 5°C higher than that of PC polymer.

From the close resemblance between the results of Fe_2O_3 catalyzed polymer, P12, and uncatalyzed polymer, PC, the same mechanism for the pyrolysis of PC polymer is also valid for the pyrolysis of P12 under

a. Run No. 50-1-2
P_f: 0.85 atm nitrogen

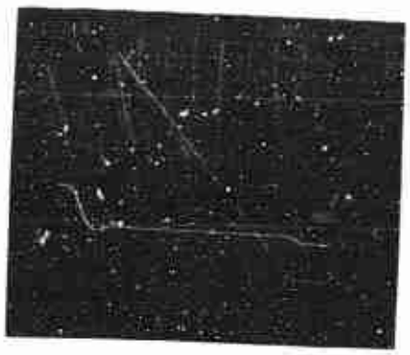

b. Run No. 50-1-6
P_f: 1.49 atm nitrogen

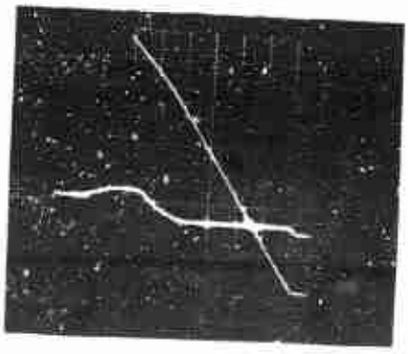

c. Run No. 50-1-12
P_f: 2.9 nitrogen

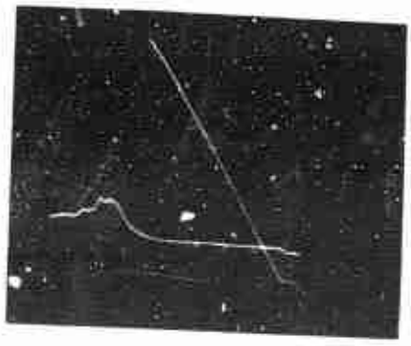

d. Run No. 50-1-18
P_f: 5.0 atm nitrogen

Fig. 30. -- Typical oscillograms of interface temperature (diagonal trace) and photocell traces for PI2 polymer at 1100°C furnace temperature and several external pressures. Time base (right to left) is 0.5 sec/(div.) for a and b, and 1 sec/(div.) for c and d. Vertical scale is 2.5 mv/(div.) for a and b, and 3.4 mv/(div.) for c and d.

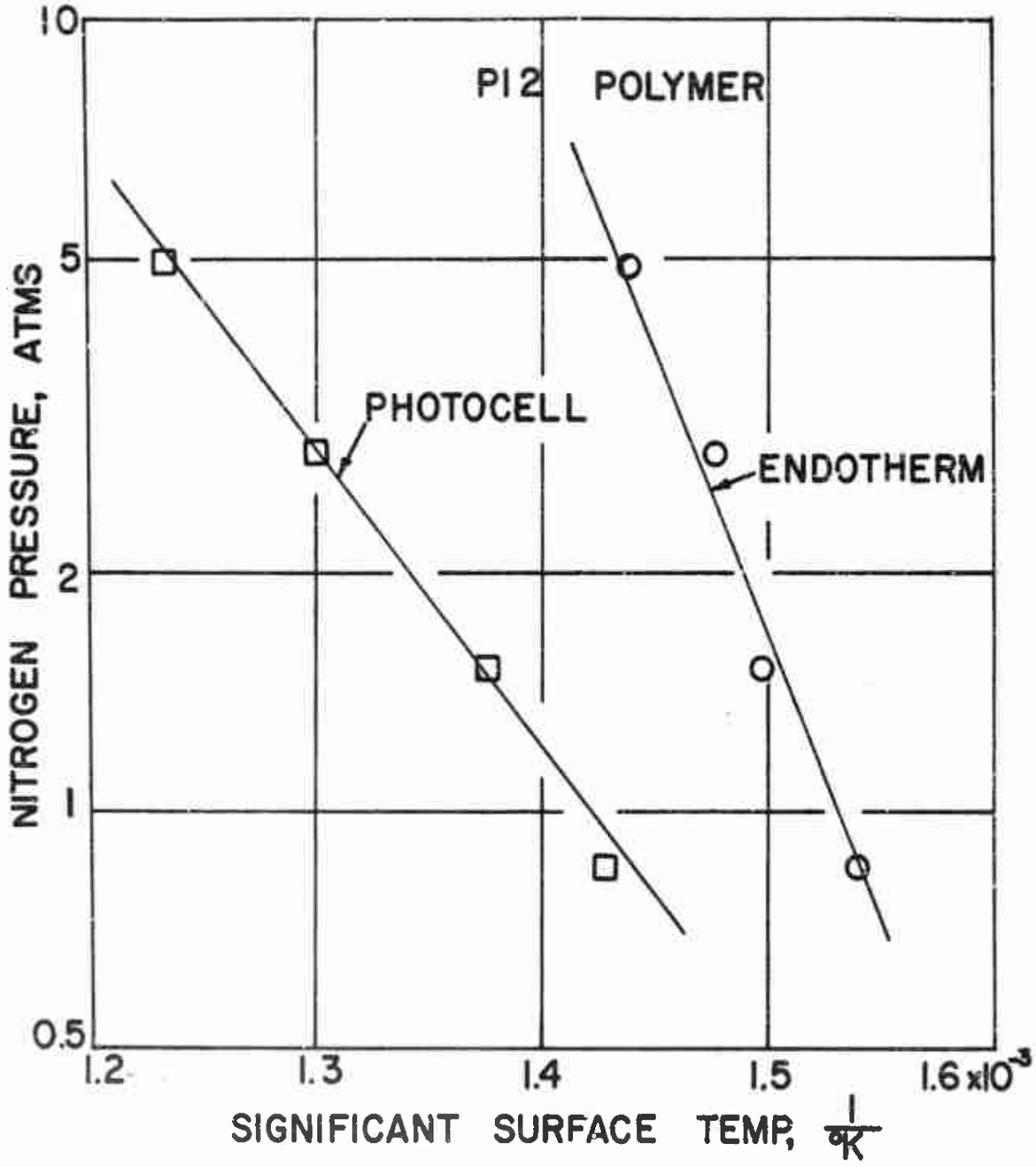

Fig. 31. -- Plots of logarithms of total nitrogen pressures versus reciprocal surface temperatures of endotherm and significant vaporization for PI2 polymer at a furnace temperature of 1100°C.

pressure. The results of PI1 polymer which contains only three per cent Fe_2O_3 and no carbon black are discussed in Appendix D.

For reference a summary of the apparent vaporization constants for catalyzed and uncatalyzed polymers is shown as Table VI.

TABLE VI

SUMMARY OF VAPORIZATION CONSTANTS FOR CATALYZED AND UNCATALYZED POLYMERS

Catalyst	Surface Temperature of Reaction		ΔH_λ		C_2	
	Endo-therm	Vaporiza-tion	Endotherm	Vaporization	Endotherm	Vaporization
	°C	°C	kcal/g-mole	kcal/g-mole		
None	375	412	32.4± 3	15.7±1.3	25.1±2.5	11.2±0.8
copper chromite	322	363	27.6±2.3	14.1±1.5	23.2±2	10.9±1
iron oxide	378	427	33.6±3.6	17.3±1	25.9±3	12.4±0.7

Experiments in Nitrogen with Propellant-like Materials

Four types of AP-containing polymers (each different in AP content) without burning rate catalyst were investigated at a furnace temperature of 1100°C and 0.85 atm. The code names for these polymers are A05, A09, A20 and A50 correaponding to roughly 5, 9, 19, and 49 per cent of AP by weight respecitvely. Fig. 32 ahows three typical oscillograms of the

a. Run No. 23-1-2
w_{AP}: 8.8%

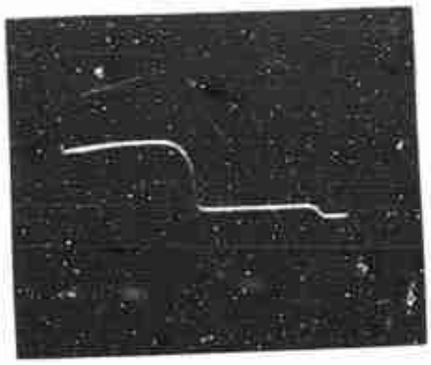

b. Run No. 36-1-3
w_{AP}: 19.4%

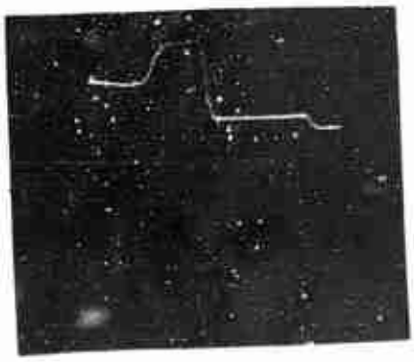

c. Run No. 27-1-3
w_{AP}: 48.5%

Fig. 32. -- Typical oscillograms of interface temperature (diagonal trace) and photocell traces for AP-containing propellant-like materials without catalyst at 1100°C furnace temperature and 0.85 atm nitrogen. Time base (right to left) is 0.5 sec/(div.) for all records. Vertical scale is 2.0 mv/(div.) for all records.

behaviors of degradation reactions of polymers containing different amounts of AP. The experimental runs with 5 per cent AP loading were not recorded by oscilloscope. Table XXV shows the data of significant reactions.

With AP in the polymer, several reactions, in addition to polymer decomposition, are possible, for example, the heterogeneous reactions between AP and binder, and between one and decomposition products of the other. The information available does not allow one to take all these reactions into consideration. However, in order to represent the real case as closely as possible, two Arrhenius expressions were used in the mathematical analysis to translate the interface temperature into surface temperature (the general procedure being the same as the example shown in the section of "The Technique of Data Analysis"). One was used in the heat transfer differential equation to represent oxidizer-modified polymer decomposition in the sample bulk, the second in the boundary condition to represent the interaction reaction at the surface. The first is presumed to be endothermic, and the second exothermic.

Fig. 33 shows the changes of the calculated characteristic surface temperatures, i.e., endotherm temperatures, exotherm temperatures and the temperatures of quick photocell response, with the quantity of AP in the polymer. Several interesting observations follow from inspection of Figs. 32 and 33:

(a) There is a significant drop of the characteristic temperatures when a small amount of AP is added to the PBAA binder. The weight loss experiments which will be discussed later show

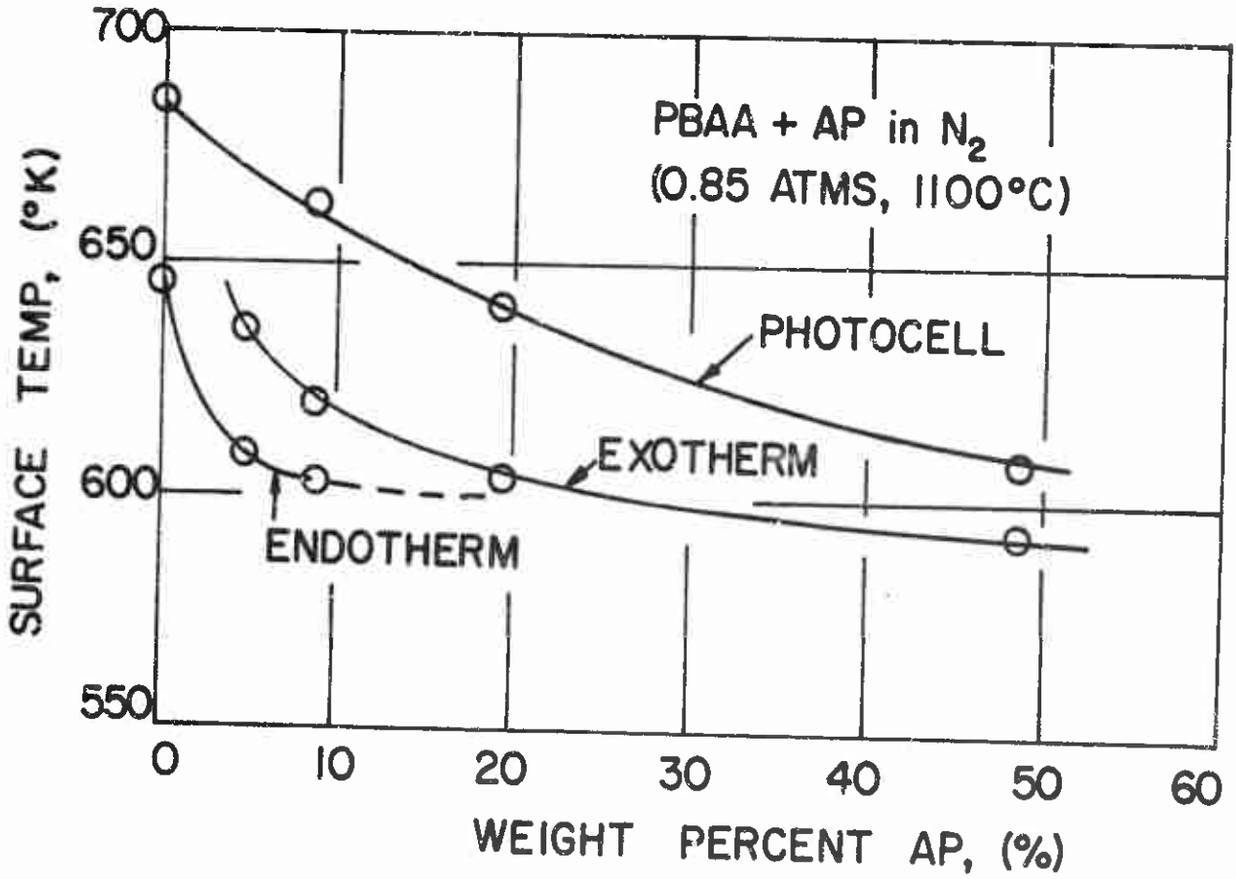

Fig. 33. -- Changes of characteristic surface temperatures as a function of quantity of AP in the polymer, without catalyst. Furnace temperature, 1100°C. Furnace pressure, 0.85 atm nitrogen.

that the PBAA binder with 9% AP produces more pyrolyzed products than pure PBAA binder at the same exposure level. These two sets of experiments demonstrate that AP participates in PBAA binder decomposition.

(b) In Fig. 33 we see that the endotherm temperature approaches 600°K at an AP level of about 20 per cent. At AP levels above 20 per cent no endothermic reaction is observed.

(c) The time lag and temperature difference between the start of the exothermic reaction and the sharp light signal detected by the photocell become smaller as the amount of AP in the polymer increases.

(d) The rate of rise of the interface temperature decreases after the photocell signal, indicating fast mass evolution. This is probably caused by the shielding effect of the evolved gases which absorb part of the incident radiation energy.

(e) For tests at low AP levels, the light signal stays at a constant level, even after the injection rod has been pulled out. (See Fig. 32.) It may be that after fast mass evolution a great deal of carbon and carbon-rich materials are produced because of incomplete oxidation reaction at these low AP levels and that what the photocell sees is the reflected light from these solid particles which are still floating in the furnace even after the injection rod has been pulled out. For the low AP tests, the films were never completely consumed.

The asymptotic surface temperature of 600°K discussed in Item (b) is interesting as compared with the surface endotherm temperature of PC polymer in vacuum which is also 600°K (see the section, "Pyrolysis Tests Under Vacuum"). This result seems to suggest that the presence of AP has assisted the pyrolysis of PBAA polymer by removal of decomposition products. The explanation starts conveniently with the mechanism postulated for PC polymer (0% AP on Fig. 33) in the previous section. When AP is present in small amount, the gasification of the volatile N(s) is augmented by AP, which generates oxidizing species represented by O_x:

$$N(s) + O_x \longrightarrow \text{small, more volatile fragments.}$$

This may be an endothermic reaction in spite of the O_x participation if it is polymer unzipping initiated by O_x. Apparently between 10 and 20 % AP, the oxidation gasification removes N(s) as fast as it is formed by the thermal process.

At low AP levels, the endotherm is followed by an exotherm, presumed to be vigorous attack by O_x on all the polymeric material. The energy supplied shortens the time to the photocell signal rise, which indicates rapid evolution of material. The reduction in the signal rise temperature may indicate that the volatilized fragments produced then are of lower molecular weight than those produced from PC polymer alone.

At high AP levels, where there is a larger supply of O_x, the oxidative degradation process wholly displaces the thermal process as the first detected reaction. The exotherm and the photocell signal rise

appear to be converging and approaching 580 to 590°K as an asymptote. This temperature is, it is speculated, the surface temperature at ignition discussed by Keller, Baer and Ryan [29].

The results plotted in Fig. 33 thus agree with propellant ignition results reported elsewhere. Furthermore, they confirm Keller's conclusion that simple thermal degradation of FBAA polymer is not an important process in ignition [28].

Five types of AP-containing polymer with catalyst, either copper chromite or iron oxide, were investigated at 1100°C furnace temperature and 0.85 atm nitrogen. These propellant-like materials are referred to as A9C, A2C, A5C, A9I and A5I whose compositions are shown in Table X. The quantity of catalyst, either iron oxide or copper chromite, always amounts to 1/20th of the weight of AP.

Fig. 34 shows five typical oscillograms of experimental results. Fig. 35 shows plots of calculated characteristic surface temperatures as a function of the amount of AP in the polymer. The data on significant reactions are summarized in Table XXVI. General trends which had been observed in the cases of uncatalyzed AP-containing polymers discussed previously were also found here.

There are, however, some significant differences between the results for catalyzed and those for uncatalyzed propellant-like materials. The most striking difference is that, at higher AP levels, the endotherm, exotherm, and photocell signal rise temperatures are lower than those found for the uncatalyzed propellant. In view of the fact that, as mentioned earlier, the copper chromite catalyst enhanced the decomposition

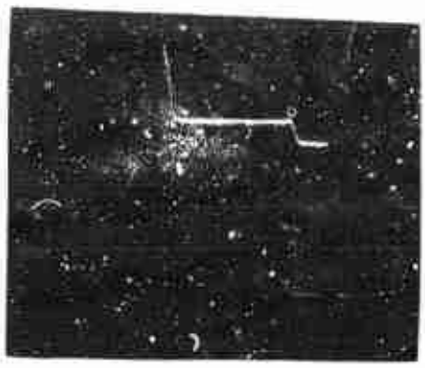

a. Run No. 24-1-4

w_{AP}: 8.8%

b. Run No. 37-1-2

w_{AP}: 19.2%

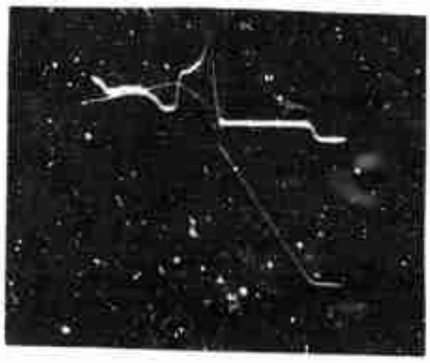

c. Run No. 28-1-3

w_{AP}: 47.3%

d. Run No. 51-1-5

w_{AP}: 8.8%

e. Run No. 52-1-3

w_{AP}: 47.3%

Fig. 34. -- Typical oscillograms of interface temperature (diagonal trace) and photocell traces for AP-containing polymers with catalyst at 1100°C furnace temperature and 0.85 atm nitrogen. The catalyst for a, b and c is copper chromite, and for d and e, iron oxide. Time base (right to left) is 0.5 sec/(div.) for all periods. Vertical scale is 2.0 mv/(div.) for a, b and c, 2.5 mv/(div.) for d, and 2.3 mv/(div.) for e.

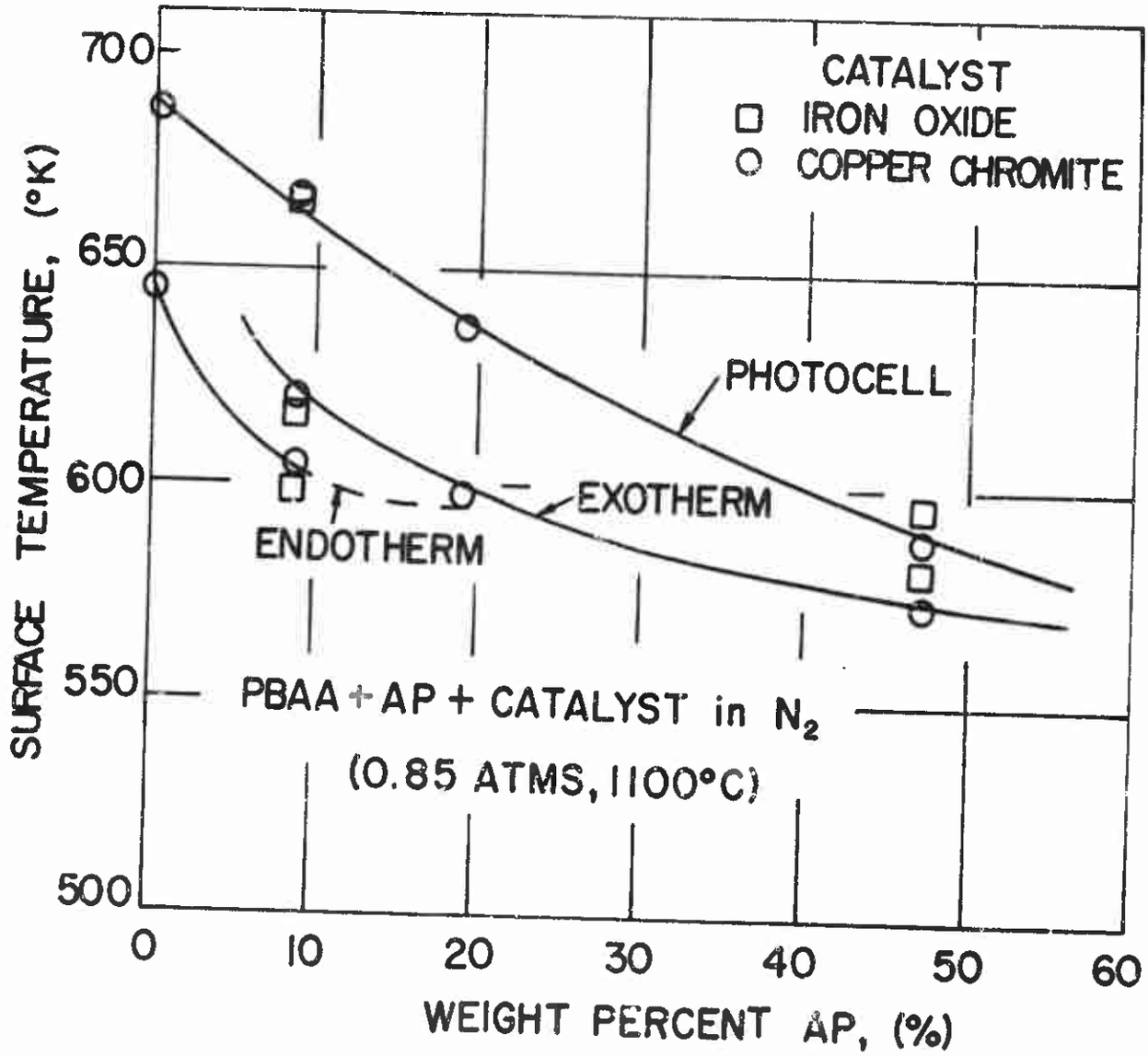

Fig. 35. -- Changes of characteristic surface temperatures as a function of quantity of AP in the polymer, with catalyst. Furnace temperature, 1100°C. Furnace pressure, 0.85 atm nitrogen.

of polymer without AP it is not possible to determine from these results the degree to which the effect is on polymer rather than on AP. That ferric oxide also reduces the temperatures at higher AP levels, yet does not appear to affect polymer decomposition, suggests that the catalysts are augmenting the effect of AP. Apparently copper chromite is, in its over-all effect, slightly more effective than ferric oxide.

The overall rate of exothermic reaction of these AP-containing polymers is related to the difference in the measured heat flux at the copper disk-polymer interface before and during the exotherm; the former is actually the interface heat flux when heating the test sample surface without reactions. This difference in heat flux is defined as the net exotherm heat flux. Shown in Fig. 36 is the plot of the calculated net exotherm heat flux as a function of weight per cent AP times the density of the test sample, which is proportional to the polymer-AP contact surface per unit volume. The slope of this plot is found to be 1.8 for both catalyzed and uncatalyzed materials.

The heat flux obtained at the interface can be used to estimate the surface heat flux by the same set of differential equations which were used to analyze the measured interface temperature history. However, surface regression would have to be considered. Because test film is thin, a near proportionality is expected to exist between the interface and surface heat fluxes; therefore, if a similar plot to Fig. 36 is made using the net exotherm surface heat flux, one would expect to obtain an almost the same slope. This slope may suggest that the reaction between AP and binder does not observe a simple kinetic order.

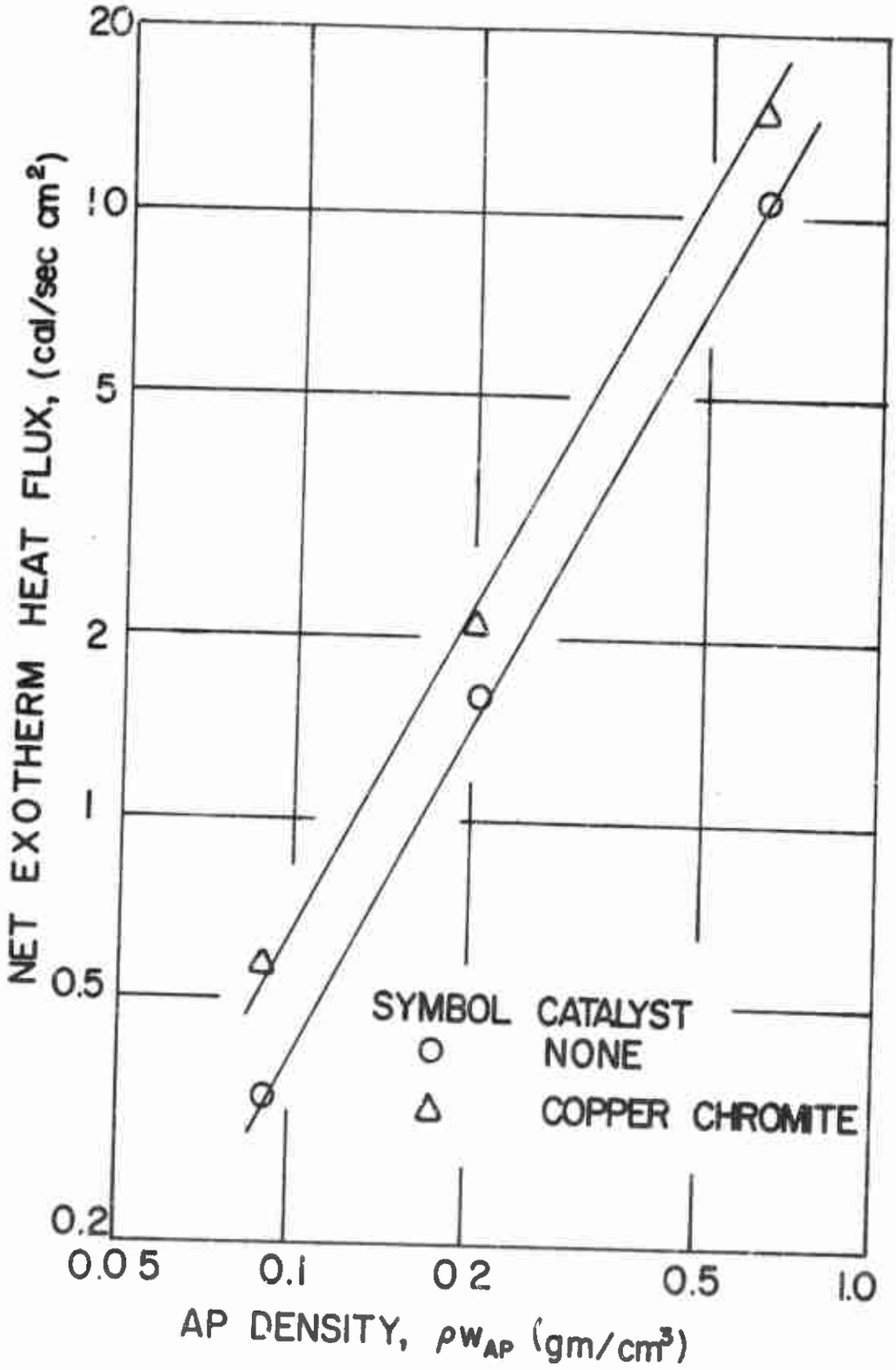

Fig. 36. -- Net exotherm heat flux as a function of AP density in the AP-containing polymers at a furnace temperature of 1100°C and 0.85 atm nitrogen.

The effect of copper chromite catalyst on the exothermic reaction can be seen from Fig. 36. On average, an increase of 30% in net exotherm heat flux because of the presence of copper chromite is calculated. This is about the increase observed in burning rate by addition of catalyst to this system. It is impossible to determine whether the effect is between oxidizer and catalyst or between binder and catalyst. In contrast to the effect on ignition, the copper chromite effect on the feedback flux is essentially uniform for high and low AP loadings.

The net exotherm heat flux for iron oxide catalyzed, AP-containing polymers were much lower than those for uncatalyzed and copper chromite catalyzed ones. This strange experimental result is clearly illustrated by the measured net exotherm heat fluxes for A50 (50% AP with no catalyst), A5C (50% AP, copper chromite) and A5I (50% AP, iron oxide) at a furnace temperature of 1100°C and a pressure of 0.85 atm nitrogen, the average measured values being 10.4 cal/(sec)(cm)^2, 15 cal/(sec)(cm)^2 and 2.4 cal/(sec)(cm)^2 respectively. Apparently the iron oxide-containing samples involve a burning characteristic considerably different from that of other two polymers.

In order to investigate possible differences of the burning characteristic of these materials, pieces of propellant-like materials, 2 cm x 0.7 cm x 0.2 cm, were cut out from these three AP-containing polymers. When placed on a piece of flat pyrophyllite, these samples were ignited with a match and burned in the atmosphere. Several important things were noticed. Total burning times were 4 second for

the A5C polymer, 6.3 seconds for the A50 polymer and 5.3 seconds for the A5I polymer. For the A50 and A5C polymers, the ratio of burning rates in the air is 1 to 1.6, which is close to the ratio of the net exotherm heat fluxes of 1 to 1.44 as shown in Fig. 36.

The burning characteristics of these materials were widely different. A5C polymer burned noisily and the flame was tinted with blue color. After combustion a little scattered ash was left. A50 polymer burned almost quietly and no characteristic color was observed in the flame. After combustion a little more loose, scattered ash was found. The flame characteristic of A5I was almost the same as that of A50. However, for the A50 the deflagration wave, with the usual flame brush, left behind a coherent residue through which, following the deflagration wave, a second reaction wave proceeded as a glowing plane. The second wave may have been air oxidation of free iron formed by reduction of Fe_2O_3 in the fuel-rich deflagration flame. The residual ash was black, and roughly the size and shape of the original sample.

When the experiment was repeated by supporting the samples on a sheet of metal, no visible flame brush but only a glowing reaction wave was observed for the A5I polymer. Again a black, coherent ash was left. For A5C and A50 polymers, no change was noted. Since the copper disk calorimeter is an excellent heat sink, the A5I polymer probably burned inside the radiation furnace with much the same mechanism as described here, and presumably generated much less energy than the other materials. This different burning process perhaps is responsible for the extremely low net exotherm heat flux observed for A5I polymer.

Five AP-containing polymers, A09, A9C, A2C, A9I and A5I were studied for their reaction behavior in nitrogen at lower furnace temperatures. As in the case of PC polymer, a decrease in significant reaction temperatures with decreasing furnace temperatures were observed. However, the decreases were greater than those found with PC polymer. See Table VII. For more data see Tables XXV and XXVI.

TABLE VII

DECREASE OF SIGNIFICANT REACTION TEMPERATURES AS A FUNCTION OF FURNACE TEMPERATURE DIFFERENCE. Pressure=0.85 atm N_2

Material Code	AP Wt %	Catalyst Wt %	Decrease of Surface Reaction Temperature (°C) Between Two Furnace Temperatures				
			Endotherm		Exotherm		Photocell Rise
			1100°C→ 950°C	950°C→ 800°C	1100°C→ 950°C	950°C→ 800°C	1100°C→ 950°C
PC	none	none	20	14	*	*	4
A09	8.83	none	25	--	20	--	6
A9C	8.78	0.44[2]	32	27	33	30	11
A2C	19.23	0.96[1]	*	*	32	24	28
A9I	8.78	0.44[2]	48	--	53	--	32
A5I	47.32	2.36[2]	*	*	44	--	40

* no reaction observed

-- no experimental data available

1 copper chromite

2 iron oxide

Examination of Table VII indicates that the presence of AP appears to be the important factor for the greater decrease in reaction temperature. The effect of AP on the decomposition of polymer was postulated earlier as a second, augmenting mechanism in which the polymer decomposition product, N(s), reacts with AP decomposition product, O_x. For a pyrolysis test at a lower heating rate, the production of N(s) per unit degree of surface temperature rise should be more than that at higher heating rate, therefore at constant aurface temperature level more N(s) will be produced at a lower heating rate than at a higher heating rate, and a lower endotherm temperature (and also exotherm temperature and temperature of photocell rise) will be observed. The catalyst effect can also be seen from Table VII. Again, as mentioned earlier, it is not possible to determine the degree to which the effect is on polymer rather than on AP.

The temperature drop with iron oxide as catalyst is more severe than copper chromite as catalyst (see Table VII). Since it has been observed that the iron oxide does not affect the decomposition of polymer, it appears that the reactions involving AP are affected significantly by iron oxide.

Comparing the results of A9I and A5I in Table VII, we find that the amount of AP from 10 to 50% by weight does not affect seriously the temperature drop. This agrees with the earlier observation that the effect of AP on the over-all reaction ia most obvious for AP levels less than 20%.

As already pointed out in the section of "The Technique of Data Analysis", the activation energies used to calculate the surface temperature histories are only approximate; therefore only one set of activation energies were used in the analysis of the results of all AP-containing polymers, catalyzed and uncatalyzed materials alike. Because the surface temperature history and temperature gradient across the test film are rather insensitive to the values of activation energy chosen until there is a significant change of interface temperature history, and because experiment/calculation matching of the latter cannot be very exact, there is some reservation about the accuracy of surface temperature after the endotherm. The net exotherm heat flux as measured by the calorimeter is exact. Its interpretation in terms of events occurring at the exposed surface is dubious.

CHAPTER VII

RADIATION FURNACE EXPERIMENTS: REACTIVE ATMOSPHERE

While a large body of literature, see for example [15, 27, 46], is available on the mechanism and kinetics of thermal degradation of polymers, there are few systematic and detailed studies of the oxidative degradation of polymers. The decomposition of ammonium perchlorate yields a number of oxidizing species: perchloric acid under some conditions, and under others oxygen, chlorine, oxides of nitrogen, and even nitrogen oxychloride. Though they are not seen in the stable decomposition products, the very potent oxidizing oxides of chlorine (Cl_2O, ClO_2 and the free radical ClO) are probably present during the decomposition process. It seems obvious that these reactive compounds must accelerate the degradation of polymers.

Since the pressure experienced by a propellant during the ignition transient is rather high and changing, the pyrolysis-promoting effect of chemically reactive agents should be studied at different pressures. Though oxygen was used exclusively in this work, the results can, hopefully, be extended to understand the effect of other reactive oxidants.

In the kind of experiment performed, three process conditions can conveniently be varied independently: the oxygen pressure, the furnace

temperature, and the fraction of specimen surface that is polymer. The surface fraction was varied by use of specimens containing different amounts of glass beads. The changes in the calorimeter temperature history and the photocell response as these conditions were systematically varied provide clues to the mechanism of polymer pyrolysis.

PC Polymer

The polymers which will be discussed are PC, G10, G20, G30, G50, and G5C. (See Table X for their complete compositions.) PC polymer is PBAA binder without catalyst, the behavior of which in the presence of nitrogen has been previously discussed. The others are PC polymer containing glass beads.

The behavior of the PC polymer in oxygen was studied at three furnace temperatures at atmospheric pressure, and at four pressures at the highest furnace temperature of 1100°C. Fig. 37 shows five typical oscilloscope records for PC polymer tests in the radiation furnace at 1100°C and 950°C under different oxygen pressures. For a furnace temperature of 800°C only photocell traces were recorded; they are not shown in Fig. 37. In Fig. 38 are five records of experiments with polymers containing glass beads, furnace conditions being 1100°C and 0.85 atm of oxygen. The surface temperature history was calculated from the interface temperature history using the same general procedure as that used with data for PCC polymer at 0.85 atm nitrogen. In this case, however, the Arrehenius expression was used in the boundary condition to represent oxidative reaction at the surface. The significant reaction temperatures are summarized in Tables XXVII and XXVIII.

a. Run No. 25-1-51
P_f: 0.85 atm oxygen
T_f: 1100°C

b. Run No. 25-1-59
P_f: 1.45 atm oxygen
T_f: 1100°C

c. Run No. 25-1-62
P_f: 2.86 atm oxygen
T_f: 1100°C

d. Run No. 25-1-67
P_f: 4.8 atm oxygen
T_f: 1100°C

e. Run No. 25-2-52
P_f: 0.85 atm oxygen
T_f: 950°C

Fig. 37. -- Typical oacillograms of interface temperature (diagonal trace) and photocell tracea for PC polymer at several oxygen preasurea and different furnace temperaturea. Time base (diagonal trace) ia 0.5 aec/(div.) for all records. Vertical scale is 2.0 mv/(div.) for a, b, c and e, and 1.8 mv/(div.) for d.

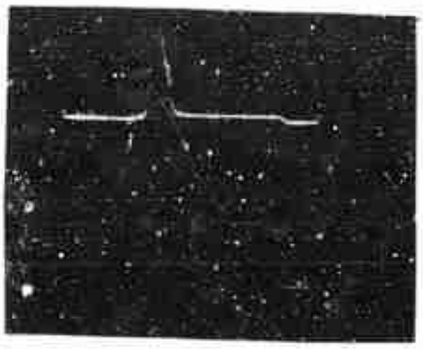

a. Run No. 39-1-1
Glass beads: 9.7%

b. Run No. 40-1-1
Glass beads: 19.4%

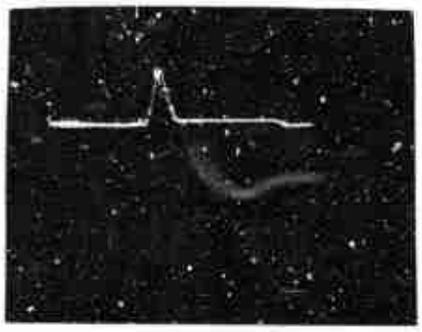

c. Run No. 41-1-4
Glass beads: 29.1%

d. Run No. 42-1-2
Glass beads: 48.5%

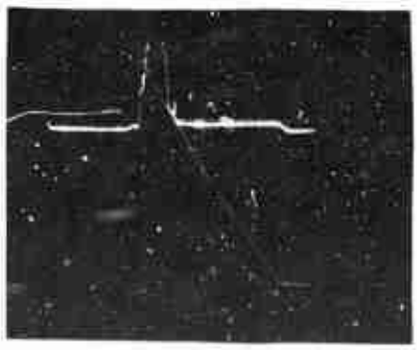

e. Run No. 43-1-1
Glass beads: 46%
With copper chromite catalyst

Fig. 38. -- Typical oscillograms of interface temperature (diagonal trace) and photocell traces for glass beads-containing PC polymers at 1100°C furnace temperature and 0.85 atm oxygen. a, b, c and d contain no catalyst. Time base (right to left) is 0.5 sec/(div.) for all records. Vertical scale is 2.0 mv/(div.) for a, b, d and e, and 2.3 mv/(div.) for c.

In these tests with oxygen an exotherm was always observed, and at surface temperatures well below (more than 100°C) those at which an endotherm was observed during heating in nitrogen at the same pressures. There can be no doubt that oxygen strongly promotes the decomposition and gasification of the polymer.

It can be seen from Table XXVII, where data and results are summarized, that the exotherm temperature is not significantly affected when pressure is varied over a six-fold range. As oxygen clearly plays a role, this observation cannot be taken as evidence that the gas phase is not involved. Possibly there is a purely physical effect of pressure to suppress the vaporization of volatile fragments, that is, to raise their vaporization temperature (the increase in the endotherm temperature with nitrogen pressure was explained in this way), compensated by a chemical effect that tends to reduce the exotherm temperature as pressure is increased.

A puzzling observation is that, for heating under a fixed oxygen pressure, the exotherm temperature bears an inverse relationship to the furnace temperature. (See Fig. 39.) A measure of the heating rate, a higher furnace temperature was expected to be accompanied by a rise in the exotherm temperature (in the way the endotherm temperature in vacuum heating was raised). The furnace temperature has another significance, however: it is also the temperature of the gaseous oxygen. It seems that one is driven to the conclusion that the first volatile polymer fragments, produced as the exotherm temperature is approached, vaporize and diffuse far enough from the surface to encounter hot oxygen. The resulting reaction

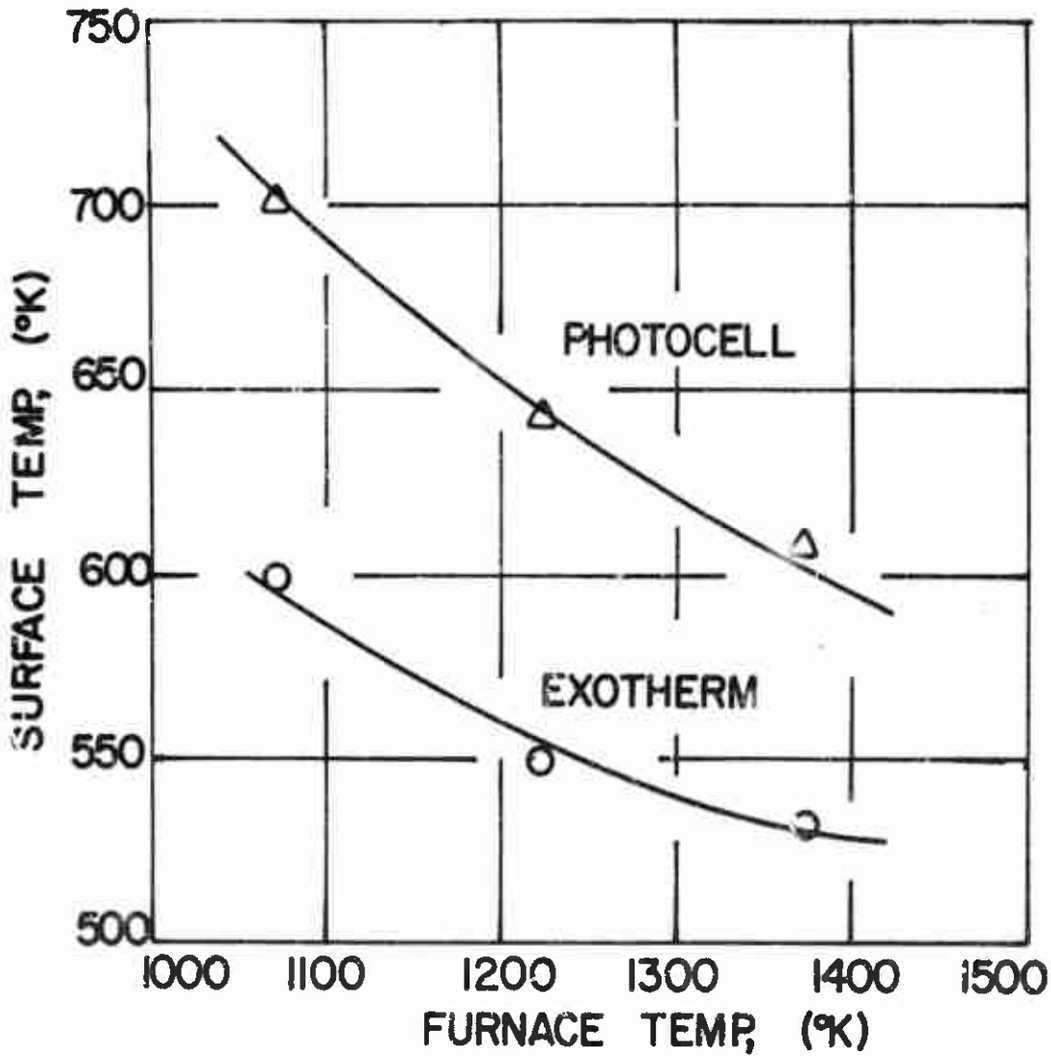

Fig. 39. -- Photocell temperature and exotherm temperature as a function of furnace temperature for PC polymer at 0.85 atm oxygen.

faster with hotter oxygen, produces both energy and reactive species that diffuse back to the polymer surface to accelerste events there.

It is not possible to say whether the initial part of the exotherm is due to heterogeneous reaction or to feed-bsck from gas phsse reaction. In either case, it must coincide closely with the start of rapid effusion of gaseous polymer fragments. Their reaction with oxygen supplies more energy to produce more fuel, bootstrapping the pyrolysis process until, it is postulated, the oxygen near the surface is pushed back by a cloud of fuel vapor. A diffusion flame, detected by the photocell, develops at the fuel vspor-oxygen mixing zone.

The polymer surface temperature at the time of the first photocell signal (called photocell temperature) is, like the exotherm temperature, less when the furnace temperature is greater, as shown in Fig. 39, but unlike the exotherm temperature, it is strongly pressure dependent as shown in Fig. 40. As oxygen temperature is increased, the difference between the photocell and the exotherm temperature drops (Fig. 39).

The photocell temperature is clearly a fictitious temperature, greater than the true surface tempersture and less than the temperature at which the gss phase reactions occur. It is used in an attempt to discuss some of the gross festures of the very complex reaction mechanism. Another defined quantity used for this purpose is the net exotherm heat flux, which has been defined earlier as the difference between the furnsce flux and the exotherm flux, both as perceived by the copper calorimeter. It is proportionsl to the difference between the rates of interface

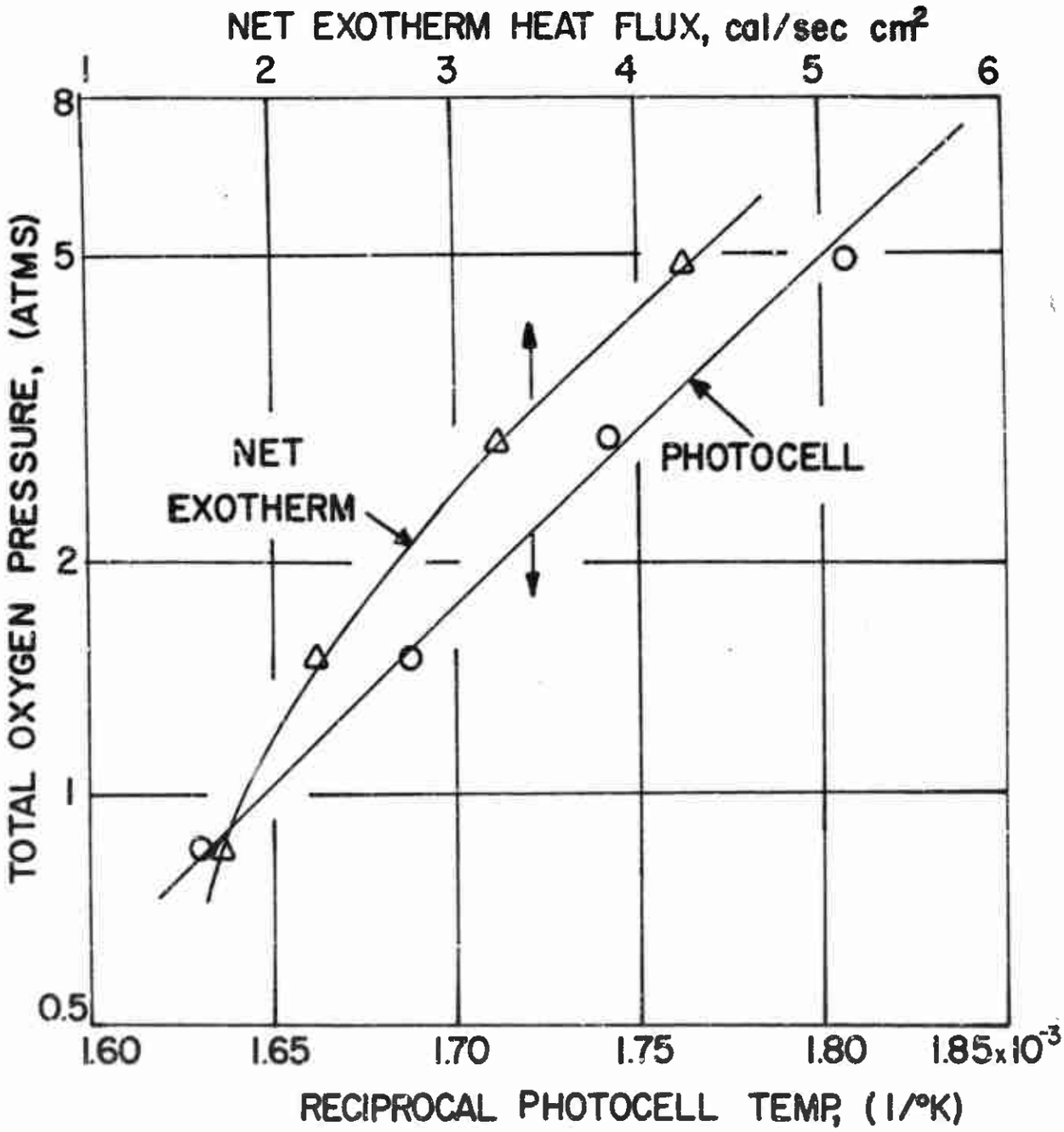

Fig. 40. -- Plot of total oxygen pressure versus net exotherm heat flux and reciprocal photocell temperature for PC polymer at a furnace temperature of 1100°C.

temperature rise before and during the exotherm. The net exotherm heat flux is taken as proportional to the over-all reaction rate. The net exotherm heat flux is plotted in Fig. 40 as a function of total oxygen pressure.

An examination of the data for polymer films containing various amounts of glass beads shows that the exotherm temperature and photocell temperature depend on available PBAA binder on the polymer surface. Shown in Fig. 41 is a plot of volume fraction of available PBAA binder in the polymer as a function of reciprocal photocell temperature. The plot of net exotherm heat flux versus volume fraction of PBAA is shown in Fig. 42.

Based on the observations and discussions presented above, we may assume that the rate of oxidative reaction of PC polymer is given by

$$\dot{r} = k(P_{O_2})^n(p)^s = Ae^{-E/RT}(P_{O_2})^n(p)^s. \qquad \text{(VII-1)}$$

Where $\dot{r}$ is the rate of oxidative reaction which is taken as proportional to the net exotherm heat flux; T is properly the surface temperature of the polymer film, which in this analysis is arbitrarily taken as the calculated photocell temperature; (P_{O_2}) is the total oxygen pressure; (p) is the volume fraction of PBAA binder; n and s are the reaction order with respect to oxygen pressure and the volume fraction of PBAA binder respectively.

The determination of E, n and s from the experimental data can be done by a trial and error procedure. For the glass beads-containing

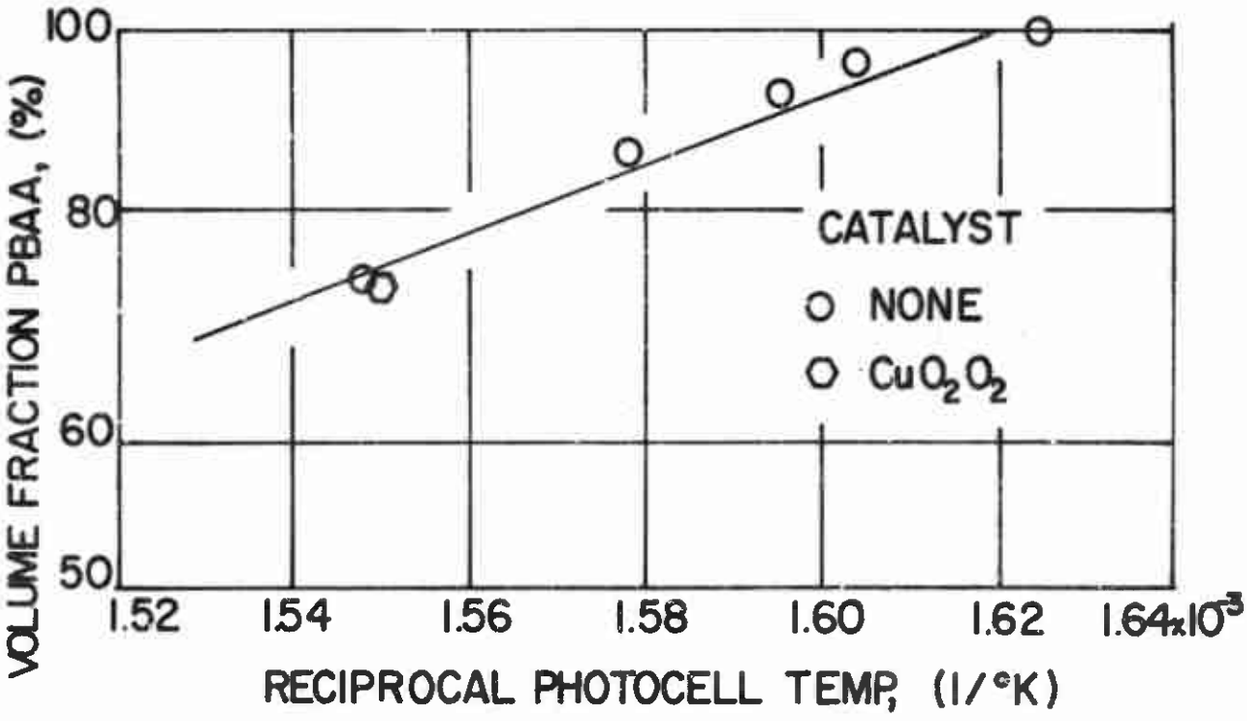

Fig. 41. -- Plot of volume fraction of PBAA fuel-binder in the polymer versus reciprocal photocell temperature for glass beads-containing polymers at a furnace temperature of 1100°C and 0.85 atm oxygen.

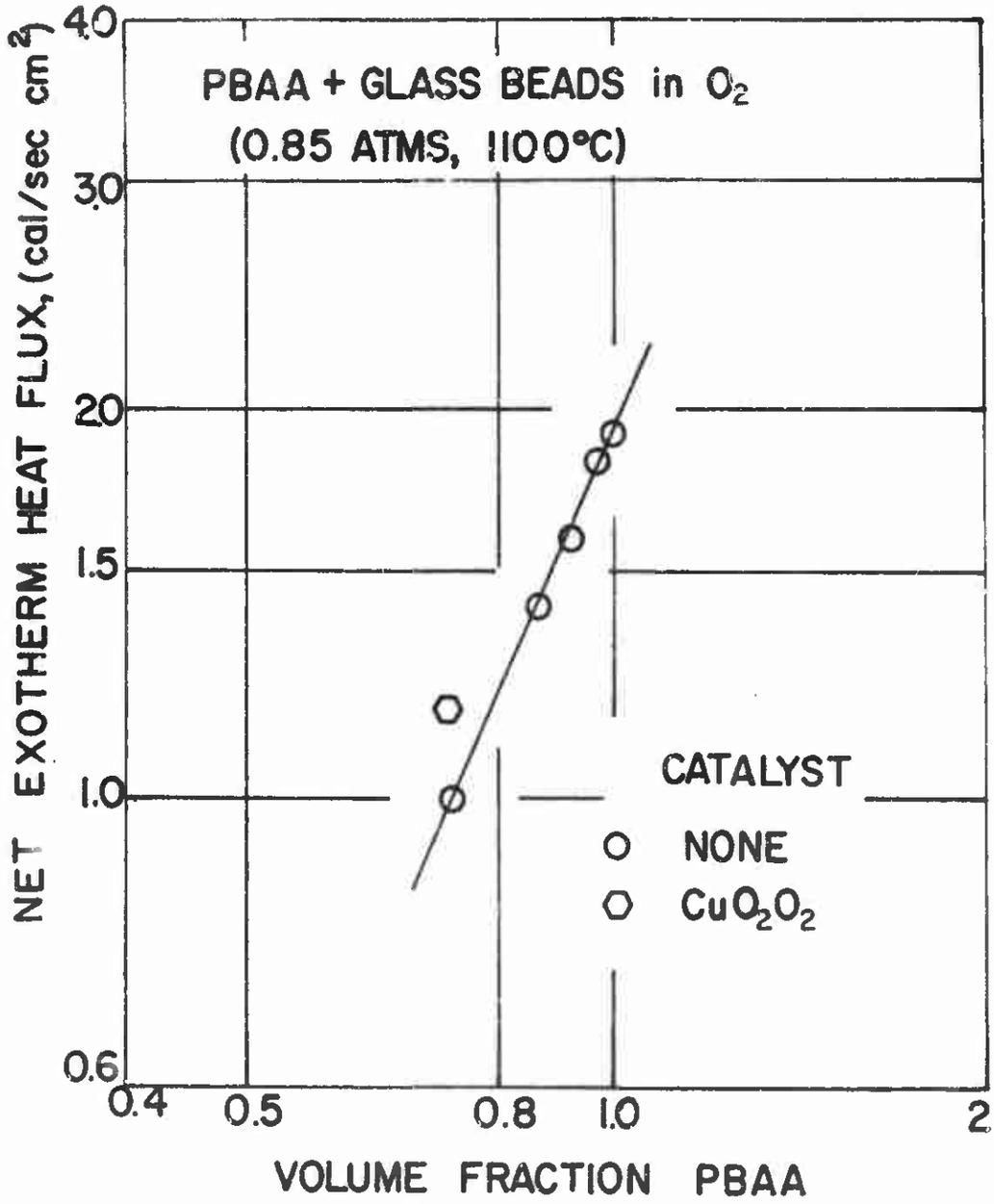

Fig. 42. -- Plot of net exotherm heat flux versus volume fraction of PBAA fuel-binder in the polymer at a furnace temperature of 1100°C and 0.85 atm oxygen.

polymers, the change of photocell temperature with the available PBAA binder is not severe, hence s can be approximately evaluated from the slope of Fig. 42. The calculated value for s is 2.2.

With PC polymer where (p) is constant, the rate of oxidative reaction becomes

$$\dot{r} \propto e^{-E/RT_{ph}} (p_{O_2})^n \ . \qquad \text{(VII-2)}$$

Mathematically the right values of E and n can be evaluated from the experimental data in the following manner. With an assumed value for n, a plot of log $[(\dot{r})/(P_{O_2})^n]$ versus $1/T_{ph}$ is made. When the best straight line is obtained, E is calculated, and a plot of (log $\dot{r}$ + E/RT_{ph}) versua log P_{O_2} is made to get n exactly. By this method E and n are found to be 19.2 kcal/g-mole and 1.52 respectively. From the values of n and s, we find that the oxidative reaction of polymer does not observe a simple kinetic order.

Polymers Containing Ammonium Perchlorate

Six AP-contsining polymers were investigated for their behavior in the chemically reactive environment of oxygen at 0.85 atm and 1100°C. Fig. 43 shows typical oscillograph records of the experiments. For calculating the surface temperatures at the times of exotherm and photocell light signal, two surface reaction terms were considered. One was assumed to approximate the heterogeneous reaction between oxygen and polymer, the other treated the reaction between polymer intermediates

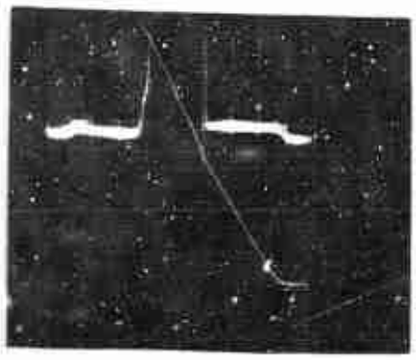

a. Run No. 23-1-23
w_{AP}: 8.8%

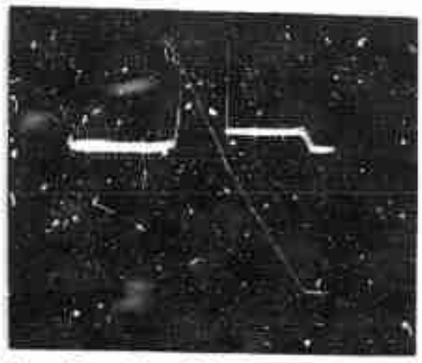

b. Run No. 24-1-22
w_{AP}: 8.8%

c. Run No. 36-1-23
w_{AP}: 19.4%

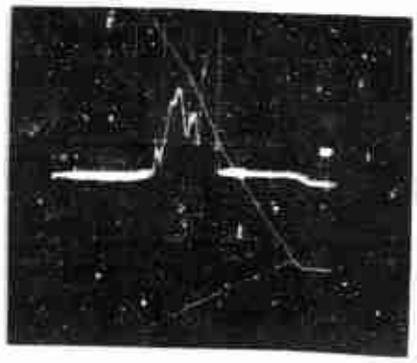

d. Run No. 37-1-22
w_{AP}: 19.2%

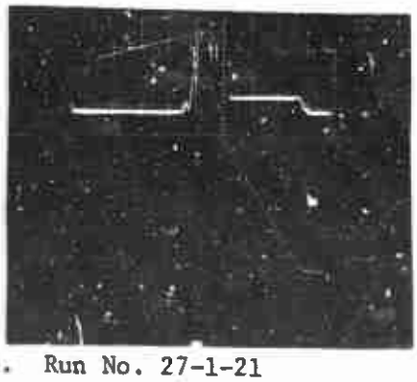

e. Run No. 27-1-21
w_{AP}: 48.5%

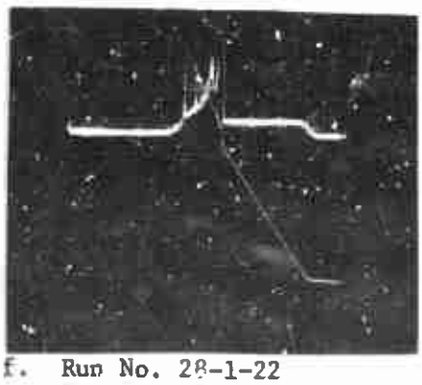

f. Run No. 28-1-22
w_{AP}: 47.3%

Fig. 43. -- Typical oscillograms of interface temperature (diagonal trace) and photocell traces for AP-containing polymers with (b,d,f) and without (a,c,e) copper chromite catalyst at 1100°C furnace temperature and 0.85 atm oxygen. Time base (right to left) is 0.5 sec/(div.) for all records. Vertical scale is 2.0 mv/(div.) for all records.

and the decomposition products of AP. The reason for addition of the latter reaction is that with AP in the polymer, all the photocell light signal in oxygen occurred at about the same time as the exotherm while a time difference is seen if AP is not present. The calculated results are shown in Table XXIX and are plotted in Figs. 44 and 45. Several phenomena are indicated from a study of these figures and tables of data in the appendix:

(a) The exotherm temperature of AP-containing polymer is generally higher than that for PC polymer (without AP). This observation suggests that AP plays no role in the initial stages of reaction between oxygen and the polymer. Also the exothermic reaction temperature is, on the average, 16°C higher than the temperature predicted from the data for polymer samples containing glass beads (inert constituent). It appears likely that at the same volumetric loading, less polymer surface is exposed when irregular AP is in the film than when the inert material is spherical glass beads.

(b) A comparison of the test results of AP-containing polymer in nitrogen and in oxygen shows a reduction in exotherm and photocell light signal temperature with oxygen. This indicates probably that oxygen attacks polymer before AP can supply oxidizing species and thus starts the chain of events earlier. This supports the view in Item (a).

(c) At all pressures the photocell break occurs almost immediately after the occurrence of the exotherm. This effect is in marked

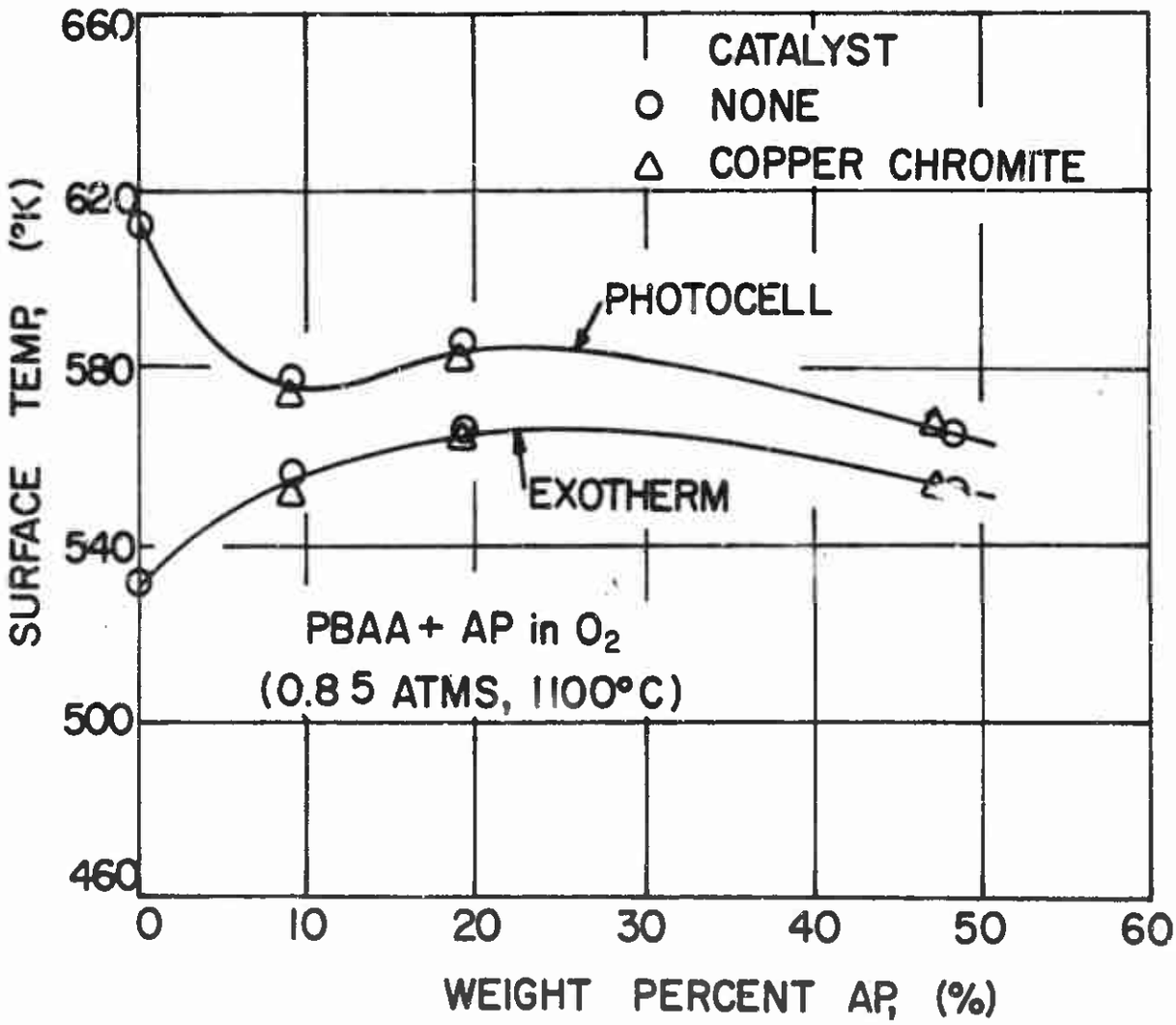

Fig. 44. -- Plot of characteristic surface temperatures versus AP levels in the catalyzed and uncatalyzed AP-containing polymers at a furnace temperature of 1100°C and 0.85 atm oxygen.

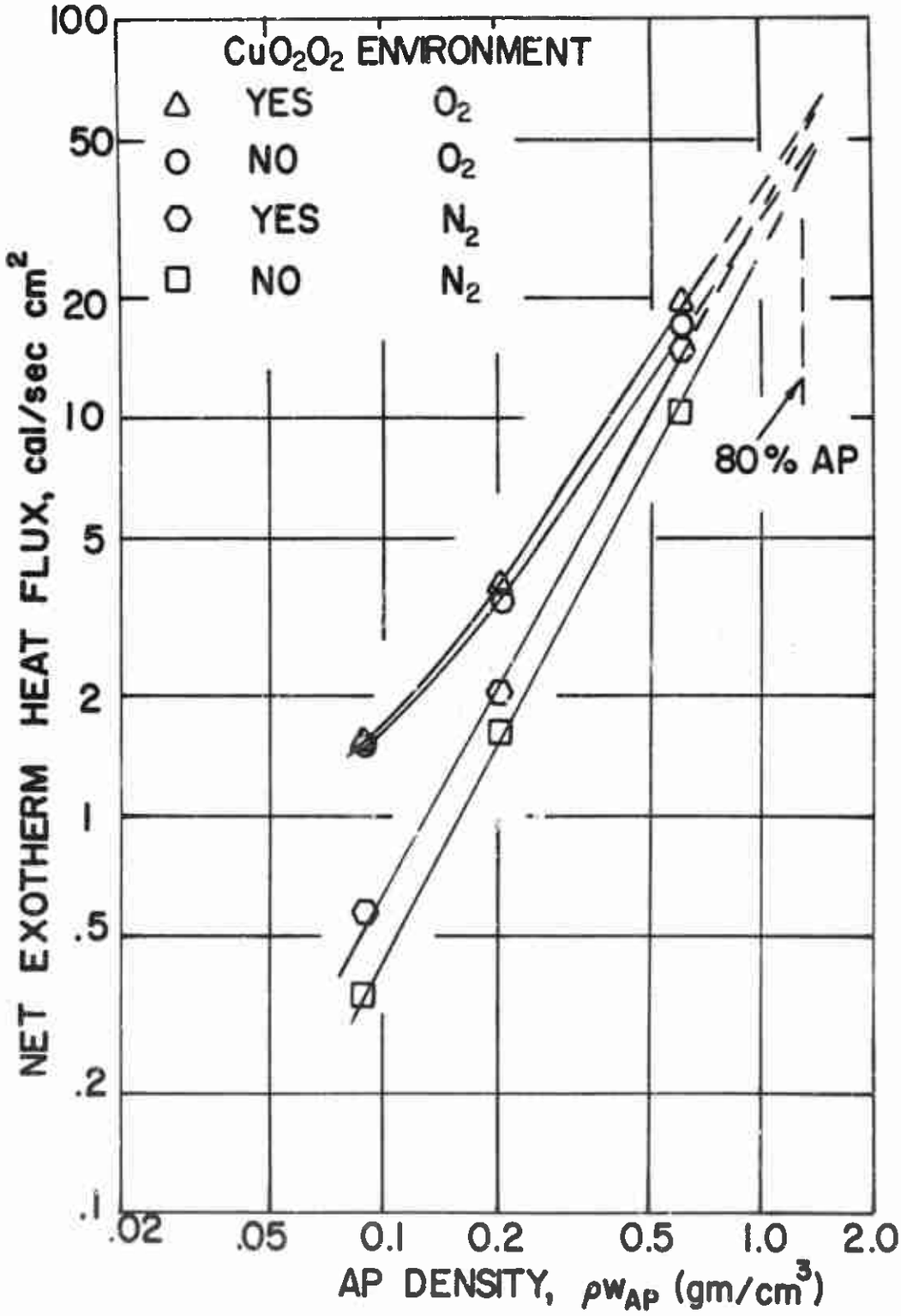

Fig. 45. -- Net exotherm heat flux as a function of AP density in AP-containing polymers. Furnace temperature, 1100°C. Pressure, 0.85 atm.

contrast to the pressure dependent time difference between the exotherm and photocell aignal observed for the PC polymer in oxygen. Loss of time lag between exotherm and photocell signal indicates that AP species become available immediately at the exotherm, then accelerate the later phases of reaction.

(d) In Fig. 44 we see that the exotherm temperature increases with AP loading for AP less than 20 per cent. This is apparently due to the dilution effect of AP. With AP loading bigger than 20 per cent, both exotherm and photocell light signal temperature decrease with increasing AP level. At these AP levels, probably the exothermic reaction of AP products and polymer intermediates is large enough to overtake the loss of available polymer surface.

(e) In Fig. 45 we see that the net exotherm heat flux of AP-containing polymers in oxygen heating increases, as in nitrogen heating, with the amount of AP per unit volume in the polymer. Unlike the nitrogen heating, the result in oxygen shows a pronounced curvature. The effect of copper chromite on the reaction in oxygen is also seen. This catalyst effect becomes more evident as the amount of AP (and slso the amount of catalyst) increases. A very important festure which is clear from this figure is that the effect of oxygen on the reaction of AP-containing polymers decresses as the smount of AP increases snd (if the extrapolation is permissible) dissppears ss the

amount of AP reaches the propellant level. This disappearance of O_2 effect as AP reactions become dominant confirms Keller's observation that the decomposition of AP is the key reaction in propellant ignition [28].

The effect of oxygen (furnace) temperature on the reactions of three AP-containing polymers, A09, A9C and A9I were studied at furnace temperatures of 950°C and 800°C. The significant reaction temperatures and net exotherm heat fluxes are shown as Table VIII. More data can be found in Tables XXX and XXXI.

TABLE VIII

SIGNIFICANT REACTION TEMPERATURES AND NET EXOTHERM HEAT FLUXES FOR LOW AP-CONTAINING POLYMERS AT 0.85 ATM OXYGEN AND DIFFERENT FURNACE TEMPERATURES

Material Code (Furnace Temp.)	Exotherm Surface Temperature	Photocell Light Signal Temperature	Net Exotherm Heat Flux
	°K	°K	cal/(sec)(cm)^2
A9C (1100°C)	552	577	1.54
A9C (950°C)	559	579	1.65
A9C (800°C)	550	571	1.72
A09 (950°C)	566	585	1.70
A9I (950°C)	553	570	1.61

Examination of the results in Table VIII shows no significant change of either exotherm or photocell light signal temperature at different

oxygen temperatures (furnace temperature). This is in marked contrast to the result for PC polymer at different oxygen temperatures. This indicates that AP species become available immediately at the exotherm which is started by oxygen-polymer heterogeneous reaction. This view is supported by the loss of time lag between exotherm and photocell light signal discussed on Item (c) on page 133. The nearly constant net exotherm heat flux is also attributed to the presence of AP species immediately at the exotherm. The effect of catalyst, either iron oxide or copper chromite in the quantities used, on the reaction of these materials is insignificant.

A09 (8.83% AP in the polymer) was investigated at a furnace temperature of 950°C and at three oxygen pressures. The significant reaction temperatures are shown as Table XXXI. A general lowering of the significant reaction temperature with increasing oxygen pressures was observed. A dropping of 20°C in the exotherm temperature and 35°C in the temperature of photocell light signal was recorded when oxygen pressure changed from 0.85 atm to 5 atm. The net exotherm heat flux is plotted in Fig. 46 as a function of total oxygen pressure. The slope of this plot was found to be 0.54. Because the exotherm temperature drops with increasing oxygen pressure, the reaction has a greater than 0.54 order dependence on oxygen.

Also plotted in Fig. 46 for comparison is the data of net exotherm heat flux of PC polymer in oxygen at 1100°C furnace temperature (Fig. 40).

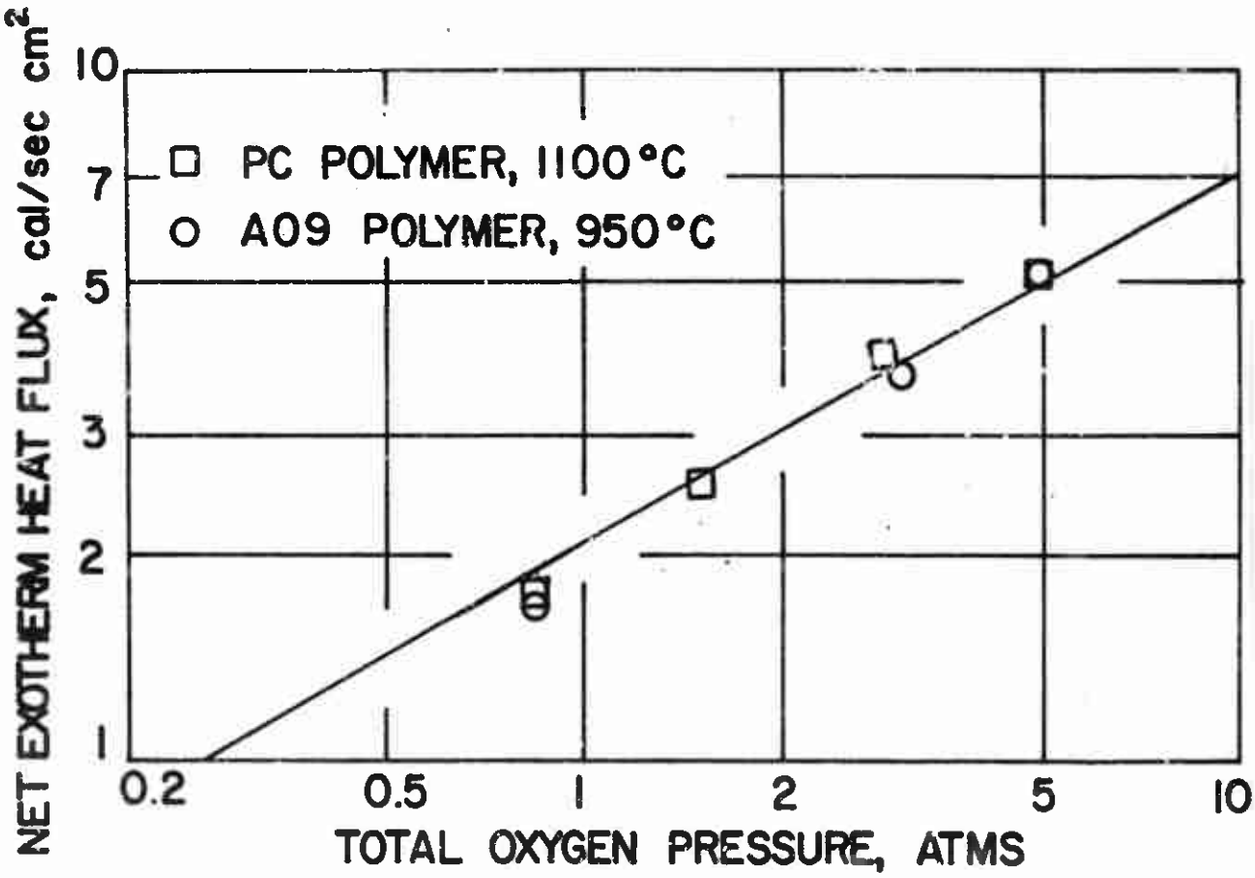

Fig. 46. -- Plot of net exotherm heat flux versus total oxygen pressure for A09 polymer at a furnace temperature of 950°C, and PCC polymer at a furnace temperature of 1100°C.

That the net flux increase during the exotherm (see Fig. 46) has the same pressure dependence for A09 at a furnace temperature of 950°C as for PC polymer at 1100°C, (though at a lower exotherm surface temperature) is regarded as a coincidence. That the form of the flux-pressure relationship is the same is probably not a coincidence. It indicates that in both cases, the initial exothermic process is reaction between polymer and oxygen.

CHAPTER VIII

IMAGING FURNACE EXPERIMENTS

Two series of experiments were carried out in the filament-imaging furnace. In one series, weight loss was determined as a function of energy input; in the other, the decomposition products were analyzed. In the weight loss experiments, four types of polymers, i.e., PC, PCC, A09, and A9C were studied in vacuum at two heating rates. PC and PCC polymers were also investigated under 0.85 atm helium and one heating rate to investigate a possible pressure effect. The vacuum tests were at an initial total pressure less than 5 mm Hg. The exact pressure was not measured.

Loss-in-Weight

In the imaging furnace, the area of uniform heat flux is very small. Sample size had to be correspondingly small, and weight loss was therefore extremely difficult to determine accurately. Fig. 19 shows a "before and after" test sample mounted on a copper strip.

The two heating rates used in this work were 21.5 cal/(sec)$(cm)^2$ and 10.3 cal/(sec)$(cm)^2$. The higher rate is more than four times the maximum used in the radiation furnace, and it closely approaches flux levels typical of propellant ignition and combustion processes. The

exposure times, controlled by a timer, ranged from 0.0 to 0.26 second for the higher heating rate and from 0.0 to 0.4 second for the lower heating rate.

Typical results of the experiments are plotted in Figs. 47, 48, and 49 with weight loss per unit area of exposure as ordinate, the exposure time as abscissa. Also marked on these figures are the times at which the surface reached the significant reaction temperatures in the radiation furnace experiments. Those marked times are good only for qualitative reference, because the significant reactions have been found to depend on heating rate, external pressure, etc. Tables XXXII, XXXIII, and XXXIV summarize the data. Several things can be observed from these figures:

(a) The rate of weight loss is small for short exposures and then increases rapidly as exposure time is increased. Apparently there is a temperature above which the degradation and vaporization become very rapid.

(b) Qualitatively speaking, all significant reactions occur at very early stages of weight loss. This provides a support to the mathematical analysis of experimental data in which the regression of material is neglected.

(c) After an initial weight loss of 2 or 3 mg/cm^2, a change to slower rates of weight loss is noted. This is possibly because part of the radiant energy is intercepted by pyrolysis products condensed on the inner face of the quartz tube which constitutes the wall of the test chamber. The condensation of

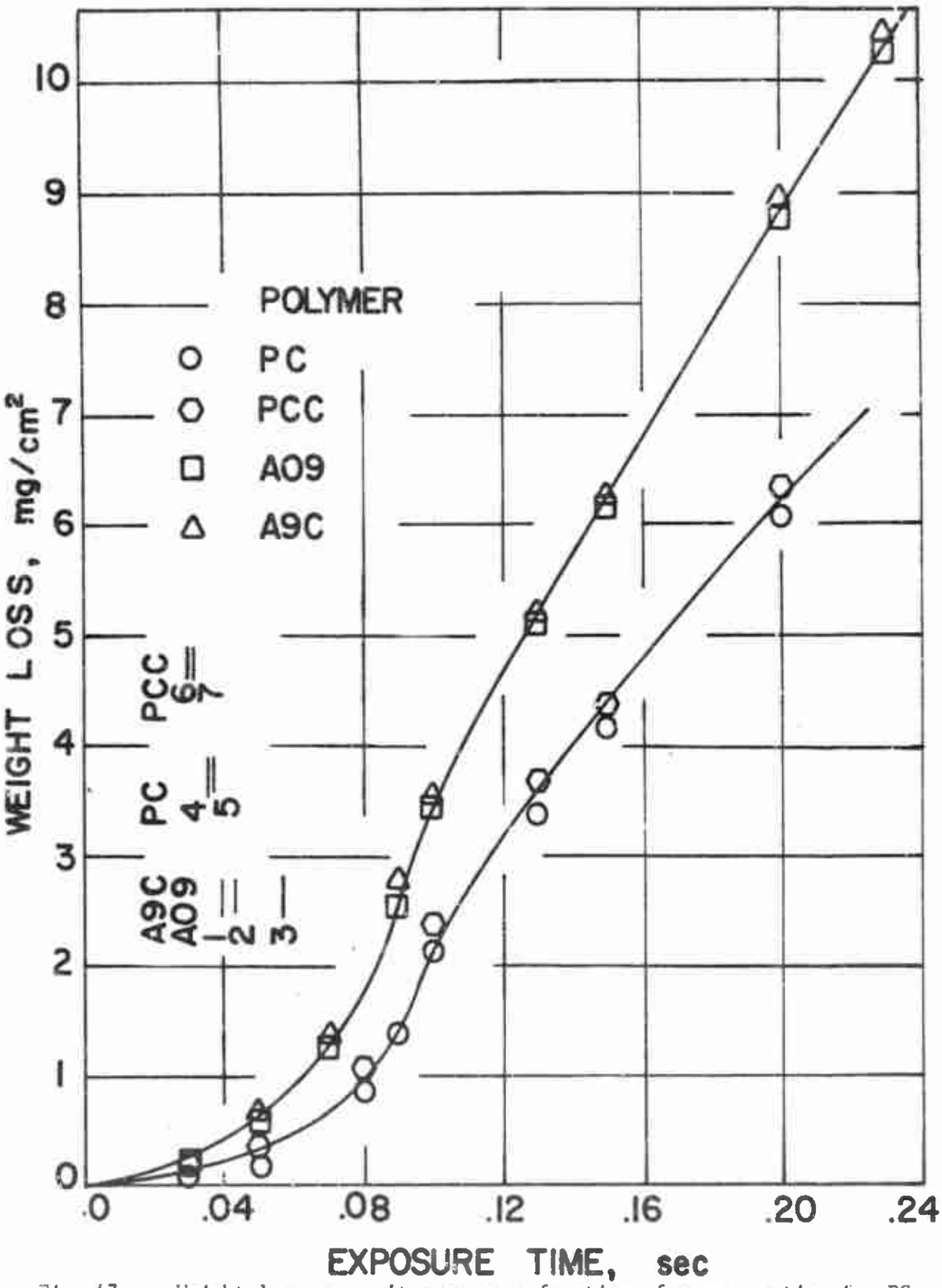

Fig. 47. -- Weight loss per unit area as a function of exposure time for PC, PCC, A09 and A9C polymers at 21.5 cal/sec cm^2 heating rate and vacuum by use of imaging furnace. The Arabic numerals from 1 to 7 show the corresponding times at this heating rate for significant reactions of these polymers in the radiation furnace at 1100°C. 1, 4 and 6 are endotherms. 2 is exotherm. 3, 5 and 7 are photocell signals. 1, 2 and 3 are data at 0.85 atm N_2. 4, 5, 6 and 7 are data in vacuum.

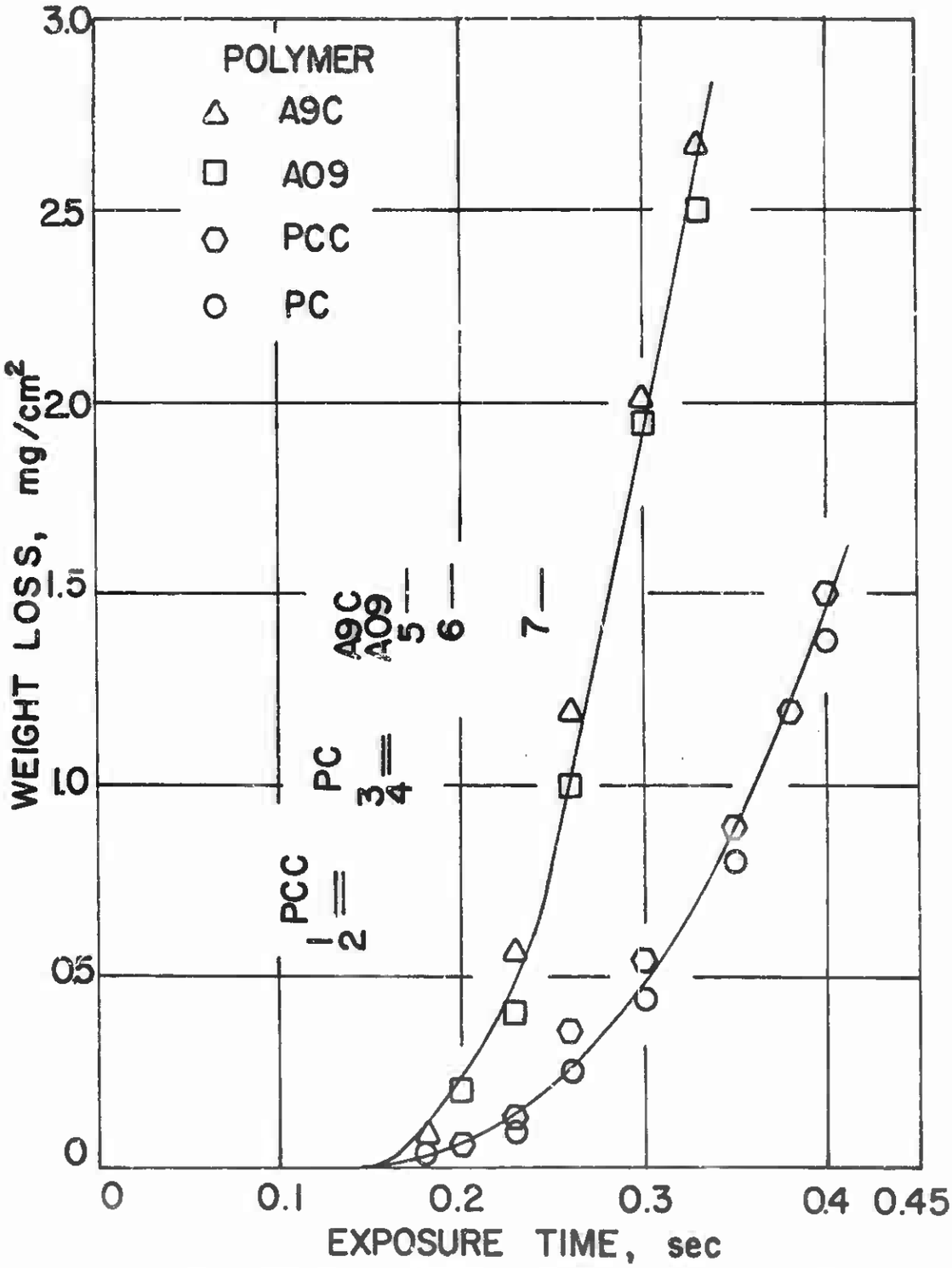

Fig. 48. -- Weight loss per unit area as a function of exposure time for PC, PCC, A09 and A9C polymers at 10.3 cal/sec cm^2 heating rate and vacuum by use of imaging furnace. The Arabic numerals from 1 to 7 show the corresponding times at this heating rate for significant reactions of these polymers in the radiation furnace at 1100°C. 1, 3 and 5 are endotherms. 6 is exotherm. 2, 4 and 7 are photocell signals. 1, 2, 3 and 4 are data in vacuum. 5, 6 and 7 are data at 0.85 atm N_2.

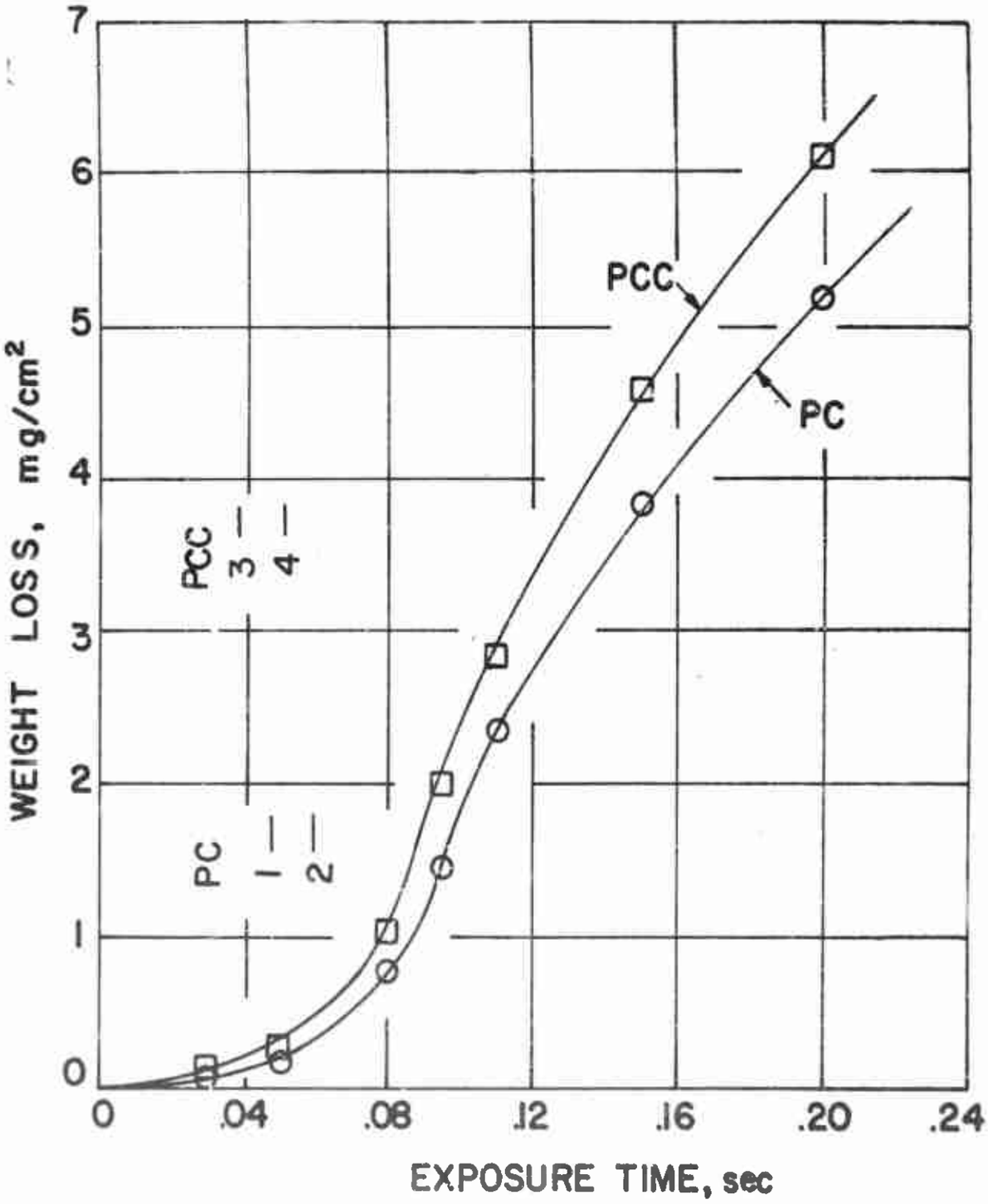

Fig. 49. -- Weight loss as a function of exposure time for PC and PCC polymers at a heating rate of 21.5 cal/sec cm^2 and 0.85 atm helium by use of imaging furnace. The Arabic numerals from 1 to 4 show the corresponding times at this heating rate for significant reactions of these polymers in the radiation furnace at 1100°C and 0.85 atm N_2. 1 and 3 are endotherms. 2 and 4 are photocell signals.

pyrolysis products on the wall was not found at the lower heating rate and therefore no inflection point on the weight loss curve was noted.

(d) Under vacuum there ia little difference in weight loss characteristica of catalyzed (PCC) and uncatalyzed (PC) polymer. However a 53°C difference of surface endotherm temperature existed between these two polymers in the radiation furnace tests. For PC polymer the examination of liquid products (to be discussed later) shows that there are many fine solid particles dispersed in the liquid. These particles may be undecomposed polymer fragments carried away from the surface by the gases evolved. These additional solid particles have compensated for the higher reaction temperaturea of PC polymer, therefore the weight loss rate of PC and PCC polymers in vacuum are about equal.

(e) For the same exposure, the weight losaes of AP-containing polymers are considerably larger than thoae of the PC and PCC polymers. Obvioualy a reaction between AP speciea and PBAA binder is taking place. See Figs. 47 and 48.

(f) Under 0.85 atm helium pressure and the same exposure, the weight loss of PC polymer is less than that of PCC polymer. No fine solid particles are found in the liquid from PC polymer. One pressure effect was apparently to suppress the ejection of undecomposed polymer fragments. Another was to raise the vaporization temperature of the volatile apecies formed from both polymers.

(g) Examination of the loss-in-weight results of both higher and lower heating rates shows that at the same total energy input the weight loss increases with the heating rate. This suggests that surface temperature is the most important factor in the reactions of pyrolysis.

The results of the weight loss experiments for PC and PCC polymers in 0.85 atm helium help to explain the results of radiation furnace tests for the same polymers. This discussion requires that the weight loss per unit area versus exposure time be converted to weight loss per unit area versus surface temperature. This can be done by use of the following one-dimensional heat transfer equation to calculate temperatures

$$\rho c \frac{\partial T}{\partial t} = k_s \frac{\partial^2 T}{\partial x^2} + Ae^{-E_a/RT} \quad . \qquad \text{(VIII-1)}$$

The boundary conditions are:

$$t = 0, \; T = T_o \quad ;$$

$$x = 0, \; -k_s \frac{\partial T}{\partial x} = \varepsilon f_s - \varepsilon o T^4 \quad . \qquad \text{(VIII-2)}$$

The results are shown in Table XXXIV and are plotted in Fig. 50.

No surface regression term was included in Eq. (VIII-1), because, first, only reactions before appreciable regression (<10μ) are of interest, second, we don't know how to calculate regressgion rate accurately and, third, no surface regression term was included in the

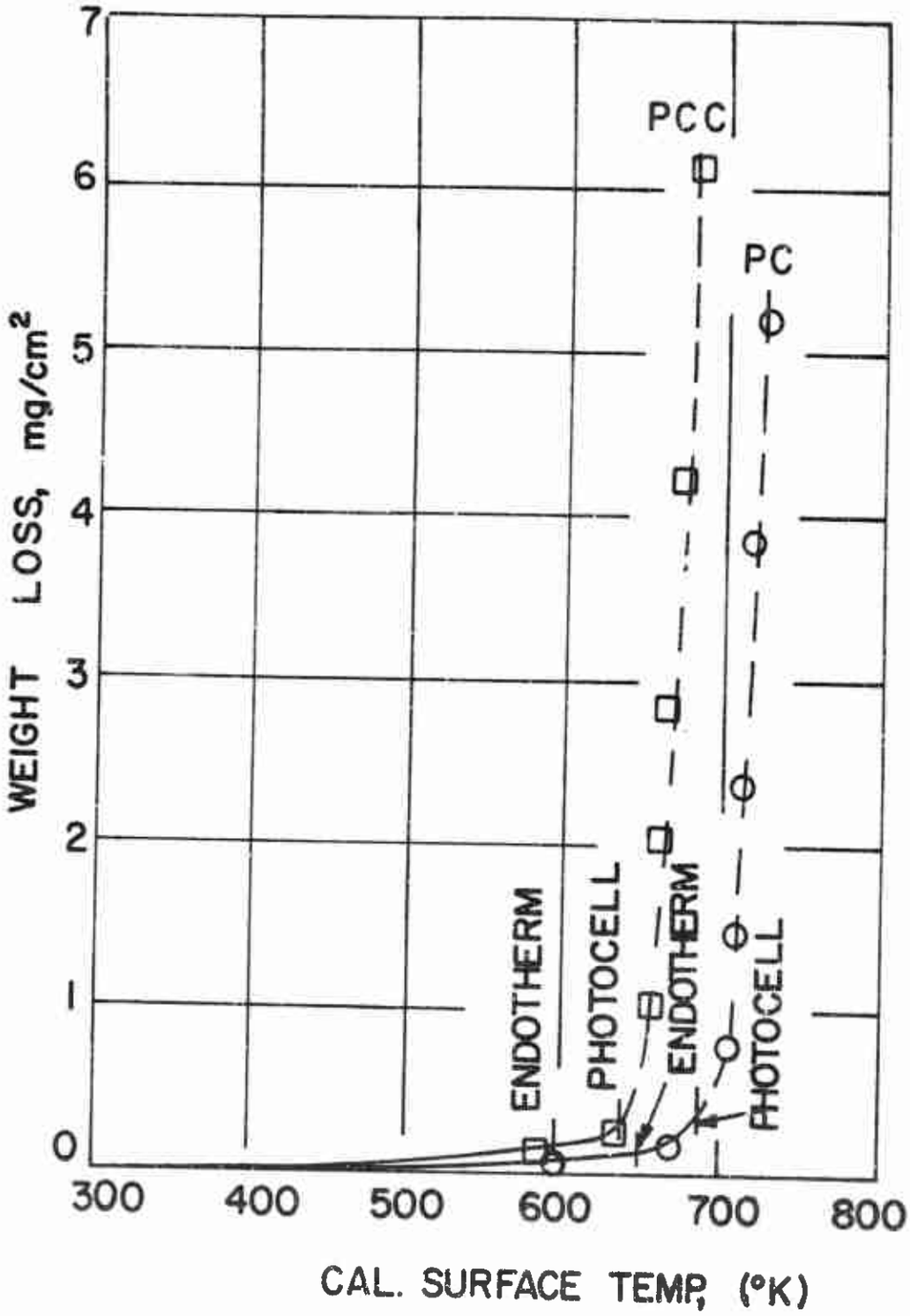

Fig. 50. -- Plots of weight loss per unit area versus calculated surface temperature for PC and PCC polymers at a heating rate of 21.5 cal/sec cm^2 and 0.85 atm helium.

analysis of the results of radiation furnace tests. In using Eq. (VIII-1) to obtain converted data for Fig. 50, the same set of kinetic parameters and surface emissivity as those used to analyze the results of PC and PCC polymers in the radiation furnace were used. To simplify the analysis all physical constants were assumed to be constant at room temperature values.

Also plotted in Fig. 50 are the significant reaction temperatures of PC and PCC polymers in the radiation furnace experiments at 0.85 atm nitrogen and 1100°C. Take PC polymer for instance. At the endotherm temperature of 648°K, little weight loss is noted (Fig. 50), but the weight loss becomes significant when the surface temperature reaches 705°K. (The assumption of a constant value of the product $k\rho c$ may result in overestimating these two temperatures.) In the radiation furnace test, the surface temperature corresponding to a sharp photocell response is 685°K. The nearness of these two temperatures is added evidence of close relationship between the appreciable weight loss and the steep photocell break, and the difference is in the direction expected as a result of the difference in heating rates.

Relative Amounts of Gaseous and Liquid Products

Another series of weight loss experiments was carried out to determine the relative amount of gaseous and liquid products at 0.85 atm helium and a heating rate of 21.5 cal/(sec)(cm)^2. Only PC polymer was studied. The liquid products were collected on a thin glass plate (cover glass), 2.2 cm by 2.2 cm, placed in front of the test sample.

Because of the added cover glass, 10.6% of energy flux was abosrbed and reflected, and the final available heat flux to the surface of test sample was reduced to 19.2 cal/(sec)(cm)^2. Table IX shows the exposure time, total weight loss per unit area, and weight per cent of liquid and gaseous products.

TABLE IX

RELATIVE AMOUNT OF LIQUID AND GASEOUS PRODUCTS AS A FUNCTION OF EXPOSURE TIME. Heating rate: 19.2 cal/(sec)(cm)^2. Polymer: PC. Pressure: 0.85 atm helium. Total weight of sample ≈ 140 mg/cm^2.

Exposure Time	Total Volatilization	Wt. Fraction Based on Total Volatilization[1]	
		Liquids	Gases[2]
sec	mg/cm^2	%	%
0.03	0.056	7.2	92.8
0.05	0.164	13.3	86.7
0.07	0.6	33.6	66.4
0.09	1.18	41.9	58.1
0.11	2.33	49.7	50.3
0.13	2.77	53.9	46.1
0.15	3.3	57.0	43.0
0.20	4.55	61.6	39.4

1 All the products are volatile at the temperature of pyrolysis.

2 The weight of gas product is obtained by subtracting the measured weight of liquid product from the total weight loss.

Fig. 51 is a plot of exposure time versus the relative amount of gaseous and liquid products. From this figure it can be seen that the ratio of gaseous to liquid products decreases as exposure time increases. Initially nearly all the vaporized materials are gaseous in nature. When exposure time reaches 0.2 sec only 39.4% of gaseous products is obtained. Also plotted in Fig. 51 are the calculated surface temperature history of PC polymer at the experimental heating rate. (No chemical reaction is considered.) From these plots we see that for temperatures below 700°K which is about the temperature of an appreciable rate of volatilization, more than 85% of vaporized products are gaseous at room temperature.

Analysis of the Decomposition Products From Imaging Furnace

The products of decomposition from PC, PCC, A09, and A9C polymers were investigated by gas chromatography, mass spectrometry and infrared spectrometry. All samples analyzed were the decomposition products of pyrolysis experiments at a heat flux of 19.2 cal/(sec)(cm)^2 and under vacuum, except for PC polymer in which both atmospheric (0.85 atm) pressure and vacuum were used. Two exposure durations, i.e., 0.2 and 0.4 sec, were used. However, the quantity of products collected from the 0.2 sec exposure duration was found to be too small to be analyzed. Analyses are reported only for tests at the 0.4 second exposure time.

After each pyrolysis test, the test chamber was filled with helium to 1.65 atm, and left at this pressure for five minutes to ensure that the gaseous products were throughly mixed. Then a valve was opened and

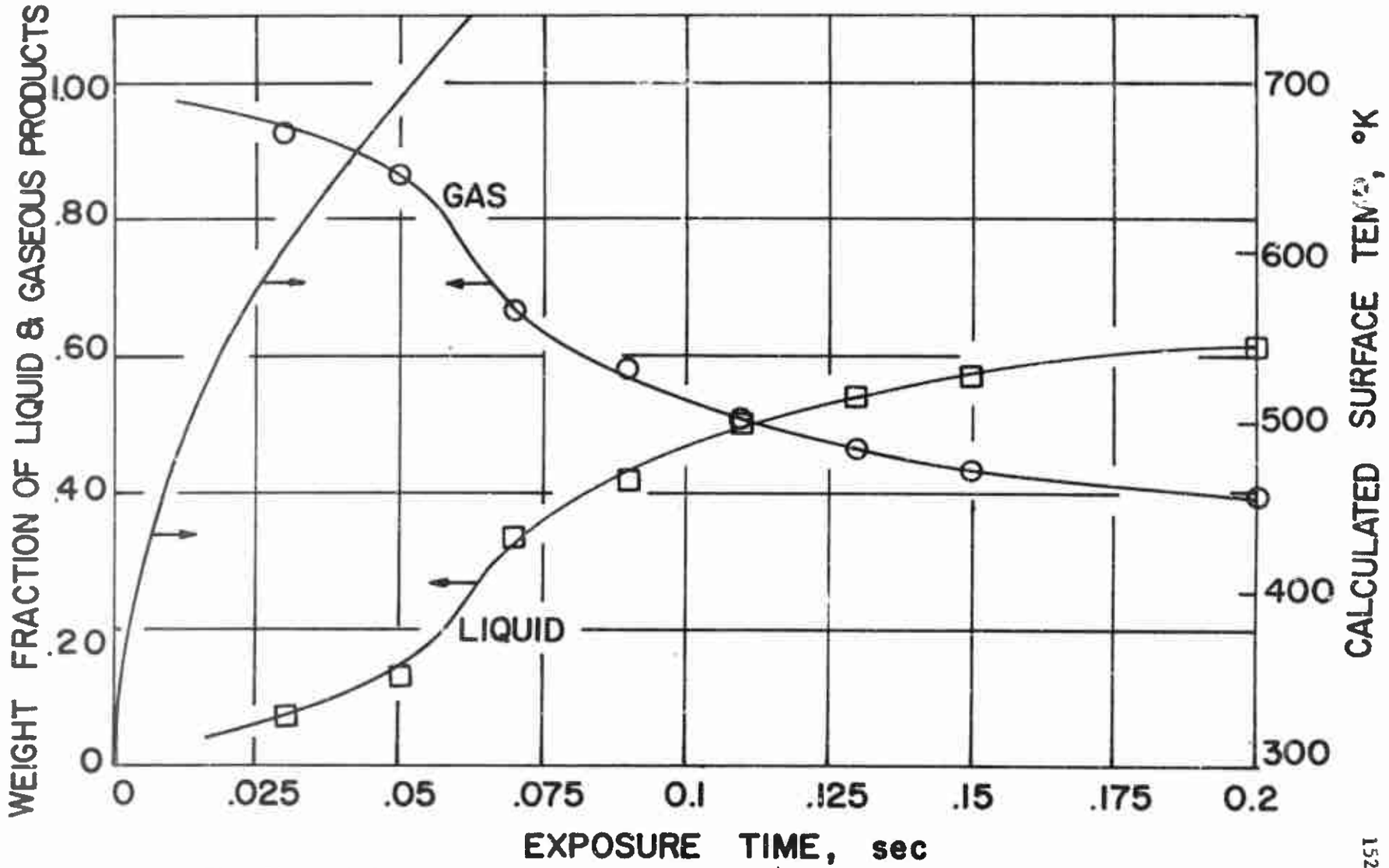

Fig. 51. -- Relative quantity of liquid products and gaseous products as a function of exposure time for PC polymer at a heating rate of 19.2 cal/sec cm^2 and 0.85 atm helium.

the gas products passed into a sample collecting chamber which had been previously evacuated. These gas products were analyzed by use of a Model 154 Perkin-Elmer Vapor Fractometer. These results are discussed below.

Results of Gas Chromatographic Analysis

The first step in this study was to select a proper column for the separation of gaseous products with reasonable resolving power and speed of analysis. Four Perkin-Elmer columns, designated as A, R, L, and M and which were recommended for hydrocarbon analysis, were investigated. Tests showed that the R column which is filled with Ucon polyglycol LB-550-X was most suitable for this system. The second step was to calibrate the selected column at the selected operating condition using standard mixtures. Two standard mixtures were used, "Hydrocarbon Mixture No. 37" and "Hydrocarbon Mixture No. 40", which were purchased from Phillips Petroleum Company. The gas chromatograph records for these two mixtures using the column R are shown in Fig. 52. Tables XVII and XVIII give identification numbers for these peaks and the certified analysis of these mixtures.

Chromatograph records for gaseous products in vacuum from PC, PCC, A09, and A9C polymers are shown in Figs. 53 and 54. With the aid of the standard calibration, peaks were identified as shown in the same figures. From these records it is apparent that the gaseous products obtained from these four polymers are very similar. The first peak of each chromatograph is ambiguous, because it occurs at the same place as

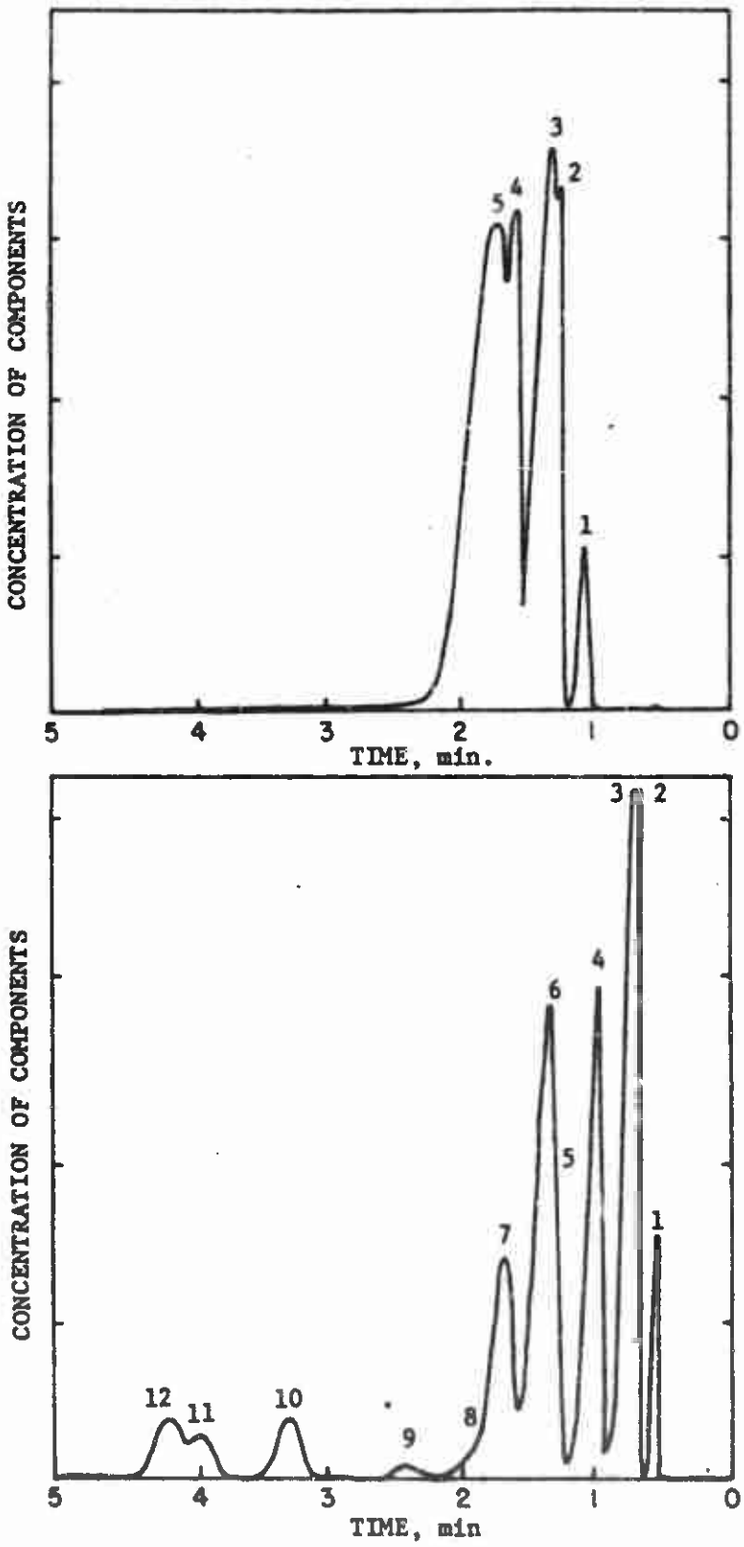

Fig. 52. -- Gas chromatographs of hydrocarbon mixture No. 37 (top) and hydrocarbon mixture No. 40 (bottom). Both are from Phillips Petroleum Company.

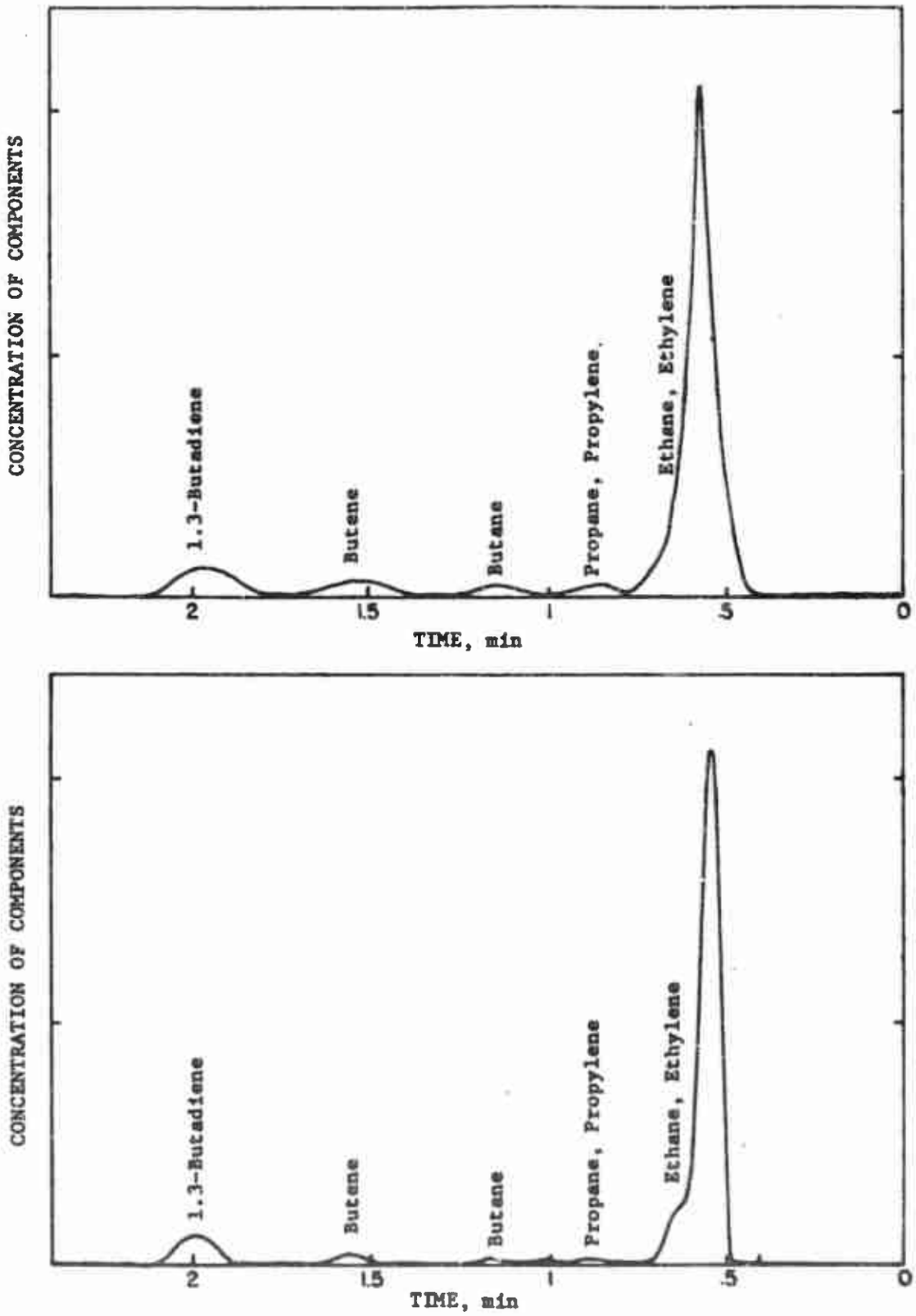

Fig. 53. -- Gas chromatographs of gaseous products in vacuum from PC polymer (top) and PCC polymer (bottom).

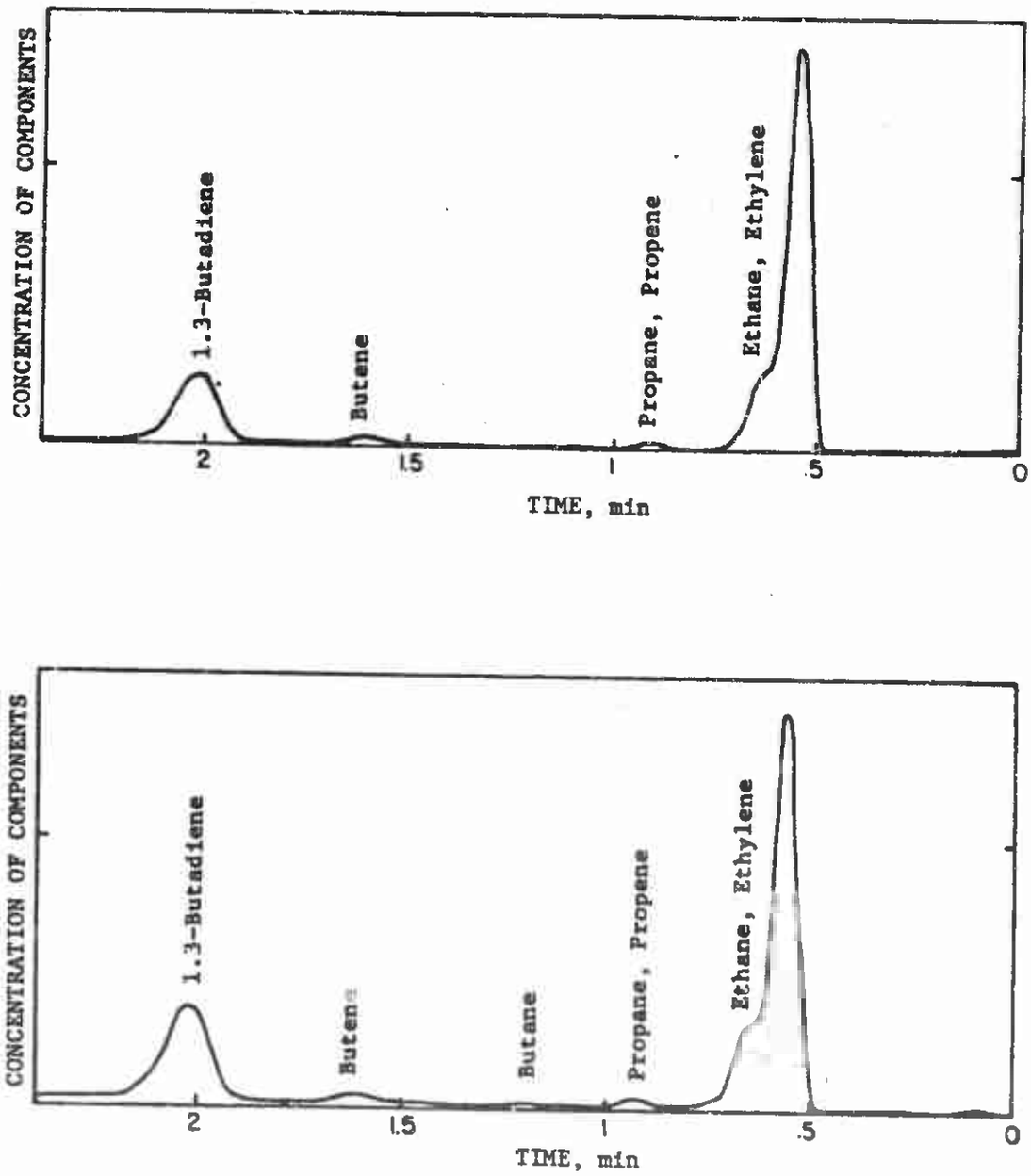

Fig. 54. -- Gas chromatographs of gaseous products in vacuum from A09 polymer (top) and A9C polymer (bottom).

the peaks for CCl_4 and CO_2. These two gases could be present in the gaseous mixtures (CCl_4 having been used to clean the test chamber and sample collecting chamber). Other peaks are identified as ethane, ethylene, propane, propylene, butane, betene, and 1, 3-butadiene. Excluding the first peak which may have contamination of CCl_4 etc., butadiene comprises 30 to 50 per cent of gas products.

An attempt was made to support the chromatographic analysis with mass spectrometry. The gaseous products were also analyzed by a conventional mass spectrometer. Unfortunately the results of products analysis show no difference from the background analysis because the mass of collected gas products was too small for the instrument employed.

The results of gas analysis are limited in value because (a) the exposure time interval (0.4 second) over which products were collected for analysis was much longer than the time required for the endotherm and the initial rapid gas evolution, and the samples therefore represent the cumulative contributions from these and subsequent processes, and (b) the quantity of gas in each sample was very small, making an accurate analysis very difficult.

Liquid Products

The liquid part of the pyrolysis products was collected on a glass plate placed in front of the test sample. Photographs are shown in Fig. 55. Because so little product was collected ($\approx$ 1 mg), no simple technique was found to determine the average molecular weight of the liquid samples.

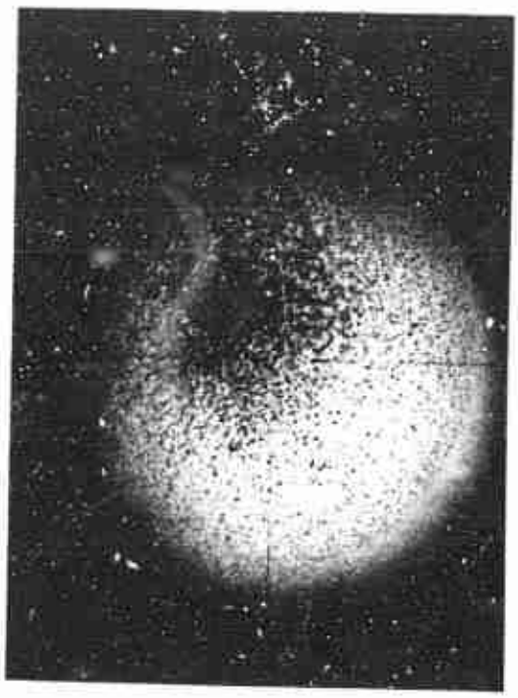

a. PC polymer

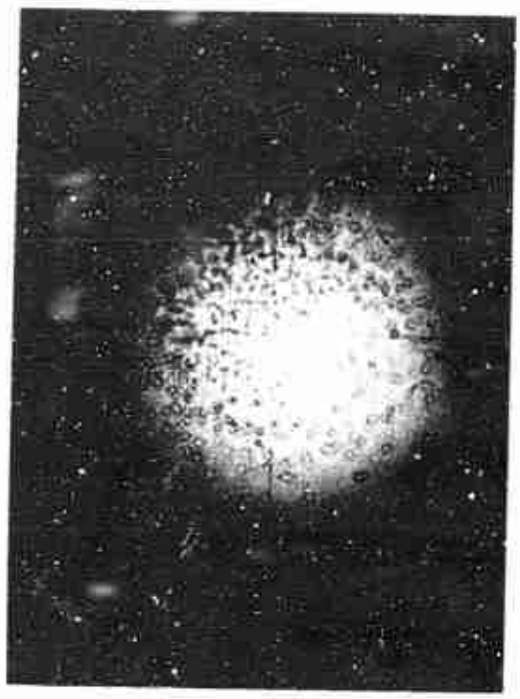

b. PC polymer
Pressure: 0.85 atm helium

1 cm

c. PCC polymer

Fig. 55. -- Pictures of liquid pyrolysis products from PC, PCC, A09 and A9C polymers by use of imaging furnace. With the exception of b all the rest were the products under vacuum (<0.1 in Hg helium).

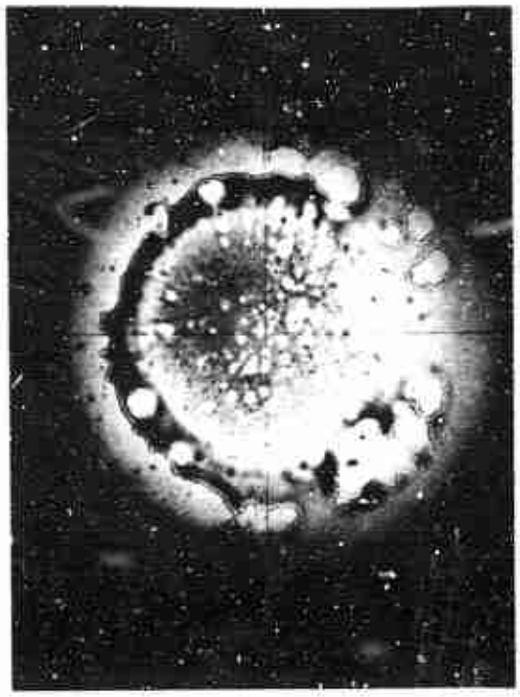

d. A09 polymer

e. A9C polymer

1 cm

Fig. 55. -- (continued).

Fortunately the liquid products collected was barely enough to be analyzed by infrared spectrometry. In addition to PC, PCC, A09, and A9C materials, the uncured PBAA plus epoxy resin, and finally a dispersion of ammonium perchlorate crystals were studied using an infrared spectrometer. Though the capability of the infrared spectrometer is limited to the identification of chemical groups, the differences in the absorption regions before and after pyrolysis should provide useful information about the roles of various polymer ingredients in the pyrolysis process.

In general there are two differences between the spectra of pyrolysis products and those of original materials, change of absorption regions and change of absorption intensities. The former is related to the change of chemical structure, and the latter to the change of the relative amount of the same chemical groups.

The interpretation of infrared spectra is based on the so called "group frequencies" which related molecules have in common. The absorption frequencies of a given group are the frequencies of vibration of bonds within the group together with combinations and harmonics of these frequencies. These frequencies are subject to interference by the neighboring atoms and the orientation of these atoms. The intensities are strongly affected by the cell length, the kind of solvent used, etc.. These things, altogether, make the interpretation of infrared spectra for a complicated molecule a rather difficult effort. The explanations made in the following paragraphs are based on the information available.

Epon Resin 828 is one of the constituents in the PBAA binder. Since the understanding of original material is always very helpful to the interpretation of pyrolysis result, the Epon Resin was analyzed by infrared spectrometer, and the result shown in Fig. 56(a). Fig. 56(b) shows the infrared spectrum obtained from the reaction product of bisphenol A and epichlorohydrin by Harms [19]. For the convenience of easy comparison, the corresponding significant absorption bands in the spectra of Epon Resin and Harm's compound are indicated by the same symbol just below the tips of the peaks. Examination of these two spectra shows a very close similarity between them. There are only a few places where the peak characteristics are different. One peak at 3500 cm^{-1} which is moderately strong in the Harm's spectrum appears very weak in the spectrum of Epon Resin 828. The other peak at 1120 cm^{-1} which is sharp and strong in the Harm's spectrum also appears very weak in the spectrum of Epon Resin 828. This wave number is probably one of the in-plane bending frequencies of = CH. Still another peak which is also strong and sharp in the Harm's spectrum but is almost completely missing in the spectrum of Epon Resis 828 is found at 870 cm^{-1} wave number. However, at 900 cm^{-1} there is a peak characteristic moderately strong and sharp in the spectrum of Epon Resin 828, yet the peak is weak in the spectrum of Harm's compound. Despite the few differences, we recognize that the basic structure of the Epon Resin 828 must be very close to that represented by Harm's formula,

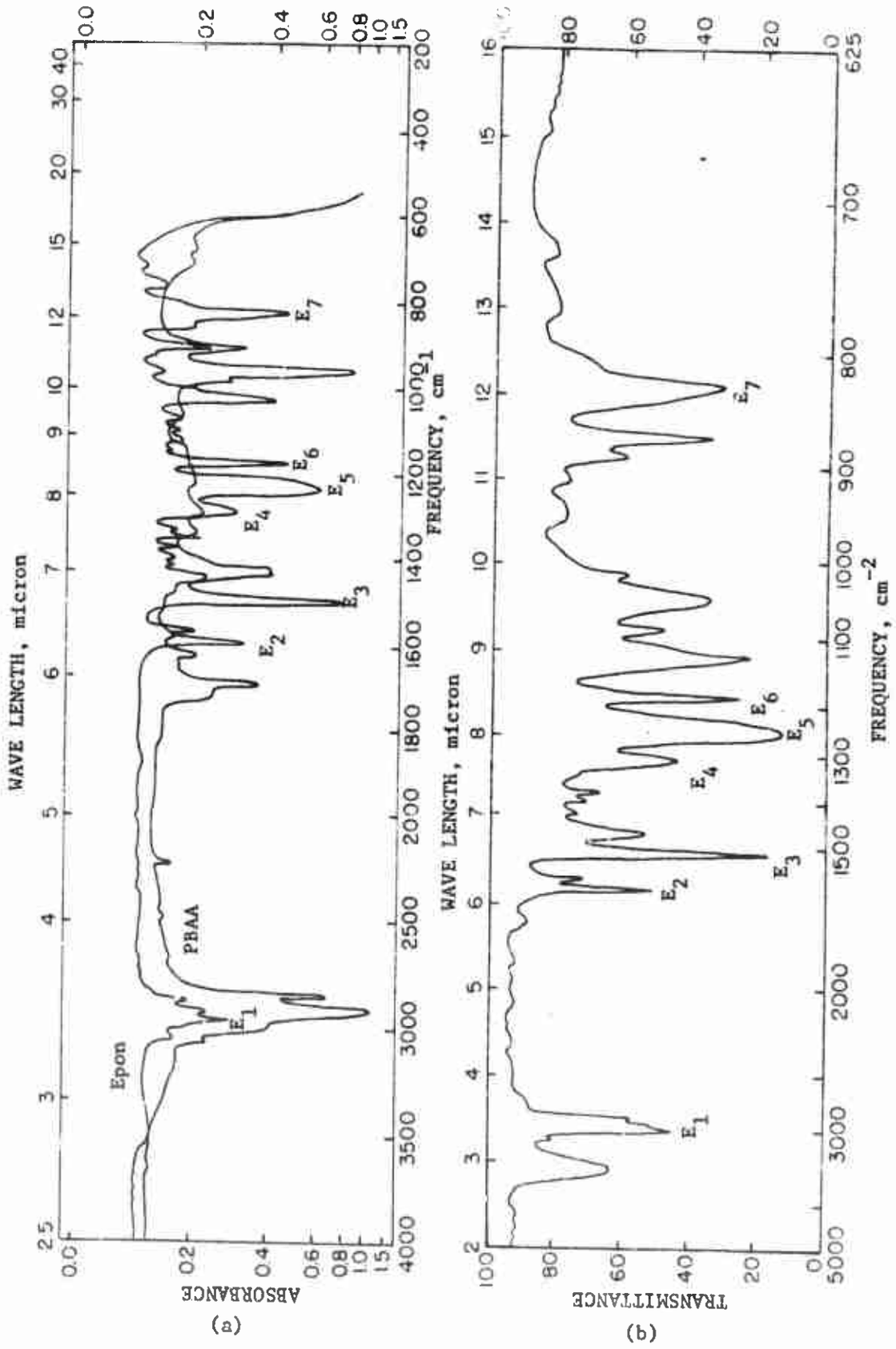

Fig. 56. -- Infrared absorption spectra of Epon Resin 828 and PBAA (a) and Harm's compound (b).

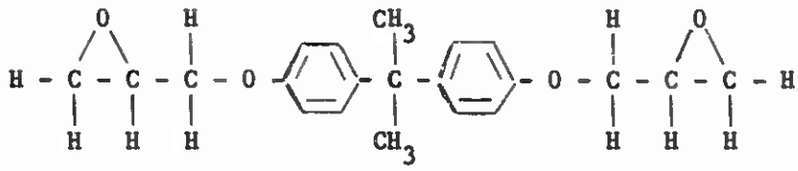

The interpretation of other significant absorption frequencies is discussed in the following. The absorption band at 3040 cm^{-1} is the stretching frequency of = CH in the benzene ring and CH in the epoxide and the bands at 2960 cm^{-1} and 2870 cm^{-1} are the stretching frequencies of C-H in $C-CH_3$, and the band at 2920 cm^{-1} is the stretching frequency of C-H in methylene group $>CH_2$. The absorption frequencies of C=C are split into three bands lying between 1500 cm^{-1} and 1600 cm^{-1}. These three frequencies and the one at 3040 cm^{-1} for =CH are the characteristic absorption frequencies of benzene ring. Between 1050 cm^{-1} and 1280 cm^{-1} lie the in-plane bending frequencies of =CH. It is possible that the absorption band for =C-O coincides with one of the bending frequencies of =CH at 1240 cm^{-1}. There are three out-of-plane bending frequencies of =CH lying between 750 cm^{-1} and 900 cm^{-1}. The absorption bands at 820 cm^{-1} and 900 cm^{-1} are probably also for the carbonyl group C-O in the epoxides.

The infrared spectrum of PO polymer is shown in Fig. 57(a). The spectrum was obtained from a microtome-cut film, 50 microns in thickness. Also shown in Fig. 57(a) is the spectrum of uncured PO polymer. The spectrum of PBAA which is one of the two main constituents of uncured PO polymer is shown in Fig. 56(a), alongside of Epon Resin, which is the other constituent. The spectrum of Epon Resin 828 has been discussed previously.

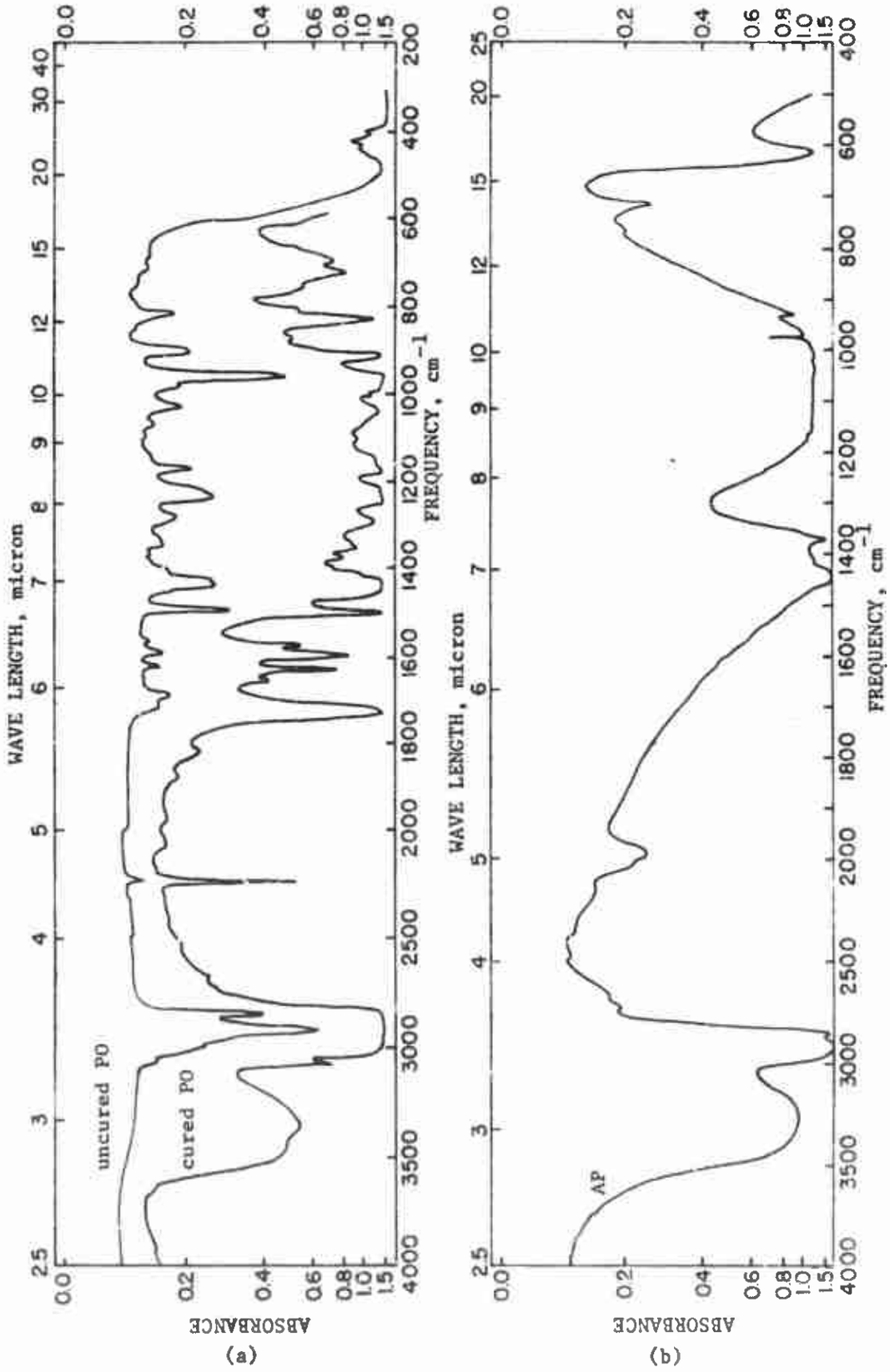

Fig. 57. -- Infrared absorption spectra of uncured and cured PO polymer (a) and AP (b).

Before we compsre the spectra of cured and uncured polymers, the spectrum of PBAA will be examined. At wave numbers 2920 cm^{-1} and 2840 cm^{-1} lie the stretching freqtency of $>CH_2$. A sharp amall peak sppearing at 2230 cm^{-1} is either stretching frequencies of C≡C, C≡N or both. C≡C probably comes from excess condensation during the polymerization and C≡N is possibly coming either from the impuritiea of acrylic acid or from slow reaction of polymer with the atmospheric nitrogen. A peak at 1720 cm^{-1} is a characteristic of csrbonyl group in esters or ketones. Two bands of C=C sre found at 1625 cm^{-1} and 1695 cm^{-1}. At 1430 cm^{-1} lie the in-plane bending frequencies of =CH and $>CH_2$. Out-of-plane bending frequencies of =CH and CH_2 are found at 950 cm^{-1} and 900 cm^{-1} respectively.

By examining the spectrum of the cured PO polymcr and the spectra of its constituents, we find that although the patterns of absorption regions look similar, there are still several notable differences:

(1) At wave number of 3360 cm^{-1}, there is an additional absorption region in the spectrum of cured polymer which may be due to the presence of O-H, resulting either from the absorption of moisture and oxygen from the stmosphere during or after the polymerization, or bonded O-H group.

(2) An incresse in the absorption intensities at 700 cm^{-1} in the cured polymer may be due to the intensification of some out-of-plane bending vibration of =CH and $>CH_2$, because of the polymerization.

(3) There is a great increase in the absorption intensity at 2230 cm^{-1}. This indicates an increase in the population of C≡C or C≡N as a result of polymerization.

(4) The increase in the absorption intensity at 1720 cm^{-1} indicates an increase of carbonyl group in the polymer which may have resulted from the absorption of oxygen from the atmoaphere. Since the polymerization was carried out in the absence of oxygen, the oxygen may get into the polymer during the long hours of exposure in the air (half a day to one day waiting for the space in the sealed oven) before polymerization in the inert environment.

There are only four major differences in the infrared spectra of the liquid decomposition products of PC and PCC polymers. (Fig. 58(a)) All of them fall between wave numbers 820 cm^{-1} and 1030 cm^{-1}. The absorption band at 1030 cm^{-1} is completely missing for the copper chromite catalyzed polymer, PCC. Weaker intensities are recorded for PCC polymer in the other three absorption bands, 820 cm^{-1}, 900 cm^{-1} and 950 cm^{-1}. These frequencies are corresponding to the out-of-plane bending vibrations of =CH in the benzene ring and out-of-plane bending vibrations of $>CH_2$ and =CH in the PBAA. During the pyrolysis the effect of copper chromite apparently is to break more of the benzene ring and double bonds in the PBAA.

A comparison of the spectra of the pyrolysis products of these two types of polymers and uncured PBAA binder indicates differences at three abaorption regions:

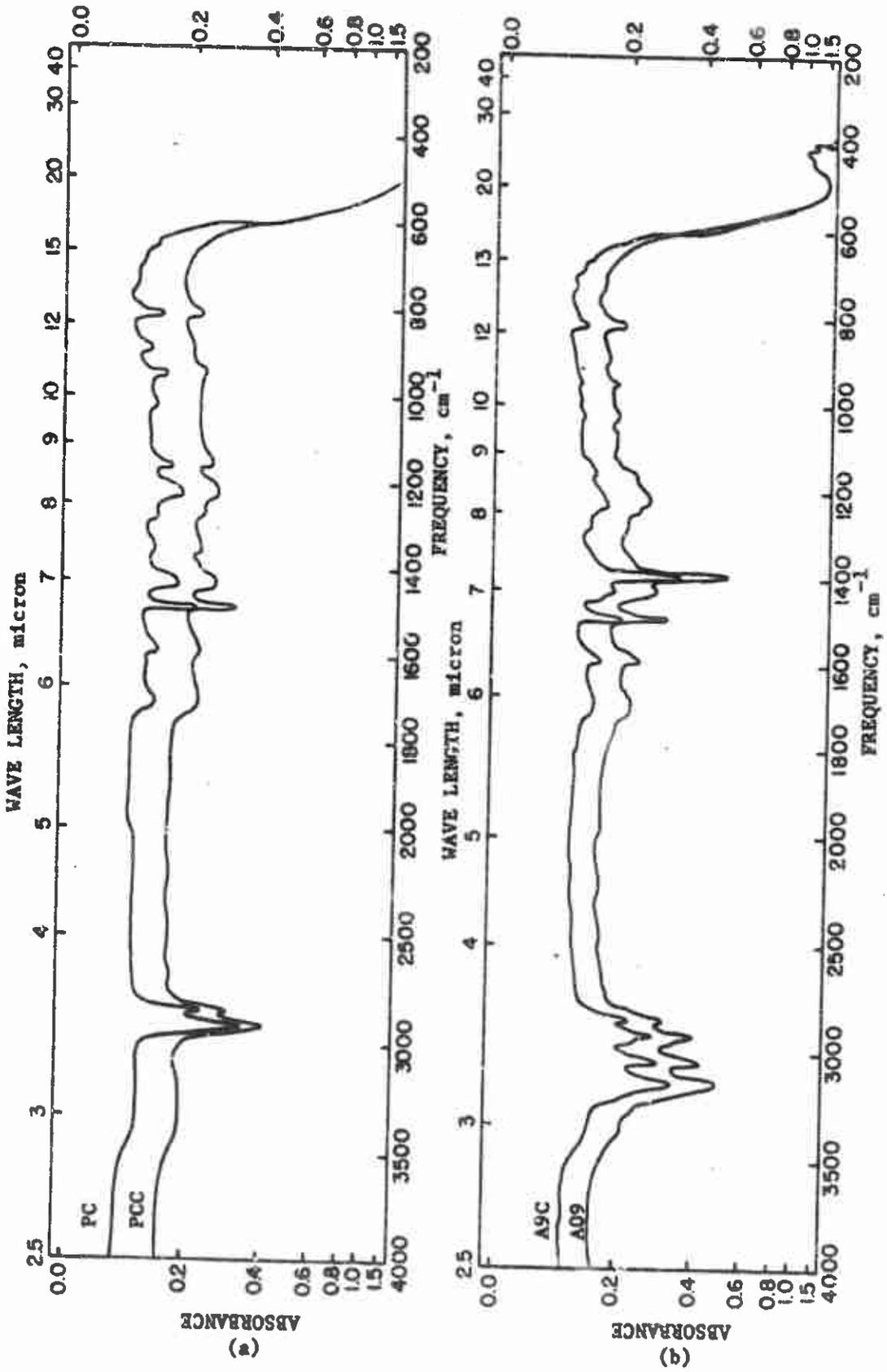

Fig. 58. -- Infrared absorption spectra of liquid products from PC polymer, PCC polymer (a) and A9C polymer, A09 polymer (b).

(1) The pyrolysis products show no absorption at 2230 cm^{-1}, indicating a disappearance of C≡N or C≡C.

(2) Also absent in the spectrum of pyrolysis products is the absorption band at 1625 cm^{-1} which is one of the frequencies of C=C.

(3) The intensity at 950 cm^{-1} for the pyrolysis products decreases appreciably. This is the out-of-plane bending frequency of =CH.

These differences seem to indicate an increase in the degree of ssturation in the liquid psrt of products as a result of pyrolysis.

Shown in Fig. 58(b) are the spectra of the liquid decomposition products of AP-containing polymers with and without copper chromite catalyst. The spectrum of AP crystal is shown in Fig. 57(b). There is no difference that can be regarded as significant between these two polymers. Since in the catalyzed AP-containing polymer the copper chromite always amounts to only one-twentieth of AP, the quantity of catalyst is very small. Apparently the character of the decomposition products depends much more on the catalyst-polymer ratio than on the catalyst-AP ratio.

It is very interesting to compare the spectrum of the liquid decomposition products of AP-containing polymers with that from the polymer without AP. In the AP-containing polymers three additionsl absorption bands can be found at 3150 cm^{-1}, 3050 cm^{-1} and 1395 cm^{-1}. These frequencies represent the N-H stretching and bending vibrstions in the primary amide group $CONH_2$. This group is obviously the result of AP-polymer interaction. The

mechanism of the interaction is possibly the reaction between NH_3 from AP and ester or ketone carbonyl which is considered a weak link in the polymer chain. Part of the considerably heavier weight loss for these two AP-containing polymers than for the polymer itself discussed earlier is probably attributed to this interaction. Apart from these three additional bands just discussed, the rest of the absorption bands are similar to the spectra of polymer without AP.

The results of product analysis discussed on the previous pages are summarized in the following. In the gas analysis a significant amount of butadiene was found, indicating that some unzipping reaction is going on during the pyrolysis process. Other products found were butane, butene, propane, propylene, ethane, ethylene, etc., indicating that there is also random scission during the pyrolysis. The analysis of liquid products shows that the catalyst, copper chromite, has an effect on the decomposition reaction, apparently by promoting attack or rupture at points of unsaturation. The liquid products of AP-containing polymers show that the effect of AP may not be wholly due to oxidizing species. NH_3 may participate in polymer decomposition. From the experiment conducted in this work we cannot be sure whether the $-NH_2$ attachment occurred at the time of pyrolysis or after the pyrolysis products deposited on the glass sample collector.

CHAPTER IX

CONCLUSIONS

Since the ignition and combuation reactions in composite propellants are very complex, the conclusions drawn from this work are possibly only valid for the PBAA-AP system studied; generalization is perhaps not justified.

Although it is recognized that the time acale of teat in thia work only approaches the time scale of interest in ignition and burning, much ignition data would seem to indicate that the same mechanism is followed for ignition times ranging from 1 sec to 1 msec. Thus it is thought that the resulta of this work are valid representations of the processes which occur in ignition and burning. The reaction temperatures quoted in the following apply to a surface heating rate of about 100°C per aecond.

With these qualifications several concluaiona are apparent.

(1) Although the thin film technique was difficult to perfect and mounting procedures must be developed separately for each type of polymer, significant information can be obtained.

(2) The pyrolysia of the PBAA fuel-binder occura in two obvious stagea. The first stage is characterized by a sudden decreaae

of temperature rising rate indicating a significant endothermic reaction. During this first endotherm, probably most of the energy received at the surface is used to decompose the polymer and only a small quantity of material escapes from the polymer surface. In the second stage a vigoroua vaporization process occurs at the polymer surface. The surface temperature difference between the appearance of the endotherm and the start of vaporization depends upon the total external preasure. Both characteristic temperatures are pressure dependent.

(3) The vaporization at the PBAA surface at significant rates has the attributes of an equilibrium process. The calculated latent heats for the vaporization process (15.7 kcal/g-mole for PC polymer) are very close to the values predicted from either the Trouton's rule (14.8 kcal/g-mole) or the Kistyakowsky's equation (15.3 kcal/g-mole) for the observed vaporization behavior of non polar materials.

(4) The addition of a copper chromite burning rate catalyst to the PBAA polymer significantly affects the decomposition reactions. The surface temperatures at which both the endotherm and vigorous vaporization occur are decreased by almost 50°C. The lower estimated latent heats and the decrease in the vaporization temperature indicate that smaller fragments are produced in the presence of the copper chromite. Such an effect on the decomposition reaction was not observed when iron oxide, also a burning rate and ignition catalyst, was added to the polymers.

(5) The addition of even small quantities of AP to the polymer significantly reduces the decomposition tempersture and greatly increases the rate of polymer decomposition at a given tempersture. A strong reaction between AP and PBAA (or between early products of decomposition) is apparent.

(6) The decomposition reaction of polymer films contsining less than 10 per cent AP includes an endothermic reaction at about 330°C which may be sssociated with polymer decomposition assisted by AP or AP products. This endothermic rsction is followed by a strongly exothermic reaction as the temperature is increased. At higher AP levele the endothermic reaction wss not detected by this thin film techniques.

(7) The decomposition of the polymer films containing AP was influenced by the presence of oxygen. At low AP levels the oxygen is the dominsnt reactive agent and the AP acts almost only as a diluent in the polymer. At higher AP levels both oxygen and AP interacted with polymer to produce the reaction temperatures lower thsn those observed in the presence of each alone. At AP levels commonly used for propellants, the AP influence predominates.

(8) The gaseous fractions of decomposition products are very similar for the catalyzed and uncatalyzed PBAA polymer and AP-containing polymer. The liquid products are also found to be quite similar. The r tion temperature is greatly different

for these materials, therefore it is rather difficult, by uee of the analytical methods available, to relate the thermal character of the decompoeition reactions to the pyrolysie products.

(9) The most important conclusion is recognized by the coneideration of the magnitude of the reaction temperatures of the polymer and the AP-PBAA films. Since the presence of AP drastically reduces the reaction temperature and increases the rate of polymer decomposition, it is obvious that the reaction of prime importance is that between AP (or AP decomposition products) and the polymer (or polymer decomposition products). The decomposition reactions of the polymer alone are almost only of academic interest. All the individual ingredients in a PBAA-AP composite propellant do not decompose as pure constituents, and the interaction reactions determine the character of the ignition response of a propellant and probably strongly affect the characteristics of the steady-state combustion.

If the assumption is granted that the heat flux measured by the copper disk calorimeter after a strong exothermic reaction is closely related to the exothermic heat flux at the test film surface, several interesting effects are noted.

(1) For AP-containing polymers in nitrogen, the magnitude of the net exothermic heat flux increases with increasing the quantity of AP per unit volume of test sample. The magnitude of this flux is about 11 cal/(sec)(cm)^2 at 0.85 atm at 50 weight per cent

AP loading for uncatalyzed sample and about 15 cal/(sec)(cm)^2 for a similar sample containing copper chromite catalyst (one-twentieth of the amount of AP). The catalyst effect is obvious.

(2) For AP-containing polymer films in oxygen, the magnitude of the net exothermic heat flux also increases with increasing quantities of AP per unit volume of test sample. The magnitude of this flux is higher than that in nitrogen. Obviously oxygen has taken part in the reaction. There is also a slight catalyst effect on the reaction, though less so than that in nitrogen. The magnitude for uncatalyzed sample is about 17 cal/(sec)(cm)^2 at 0.85 atm oxygen at 50 weight per cent AP, and for catalyzed sample 20 cal/(sec)(cm)^2.

(3) In Fig. 45 we see that the effect of oxygen on the reaction of AP-containing polymers decreases as the amount of AP in the polymer increases and disappears as the amount of AP reaches the propellant level. This disappearance of the O_2 effect as AP loading goes up confirms Keller's observation [28].

The analysis of decomposition products as related to other information indicates the following.

(1) The detailed mechanism of the AP-PBAA interaction is not completely understood. However, the infrared analysis shows an existence of $-CONH_2$ groups in the liquid decomposition products from AP-containing films. This may indicate an attack on the carboxyl group in the PBAA binder by NH_3, which is one of the AP decomposition products.

(2) For copper chromite-catalyzed materials it is suggested that the important factor appears to be the catalyst to PBAA ratio rather than the catalyst to AP ratio. At low AP levels (the amount of catalyst always amounts to one-twentieth of AP) the difference of reaction temperatures between catalyzed and uncatalyzed materials is negligible; however, a 20°C difference in the reaction temperature is noted at 50 weight per cent AP level. The addition of iron oxide catalyst to the AP-PBAA resulted in a similar reduction in the reaction temperature at higher AP levels. Since both the copper chromite and iron oxide used are known to be effective ignition catalysts [28], the effect of catalyst at low AP levels may be quite different from its effect in propellants.

(3) The results of the ignition experiment in oxygen for PBAA binder and glass bead-containing polymers strongly suggest that the reaction between the polymer and oxygen begins with a heterogeneous oxidative reaction which is followed by a homogeneous gas phase reaction which leads to ignition. The reaction appears to be dependent on the total oxygen pressure to the 1.5th power and on the available polymer surface to the second power. The whole process very likely involves polymer radical fragments.

APPENDIX A

THERMAL PROPERTIES OF VARIOUS POLYMERS AND PROPELLANT-LIKE MATERIALS

Determination of Thermal Properties

Thermal properties of PBAA binder with and without copper chromite catalyst and thermal diffusivity of ammonium perchlorste were measured by L. S. Bouck and were reported on the "Technical Report on Ignition and Combustion of Solid Propellant", AFOSR 62-99, Department of Chemical Engineering, University of Utah. The properties of other materials used in this work were calculated from Bouck's values and published data on AP, copper chromite, iron oxide and carbon black. (See footnote of Tabls XI for manufaturers and sources of published data on physical properties.) The measurement techniques for the above two basic polymers and the methods of calculation for the properties of other materials are discussed below. Table XI summarizes the thermal properties of these materials. Table X gives their chemical compositions.

Density

Catalyzed and uncatalyzed PBAA binder without carbon black were measured by water displacement. An experimental accuracy of $\pm$ 2% is anticipated. The densities of other polymers were calculated from the densities of their constituents, considering no change of volume.

Heat Cepacity

The haat capacities of the two basic polymers were datermined et two temparature by use of a Dewar-flask calorimeter. The calorimeter was calibrated by means of copper bars of known heat capacity, and calorimeter temperature changes were recorded to the nearest 0.01°C with a Beckman differential thermometer. The initial sample temparatura was approximately 95°C, and the final sample temperature was about 25°C. The anticipated accuracy is ± 3%. The heat capacities of othar materials were calculatad from the heat capacities of constituents.

Thermal Diffusivity

An unsteady state technique was used to determine the thermal diffusivity of catalyzed and uncatalyzed polymer. Cylindrical samplas of these materials were prepared with fine thermocouples mounted in their geometric centers. These cylinders were quickly immersed in an agitated bath. The bath temperature was different from the initial cylinder temparature. The center temperature-time relationship was recorded and was used to calculate the sample diffusivity in the manner described below.

If a plot is made of tha logarithm of the rates of the difference batween the cylinder center temperature and the bath temperature to the initial temperature difference against linear time, it is found that after a short time the plot became a straight line. During this period [page 228, 11] we have

$$\frac{v-v_o}{v_b-v_o} = G_o \exp\left\{-\alpha t(\gamma_1{}^2 + \beta_1{}^2)\right\} , \qquad \text{(A-1)}$$

where v, v_o, and v_b are respectively the center temperature, initial temperature and bath temperature; α is the material thermal diffusivity; t is time and G_o is a time-invariant constant. The constants γ_1, and β_1 are respectively the smallest roots of the equations,

$$\gamma \ell_c \tan\gamma \ell_c = \frac{h\ell_c}{k_s} , \qquad \text{(A-2)}$$

and

$$r_c \beta J_1(r_c \beta) = \frac{hr_c}{k_s} J_o(r_c \beta) , \qquad \text{(A-3)}$$

where r_c is the cylindrical radius, ℓ_c the half-cylinder height, k_s the solid thermal conductivity and h the surface heat transfer coefficient between the surface and agitated bath (assume constant over the surface).

The surface heat transfer coefficient was determined by immersing a 2.5 cm o.d. by 5 cm high copper cylinder in the agitated baths. In the case of copper, the terms $\frac{h\ell_c}{k_s}$ and $\frac{hr_c}{k_s}$ are so small that a limiting form of Eq. (A-1) which neglects the temperature gradient in the solid can be used. In the agitated water bath h was found to be 0.025 cal/(cm)(sec)(°C). Sample position and agitation was controlled to ensure that these same values would apply in the tests on polymers.

In the case of the thermal diffusivity determinations on the polymers, $\frac{hr_c}{k_s}$ and $\frac{hl_c}{k_s}$ were greater than 100, and the roots of Eq. (A-1) are γ_1 = 1.57 and β_1 = 2.40. These values are essentially independent of h or k_s; and the thermal diffusivity can be evaluated directly. In these tests the initial solid temperature was 95°C and the bath temperature 25°C.

The thermal diffusivities of other materials were calculated from the equation

$$\alpha = \frac{k_s}{\rho c}$$

The calculation of thermal conductivity k_s is discussed in the following section.

Thermal Conductivity

The thermal conductivity of catalyzed and uncatalyzed polymer was calculated from the volumetric loading and the thermal conductivities of the constituents by use of the Maxwell equation [14],

$$\frac{k_s}{k_a} = \frac{2 + \nu - 2\eta(1-\nu)}{2 + \nu + \eta(1-\nu)} \quad .$$

Where ν is the ratio of the thermal conductivities of the discontinuous phase to that of the continuous phase, η is the volume fraction of the discontinuous phase, and k_a is the thermal conductivity of the continuous phase.

When there are more than two solids present in the polymer, the thermal conductivity is calculated by considering only one solid at a time.

APPENDIX B

THE NUMERICAL SOLUTION TO EQUATION (VI-1)

Eq. (VI-1) was used to convert the temperature history measured by copper disk to a temperature history for the surface of films. For convenience the heat conduction equation and its boundary conditions are reproduced as follows:

For $0 < x < \ell$ (see Fig. 20 for physical model)

$$\rho c \frac{\partial T}{\partial t} = k_s \frac{\partial^2 T}{\partial x^2} + Ae^{-E_a/RT} . \tag{B-1}$$

The boundary conditions are that for

$$t = 0,\ T = T_o ; \tag{B-2}$$

$$x = 0,\ -k_s \frac{\partial T}{\partial x} = \varepsilon f_s + Be^{-E_b/RT} + Ce^{-E_c/RT} - L_{rs} + G_c ; \tag{B-3}$$

$$x = \ell,\ -a_e k_s \frac{\partial T}{\partial x} = al\rho' c' \left(\frac{dT}{dt}\right)_{x=\ell} + L_v + L_d + L_{rb} . \tag{B-4}$$

Where

x = distance from the surface of the test film, cm.

A,B,C = pre-exponential factors of condensed phase reaction and surface reactions, $cal/(cm)^3(sec)$ for A, and $cal/(cm)^2(sec)$ for B and C.

E_a, E_b, E_c = Activation energies of condensed phase reaction and surface reaction, cal/g-mole.

ε = surface emissivity, 0.9 by assumption.

a_e = exposure area, cm^2.

a = area of copper disk gage, one side only, cm^2.

ℓ = thickness of test film, cm.

L = thickness of copper disk, cm.

ρ, ρ' = densities of test film and copper disk, g/cm^3.

c, c' = heat capacities of test film and copper disk, cal/(g)(°C).

L_{rs}, L_{rb} = rates of heat loss through radiation from the surface of test film and back of copper disk, cal/(sec)$(cm)^2$ for L_{rs}, and cal/sec for L_{rb} .

L_d, L_v = rates of heat loss through conduction and convection, cal/sec.

G_c = rate of energy gain at test film surface through convection, cal/(sec)$(cm)^2$.

L_{rs} and L_{rb} can be evaluated from Stefan-Boltzmann law of radiation. Assuming that the test sample in the radiation furnace facing a black body enclosure, we have the rate of heat loss through radiation

$$L_{rs} = \sigma \varepsilon T_s^4 \tag{B-5}$$

and $$L_{rb} = \sigma \varepsilon_c a(T_i^4 - T_o^4) . \tag{B-6}$$

Since

$$\sigma = 1.354 \times 10^{-12} cal/(cm)^2 (°K)^4 (sec) ,$$

$$a = 1.33 \ cm^2 ,$$

ε_c = emissivity of back face of copper disk gage, 0.6 by assumption,

then $L_{rb} = 1.08\text{x}10^{-12}(T_i^{\,4} - T_o^{\,4})$, (B-6s)

where T_i is the temperature of copper disk gage.

Except for the thermocouple wires there was no physical contact of the copper disk with other objects. Most conduction loss is through these wires. These wires are quite long and well insulated; and since the temperature history of copper disk, when exposed to constant heat flux, is almost linear with time, the conduction loss can be evaluated by considering these wires as two semi-infinite body with the surface temperature rising linearly with time, thus

$$T(t) = C_s t + T_o \ , \qquad \text{(B-7)}$$

where C_s is a constant.

By use of this model it is found that [page 63, 11]

$$T(t) - T_o = 4C_s t i^2 \text{erfc} \frac{x}{2\sqrt{\alpha t}} \ , \qquad \text{(B-8)}$$

and the conduction loss,

$$L_d = -a_w k_w \left(\frac{\partial T}{\partial x}\right)_{x=0} = 2a_w k_w (T_i - T_o) \frac{1}{\sqrt{\alpha \pi t}} \ , \qquad \text{(B-9)}$$

where a_w is the cross sectional area of thermocouple wire, and k_w is the thermal conductivity of the wire. For this system,

$$L_d = 6.142\text{x}10^{-4} \frac{T_i - T_o}{\sqrt{\alpha \pi t}} \ . \qquad \text{(B-10)}$$

The energy transfer to the surface of test sample per unit area through natural convection can be calculated by the following equation

$$G_c = \bar{h}(T_f - T_s) \ , \qquad \text{(B-11)}$$

where $\bar{h}$ is the average value of transient heat transfer coefficient and has been determined experimentally, by use of a blackened copper disk gage, as a function of gas temperature and furnace pressure.

The method of measurement of transient heat-transfer coefficients employed the copper disk gage described earlier (Chapter V) with the gage surface being coated with a layer of optical black lacquer. Two to three measurements were made for each furnace pressure and temperature condition. The magnitude of natural convection, G_c , was calculated by subtracting the rate of radiation heat transfer in vacuum from the total heat transfer rate at test condition. $\bar{h}$ was calculated from Eq. (B-11), where T_s was taken as the observed copper disk temperature at one second of exposure. The results are shown in Table XV and Fig. 59. From Fig. 59 it can be seen that the natural convection at high temperature and low pressure is considerably lower than steady-state result estimated from Hellum's calculation [21]. To calculate G_c for the test films at experimental furnace temperature and pressure, it was assumed that $\bar{h}$ measured by a blackened copper disk gage was valid for the black face of polymer films.

Since at low furnace temperatures the measured transient heat-transfer coefficients tend to approach the calculated steady-state

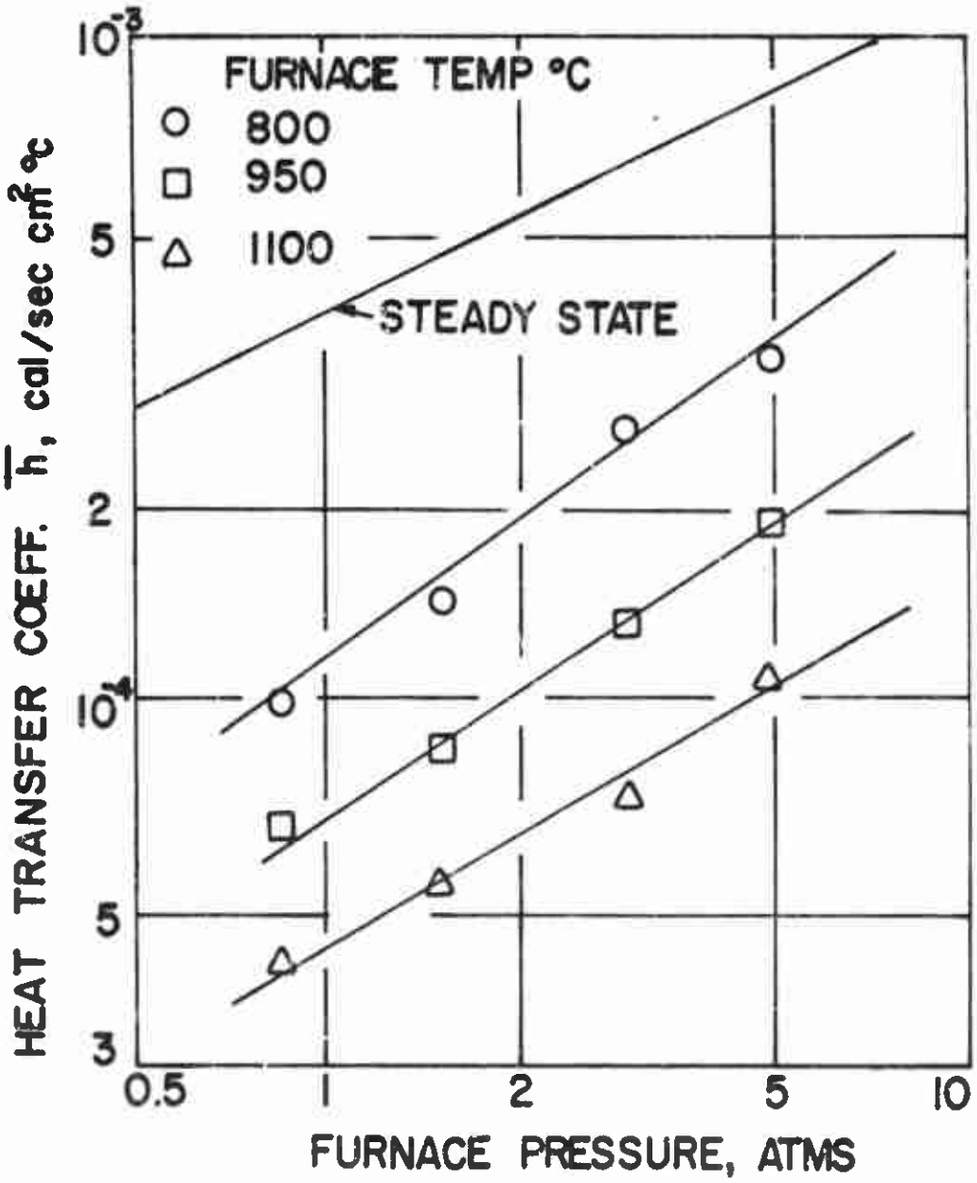

Fig. 59. -- Convective heat transfer coefficient as a function of furnace pressure and temperature measured by a blackened copper disk gage. The steady state value is from Hellum's calculation [21].

values, the assumption was made that the transient heat-transfer coefficient, $\bar{h}$, from the cold gases behind the gage to the copper disk gage was the steady-state heat-transfer coefficient. The rate of heat loss, L_v, from the back face of copper disk could be calculated.

When applying finite difference technique to Eqs. (B-1) to (B-4), several factors must be considered:

(1) The reaction occurring within the first half increment near the surface is considered as a surface reaction.

(2) The heat flux at the polymer film and copper disk interface is calculated by assuming that the temperatures at the three nodes nearest the copper disk can be approximated by a parabolic temperature profile. (See Fig. 60.)

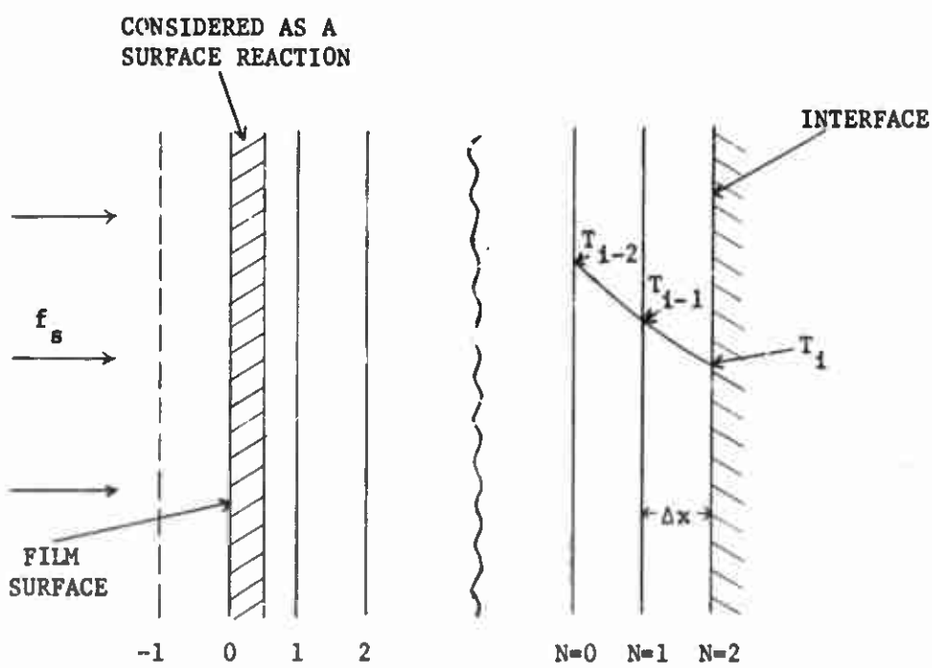

Fig. 60.-- A sketch of divisions for numerical solution.

A parabolic function passing T_{i-2}, T_{i-1} and T_i can be expressed by

$$T(x) = T(N\Delta x) = c_1 + c_2(N\Delta x) + c_3(N\Delta x)^2 , \tag{B-12}$$

at

$$\left.\begin{aligned} N &= 0, \quad T_{i-2} = c_1 ; \\ N &= 1, \quad T_{i-1} = c_1 + c_2\Delta x + c_3\Delta x^2 ; \\ N &= 2, \quad T_i = c_1 + 2c_2\Delta x + 4c_3\Delta x^2 . \end{aligned}\right\} \tag{B-13}$$

Solving Eq. (B-13) simultaneously, we have

$$c_1 = T_{i-2} ,$$

$$c_2 = \frac{1}{2\Delta x}(-3T_{i-2} + 4T_{i-1} - T_i) ,$$

$$c_3 = \frac{1}{2\Delta x^2}(T_{i-2} - 2T_{i-1} + T_i) ,$$

and

$$T(x) = T_{i-2} + \left(\frac{-3T_{i-2}+4T_{i-1}-T_i}{2}\right)N + \left(\frac{T_{i-2}-2T_{i-1}+T_i}{2}\right)N^2 . \tag{B-14}$$

The heat flux at the interface is

$$\begin{aligned} f_i &= -k_s\left(\frac{dT}{dx}\right)_{\text{interface}} \\ &= -k_s \frac{1}{\Delta x}\left(\frac{dT}{dN}\right)_{N=2} \\ &= \frac{-T_{i-2}+4T_{i-1}-3T_i}{2\frac{\Delta x}{k_s}} . \end{aligned} \tag{B-15}$$

After some algebraic operation, the finite differences approximation to Eqs. (B-1) to (B-4) becomes

$$T_{i,j+1} = \frac{1}{2}(T_{i-1,j}+T_{i+1,j}) + \frac{\alpha\Delta t}{k_s} Ae^{-E_s/RT_{i,j}} \; ; \qquad \text{(B-16)}$$

$$t = 0, \quad T = T_0 \; ;$$

$$T_{-1,j} = \frac{T_{1,j} + \frac{2\Delta x}{k_s}\{G_{0,j}+(0.25T_{1,j} - 0.5T_{0,j})PG\}}{1 - 0.5\frac{\Delta x}{k_s}PG} \; , \qquad \text{(B-18)}$$

where $G_{0,j} = \varepsilon f_s + Be^{-E_b/RT_{0,j}} + Ce^{-E_c/RT_{0,j}} + 0.5A\Delta x e^{-E_a/RT_{0,j}}$

$$-\sigma\varepsilon T_{0,j}^4 + \bar{h}(T_f - T_{0,j}) \; ,$$

$$PG = \left(\frac{\partial G}{\partial T}\right)_{0,j}$$

$$= B\frac{E_b}{RT_{0,j}^2} e^{-E_b/RT_{0,j}} + C\frac{E_c}{RT_{0,j}^2} e^{-E_c/RT_{0,j}}$$

$$+ 0.5A\Delta x \frac{E_a}{RT_{0,j}^2} e^{-E_a/RT_{0,j}} - 4\sigma\varepsilon T_{0,j}^3 - \bar{h} \; .$$

$$T_{MI,j+1} = T_{MI,j} + \frac{\Delta t}{aL\rho' c'} \left[\frac{4T_{MI-1,j} - T_{MI-2,j} - 3T_{MI,j}}{2\frac{\Delta x}{a_e k_s}} \right.$$

$$-\ell_{rb}(T_{MI,j}^4 - T_o^4) - \ell_d \frac{T_{MI,j} - T_o}{\sqrt{t}} - \ell_v(T_{MI,j} - T_o)$$

$$\left. +0.5A\Delta x \; e^{-E_a/RT_{MI,j}} \right] \; . \qquad \text{(B-19)}$$

Where the first subscripts in $T_{i,j}$ and $G_{0,j}$ stand for position in the test film, and the second subscripts, time. ℓ_{rb}, ℓ_d and ℓ_v respectively stand for the coefficient for rates of heat loss by radiation, conduction and convection. MI, MI-1 and MI-2 indicate position at interface, one Δx from interface and two Δx from interface, respectively.

The FORTRAN program written to solve Eqs. (B-1) to (B-4) is shown as Table XXXV. A brief description of the program follows: The one dimensional heat conduction equation, Eq. (VI-1), is solved by use of the explicit Schmidt method. The language is FORTRAN IV as employed by an IBM 7044 computer.

There are four input cards. The input information includes (a) experimental conditions: furnace temperature and heat flux, (b) physical properties: density, thermal conductivity etc., (c) kinetic parameters: activation energies and pre-exponential constants, (d) control parameters: maximum temperature, maximum exposure time, number of divisions etc., and (e) values of various heat losses. Table XXXVI defines all variables appeared in Table XXXV.

The output information includes (a) reproduction of all input information, (b) printing out of calculated surface temperature and interface temperature history, rate of temperature rise at the interface and surface, temperature gradient across the polymer film at the moment of output etc.

The order of operstions in the program can be seen from the flow sheet shown in Fig. 61. First, start temperatures at the time of input KOUNT by use of a semi-infinite body model without reactions are calculated. The subsequent temperatures are calculated by the one-dimensional

heat conduction equation for each new KOUNT which ia increaaed by one after each cycle of calculation. After every KL cyclea of calculation, the calculated temperaturea are stored and the rate of temperature riae at the interface and aurface ia calculated. The output criteria are aeveral, (a) when 1.0 - 0.6DP ia equal and leaa than zero, (b) when the aurface temperature is bigger than input maximum temperature, and (c) when the number of KOUNT is bigger than the input KOMAX. At the time of output the temperature gradient ia calculated.

An eatimate of the accuracy of thia program, uaing MI=10, or 8 diviaiona, waa evaluated by compariaon to the reault of analytical solution. (See Appendix C.) After 5000 time cyclea the numerically determined temperaturea were within 0.3% of the analytical temperature.

APPENDIX C

ANALYTICAL SOLUTION TO THE LINEARIZED FORM OF EQUATION (VI-1)

The equations to be solved here are essentially the same as in Appendix B, except that there is no reaction term and heat losses. These equations are shown as follows:

For $0 < x < \ell$ (see Fig. 20)

$$\rho c \frac{\partial T}{\partial t} = k_s \frac{\partial^2 T}{\partial x^2} \quad . \tag{C-1}$$

The boundary conditions are that when,

$$\left.\begin{aligned} &t = 0, \quad T = T_o \ ; \\ &x = 0, \quad -k_s \frac{\partial T}{\partial x} = \varepsilon f_s = F \ ; \text{ and} \\ &x = \ell, \quad -k_s \frac{\partial T}{\partial x} = L\rho' c' \frac{dT}{dt} = B_c \frac{dT}{dt} \quad . \end{aligned}\right\} \tag{C-2}$$

The Laplace transformation of Eq. (C-1) with respect to t gives the result,

$$P\bar{v} = \alpha \frac{d^2 \bar{v}}{dx^2} \quad . \tag{C-3}$$

Here the transform of temperature T is $\bar{v}$. The transform variable is P.

The transformed boundary conditions are that when,

$$x = 0, \quad -k_a \frac{d\bar{v}}{dx} = \frac{\bar{F}}{P}, \text{ and} \tag{C-4}$$

$$x = \ell, \quad -k_s \frac{d\bar{v}}{dx} = B_c P\bar{v} . \tag{C-5}$$

If $\quad q^2 = \frac{P}{\alpha}$, Eq. (C-3) becomes

$$\frac{d^2\bar{v}}{dx^2} - q^2\bar{v} = 0 . \tag{C-6}$$

The general solution to Eq. (C-6) ia

$$\bar{v} = D_1 e^{-qx} - D_2 e^{qx} , \tag{C-7}$$

where D_1 and D_2 are integration constants.

By use of the boundary conditions D_1 and D_2 can be evaluated. From the first boundary condition it is found that

$$D_1 qk_s - D_2 qk_s = \frac{F}{P} . \tag{C-8}$$

From the second boundary condition we have

$$D_1 qk_a{}^{-q\ell} - D_2 qk_a e^{q\ell} = B_c P(D_1 e^{-q\ell} + D_2 e^{q\ell}) . \tag{C-9}$$

Solution of Eqs. (C-8) and (C-9) for D_1 and D_2 shows that

$$D_1 = \frac{F}{qk_sP} \frac{B_cPe^{q\ell} + qk_se^{q\ell}}{B_cP(e^{q\ell} + e^{-q\ell}) + qk_s(e^{q\ell} - e^{-q\ell})} , \qquad \text{(C-10)}$$

and

$$D_2 = \frac{F}{qk_sP} \frac{(qk_s - B_cP)e^{-q\ell}}{B_cP(e^{q\ell} + e^{-q\ell}) + qk_s(e^{q\ell} - e^{-q\ell})} . \qquad \text{(C-11)}$$

When the values of D_1 and D_2 sre introduced into Eq. (C-7) it is found that

$$\bar{v} = \frac{F}{qk_sP} \frac{\cosh q(\ell - x) + \xi q \sinh q(\ell - x)}{\sinh q\ell + \xi q \cosh q\ell} , \qquad \text{(C-12)}$$

where

$$\xi = \frac{B_c}{\rho c} = \frac{L\rho' c'}{c} = \frac{B_c\alpha}{k_s} .$$

If $\lambda = P$, $\mu = q = \sqrt{\frac{\lambda}{\alpha}}$, then Eq. (C-12) becomes

$$\bar{v} = \frac{F}{\mu k_s\lambda} \frac{\cosh \mu(\ell-x) + \xi\mu \sinh \mu(\ell-x)}{\sinh \mu\ell + \xi\mu \cosh \mu\ell} . \qquad \text{(C-13)}$$

By the use of the Inversion Theorem for the Laplace transformation, Eq. (C-13) becomes

$$T = \frac{F}{k_s} \frac{1}{2\pi i} \int_{\gamma-i\infty}^{\gamma+i\infty} \frac{e^{\lambda t}\{\cosh \mu(\ell-x) + \xi\mu \sinh \mu(\ell-x)\}\, d\lambda}{(\sinh \mu\ell + \xi\mu \cosh \mu\ell)\mu\lambda} . \qquad \text{(C-14)}$$

The integral of Eq. (C-14) is evaluated by use of the Theory of Residues, thus

$$\text{Integral} = 2\pi i \text{ (the sum of the residues at the poles of integrand).} \tag{C-15}$$

One pole is at $\lambda = \mu = 0$. To find the residue of this pole, it is necessary to expand the denominator of the integrand in Eq. (C-14) about 0, thus

$$\frac{e^{\lambda t}\{\cosh \mu(\ell - x) + \xi\mu \sinh \mu(\ell - x)\}}{\mu\lambda\ (\sinh \mu\ell + \xi\mu \cosh \mu\ell)}$$

$$= \frac{e^{\lambda t}\{\cosh \mu(\ell - x) + \xi\mu \sinh \mu(\ell - x)\}}{\lambda^2\left\{\frac{\ell}{\alpha}\left(1 + \frac{(\mu\ell)^2}{3!} + \frac{(\mu\ell)^4}{5!} + \cdots\right) + \frac{\xi}{\alpha}\left(1 + \frac{(\mu\ell)^2}{2!} + \frac{(\mu\ell)^4}{4!} + \cdots\right)\right\}} . \tag{C-16}$$

This integrand has a pole of order 2 at $\lambda = 0$, therefore the residue for this pole is

$$\lim_{\lambda\to 0} \frac{d}{d\lambda} \frac{e^{\lambda t}\{\cosh \mu(\ell - x) + \xi\mu \sinh \mu(\ell - x)\}}{\frac{\ell}{\alpha}\left(1 + \frac{(\mu\ell)^2}{3!} + \frac{(\mu\ell)^4}{5!} + \cdots\right) + \frac{\xi}{\alpha}\left(1 + \frac{(\mu\ell)^2}{2!} + \frac{(\mu\ell)^4}{4!} + \cdots\right)}$$

$$= \frac{\alpha t}{\ell+\xi} + \frac{\frac{1}{2}(\ell-x)^2 + \xi(\ell-x)}{\ell+\xi} - \frac{\frac{\ell^2}{6}(\ell + 3\xi)}{(\ell+\xi)^2} . \tag{C-17}$$

The other poles sre roots of the equstion

$$\sinh \mu\ell + \xi\mu \cosh \mu\ell = 0,$$

or $\tanh \mu\ell = -\mu\xi.$

If $\mu\ell = i\beta_s$,

then $\lambda = \alpha\mu^2 = -\dfrac{\alpha\beta_s^{\,2}}{\ell^2}$,

and $\text{itsn}\ \beta_s = -\xi\mu = -i\dfrac{\xi\beta_s}{\ell}$,

or $\tan \beta_s = -\dfrac{\xi\beta_s}{\ell}$, (C-18)

where β_s is positive non-zero root.

For one β_s, the residue is

$$\frac{\exp(-\frac{\alpha\beta_s^{\,2}}{\ell^2}t)\ \{\cosh i\beta_s\ (1-\frac{x}{\ell}) + \frac{\xi}{\ell}i\beta_s \sinh i\beta_s(1-\frac{x}{\ell})\}}{\frac{d}{d\lambda}\mu\lambda\ (\sinh \mu\ell + \xi\mu \cosh \mu\ell)}$$

$$= -\frac{2\ell\ \exp(-\frac{\alpha\beta_s^{\,2}}{\ell^2}t)\ \{\cos \beta_s(1-\frac{x}{\ell}) - \frac{\xi}{\ell}\beta_s \sin \beta_s(1-\frac{x}{\ell})\}}{\beta_s^{\,2} \cos \beta_s\ (1 + \frac{\xi}{\ell} + \frac{\beta_s^{\,2}\xi^2}{\ell^2})}$$

(C-19)

By combining Eqs. (C-14), (C-15), (C-17) and (C-18) the vslue of the tempersture of the film is found to be

$$T = \frac{F}{k_s}\left[\frac{\alpha t}{\ell+\xi} + \frac{\frac{1}{2}(\ell-x)^2 + \xi(\ell-x)}{\ell+\xi} - \frac{\frac{\ell^2}{6}(\ell+3\xi)}{(\ell+\xi)^2}\right.$$

$$\left. - 2\ell \sum_{\beta_s} \frac{\exp\left(-\frac{\alpha\beta_s^2}{\ell^2}t\right)\left\{\cos\beta_s\left(1-\frac{x}{\ell}\right) - \frac{\xi}{\ell}\beta_s \sin\beta_s\left(1-\frac{x}{\ell}\right)\right\}}{\beta_s^2 \cos\beta_s\left(1+\frac{\xi}{\ell}+\frac{\beta_s^2\xi^2}{\ell^2}\right)}\right] + T_o \, . \tag{C-20}$$

At the interfsce

$$T_i = \frac{F}{k_s}\left[\frac{\alpha t}{\ell+\xi} - \frac{\frac{\ell^2}{6}(\ell+3\xi)}{(\ell+\xi)^2}\right.$$

$$\left. - 2\ell \sum_{\beta_s} \frac{\exp\left(-\frac{\alpha\beta_s^2 t}{\ell^2}\right)}{\beta_s \cos\beta_s\left(1+\frac{\xi}{\ell}+\frac{\beta_s^2\xi^2}{\ell^2}\right)}\right] + T_o \, . \tag{C-21}$$

At the film surface

$$T_s = \frac{F}{k_s}\left[\frac{\alpha t}{\ell+\xi} + \frac{\frac{1}{2}\ell(\ell+2\xi)}{\ell+\xi} - \frac{\ell^2(\ell+3\xi)}{6(\ell+\xi)^2}\right.$$

$$\left. -2\ell \sum_{\beta_s} \frac{\left(\cos\beta_s - \frac{\xi\beta_s}{\ell}\sin\beta_s\right)\exp\left(-\frac{\alpha\beta_s^2}{\ell^2}t\right)}{\beta_s^2 \cos\beta_s\left(1+\frac{\xi}{\ell}+\frac{\beta_s^2\xi^2}{\ell^2}\right)}\right] + T_o \, . \tag{C-22}$$

Eqs. (C-20), (C-21) and C-22) serve as an essential check to the accuracy of the numerical method for solving the heat transfer equations in Appendix B. The FORTRAN program used to evaluate the infinite series of Eqs. (C-20), (C-21) and (C-22) are shown as Table XXXVII. The discussion of this program is as follows: The objective of this program is to evaluate the infinite series appearing in Eqs. (C-20), (C-21) and (C-22). Two input cards are used. They include the physical properties of test sample, heat flux, control parameter, RESI (see definition of variables in Table XXXVII), and the first six roots of the equation

$$\tan \beta_s = - \frac{\xi \beta_s}{\ell} .$$

These roots are taken from Carslaw and Jaeger [page 492, 11]. The output information includes the reproduction of input information, calculated surface and interface temperature history and the temperature gradient at the time of output.

The pattern of the computer program can be seen from the flow sheet, Fig. 62. Since the analytical solutions involve infinite series, a criterion has to be established to determine when to stop adding additional terms. This criterion is determined by RESI. Each calculated value after the seventh term in the infinite series is made to compare with RESI. If the calculated value is bigger than RESI the calculation goes on to the next term, and if equal or smaller the calculation goes on to calculate the next time step. The final output criterion is when the calculated surface temperature is bigger than 450°C. At the time of output the temperature gradient across the test film is calculated. The definition of variables used in this program is shown as Table XXXVIII.

For a very short exposure time, the polymer film acta like a semi-infinite body, the surface temperature of which can be exactly calculated. This surface temperature calculated from the semi-infinite body at a very short exposure time was used to check the accuracy of the evaluation of the infinite series in this program. The result of comparison was nearly exact, because for an exposure time less than 0.1 sec the surface temperature calculated from this program is, on the average, within 0.023°C of the same temperature from the semi-infinite body at a heating rate of 4.82 cal/(sec)(cm)^2. Therefore the criterion used to evaluate the infinite series in this program was justified.

APPENDIX D

EXPERIMENTAL RESULTS OF PI1 POLYMER IN NITROGEN IN THE RADIATION FURNACE

PI1 polymer contained 100 parts of PBAA binder, 3 parts of Fe_2O_3 and no carbon black. The purpose of the study was to determine whether Fe_2O_3 was suitable for use as an inert opaque ingredient. The experiments were conducted at a furnace temperature of 1100°C and at several pressures. The initial rate of temperature rise was employed to estimate the emissivity of the polymer surface. It was calculated to be 0.55 ± 0.02. One of the peculiar results of these experiments was that no sudden or even gradual decrease of temperature rising rate signifying the endothermic decomposition process was ever observed. Instead, the opposite case was actually noted in which a slow increase in the rate of temperature rise started to occur at interface temperature of about 380°C. When the test samples were removed from the furnace before, during and after the region of the rate change and the surface examined, a progressive darkening of the color was clearly observed. The influence of darkening was to overshadow the effect of the decomposition reaction which resulted in the observed temperature history. Because of this, the use of iron oxide as an opaquing material was discontinued. The data of significant reactions are shown as Table XXIV.

APPENDIX E

CALIBRATION OF THE SENSITIVITIES OF GALVANOMETER M-100-350

The sensitivity of a galvanometer used in the Visicorder depends upon the series and shunt resistances connected with it. Galvanometer M-100-350 was calibrated in series with each of the resistors used in this work with two input voltage sources: (1) a Leeds & Northrup potentiometer, and (2) a copper disk gage and a thermometer. In the first case a known emf output from the potentiometer was fed into the galvanometer in the Visicorder through a series resistor and, also in series, a pair of thermocouple extension wires of the same length as those used to transmit the signal from the copper disk calorimeter to the galvanometer. The procedure of calibration for all series resistor were the same, starting with a zero voltage output from the potentiometer, followed by successive increments of 5 mv. With each emf output, the corresponding deflection of the galvanometer was recorded on the Visicorder recording paper. A slight non-linearity of 2.3 $\pm$ 0.2 % for deflection sensitivity was found for all series resistors when the galvanometer deflected from zero to six inches (width of recording sheet). The values shown as Table XVI were the average values of the measured sensitivities across the width of the recording sheet.

Before the copper disk gage and thermometer were used to calibrate the galvanometer, the copper disk gage itself (effectively a copper-constantan thermocouple) was calibrated at two temperatures, i.e., the freezing point and the boiling point of pure water. It was found that the temperature converted (according to the Conversion Tables for Thermocouples, Leeds & Northrup Co.) from the emf output of the copper disk gage measured by the potentiometer at these two temperatures were within $\pm$ 0.1°C of thermometer reading. Thus calibrated, the copper disk calorimeter was then used to drive the galvanometer in series with each of the several resistors. Because of the limitation of the temperature range of liquid water, the maximum deflection on the Visicorder record was about two inches, and the range of calibration was thus limited. The results of sensitivities determined were about 0.7% lower than those reported in Table XVI. In this work the sensitivity values found by use of the potentiometer were employed. The slight non-linearity of the sensitivities was taken into account.

APPENDIX F

TABLES X TO XXXVIII

TABLE X

COMPOSITIONS OF VARIOUS POLYMERS AND PROPELLANT-LIKE MATERIALS

Material Code	Ingredients (Weight Per Cent)	
PO	15	Epon Resin 828 (epoxides)
	85	Polybutadiene-acrylic acid
PC	2.91	Carbon black
	14.56	Epon Resin 828 (epoxides)
	82.53	Polybutadiene-acrylic acid
PCC	2.91	Carbon black
	9.71	Copper chromite
	13.11	Epon Resin 828 (epoxides)
	74.27	Polybutadiene-acrylic acid
G10	2.91	Carbon black
	9.71	Glass beads
	13.11	Epon Resin 828 (epoxides)
	74.27	Polybutadiene-acrylic acid
G20	2.91	Carbon black
	19.40	Glass beads
	11.66	Epon Resin 828 (epoxides)
	66.03	Polybutadiene-acrylic acid
G30	2.91	Carbon black
	29.10	Glass beads
	10.18	Epon Resin 828 (epoxides)
	57.81	Polybutadiene-acrylic acid
G50	2.91	Carbon black
	48.53	Glass beads
	7.28	Epon Resin 828 (epoxides)
	41.28	Polybutadiene-acrylic acid
G5C	2.91	Carbon black
	5.11	Copper chromite
	45.99	Glass beads
	6.90	Epon Resin 828 (epoxides)
	39.09	Polybutadiene-acrylic acid

(continued)

TABLE X (continued)

Material Code	Ingredients (Weight Per Cent)	
PI1	2.91	Iron Oxide
	14.56	Epon Resin 828 (epoxides)
	82.53	Polybutadiene-acrylic acid
PI2	2.91	Carbon black
	9.71	Iron oxide
	13.11	Epon Resin 828 (epoxides)
	74.27	Polybutadieoe-acrylic acid
A05	2.91	Carbon black
	4.86	Ammonium perchlorate
	13.83	Epon Resin 828 (epoxides)
	78.40	Polybutadiene-acrylic acid
A09	2.91	Carbon black
	8.83	Ammonium perchlorate
	13.24	Epon Resin 828 (epoxidea)
	75.02	Polybutadiene-acrylic acid
A9C	2.91	Carbon bleck
	8.78	Ammonium perchlorate
	0.44	Copper chromite
	13.18	Epon Reain 828 (epoxides)
	74.69	Polybutadiene-acrylic acid
A20	2.91	Carbon black
	19.42	Ammonium perchlorate
	11.66	Epon Resin 828 (epoxides)
	66.01	Polybutadiene-acrylic acid
A2C	2.91	Carbon black
	0.96	Copper chromite
	19.23	Ammonium perchlorate
	11.52	Epon Resin 828 (epoxides)
	65.38	Polybutadiene-acrylic acid
A50	2.91	Carbon black
	48.54	Ammonium perchlorate
	7.28	Epon Resin 828 (epoxides)
	41.27	Polybutadiene-acrylic acid

(continued)

TABLE X (continued)

Material Code	Ingredients (Weight Per Cent)	
A5C	2.91	Carbon black
	2.36	Copper chromite
	47.32	Ammonium perchlorate
	7.10	Epon Resin 828 (epoxides)
	40.21	Polybutadiene-acrylic acid
A9I	2.91	Carbon black
	8.78	Ammonium perchlorate
	0.44	Iron oxide
	13.18	Epon Resin 828 (epoxides)
	74.69	Polybutadiene-acrylic acid
A5I	2.91	Carbon black
	2.36	Iron oxide
	47.32	Ammonium perchlorate
	7.10	Epon Resin 828 (epoxides)
	40.21	Polybutadiene-acrylic acid

TABLE XI

SUMMARY OF THERMOPHYSICAL PROPERTIES
Except aa noted all valuea are at 60°C.

Material[1]	Density	Heat Capacity	Thermal Diffusivity	Thermal Conductivity	Thermal Responsivity $\sqrt{k_s \rho c}$
	g/cm^3	cal/g°C	cm^2/sec	cal/sec cm°C	cal/sec$^{1/2}$ cm^2°C
ammonium[2] perchlorate	1.95	0.275	2.22×10^{-3}	1.19×10^{-3}	2.52×10^{-2}
copper chromite[3]	6.15[4]	0.146	2.417	2.17	1.47
iron oxide[5]	5.12[4]	0.168	1.639	1.41	1.10
carbon black[6]	1.88[4]	0.204	0.407	0.156	0.774
PO[2]	0.956	0.465	0.983	0.437	1.39
PC	0.970	0.457	0.974	0.432	1.38
PCC	1.123	0.418	0.988	0.464	1.48
G10	1.033	0.432	1.037	0.463	1.44
G20	1.104	0.408	1.11	0.502	1.504
G30	1.189	0.381	1.21	0.547	1.57
G50	1.40	0.331	1.464	0.678	1.687

(continued)

TABLE XI (continued)

Material	Density	Heat Capacity	Thermal Diffusivity	Thermal Conductivity	Thermal Responsivity $\sqrt{k_s \rho c}$
	g/cm^3	cal/g°C	cm^2/sec	cal/sec cm°C	$cal/sec^{1/2}\ cm^2 \cdot C$
G5C	1.459	0.321	1.471×10^{-3}	0.690×10^{-3}	1.798×10^{-2}
A05	0.999	0.449	0.989	0.443	1.409
A09	1.015	0.441	1.015	0.454	1.426
A9C	1.019	0.440	1.016	0.455	1.429
A20	1.076	0.421	1.072	0.486	1.484
A2C	1.084	0.421	1.066	0.487	1.492
A50	1.290	0.367	1.288	0.611	1.701
A5C	1.315	0.362	1.293	0.615	1.710
A9I	1.019	0.440	1.015	0.455	1.427
A5I	1.313	0.362	1.291	0.614	1.709
PI1	0.979	0.449	1.002	0.440	1.390
PI2	1.053	0.429	0.976	0.441	1.411

(continued)

TABLE XI (continued)

1 For compositions see Table X.

2 The ammonium perchlorate was obtained from the American Potash and Chemical Corporation and was designated as 50 per cent less than 10 microns. The thermophysical properties for AP (at 60°C) are taken from AIAA Journal 4, 663-666 (1966). The values for the thermal diffusivity were confirmed in our laboratory. The thermophysical properties for PO polymer are taken from the Technical Report on "Ignition and Combustion of Solid Propellants", AFOSR 62-99 (1962). University of Utah, Department of Chemical Engineering.

3 Copper Chromite Catalyst, Cu-0202 P, obtained from Harshaw Chemical Company and contains approximately 82 per cent CuO and 17 per cent Cr_2O_3. The weight-average particle diameter is 3.7 microns. The thermophysical properties of copper chromite are calculated from CuO and Cr_2O_3 according to weight per cent. The values for the last two materials are from "Handbook of Physics and Chemistry" 44th edition, CRP Company.

4 These values are at 20°C.

5 Pure red iron oxide, code R-1599, obtained from C. K. Williams and Company. Particle size ranged from less than one micron to ten microns in diameter, with 55.0 per cent of the particles having diameters of less than 0.25 microns.

6 A rubber-reinforcing carbon black, Philblack E, obtained from Phillips Petroleum Company. Philblack E has a surface area of 142 square meters per gram.

TABLE XII

HEAT FLUX DISTRIBUTION ALONG THE LONGITUDINAL (AXIAL) TRAVERSE IN THE FOCUS VOLUME OF IMAGING FURNACE

Distance From Optical Axis		Heat Flux	Normalized Heat Flux+
turn*	cm	cal/sec cm^2	
-7.5	-1.179	6.39	0.288
-6.5	-1.022	7.62	0.343
-5.5	-0.865	9.41	0.424
-4.5	-0.707	11.85	0.534
-3.5	-0.550	14.80	0.666
-2.5	-0.393	18.12	0.816
-1.5	-0.236	20.71	0.932
-1.0	-0.157	21.52	0.969
-0.5	-0.079	22.10	0.995
0.0	0.0	22.21	1.0
+0.5	+0.079	22.13	0.996
+1.0	+0.157	21.40	0.964
+1.5	+0.236	20.76	0.935
+2.5	+0.393	18.40	0.828
+3.5	+0.550	14.96	0.674
+4.5	+0.707	12.40	0.558
+5.5	+0.865	9.48	0.427
+6.5	+1.022	7.02	0.316
+7.5	+1.179	4.72	0.213
+8.5	+1.336	2.70	0.122
+9.5	+1.493	1.05	0.047

+ heat flux measured divided by maximum hest flux, 22.2 cal/sec cm^2.

* corresponding to number of turnings made by longitudinal screw on the screw driven positioning table. 0 turn is the position for maximum flux. "+" means movement in the direction of image reflector, "-" in the opposite direction. One complete turn corresponds to a displacement of 0.1572 cm.

TABLE XIII

HEAT FLUX DISTRIBUTION ALONG THE HORIZONTAL TRAVERSE IN THE FOCUS VOLUME OF IMAGING FURNACE AT LONGITUDINAL POSITION -1 TURN FROM CENTER

Distance From Optical Axis		Heat Flux	Normalized Heat Flux+
turns*	cm	cal/sec cm^2	
-8	-1.258	0.62	0.029
-7	-1.100	1.43	0.067
-6	-0.943	3.32	0.155
-5	-0.786	7.18	0.336
-4	-0.629	12.72	0.594
-3	-0.472	16.75	0.783
-2	-0.314	20.13	0.941
-1.5	-0.236	21.22	0.992
-1.0	-0.157	21.40	1.0
-0.5	-0.079	21.38	0.999
0.0	0.0	21.40	1.0
+0.5	+0.079	21.40	1.0
+1.0	+0.157	21.39	1.0
+1.5	+0.236	21.41	1.0
+2.0	+0.314	20.02	0.936
+3.0	+0.472	16.90	0.790
+4.0	+0.629	13.21	0.617
+5.0	+0.786	7.20	0.336
+6.0	+0.943	2.92	0.136
+7.0	+1.100	1.02	0.048
+8.0	+1.258	0.35	0.016

+ hest flux measured divided by maximum flux, 21.4 cal/sec cm^2.

* corresponding to number of turnings made by horizontal screw on the screw driven positioning table. 0 turn is the position of center. "+" means movement to the right, facing image reflector, "-" to the left. One complete turn corresponds to a displacement of 0.1572 cm.

TABLE XIV

HEAT FLUX DISTRIBUTION ALONG VERTICAL TRAVERSE OF THE FOCUS VOLUME OF IMAGING FURNACE AT LONGITUDINAL (AXIAL) POSITION -1 TURN FROM CENTER

Distance From Optical Axia		Heat Flux	Normalized Heat Flux+
turns*	cm	cal/aec cm^2	
-9	-1.152	0.51	0.024
-8	-1.024	1.42	0.066
-7	-0.896	2.75	0.129
-6	-0.768	5.58	0.261
-5	-0.64	10.80	0.505
-4	-0.512	16.05	0.75
-3	-0.384	19.25	0.90
-2.75	-0.352	19.95	0.932
-2.5	-0.32	20.50	0.958
-2.0	-0.256	21.38	0.999
-1.5	-0.192	21.42	1.0
-1.0	-0.128	21.40	1.0
-0.5	-0.064	21.39	1.0
0.0	0.0	21.40	1.0
+0.5	+0.064	21.38	0.999
+1.0	+0.128	21.41	1.0
+1.5	+0.192	21.39	1.0
+2.0	+0.256	21.38	0.999
+2.5	+0.32	20.48	0.957
+2.75	+0.352	20.00	0.935
+3.0	+0.384	19.52	0.912
+3.50	+0.448	17.98	0.840
+4.0	+0.512	15.45	0.722
+5.0	+0.64	10.26	0.479
+6.0	+0.768	5.04	0.236
+7.0	+0.896	2.52	0.118
+8.0	+1.024	1.10	0.052

+ heat flux measured divided by maximum flux, 21.4 cal/aec cm^2.

* correaponding to number of turnings made by vertical screw on the acrew driven positioning tsble. 0 turn ia the poaition center. "+" meana movement in the "up" direction, "-" "down" direction. One complete turn correaponda to a displacement of 0.128 cm.

TABLE XV

SUMMARY OF TRANSIENT HEAT FLUX MEASUREMENTS BY COPPER DISK GAGES FOR THE SEALED RADIATION FURNACE

Furnace Temp. °C	Furnace Pressure atm	Total Heat Flux cal/sec cm^2	Convective Heat Flux[1] cal/sec cm^2	Convective Heat Transfer Coefficient[2] cal/sec cm^2 °C
800	~0.01	1.736	-----	-----
802	0.85	1.834	0.098	1.03×10^{-4}
800	1.53	1.876	0.140	1.45
801	2.89	1.984	0.248	2.70
789	4.90	2.061	0.325	3.32
952	~0.01	2.940	-----	-----
950	0.85	2.997	0.057	0.68
948	1.52	3.017	0.077	0.89
950	2.92	3.058	0.118	1.35
950	4.93	3.109	0.169	1.90
1100	~0.01	4.621	-----	-----
1102	0.85	4.652	0.031	0.43
1101	1.50	4.663	0.042	0.56
1099	2.95	4.679	0.058	0.75
1100	4.90	4.709	0.088	1.13

1 The convective heat flux was calculated as the observed flux less the measured flux under vacuum (≈0.01 atm using vacuum pump).

2 The solid to gas temperature difference was taken to be the observed value after 1 sec.

TABLE XVI

SENSITIVITIES OF GALVANOMETER M-100-350 WITH DIFFERENT SERIES RESISTANCES

Resistor	Sensitivity	
ohms	inch/mv	mv/inch
280	4.44×10^{-1}	2.255
330	3.796	2.635
380	3.34	3.001
430	3.005	3.325
480	2.743	3.642
530	2.54	3.94

TABLE XVII

HYDROCARBON MIXTURE NO. 37, LOT 13
(From Phillips Petroleum Company)

Component	Weight Per Cent	Mole Per Cent	Identification Number
cis-Butene-2	19.07	19.07	5
trans-Butene-2	21.85	21.85	4
n-Butane	14.59	14.08	2
Butadiene	17.08	17.72	5
Butene-1	16.69	16.69	3
Isobutylene	7.05	7.05	3
Isobutane	3.64	3.52	1
Propane	Trace	Trace	
Propylene	Trace	Trace	
Neopentane	0.02	0.01	
n-Pentane	0.01	0.01	
Total	100.00	100.00	

TABLE XV

SUMMARY OF TRANSIENT HEAT FLUX MEASUREMENTS BY COPPER DISK GAGES FOR THE SEALED RADIATION FURNACE

Furnace Temp. °C	Furnace Pressure atm	Total Heat Flux cal/sec cm^2	Convective Heat Flux[1] cal/sec cm^2	Convective Heat Transfer Coefficient[2] cal/sec cm^2 °C
800	~0.01	1.736	-----	-----
802	0.85	1.834	0.098	1.03×10^{-4}
800	1.53	1.876	0.140	1.45
801	2.89	1.984	0.248	2.70
789	4.90	2.061	0.325	3.32
952	~0.01	2.940	-----	-----
950	0.85	2.997	0.057	0.68
948	1.52	3.017	0.077	0.89
950	2.92	3.058	0.118	1.35
950	4.93	3.109	0.169	1.90
1100	~0.01	4.621	-----	-----
1102	0.85	4.652	0.031	0.43
1101	1.50	4.663	0.042	0.56
1099	2.95	4.679	0.058	0.75
1100	4.90	4.709	0.088	1.13

1 The convective heat flux was calculated as the observed flux less the measured flux under vacuum (≈0.01 atm using vacuum pump).

2 The solid to gas temperature difference was taken to be the observed value after 1 sec.

TABLE XVI

SENSITIVITIES OF GALVANOMETER M-100-350 WITH DIFFERENT SERIES RESISTANCES

Resistor	Sensitivity	
ohms	inch/mv	mv/inch
280	4.44×10^{-1}	2.255
330	3.796	2.635
380	3.34	3.001
430	3.005	3.325
480	2.743	3.642
530	2.54	3.94

TABLE XVII

HYDROCARBON MIXTURE NO. 37, LOT 13
(From Phillips Petroleum Company)

Component	Weight Per Cent	Mole Per Cent	Identification Number
cis-Butene-2	19.07	19.07	5
trans-Butene-2	21.85	21.85	4
n-Butane	14.59	14.08	2
Butadiene	17.08	17.72	5
Butene-1	16.69	16.69	3
Isobutylene	7.05	7.05	3
Isobutane	3.64	3.52	1
Propane	Trace	Trace	
Propylene	Trace	Trace	
Neopentane	0.02	0.01	
n-Pentane	0.01	0.01	
Total	100.00	100.00	

TABLE XVIII

STANDARD HYDROCARBON MIXTURE 40, LOT 16
(From Phillips Petroleum Company)

Component	Weight Per Cent	Mole Per Cent	Identification Number
Ethane	2.78	4.70	1
Propane	14.89	17.16	2
Propylene	16.07	19.40	3
Isobutane	19.53	17.08	4
Isobutylene	15.18	13.75	6
Normal Butane	6.84	5.98	5
Butadiene-1,3	0.02	0.02	8
Butene-1	9.85	8.92	6
trans-Butene-2	11.81	10.69	7
cis-Butene-2	0.69	0.62	8
Isopentane	1.14	0.80	9
Normal Pentane	Trace	Trace	10
Pentene-1	0.59	0.43	10
trans-Pentene-2	0.27	0.19	11
cis-Pentene-2	0.33	0.24	12
2-Methylbutene-2	Trace	Trace	10
Ethylene	0.01	0.02	1
Total	100.00	100.00	

The composition of this mixture is reported as accurate to 0.05 weight per cent.

TABLE XIX

SUMMARY OF EXPERIMENTAL DATA OF PC POLYMER IN VACUUM

Run No.*	T_f	f_i	Endotherm			Photocell Signal			Kinetic Parameters	
			t	T_i	T_s	t	T_i	T_s	A	E_a
	°K	$\frac{cal}{sec\ cm^2}$	sec	°K	°K	sec	°K	°K	cal/sec cm^3	kcal/g-mole
25-0-1	1373	3.85	6.52	544	624	----	----	----	$3x10^{17}$	43
25-0-2	"	3.95	6.46	552	632	----	----	----	"	"
25-0-3	"	3.88	6.4	542	622	----	----	----	"	"
25-0-4	"	3.91	7.5	559	639	----	----	----	"	"
25-0-5	"	3.99	6.37	551	631	----	----	----	"	"
25-0-7	"	3.86	6.38	550	630	----	----	----	"	"
25-0-9	"	4.00	6.0	522	602	----	----	----	"	"
25-0-10	"	3.74	6.66	561	641	6.81	567	658	"	"
25-0-12	"	3.70	6.65	528	608	6.76	532	618	"	"
25-0-13	"	3.88	6.19	542	622	6.27	545	631	"	"
25-0-14	"	3.99	6.26	513	593	6.34	516	602	"	"
25-0-21	1223	2.42	10.62	549	600	10.90	555	610	$5x10^{17}$	43
25-0-22	"	2.36	11.2	565	616	----	----	----	"	"
25-0-23	"	2.46	11.6	569	620	11.86	574	629	"	"
25-0-24	"	2.60	7.71	549	600	----	----	----	"	"

(continued)

TABLE XIX (continued)

Run No.*	T_f	f_i	Endotherm			Photocell Signal			Kinetic Parameters	
			t	T_i	T_s	t	T_i	T_s	A	E_a
	°K	$\frac{cal}{sec\ cm^2}$	sec	°K	°K	sec	°K	°K	cal/sec cm^3	kcal/g-mole
25-0-25	1223	2.42	8.43	563	614	8.62	567	622	$5x10^{17}$	43
25-0-27	"	2.38	7.90	547	598	8.16	552	607	"	"
25-0-28	"	2.50	8.13	560	611	8.33	564	619	"	"
25-0-41	1073	1.37	14.89	582	612	----	----	----	$5x10^{17}$	43
25-0-42	"	1.40	14.34	565	595	----	----	----	"	"
25-0-43	"	1.51	13.82	548	578	----	----	----	"	"
25-0-44	"	1.45	14.17	560	590	----	----	----	"	"
25-0-45	"	1.47	14.05	564	594	14.48	570	601	"	"
25-0-46	"	1.39	14.72	583	613	15.04	587	618	"	"
25-0-48	"	1.45	14.56	563	593	14.76	569	590	"	"

*The first two numbers in the Run No. designate the kind of polymer studied. 25 stands for PC, 32 for PCC, 21 for PI1, 50 for PI2, 22 for A05, 23 for A09, 36 for A20, 27 for A50, 24 for A9C, 37 for A2C, 28 for A5C, 51 for A9I, 52 for A5I, 39 for G10, 40 for G20, 41 for G30, 42 for G50, and 43 for G5C.

---- No photocell data was taken.

TABLE XX

SUMMARY OF EXPERIMENTAL DATA OF PCC POLYMER IN VACUUM

Run No.*	T_f	f_i	Endotherm			Photocell Signal			Kinetic Parameters	
			t	T_i	T_s	t	T_i	T_a	A	E_a
	°K	$\frac{cal}{sec\ cm^2}$	sec	°K	°K	sec	°K	°K	cal/sec cm^3	kcal/g-mole
32-0-1	1373	3.80	5.37	499	571	5.57	506	584	$15x10^{15}$	37
32-0-2	"	3.92	4.51	465	537	----	----	----	"	"
32-0-3	"	3.84	5.59	492	564	----	----	----	"	"
32-0-5	"	3.90	5.37	500	572	----	----	----	"	"
32-0-6	"	3.78	5.31	487	559	----	----	----	"	"
32-0-8	"	3.99	5.15	509	581	----	----	----	"	"
32-0-9	"	4.00	5.48	523	595	----	----	----	"	"
32-0-10	"	3.94	5.16	512	584	5.23	515	593	"	"
32-0-12	"	4.09	5.11	513	585	5.29	518	596	"	"
32-0-13	"	3.99	6.00	508	580	6.12	512	590	"	"
32-0-14	"	3.81	5.85	488	560	5.98	493	561	"	"
32-0-21	1223	2.42	9.8	504	551	----	----	----	$25x10^{15}$	37
32-0-22	"	2.54	9.5	506	553	----	----	----	"	"
32-0-23	"	2.67	10.11	519	566	----	----	----	"	"
32-0-25	"	2.32	11.2	491	538	11.46	497	548	"	"

(continued)

TABLE XX (continued)

Run No.*	T_f	f_i	Endotherm			Photocell Signal			Kinetic Parameters	
			t	T_i	T_s	t	T_i	T_s	A	E_a
	°K	$\frac{cal}{sec\ cm^2}$	sec	°K	°K	sec	°K	°K	cal/sec cm^3	kcal/g-mole
32-0-26	1223	2.31	10.4	532	579	----	----	----	$25x10^{15}$	37
32-0-27	"	2.51	9.38	480	527	9.60	485	536	"	"
32-0-28	"	2.67	10.20	512	559	10.41	517	568	"	"
32-0-41	1073	1.56	13.32	532	561	----	----	----	$25x10^{15}$	37
32-0-43	"	1.38	14.05	504	533	14.57	511	540	"	"
32-0-44	"	1.54	13.25	535	564	13.62	540	569	"	"
32-0-45	"	1.57	14.53	520	549	----	----	----	"	"
32-0-46	"	1.41	14.1	515	540	----	----	----	"	"
32-0-47	"	1.48	13.31	521	551	13.72	527	556	"	"

* See footnote in Table XIX.

---- No photocell dsts was taken.

TABLE XXI

SUMMARY OF EXPERIMENTAL DATA OF PC POLYMER IN INERT GAS, N_2

Run No.*	T_f	P_f	f_i	Endotherm			Photocell Signal			Kinetic Parameters	
				t	T_i	T_s	t	T_i	T_s	A	E_a
	°K	atm	cal / aec cm^2	sec	°K	°K	sec	°K	°K	cal/aec cm^3	kcal/g-mole
25-1-1	1373	0.85	3.98	2.48	567	649	----	----	----	$1x10^{17}$	43
25-1-2	"	"	3.90	2.58	562	644	3.10	606	691	"	"
25-1-3	"	"	3.85	2.48	568	650	2.98	602	687	"	"
25-1-4	"	"	3.79	2.48	553	635	3.04	590	675	"	"
25-1-5	"	"	4.03	2.50	571	653	2.98	603	688	"	"
25-1-6	1373	1.53	3.99	2.61	592	672	3.27	655	740	$4x10^{16}$	43
25-1-7	"	1.52	3.97	2.52	578	658	3.39	652	737	"	"
25-1-8	"	1.48	4.02	2.56	586	666	3.36	660	745	"	"
25-1-9	"	1.50	3.91	2.54	580	660	3.43	651	736	"	"
25-1-11	1373	2.95	3.93	2.77	599	679	----	----	----	$2x10^{16}$	43
25-1-12	"	2.89	3.95	2.81	603	683	----	----	----	"	"
25-1-13	"	2.89	4.08	2.74	593	673	----	----	----	"	"
25-1-14	"	2.90	4.05	2.73	593	673	----	----	----	"	"
25-1-16	1373	4.95	3.98	2.68	611	693	----	----	----	$8x10^{15}$	43
25-1-17	"	4.93	4.04	2.64	614	696	4.02	727	814	"	"
25-1-18	"	4.84	3.95	2.67	621	703	4.05	734	821	"	"
25-1-19	"	5.02	3.95	2.74	618	700	4.07	730	817	"	"
25-1-20	"	4.93	4.06	2.64	609	691	3.90	720	807	"	"
25-2-1	1223	0.85	2.48	4.06	571	622	5.16	624	678	$15x10^{16}$	43
25-2-2	"	"	2.48	4.13	574	625	5.35	634	688	"	"
25-2-3	"	"	2.55	3.86	587	638	4.59	623	677	"	"
25-3-1	1073	0.85	1.50	7.75	585	616	----	----	----	$15x10^{16}$	43
25-3-2	"	"	1.47	7.51	580	611	----	----	----	"	"

*See footnote in Table XIX. ---- No photocell data was taken.

TABLE XXII

SUMMARY OF EXPERIMENTAL DATA OF PCC POLYMER IN INERT GAS, N_2

Run No.*	T_f	P_f	f_i	Endotherm			Photocell Signal			Kinetic Parameters	
				t	T_i	T_s	t	T_i	T_a	A	E_a
	°K	atm	$\frac{cal}{sec\ cm^2}$	sec	°K	°K	sec	°K	°K	cal/sec cm^3	kcal/g-mole
32-1-1	1373	0.85	3.88	2.17	.9	604	----	----	----	$6x10^{15}$	37
32-1-2	"	"	3.78	2.19	511	586	2.63	548	627	"	"
32-1-3	"	"	3.86	2.12	514	589	2.60	552	631	"	"
32-1-4	"	"	4.05	2.02	525	600	2.55	571	650	"	"
32-1-6	1373	1.50	3.88	2.30	539	614	----	----	----	$3x10^{15}$	37
32-1-7	"	1.48	3.97	2.24	537	612	3.06	605	684	"	"
32-1-8	"	1.52	4.06	2.22	535	610	3.00	607	685	"	"
32-1-11	1373	2.23	3.94	2.36	549	624	3.29	625	704	$1.5x10^{15}$	37
32-1-12	"	2.27	3.86	2.34	542	617	3.22	616	695	"	"
32-1-13	"	2.16	3.74	2.50	545	620	3.41	618	697	"	"
32-1-16	1373	3.04	3.89	2.31	561	636	3.28	649	728	$1x10^{15}$	37
32-1-17	"	3.04	3.82	2.35	553	628	3.32	635	714	"	"
32-1-18	"	2.85	3.89	2.31	557	632	3.26	643	722	"	"
32-1-19	"	2.90	3.97	2.38	554	629	3.29	641	720	"	"
32-1-21	1373	5.02	3.90	2.67	571	644	----	----	----	$5x10^{14}$	37
32-1-22	"	4.86	3.98	2.54	568	641	3.87	686	766	"	"
32-1-24	"	4.90	4.04	2.62	575	648	3.83	695	775	"	"
32-1-25	"	4.95	3.94	2.48	577	650	3.76	688	768	"	"

* See footnote in Table XIX.

---- No photocell data was taken.

TABLE XXIII

SUMMARY OF EXPERIMENTAL DATA OF PI2 POLYMER IN INERT GAS, N_2

Run No.*	T_f	P_f	f_i	Endotherm			Photocell Signal			Kinetic Parameters	
				t	T_i	T_s	t	T_i	T_s	A	E_a
	°K	atm	$\frac{cal}{sec\ cm^2}$	sec	°K	°K	sec	°K	°K	kcal/sec cm^3	kcal/g-mole
50-1-1	1373	0.85	3.96	2.63	580	660	3.12	623	708	$1x10^{17}$	43
50-1-2	"	"	4.00	2.63	568	648	3.20	615	700	"	"
50-1-3	"	"	3.95	2.48	559	639	3.06	604	689	"	"
50-1-4	"	"	4.05	2.53	576	656	3.01	619	704	"	"
50-1-6	1373	1.49	4.11	2.73	595	675	3.50	657	742	$4x10^{16}$	43
50-1-7	"	1.53	3.99	2.74	586	666	3.26	631	716	"	"
50-1-8	"	1.53	4.01	2.63	590	670	3.16	638	723	"	"
50-1-9	"	1.55	4.07	2.50	583	663	3.16	642	727	"	"
50-1-11	1373	2.89	4.00	2.76	600	680	----	----	----	$2x10^{16}$	43
50-1-12	"	2.79	4.12	2.72	595	675	3.75	682	767	"	"
50-1-13	"	2.90	3.89	2.98	596	676	4.06	685	770	"	"
50-1-16	1373	4.93	4.03	2.84	603	683	----	----	----	$8x10^{15}$	43
50-1-17	"	4.79	3.92	3.05	602	682	4.77	715	801	"	"
50-1-18	"	5.01	4.02	3.04	620	700	4.33	729	815	"	"
50-1-19	"	5.08	3.95	2.81	621	701	4.30	733	819	"	"

* See footnote in Table XIX.

---- No photocell data was taken.

TABLE XXIV

SUMMARY OF EXPERIMENTAL DATA OF PI1 POLYMER IN INERT GAS, N_2

Run No.*	T_f	P_f	f_i	Exotherm		
				t	T_i	T_s+
	°K	atm	cal/sec cm^2	sec	°K	°K
21-1-1	1373	0.85	2.14	6.00	648	698
21-1-2	"	0.85	2.10	5.97	643	693
21-1-11	"	2.89	2.20	6.30	663	713
21-1-12	"	2.88	2.17	6.20	651	701
21-1-16	"	4.89	2.25	6.00	661	711

*See footnote in Table XIX.

+The tempersture drop across this polymer film is evaluated by multiplying the temperature drop across PC polymer film by a measured surface emissivity of 0.55 and dividing the product by 0.9 which is the assumed surface emissivity for PC polymer.

TABLE XXV

SUMMARY OF EXPERIMENTAL DATA OF AP-CONTAINING POLYMERS WITHOUT CATALYST IN INERT GAS, N_2
AT VARIOUS FURNACE TEMPERATURES
Presaure:0.85 atm N_2

Run No.*			Endotherm			Exotherm				Photocell Signal			Kinetic Parameters+	
	T_f	f_i	t	T_i	T_s	t	T_i	T_s	f_e	t	T_i	T_a	A	B
	°K	$\frac{cal}{sec\ cm^2}$	sec	°K	°K	sec	°K	°K	$\frac{cal}{sec\ cm^2}$	sec	°K	°K	$\frac{cal}{sec\ cm^3}$	$\frac{cal}{sec\ cm^2}$
22-1-1	1373	3.97	1.90	522	603	2.11	543	632	4.16	----	----	----	$9.3x10^{17}$	$1.2x10^{26}$
22-1-2	"	3.88	1.97	531	612	2.18	551	640	4.08	----	----	----	"	"
22-1-3	"	4.05	1.93	526	607	2.14	546	635	4.26	----	----	----	"	"
23-1-1	1373	4.06	1.94	523	603	2.10	538	624	4.31	2.33	556	660	$9.0x10^{17}$	$2.5x10^{26}$
23-1-2	"	3.97	1.94	529	609	2.09	537	623	4.59	2.38	563	667	"	"
23-1-3	"	4.03	1.82	512	592	1.96	524	610	4.24	2.14	545	649	"	"
23-1-4	"	3.88	1.81	522	602	1.91	533	619	4.19	2.16	566	670	"	"
36-1-1	1373	4.12	None	None	None	1.77	515	596	5.82	1.89	534	630	$8.5x10^{17}$	$5.0x10^{26}$
36-1-3	"	3.85	"	"	"	1.79	526	596	5.15	1.95	551	647	"	"
36-1-4	"	3.98	"	"	"	1.89	532	613	5.75	2.05	555	651	"	"
36-1-5	"	4.19	"	"	"	1.78	520	601	5.73	1.94	543	639	"	"
27-1-1	1373	4.02	None	None	None	1.76	522	590	15.04	1.74	521	605	$6.5x10^{17}$	$1.5x10^{27}$
27-1-2	"	4.03	"	"	"	1.77	521	589	13.45	1.79	525	609	"	"
27-1-3	"	3.95	"	"	"	1.62	525	593	14.73	1.62	525	609	"	"
23-2-1	1223	2.56	2.93	532	580	3.17	547	599	2.71	----	----	----	$9.0x10^{17}$	$2.5x10^{26}$
23-2-2	"	2.52	2.86	530	578	3.21	554	606	2.64	----	----	----	"	"
23-2-3	"	2.44	2.87	524	572	3.14	541	593	2.64	3.62	578	656	"	"

*See footnote in Table XIX.
+The activation energies for these tests are 43 kcal/g-mole for E_a and 75 kcal/g-mole for E_b.
---No photocell data was taken.

TABLE XXVI

SUMMARY OF EXPERIMENTAL DATA OF AP-CONTAINING POLYMERS WITH CATALYST IN INERT GAS, N_2
AT VARIOUS FURNACE TEMPERATURES
Pressure: 0.85 atm N_2

Run No.*			Endotherm			Exotherm				Photocell Signal			Kinetic Parameters+	
	T_f	f_i	t	T_i	T_s	t	T_i	T_s	f_e	t	T_i	T_s	A	B
	°K	$\frac{cal}{sec\ cm^2}$	sec	°K	°K	sec	°K	°K	$\frac{cal}{sec\ cm^2}$	sec	°K	°K	$\frac{cal}{sec\ cm^3}$	$\frac{cal}{sec\ cm^2}$
24-1-1	1373	4.01	1.80	525	605	1.92	536	619	4.66	2.14	565	667	9.0×10^{17}	2.5×10^{26}
24-1-2	"	4.07	1.76	524	604	1.90	537	620	4.40	2.14	567	669	"	"
24-1-3	"	4.02	1.80	526	606	1.95	539	622	4.81	2.12	564	666	"	"
24-1-4	"	3.88	1.83	520	600	1.95	532	615	4.32	2.14	561	663	"	"
24-1-5	"	4.08	1.81	529	609	1.97	543	626	4.72	2.14	569	671	"	"
37-1-1	1373	4.04	None	None	None	1.75	518	599	6.06	1.97	549	645	8.5×10^{17}	5.5×10^{26}
37-1-2	"	4.00	"	"	"	1.77	520	601	5.82	2.00	557	653	"	"
37-1-3	"	3.93	"	"	"	1.75	515	596	6.10	1.99	550	646	"	"
37-1-4	"	4.02	"	"	"	1.73	513	594	6.17	1.96	546	642	"	"
28-1-1	1373	3.88	None	None	None	1.76	509	578	21.81	1.76	509	593	6.5×10^{17}	3.0×10^{27}
28-1-2	"	4.13	"	"	"	1.78	515	584	15.12	1.76	516	600	"	"
28-1-3	"	3.95	"	"	"	1.68	495	564	19.73	1.68	492	576	"	"
28-1-4	"	3.87	"	"	"	1.60	498	567	8.49§	1.63	503	587	"	"
28-1-5	"	3.87	"	"	"	1.61	499	568	10.58§	1.61	499	583	"	"
51-1-1	1373	3.82	1.76	517	597	1.88	530	613	4.22	2.12	562	664	9.0×10^{17}	2.5×10^{26}
51-1-2	"	4.04	1.80	528	608	1.92	538	621	4.14	2.16	569	671	"	"
51-1-4	"	3.86	1.72	514	594	1.85	528	611	3.90	2.10	559	661	"	"
51-1-5	"	3.94	1.74	520	600	1.90	535	618	3.96	2.14	565	667	"	"
52-1-1	1373	3.90	None	None	None	1.77	511	580	7.10	1.79	515	597	6.5×10^{17}	2.0×10^{27}
52-1-2	"	3.88	"	"	"	1.82	519	588	6.52	1.82	519	601	"	"
52-1-3	"	4.01	"	"	"	1.62	510	579	5.87	1.61	509	591	"	"
52-1-4	"	3.86	"	"	"	1.78	513	582	5.61	1.78	513	595	"	"

(continued)

TABLE XXVI (continued)

Run No.*			Endotherm			Exotherm				Photocell Signal			Kinetic Parameters+	
	T_f	f_i	t	T_i	T_s	t	T_i	T_s	f_e	t	T_i	T_s	A	B
	°K	$\frac{cal}{sec\ cm^2}$	sec	°K	°K	sec	°K	°K	$\frac{cal}{sec\ cm^2}$	sec	°K	°K	$\frac{cal}{sec\ cm^3}$	$\frac{cal}{aec\ cm^2}$
24-2-1	1223	2.44	2.96	528	576	3.17	536	588	2.79	3.84	578	556	$9x10^{17}$	$2.5x10^{26}$
24-2-2	"	2.42	2.95	522	570	3.20	532	584	2.97	3.75	577	555	"	"
26-2-3	"	2.36	3.07	526	574	3.29	537	589	2.60	3.76	578	556	"	"
37-2-1	1223	2.43	None	None	None	3.05	521	571	3.54	3.41	549	623	$8.5x10^{17}$	$5.5x10^{26}$
37-2-2	"	2.40	"	"	"	2.95	510	560	2.96	3.44	539	613	"	"
51-2-1	1223	2.40	3.0	505	554	3.18	512	563	2.52	3.77	552	626	$9x10^{17}$	$2.5x10^{26}$
51-2-2	"	2.38	2.98	496	545	3.20	508	560	2.56	3.85	565	639	"	"
51-2-3	"	2.37	2.93	504	553	3.11	514	566	2.62	3.69	554	628	"	"
52-2-1	1223	2.35	None	None	None	2.77	496	536	5.21	2.37	493	554	$6.5x10^{17}$	$2.04x10^{27}$
52-2-2	"	2.44	"	"	"	2.78	500	540	5.56	2.75	497	558	"	"
24-3-1	1073	1.51	5.21	521	545	5.61	530	556	1.70	----	----	----	$9x10^{17}$	$2.5x10^{26}$
24-3-2	"	1.49	5.12	520	544	5.54	527	553	1.98	----	----	----	"	"
24-3-3	"	1.53	5.04	525	549	5.47	536	562	2.02	----	----	----	"	"
37-3-1	1073	1.43	5.12	509	531	5.35	517	540	2.47	----	----	----	$8.5x10^{17}$	$8.5x10^{26}$
37-3-2	"	1.56	5.18	515	537	5.30	514	537	2.36	----	----	----	"	"
37-3-3	"	1.48	5.16	512	533	5.48	525	548	2.39	----	----	----	"	"

*See footnote of Table XIX.

+The activation energies for these testa are 43 kcal/g-mole for E_a and 75 kcal/g-mole for E_b.

---No photocell data was taken.

§ This dsta ia rejected in the calculation of average f_e.

TABLE XXVII

SUMMARY OF EXPERIMENTAL DATA OF PC POLYMER IN OXYGEN

Run No.*				Exotherm				Photocell Signal			Kinetic Parameters	
	T_f	P_f	f_i	t	T_i	T_s	f_e	t	T_i	T_s	B	E_b
	°K	atm	$\frac{cal}{sec\ cm^2}$	sec	°K	°K	$\frac{cal}{sec\ cm^2}$	sec	°K	°K	$\frac{cal}{sec\ cm^2}$	$\frac{kcal}{g\text{-}mole}$
25-1-51	1373	0.85	3.82	1.32	442	524	5.38	1.66	494	608	$4x10^9$	26
25-1-52	"	"	3.95	1.37	455	537	6.07	1.64	501	615	"	"
25-1-53	"	"	4.11	1.36	458	540	6.21	1.59	508	622	"	"
25-1-54	"	"	4.06	1.25	447	529	5.59	1.54	498	612	"	"
25-1-55	"	"	3.92	1.13	449	531	6.12	1.35	495	609	"	"
25-1-56	1373	1.55	4.05	1.26	450	532	7.70	1.42	486	600	$6x10^9$	26
25-1-57	"	1.45	3.96	1.33	453	535	6.25	1.47	481	595	"	"
25-1-58	"	1.50	3.92	1.11	448	530	6.12	1.24	475	589	"	"
25-1-59	"	1.50	3.94	1.08	444	526	6.06	1.18	472	586	"	"
25-1-61	1373	2.89	3.95	1.29	443	526	7.32	1.34	455	569	$8x10^9$	26
25-1-62	"	2.86	4.08	1.28	452	535	7.70	1.32	463	577	"	"
25-1-63	"	2.80	4.01	1.27	447	520	8.04	1.33	461	575	"	"
25-1-65	"	2.89	4.03	1.34	455	538	8.32	1.38	466	580	"	"
25-1-66	1373	4.89	4.09	1.23	447	531	9.31	1.25	449	560	$1x10^{10}$	26
25-1-67	"	4.80	4.00	1.07	434	518	9.19	1.07	434	545	"	"
25-1-68	"	4.80	4.08	1.13	437	521	8.50	1.13	437	548	"	"
25-1-69	"	5.02	3.95	1.13	444	528	9.35	1.15	446	557	"	"
25-1-70	"	4.89	3.92	1.12	435	519	9.12	1.13	436	547	"	"

(continued)

TABLE XXVII (continued)

Run No.*				Exotherm				Photocell Signal			Kinetic Parameters	
	T_f	P_f	f_i	t	T_i	T_s	f_e	t	T_i	T_s	B	E_b
	°K	atm	$\frac{cal}{sec\ cm^2}$	sec	°K	°K	$\frac{cal}{sec\ cm^2}$	sec	°K	°K	$\frac{cal}{aec\ cm^2}$	$\frac{kcal}{g\text{-}mole}$
25-2-51	1223	0.85	2.44	2.53	495	547	4.22	3.06	562	651	3.5×10^9	26
25-2-52	"	"	2.46	2.68	490	542	3.99	3.16	545	634	"	"
25-2-53	"	"	2.52	2.62	504	556	3.82	3.10	555	644	"	"
25-3-51	1073	0.85	1.41	7.47	578	599	2.63	8.40	635	701	2.5×10^9	26
25-3-52	"	"	1.60	7.50	581	602	2.82	8.48	640	706	"	"
25-3-53	"	"	1.43	7.40	572	593	2.58	8.31	630	696	"	"

* See footnote in Table XIX.

TABLE XXVIII

SUMMARY OF EXPERIMENTAL DATA OF GLASS BEADS-CONTAINING POLYMERS IN OXYGEN
Furnace Pressure:0.85 atm. Furnace Temperature:1100°C

Run No.*		Exotherm				Photocell Signal			Kinetic Parameters	
	f_i	t	T_i	T_s	f_e	t	T_i	T_s	B	E_b
	$\frac{cal}{sec\ cm^2}$	sec	°K	°K	$\frac{cal}{sec\ cm^2}$	sec	°K	°K	$\frac{cal}{sec\ cm^2}$	$\frac{kcal}{g\text{-}mole}$
39-1-1	3.97	1.49	464	542	5.81	1.85	513	621	4.0×10^9	26
39-1-2	4.00	1.27	453	531	5.49	1.61	502	614	"	"
39-1-3	4.10	1.26	459	537	6.05	1.67	513	634	"	"
39-1-4	3.92	1.28	451	529	5.60	1.70	526	627	"	"
39-1-5	4.02	1.17	460	538	6.19	1.54	519	621	"	"
40-1-1	3.84	1.33	461	535	4.94	1.75	518	626	3.7×10^9	26
40-1-2	3.92	1.40	468	542	5.62	1.80	526	634	"	"
40-1-4	3.85	1.36	462	536	5.52	1.78	513	621	"	"
40-1-5	4.00	1.50	464	538	5.89	1.84	519	627	"	"
41-1-1	3.92	1.49	468	537	5.26	1.90	622	632	3.3×10^9	26
41-1-2	3.93	1.59	475	544	5.60	1.99	532	642	"	"
41-1-4	3.84	1.55	474	543	5.38	1.95	528	638	"	"
41-1-5	3.90	1.43	467	536	4.90	1.80	516	626	"	"
42-1-1	3.91	1.53	491	552	4.83	1.83	530	652	3.0×10^9	26
42-1-2	3.93	1.56	477	538	5.20	1.94	527	642	"	"
42-1-4	3.87	1.40	481	542	4.69	1.68	537	645	"	"
43-1-1	3.90	1.61	491	552	5.20	1.94	532	645	3.0×10^9	26
43-1-2	3.97	1.60	486	547	5.24	1.93	530	647	"	"
43-1-3	3.89	1.33	477	538	4.83	1.64	528	643	"	"

* See footnote in Table XIX.

TABLE XXIX

SUMMARY OF EXPERIMENTAL DATA OF AP CONTAINING POLYMERS IN OXYGEN
Furnace Pressure: 0.85 atm O_2. Furnace Temperature: 1100°C

Run No.*		Exotherm				Photocell Signal			Kinetic Parameters			
	f_i	t	T_i	T_s	f_e	t	T_i	T_s	B	E_b	C	E_c
	$\frac{cal}{sec\ cm^2}$	sec	°K	°K	$\frac{cal}{sec\ cm^2}$	sec	°K	°K	$\frac{cal}{sec\ cm^2}$	$\frac{kcal}{g\text{-}mole}$	$\frac{cal}{sec\ cm^2}$	$\frac{kcal}{g\text{-}mole}$
23-1-21	4.00	1.48	477	557	5.62	1.51	481	579	3.8×10^9	26	3.5×10^{16}	45
23-1-23	3.92	1.53	474	554	5.53	1.56	480	578	"	"	"	"
23-1-24	4.07	1.38	474	554	5.55	1.39	467	565	"	"	"	"
23-1-25	3.97	1.41	482	562	5.40	1.43	486	584	"	"	"	"
24-1-21	3.97	1.52	472	552	5.84	1.54	474	572	3.8×10^9	26	3.5×10^{16}	45
24-1-22	4.06	1.46	473	553	5.40	1.49	477	575	"	"	"	"
24-1-23	4.00	1.46	480	560	5.79	1.48	485	583	"	"	"	"
24-1-24	3.96	1.42	465	545	5.08	1.45	470	568	"	"	"	"
24-1-25	3.99	1.40	469	549	5.52	1.43	475	573	"	"	"	"
36-1-21	4.06	1.69	493	570	8.09	1.68	492	586	3.5×10^9	26	7×10^{16}	45
36-1-22	3.98	1.51	497	574	7.41	1.54	502	596	"	"	"	"
36-1-23	3.94	1.51	479	556	6.87	1.53	483	577	"	"	"	"
36-1-24	3.94	1.54	487	564	7.24	1.56	490	584	"	"	"	"
37-1-21	3.87	1.63	475	552	7.46	1.62	474	568	3.5×10^9	26	9×10^{16}	45
37-1-22	3.87	1.65	496	573	7.95	1.63	492	586	"	"	"	"
37-1-23	3.93	1.58	490	567	7.81	1.56	486	580	"	"	"	"

(continued)

TABLE XXIX (continued)

Run No.*		Exotherm				Photocell Signal			Kinetic Parameters			
	f_i	t	T_i	T_s	f_e	t	T_i	T_s	B	E_b	C	E_c
	$\frac{cal}{sec\ cm^2}$	sec	°K	°K	$\frac{cal}{sec\ cm^2}$	sec	°K	°K	$\frac{cal}{sec\ cm^2}$	$\frac{kcal}{g\text{-}mole}$	$\frac{cal}{sec\ cm^2}$	$\frac{kcal}{g\text{-}mole}$
27-1-21	3.90	1.74	470	540	22.10	1.74	470	555	2.5×10^9	26	2×10^{17}	45
27-1-22	3.98	1.92	492	562	21.25	1.90	490	575	"	"	"	"
27-1-23	3.83	1.35	476	546	20.09	1.32	472	557	"	"	"	"
27-1-24	3.88	1.55	489	559	20.78	1.54	488	573	"	"	"	"
28-1-21	3.83	1.50	473	543	24.25	1.48	470	555	2.5×10^9	26	2×10^{17}	45
28-1-22	3.86	1.58	487	557	23.72	1.56	487	572	"	"	"	"
28-1-23	3.98	1.53	492	562	23.21	1.52	491	576	"	"	"	"
28-1-24	4.07	1.55	479	549	24.11	1.55	479	564	"	"	"	"

* See footnote in Table XIX.

TABLE XXX

SUMMARY OF EXPERIMENTAL DATA OF A9C AND A9I POLYMERS AT LOWER FURNACE TEMPERATURES
Furnace Pressure: 0.85 atm O_2

Run No.*			Exotherm				Photocell Signal			Kinetic Parameters			
	T_f	f_i	t	T_i	T_s	f_e	t	T_i	T_s	B	E_b	C	E_c
	°K	$\frac{cal}{sec\ cm^2}$	sec	°K	°K	$\frac{cal}{sec\ cm^2}$	sec	°K	°K	$\frac{cal}{sec\ cm^2}$	$\frac{kcal}{g\text{-}mole}$	$\frac{cal}{sec\ cm^2}$	$\frac{kcal}{g\text{-}mole}$
24-2-51	1223	2.46	2.72	512	561	4.10	2.91	512	579	3.8×10^9	26	3.5×10^{16}	45
24-2-52	1223	2.51	2.77	508	557	4.16	2.79	511	578	"	"	"	"
24-3-51	1073	1.47	5.25	529	549	3.23	5.25	529	570	3.8×10^9	26	3.5×10^{16}	45
24-3-52	1073	1.49	5.40	530	550	3.16	5.36	531	572	"	"	"	"
51-2-51	1223	2.53	2.86	508	557	4.21	2.86	508	575	3.8×10^9	26	3.5×10^{16}	45
51-2-52	1223	2.46	2.88	499	548	4.00	2.84	497	564	"	"	"	"

*See footnote in Table XIX.

TABLE XXXI

SUMMARY OF EXPERIMENTAL DATA OF A09 POLYMER IN DIFFERENT OXYGEN PRESSURES
Furnace Temperature:950°C

Run No.*			Exotherm				Photocell Signal			Kinetic Parameters			
	P_f	f_i	t	T_i	T_s	f_e	t	T_i	T_s	B	E_b	C	E_c
	°K	$\frac{cal}{aec\ cm^2}$	sec	°K	°K	$\frac{cal}{sec\ cm^2}$	sec	°K	°K	$\frac{cal}{sec\ cm^2}$	$\frac{kcal}{g\text{-}mole}$	$\frac{cal}{sec\ cm^2}$	$\frac{kcal}{g\text{-}mole}$
23-2-51	0.85	2.48	2.74	515	564	4.22	2.74	515	582	3.8×10^9	26	3.5×10^{16}	45
23-2-52	0.85	2.48	2.82	520	569	4.09	2.83	521	588	"	"	"	"
23-2-53	0.85	2.49	2.90	512	561	4.08	2.91	513	580	"	"	"	"
23-2-54	0.85	2.56	2.93	519	568	4.44	2.95	521	588	"	"	"	"
23-2-56	3.04	2.47	2.35	504	555	6.20	2.33	502	564	1.5×10^{10}	26	3.5×10^{16}	45
23-2-57	3.05	2.54	2.39	507	558	6.10	2.37	505	567	"	"	"	"
23-2-61	5.07	2.52	2.12	488	541	7.36	2.09	485	545	2.5×10^{10}	26	3.5×10^{16}	45
23-2-62	4.91	2.55	2.08	495	548	7.70	2.06	493	553	"	"	"	"

*See footnote in Table XIX.

TABLE XXXII

WEIGHT LOSS AS A FUNCTION OF EXPOSURE TIME
FOR PC, PCC, A09 AND A9C POLYMERS

Heat Flux, 21.5 cal/sec cm^2, Pressure, < 0.1 in Hg N_2

Exposure Time	PC	PCC	A09	A9C
sec	mg/cm^2	mg/cm^2	mg/cm^2	mg/cm^2
0.03	0.063	0.201	0.260	----
0.05	0.189	0.394	0.597	0.660
0.07	0.692	----	1.258	1.383
0.08	0.817	1.069	----	----
0.09	1.382	----	2.547	2.767
0.1	2.152	2.370	3.458	3.553
0.13	3.370	3.678	5.093	5.219
0.15	4.162	4.338	6.162	6.288
0.20	6.086	6.351	8.803	8.991
0.25	----	----	11.318	11.506

---- No data was taken.

TABLE XXXIII

WEIGHT LOSS AS A FUNCTION OF EXPOSURE TIME
FOR PC, PCC, A09 AND A9C POLYMERS

Heat flux, 10.3 cal/sec cm^2. Pressure, < 0.1 in Hg N_2

Exposure Time	PC	PCC	A09	A9C
sec	mg/cm^2	mg/cm^2	mg/cm^2	mg/cm^2
0.00	0.0	0.0	0.0	0.0
0.16	----	----	----	----
0.18	0.0	----	----	0.094
0.20	----	0.063	0.189	----
0.23	0.094	0.138	0.409	0.566
0.26	0.252	0.359	1.006	1.195
0.30	0.440	0.552	1.949	2.044
0.33	----	----	2.515	2.672
0.35	0.805	0.893	3.119	3.301
0.38	----	1.195	----	----
0.40	1.377	1.509	4.175	4.401
0.45	2.138	2.264	----	----

---- No dsta was taken.

TABLE XXXIV

WEIGHT LOSS AS A FUNCTION OF EXPOSURE TIME
FOR PC AND PCC POLYMERS

Heating rate, 21.5 cal/sec. Pressure, 0.85 atm Helium

Exposure Time	PC	Surface Temp.	PCC	Surface Temp.
sec	mg/cm^2	°K	mg/cm^2	°K
0.0	0.0	300	0.0	300
0.03	0.062	595	0.130	584
0.05	0.180	669	0.272	633
0.08	0.768	705	1.040	655
0.095	1.462	709	2.016	659
0.11	2.364	711	2.854	664
0.15	3.857	718	4.218	673
0.20	5.203	726	6.137	682

TABLE XXXV

LISTING OF FORTRAN PROGRAM TO SOLVE EQUATIONS (B-1) TO (B-4) NUMERICALLY


```
$IBFTC MAIN
      0DIMENSION T(201),V(201),TS(800),TI(800),FLUXI(800),DTSI(800),
      1FLUXSI(800),TIME(800),DEPTH(201),RATEMS(800),RATEMI(800),
      2FLUXP(800)
       COMMON T,KOUNT,DELTAX,TEMPIN,FLUXS,CONDTY,MI,ALDELT
     1 READ 9, RUN,DISH,TEMPF,KL,H,THICK,WEIGTC
       READ 2, A,EA,B,EB,C,EC,S1,S2,S3
       READ 3, FLUXS,ALFA,CONDTY,DENSTY,CAPATY,EPSIRN,TEMPIN
       READ 4, TSMAX,KOUNT,KOMAX,MI
       READ 5, COSS1, COSS2, COSS3,COSS4,COSS5,CHC
     2 FORMAT (6E8.3, 3F8.5)
     3 FORMAT (7F8.5)
     4 FORMAT (F8.5, 3I8)
     5 FORMAT (6E9.3)
     9 FORMAT (3F8.5,I8,3F8.4)
   900FORMAT (110H0   RUN    DISH     DELTAX      DELTAT          KL
      1 MI  H        THICK                                          )
    91 FORMAT (1H ,2F8.3,2F12.7,2I8,2F8.4)
   200FORMAT (99H0  A           EA          B          EB          C
      1   EC       S1        S2        S3                           )
    21 FORMAT (1H ,6E11.3,3F8.1)
   300FORMAT (99H0    FLUXS        ALFA        CONDTY      DENSTY      CA
      1PATY      EPSIRN    TEMPIN          WEIGTC                    )
    31 FORMAT (1H , 8F12.6)
   400FORMAT (90H0      TEMPF      TSMAX          KA    KOMAX     KN    KO
      1UNT  COSS5          CHC                                       )
    41 FORMAT (1H , 2F12.5,4I8,E12.3,E12.5)
    50 FORMAT (53H0  COSS1        COSS2        COSS3        COSS4     )
    51 FORMAT (1H , 4E12.4)
   100 FORMAT (53H0   TSEMIN       T2L         T(1)         PG          G  )
   101 FORMAT (1H , 3F12.5, 2E12.4)
   110 FORMAT (53H0     DEPTH(I)  T(I)                                 )
   111 FORMAT (1H , 2F12.5)
  1200FORMAT (125H0     TIME(I)   TS(I)        TI(I)        FLUXI(I)
      1FLUXP(I)   DTSI(I)     RATEMS(I)       RATEMI(I)          FLUXSI(I
      2)       )
   121 FORMAT (1H , 6F12.5, 2E16.6, F12.5)
       T(1)=0.0
       PG=0.0
       G=0.0
       CI=MI-2
       DELTAX=THICK/CI
       DELCON=DELTAX/CONDTY
       DELCO2=2.0*DELCON
       DELTAT=0.5*(DELTAX**2)/ALFA
       ALDELT=ALFA*DELTAT
       DETLDC=DELTAT/(0.093*WEIGTC)
       EPFLUS=EPSIRN*FLUXS
       EPSIGM=0.000000000013545*EPSIRN
       S1B=S1*B
       S2C=S2*C
       S3A=S3*A
       S3ADX=S3A*DELTAX*0.5
       RR=1.0/1.987
       EBRR=EB*RR
       S1BEBR=S1B*EBRR
       ECRR=EC*RR
       S2CECR=S2C*ECRR
       EARR=EA*RR
```

```
      S3AEAR=S3ADX*EARR
      CALL TEMPB
      KA=KOUNT
      KN=KOUNT
      MIJ=MI-1
      MIP=MI-2
      ROTEM4=8100000000.0
      CE=COSS4*EPSIGM
      CE4=4.0*CE
      CC5=COSS5*CHC
      ALS3A=ALDELT*S3A
      I=0
      HA=1.327*H
   12 KOUNT=KOUNT+1
      CC=-1.0/T(2)
      CC2=CC*CC
      IF (KOUNT-KOMAX) 13, 24, 24
  130PG=CC2*S1BEBR*EXP(CC*EBRR)+CC2*S2CECR*EXP(CC*ECRR)+CC2*S3AEAR*EXP
     1(CC*EARR)-CE4*T(2)**3-CC5
      DP=DELCON*PG
      IF (1.0-0.6*DP) 24, 16, 16
  160G=EPFLUS+S1B*EXP(CC*EBRR)+S2C*EXP(CC*ECRR)+S3ADX*EXP(CC*EARR)-CE*
     1T(2)**4+CC5*(TEMPF-T(2))
      T(1)=(T(3)+DELCO2*(G+PG*(0.25*T(3)-0.5*T(2))))/(1.0-0.5*DP)
      V(2)=0.5*(T(1)+T(3))
      DO 18 M=3,MIJ
   18 V(M)=0.5*(T(M-1)+T(M+1))+(ALS3A*EXP(-EARR/T(M)))/CONDTY
      COUNT=KOUNT
     0V(MI)=T(MI)+DETLDC*((HA*(4.0*T(MIJ)-T(MIP)-3.0*T(MI)))/DELCO2
     1-COSS1*(T(MI)**4-ROTEM4)-COSS2*(T(MI)-300.)/SQRT(DELTAT*COUNT)
     2-COSS3*(T(MI)-300.)+S3ADX*EXP(-EA/(1.987*T(MI))))
      DO 19 M=2,MI
   19 T(M)=V(M)
      IF (T(2)-TSMAX) 22, 24, 24
   22 IF (KL+KN-KOUNT) 26,26,12
   26 I=I+1
      TIME(I)=DELTAT*COUNT
      TI(I)=T(MI)
      TS(I)=T(2)
      FLUXI(I)=(T(MIJ)-T(MI))/DELCON
      FLUXP(I)=(4.0*T(MIJ)-T(MIP)-3.0*T(MI))/DELCO2
      DTSI(I)=TS(I)-TI(I)
      FLUXSI(I)=DTSI(I) /(DELCON*CI)
      KN=KOUNT
      KOUNT=KOUNT+1
      CC=-1.0/T(2)
      CC2=CC*CC
     0PG=CC2*S1BEBR*EXP(CC*EBRR)+CC2*S2CECR*EXP(CC*ECRR)+CC2*S3AEAR*EXP
     1(CC*EARR)-CE4*T(2)**3-CC5
      DP=DELCON*PG
      IF (1.0-0.6*DP) 24, 36, 36
  360G=EPFLUS+S1B*EXP(CC*EBRR)+S2C*EXP(CC*ECRR)+S3ADX*EXP(CC*EARR)-CE*
     1T(2)**4+CC5*(TEMPF-T(2))
      T(1)=(T(3)+DELCO2*(G+PG*(0.25*T(3)-0.5*T(2))))/(1.0-0.5*DP)
      V(2)=0.5*(T(1)+T(3))
      DO 500 M=3,MIJ
  500 V(M)=0.5*(T(M-1)+T(M+1))+(ALS3A*EXP(-EARR/T(M)))/CONDTY
      COUNT=KOUNT
     0V(MI)=T(MI)+DETLDC*((HA*(4.0*T(MIJ)-T(MIP)-3.0*T(MI)))/DELCO2
```

```
     1-COSS1*(T(MI)**4-ROTEM4)-COSS2*(T(MI)-300.)/SQRT(DELTAT*COUNT)
     2-COSS3*(T(MI)-300.)+S3ADX*EXP(-EA/(1.987*T(MI))))
      DO 600 M=2,MI
  600 T(M)=V(M)
      RATEMS(I)=(T(2)-TS(I))/DELTAT
      RATEMI(I)=(T(MI)-TI(I))/DELTAT
      GO TO 12
   24 KK=(KOUNT-KA)/KL
      DEPTH(2)=0.0
      DO 400 M=3,MI
  400 DEPTH(M)=DEPTH(M-1)+DELTAX
      T2L=T(2)
      COUNT=KOUNT
      ALFTIM=ALDELT*COUNT
      SALTI=SQRT(ALFTIM)
      TSEMIN=TEMPIN+(1.12838*FLUXS*SALTI)/CONDTY
      PRINT 90
      PRINT 91,(RUN,DISH,DELTAX,DELTAT,KL,MI,H,THICK)
      PRINT 20
      PRINT 21,(A,EA,B,EB,C,EC,S1,S2,S3)
      PRINT 30
      PRINT 31,(FLUXS,ALFA,CONDTY,DENSTY,CAPATY,EPSIRN,TEMPIN,WEIGTC)
      PRINT 40
      PRINT 41,(TEMPF ,TSMAX,KA,KOMAX,KN,KOUNT,COSS5,CHC)
      PRINT 50
      PRINT 51, (COSS1,COSS2,COSS3, COSS4)
      PRINT 100
      PRINT 101, (TSEMIN,T2L,T(1),PG,G)
      PRINT 110
      PRINT 111, (DEPTH(I),T(I),I=2,MI)
      PRINT 120
     OPRINT 121, (TIME(I),TS(I),TI(I),FLUXI(I),FLUXP(I),DTSI(I),
     1  RATEMS(I),RATEMI(I),FLUXSI(I),I=1,KK)
      GO TO 1
      END
$IBFTC TEMPB
      SUBROUTINE TEMPB
      DIMENSION T(201),V(201),P(5),DEPTH(201)
      COMMON T,KOUNT,DELTAX,TEMPIN,FLUXS,CONDTY,MI,ALDELT
      COUNT=KOUNT
      ALFTIM=ALDELT*COUNT
      SALTI=SQRT(ALFTIM)
      SALFLU=SALTI*FLUXS
      T(2)=TEMPIN+1.12838*SALFLU/CONDTY
      DEPTH(2)=0.0
      DO 200 M=3,MI
      DEPTH(M)=DEPTH(M-1)+DELTAX
      ARG=0.5*DEPTH(M)/SALTI-1.0
      IF (0.95-ARG) 180, 181, 181
  180 T(M)=TEMPIN
      GO TO 200
  181 P(1)=ARG
      P(2)=2.*ARG*P(1)-1.
      P(3)=2.*ARG*P(2)-P(1)
      P(4)=2.*ARG*P(3)-P(2)
      PIERFC=0.32746-0.50557*P(1)+0.23213*P(2)-0.0608*P(3)+0.00516*P(4)
      T(M)=TEMPIN+SALFLU*PIERFC/CONDTY
  200 CONTINUE
      RETURN
      END
```

TABLE XXXVI

DEFINITION OF VARIABLE NAMES USED IN TABLE XXXV

Variable	Use
A	Pre-exponential factor in Arrhenius expressions (reaction in the bulk of test sample).
ALDELT	Dummy defined as ALFA*DELTAT.
ALFA	Thermal diffusivity, $k_s/\rho c$.
ALFTIM	Dummy defined as ALDELT*COUNT.
ALS3A	Dummy defined as ALDELT*S3A.
ARG	Dummy defined as $\frac{1}{2}\frac{\text{DEPTH(M)}}{\text{SALTI}} - 1.0$.
B	Pre-exponential factor in Arrhenius expressions (surface reaction # 1).
C	Pre-exponential factor in Arrhenius expressions (surface reaction # 2).
CAPATY	Heat capacity of test film.
CC	Reciprocal surface temperature in minus sign.
CC2	Dummy defined as CC*CC.
CC5	Dummy defined as COSS5*CHC.
CE	Dummy defined as COSS4*EPSIGM.
CE4	Dummy defined as 4.0*CE.
CHC	Transient heat transfer coefficient between environment and copper disk gage, estimated for total exposed sres.
CI	Number of divisions in the test film.
CONDTY	Thermal conductivity of test film.
COSS1	Coefficient of radiation loss from back face of copper disk.
COSS2	Coefficient of conduction loss through two thermocouple wires.
COSS3	Coefficient of convection loss from back face of copper disk.
COSS4	Control parameter for radiation loss from test film to environment, which has values of either 1 or 0.

(continued)

TABLE XXXVI (continued)

Variable	Use
COSS5	Control paramenter for energy gain by convection from environment to test film which has values of either 1 or 0.
COUNT	Floating point number for KOUNT.
DELCO2	Dummy defined as 2.0*DELCON.
DELCON	ΔX divided by thermal conductivity of test film.
DELTAT	ΔT, time increment.
DELTAX	ΔX, space increment.
DENSTY	Density of test film.
DEPTH	Depth measured from surface.
DETLDC	Dummy defined as DELTAT/(0.093*WEIGTC).
DISH	Identification number of test sample.
DP	Dummy defined as DELCON*PG.
DTSI	Difference between surface and interface temperature.
EA	Activation energy of condensed phase reaction.
EARR	Dummy defined as EA*RR.
EB	Activation energy of surface reaction # 1.
EBRR	Dummy defined as EB*RR.
EC	Activation energy of surface reaction #2.
ECRR	Dummy defined as EC*RR.
EPFLUS	Effective incident radiation energy at the test film surface.
EPSIGM	Dummy defined as 1.3545×10^{-12}*EPSIRN.
EPSIRN	Emissivity of test film surface.
FLUXI	Heat flux at the interface estimated from the last ΔX division next to interface.
FLUXP	Heat flux at the interface estimated by assuming a parabola through the last three nodal points next to interface.
FLUXS	Incident heat flux.
FLUXSI	Heat flux at the interface estimated by assuming a linear temperature gradient between the surface and interface temperature.
G	Dummy defined in Eq. (B-18).
H	Exposure area divided by copper disk area.
HA	Actual exposure area.

(continued)

TABLE XXXVI (continued)

Variable	Use
I	A parameter used to store calculated values and control the print out.
KA	Input KOUNT.
KK	Total rows of print out.
KL	A parameter used to control the interval of each print out.
KN	A variable which is set equal to previous value of KOUNT before going on to next KL cycles of calculation.
KOMAX	Maximum number of time increment.
M	Do-loop parameter.
MI	Node number at the interface.
MIJ	Node number at one ΔX from interface.
MIP	Node number at two ΔX from interface.
P	Chebyshev Polynomials.
PG	Dummy defined in Eq. (B-18).
RATEMI	Rate of temperature rise at the interface.
RATEMS	Rate of temperature rise at the surface.
RR	Reciprocal gas constant.
RUN	Identification number for a computer run.
S1	Control parameter for surface reaction # 1 which has valuea of ± 1 or 0.
S2	Control parameter for surface reaction # 2 which has values of ± 1 or 0.
S3	Control parameter for condensed phase reaction which has values of ± 1 or 0.
S1B	Dummy defined as S1*B.
S1BEBR	Dummy defined as S1B*EBRR.
S2C	Dummy defined as S2*C.
S2CECR	Dummy defined as S2C*ECRR.
S3A	Dummy defin as S3*A.
S3ADX	Dummy defin as 0.5*S3A*DELTAX.

(continued)

TABLE XXXVI (continued)

Variable	Use
S3AEAR	Dummy defined as S3ADX*EARR.
SALFLU	Dummy defined aa SALTI*FLUXS.
SALTI	Dummy defined as $\sqrt{\text{ALFTIM}}$.
T	Temperaturea which are aet equal to V.
T2L	The higheat calculated surface temperature.
TEMPF	Furnace temperature.
TEMPIN	Initial temperature of the teat aample.
THICK	The thickness of the teat sample.
TI	Interface temperature.
TIME	Accumulated time of expoaure.
TS	Surface temperature.
TSEMIN	Maximum aurface temperature when the teat aample ia a aemi-infinite body.
TSMAX	Maximum surface temperature.
V	Calculated temperatures at KOUNT=KOUNT + 1.
WEIGHTC	Weight of copper diak.

FIGURE 61

FLOW DIAGRAM OF FORTRAN PROGRAM IN TABLE XXXV

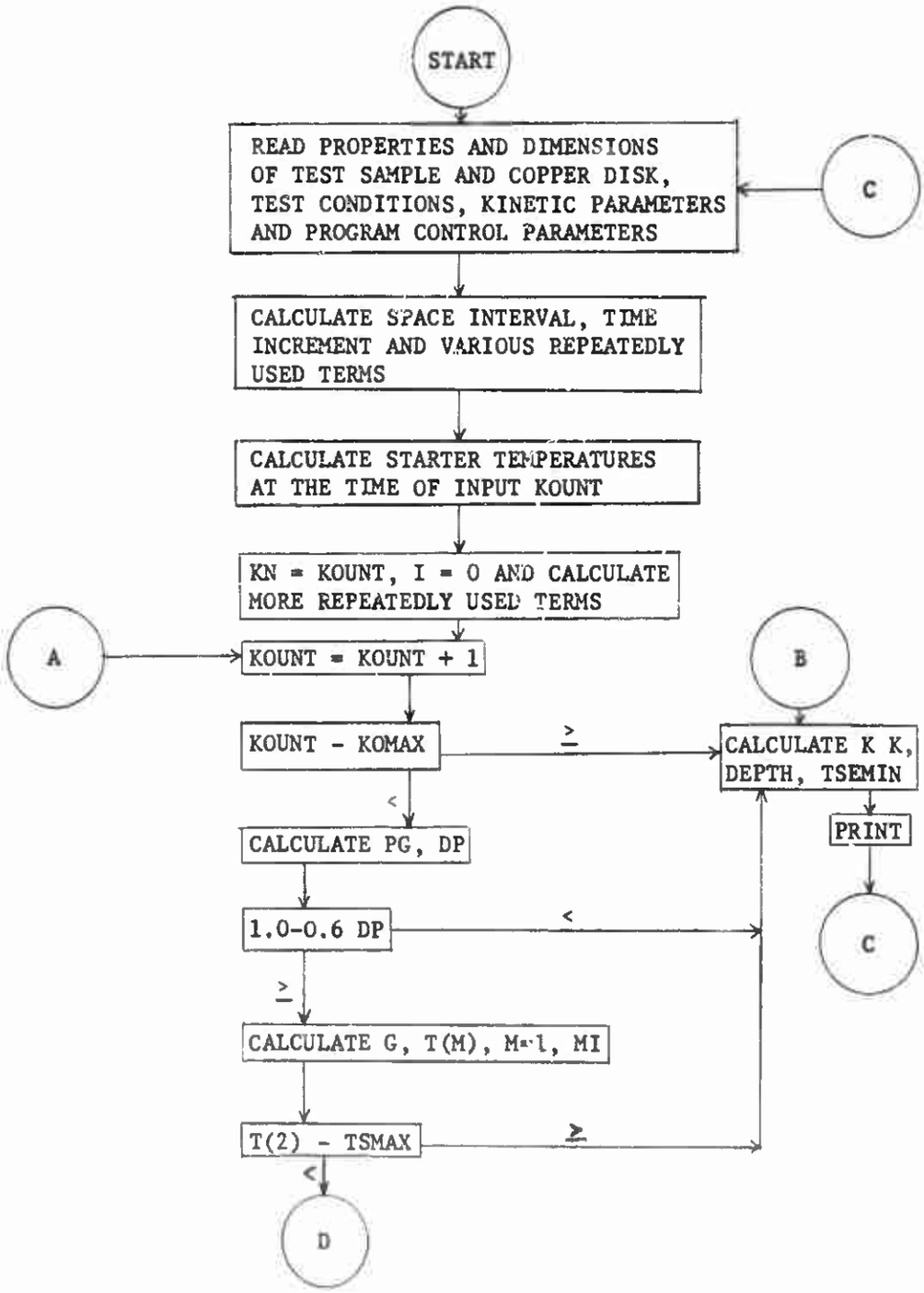

(continued)

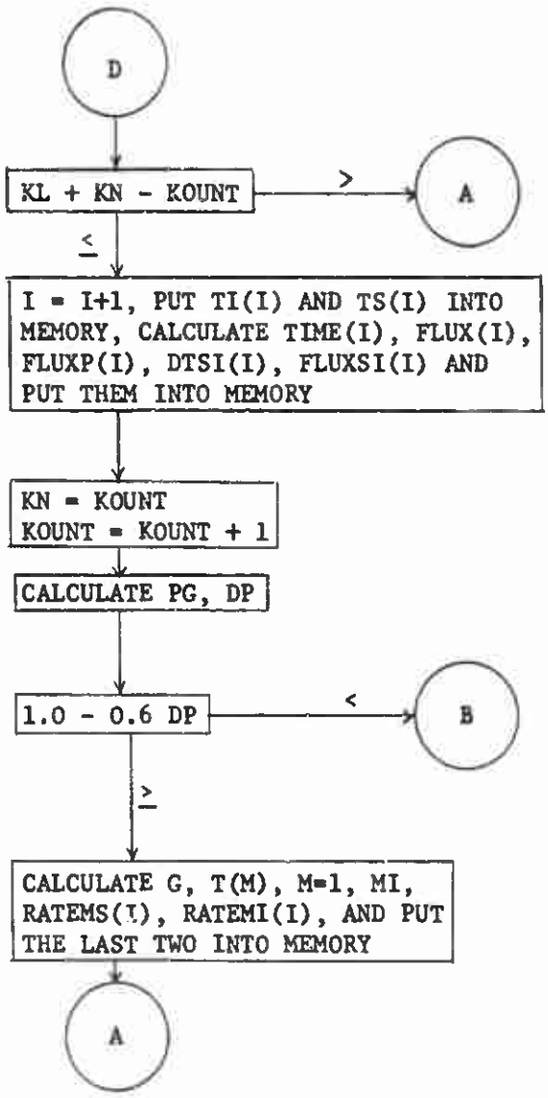
D
KL + KN - KOUNT
>
A
≤
I = I+1, PUT TI(I) AND TS(I) INTO MEMORY, CALCULATE TIME(I), FLUX(I), FLUXP(I), DTSI(I), FLUXSI(I) AND PUT THEM INTO MEMORY
KN = KOUNT
KOUNT = KOUNT + 1
CALCULATE PG, DP
1.0 - 0.6 DP
<
B
≥
CALCULATE G, T(M), M=1, MI, RATEMS(I), RATEMI(I), AND PUT THE LAST TWO INTO MEMORY
A

TABLE XXXVII

LISTING OF FORTRAN PROGRAM TO CALCULATE TEMPERATURES IN EQUATIONS (C-20), (C-21) and (C-22)


```
$IBFTC MAIN
      0DIMENSION TIME(100),UI(100),US(100),BETA(100),BETAI(100),
      1          BETAS(100),DEPTH(20),UB(20),FFLUX(100),SUMI(101),
      2          SUMS(101),SUMB(101) ,FLUXI(100), DUSI(100)
      0COMMON BETA,BBS,DENO,UOMI1,ARG,HCR,HCR1,CONSTT,UOMB1,UOMB3,
      1       DEPTH,UOMB4,BETAD,QUOTB,SUMB,JJ,K1
    1 READ 3,RUN,FLUX,HCR, CONST,T,RESI,CDR
    2 READ 4,(BETA(J),J=1,6)
    3 FORMAT (6F12.0, F8.0)
    4 FORMAT (6F12.0)
    5 FORMAT (1H ,F6.2,2F10.4,2E10.4,3F10.4)
    6 FORMAT (1H ,8F10.6)
    7 FORMAT (1H ,2F12.6)
  510FORMAT (72H0 TIME      UI        US        BETAI      BETAS     FFLUX
    1 FLUXI      DUSI       )
   71 FORMAT (24H0   DEPTH          UB          )
  610FORMAT (85H0  RUN       FLUX        HCR        CONST      TTIME      T
    1          RESI       CDR                                              )
      RFLUX=1.0/FLUX
      DIV=1.0/(1.0+HCR)
      TERM2=0.5*(1.0+2.0*HCR)*DIV
      TERM3=0.16667*(1.0+3.0*HCR)*(DIV**2)
      TIME(1)=0.0
      I=1
   13 TERM1=CONST*(HCR**2)*DIV*TIME(I)
      TER13=TERM1-TERM3
      SUMS(1)=0.0
      SUMI(1)=0.0
      CONSTT=-CONST*TIME(I)
      HCR1=1.0+HCR
      DO 20 J=1,6
      JJ=J
      CALL BDAN
      UOMI2=(1.0+BBS)*UOMI1
      UOMI3=1.0/COS(BETA(J))
      QUOTS=UOMI2/DENO
      QUOTI=UOMI1*UOMI3/DENO
      SUMI(J+1)=SUMI(J)+QUOTI
   20 SUMS(J+1)=SUMS(J)+QUOTS
      J=6
   19 IF(QUOTI-RESI ) 22,21,21
   21 J=J+1
      BETA(J)=BETA(J-1)+3.1416
      JJ=J
      CALL BDAN
      UOMI3=1.0/COS(BETA(J))
      QUOTI=UOMI1*UOMI3/DENO
      SUMI(J+1)=SUMI(J)+QUOTI
      GO TO 19
   22 BETAI(I)=BETA(J)
      TERM4I=2.0*SUMI(J+1)
      UI(I)=FLUX*(TER13-TERM4I)
      J=6
   29 IF(QUOTS-RESI ) 32,31,31
   31 J=J+1
      BETA(J)=BETA(J-1)+3.1416
      BBS=(BETA(J)*HCR)**2
      DENO=BETA(J)**2*(HCR1+BBS)
      ARG=CONSTT*BBS
```

```
      UOMI1=EXP(ARG)
      UOMI2=(1.0+BBS)*(UOMI1)
      QUOTS=UOMI2/DENO
      SUMS(J+1)=SUMS(J)+QUOTS
      GO TO 29
   32 BETAS(I)=BETA(J)
      TERM4S=2.0*SUMS(J+1)
      US(I)=FLUX*(TER13+TERM2-TERM4S)
      DUSI(I)=US(I)-UI(I)
      FFLUX(I)=DUSI(I)*RFLUX
      SUMB(1)=0.0
      DEPTH(10)=0.99
      DO 100 K=10,11
      K1=K
      TERM2B=(0.5*(1.0-DEPTH(K1))**2+HCR*(1.0-DEPTH(K1)))*DIV
      DO 801 J=1,6
      JJ=J
      CALL BULK
  801 CONTINUE
      J=6
  791 IF(QUOTB-RESI ) 821,811,811
  811 J=J+1
      BETA(J)=BETA(J-1)+3.1416
      JJ=J
      CALL BULK
      GO TO 791
  821 TERM4B=2.0*SUMB(J+1)
      UB(K1)=FLUX*(TER13+TERM2B-TERM4B)
      DEPTH(K1+1)=1.0
  100 CONTINUE
      FLUXI(I)=(UB(10)-UB(11))*CDR
      IF(US(I)-450.0) 12,11,11
   12 I=I+1
      TIME(I)=TIME(I-1)+T
      GO TO 13
   11 TTIME=TIME(I)
      II=I
      SUMB(1)=0.0
      DEPTH(1)=0.0
      DO 40 K=1,11
      K1=K
      TERM2B=(0.5*(1.0-DEPTH(K1))**2+HCR*(1.0-DEPTH(K1)))*DIV
      DO 80 J=1,6
      JJ=J
      CALL BULK
   80 CONTINUE
      J=6
   79 IF(QUOTB-RESI ) 82,81,81
   81 J=J+1
      BETA(J)=BETA(J-1)+3.1416
      JJ=J
      CALL BULK
      GO TO 79
   82 TERM4B=2.0*SUMB(J+1)
      UB(K1)=FLUX*(TER13+TERM2B-TERM4B)
   40 DEPTH(K1+1)=DEPTH(K1)+0.1
      PRINT 61
      PRINT 6, (RUN,FLUX,HCR,CONST,TTIME,T,RESI,CDR)
      PRINT 51
```

```
      0PRINT 5, (TIME(I),UI(I),US(I),BETAI(I),BETAS(I),FFLUX(I),
      1 FLUXI(I), DUSI(I), I=1,II)
       PRINT 71
       PRINT 7,(DEPTH(J),UB(J),J=1,11)
       GO TO 1
       END
$IBFTC BDAN
       SUBROUTINE BDAN
       DIMENSION BETA(100),DEPTH(20),SUMB(101)
      0COMMON BETA,BBS,DENO,UOMI1,ARG,HCR,HCR1,CONSTT,UOMB1,UOMB3,
      1        DEPTH,UOMB4,BETAD,QUOTB,SUMB,JJ,K1
       J=JJ
       BBS=(BETA(J)*HCR)**2
       DENO=BETA(J)**2*(HCR1+BBS)
       ARG=CONSTT*BBS
       UOMI1=EXP(ARG)
       RETURN
       END
$IBFTC BULK
       SUBROUTINE BULK
       DIMENSION BETA(100),DEPTH(20),SUMB(101)
      0COMMON BETA,BBS,DENO,UOMI1,ARG,HCR,HCR1,CONSTT,UOMB1,UOMB3,
      1        DEPTH,UOMB4,BETAD,QUOTB,SUMB,JJ,K1
       J=JJ
       BBS=(BETA(J)*HCR)**2
       DENO=BETA(J)**2*(HCR1+BBS)
       ARG=CONSTT*BBS
       UOMB1=EXP(ARG)
       UOMB3=1.0/COS(BETA(J))
       BETAD=BETA(J)*(1.0-DEPTH(K1))
       UOMB4=COS(BETAD)-HCR*BETA(J)*SIN(BETAD)
       QUOTB=UOMB1*UOMB4*UOMB3/DENO
       SUMB(J+1)=SUMB(J)+QUOTB
       RETURN
       END
```

TABLE XXXVIII

DEFINITION OF VARIABLE NAMES USED IN TABLE XXXVII

Variable	Use
ARG	Dummy defined as CONSTT*BBS.
BBS	Dummy defined as (BETA(J)*HCR)**2.
BETA	Roots of Eq. (C-18).
BETAD	Dummy defined as BETA(J)*(1.0-DEPTH(K1)).
BETAI	Maximum BETA(J) used to calculate interface temperature at each TIME.
BETAS	Maximum BETA(J) used to calculate surface temperature at each TIME.
CDR	Thermal conductivity of test film divided by one-hundredth of film thickness.
CONST	Dummy defined as α/ξ^2.
CONSTT	Dummy defined as -CONST*TIME(I).
DENO	Dummy defined as BETA(J)**2*(HCR1+BBS).
DEPTH	Depth divided by film thickness.
DIV	Dummy defined as 1.0/(1.0+HCR).
DUSI	Difference between surface and interface temperature.
FFLUX	Ratio of calculated heat flux by assuming a linear temperature gradient between surface temperature and interface temperature to incident heat flux.
FLUX	Dummy defined as $f_s \ell/k_s$.
FLUXI	Interface heat flux calculated by assuming a linear temperature gradient within the last one-hundredth of film thickness next to interface.
HCR	Dummy defined as $L\rho' c'/\rho c$.
HCRI	Dummy defined as HCR+1.0.
I	Number of time increment.
II	Dummy which is set equal to I.
J	Number used to identify different BETA(J).

(continued)

TABLE XXXVIII (continued)

Variable	Use
JJ	Dummy which is set equal to J.
K	Do-loop parameter.
K1	Dummy which is set equal to K.
QUOTB	Dummy defined as UOMB1*UOMB4*UOMB3/DENO.
QUOT1	Dummy defined as UOM11*UOM13/DENO.
QUOTS	Dummy defined as UOM12/DENO.
RES1	Input value for calculated QUOTB, QUOT1 and QUOTS to compare with.
RFLUX	Reciprocal FLUX.
RUN	Identification number of a computer run.
SUMB	Summation of QUOTB.
SUM1	Summation of QUOT1.
SUMS	Summation of QUOTS.
T	Time increment between each cycle of calculation.
TERM1	Dummy defined as CONST*(HCR**2)*DIV*TIME(1).
TER13	Dummy defined as TERM1-TERM3.
TERM2	Dummy defined as 0.5*(1.0+2.0*HCR)*(DIV).
TERM3	Dummy defined as 0.16667*(1.0+3.0*HCR)*(DIV**2).
TERM2B	Dummy defined as (0.5*(1.0-DEPTH(K1))**2+HCR*(1.0-DEPTH(K1)))*DIV.
TERM4B	Dummy defined as 2.0*SUMB(J+1).
TERM41	Dummy defined as 2.0*SUM1(J+1).
TERM4S	Dummy defined as 2.0*SUMS(J+1).
TIME	Accumulated time of exposure to FLUX.
TTIME	Maximum exposure time.
UB	Temperatures in the polymer bulk surface and interface.
U1	Interface temperatures.
UOMB1	Dummy defined as EXP(ARG).
UOMB3	Reciprocal COS(BETA(J)) in the SUBROUTINE BULK.
UOMB4	Dummy defined as COS(BETAD)-HCR*BETA(J)*SIN(BETAD).
UOM12	Dummy defined as (1.0+BBS)*UOM11.
UOM13	Reciprocal COS(BETA(J)) in the main program.
US	Surface temperatures.

FIGURE 62

FLOW DIAGRAM OF FORTRAN PROGRAM IN TABLE XXXVII

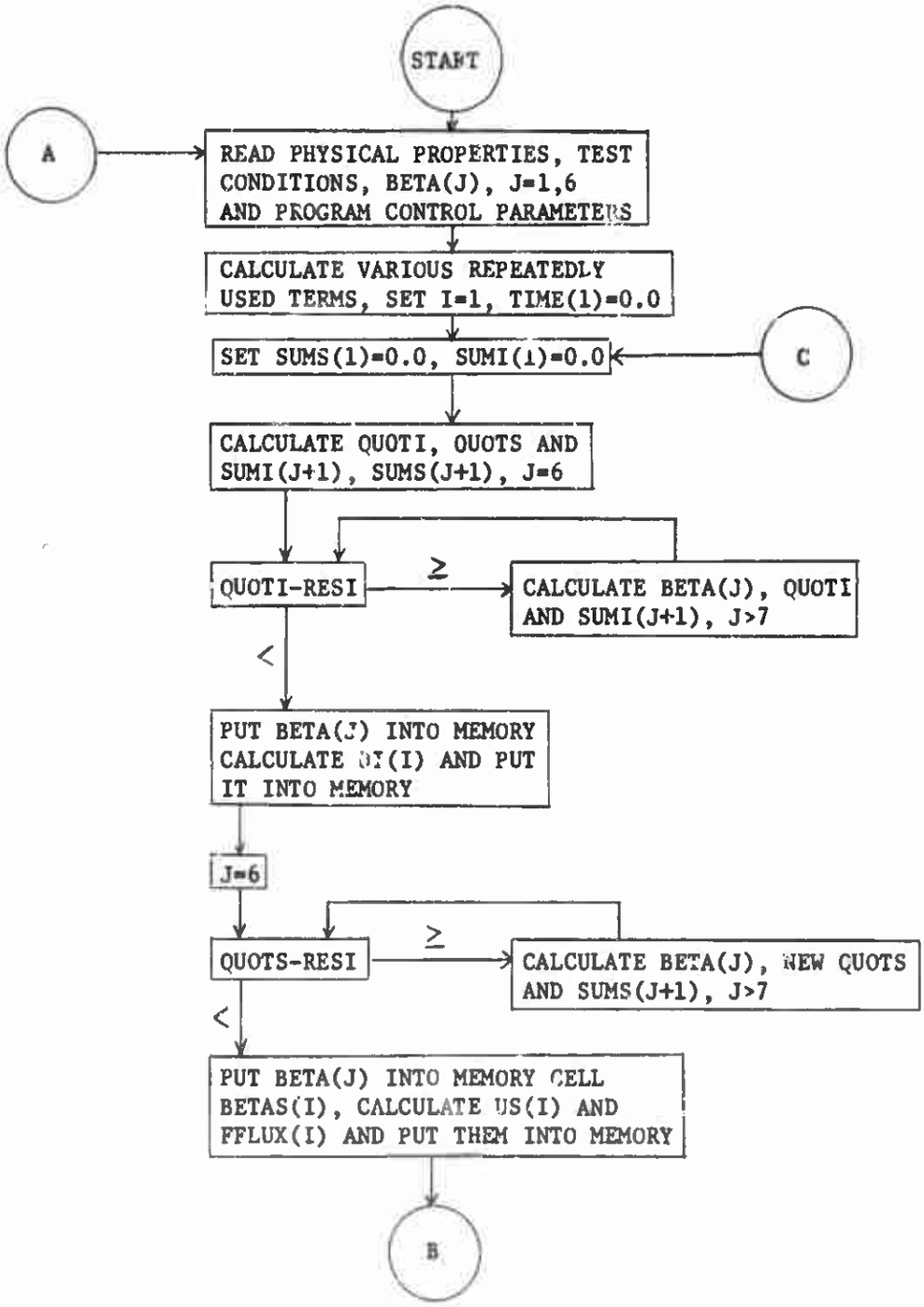

(continued)

FIGURE 62 (continued)

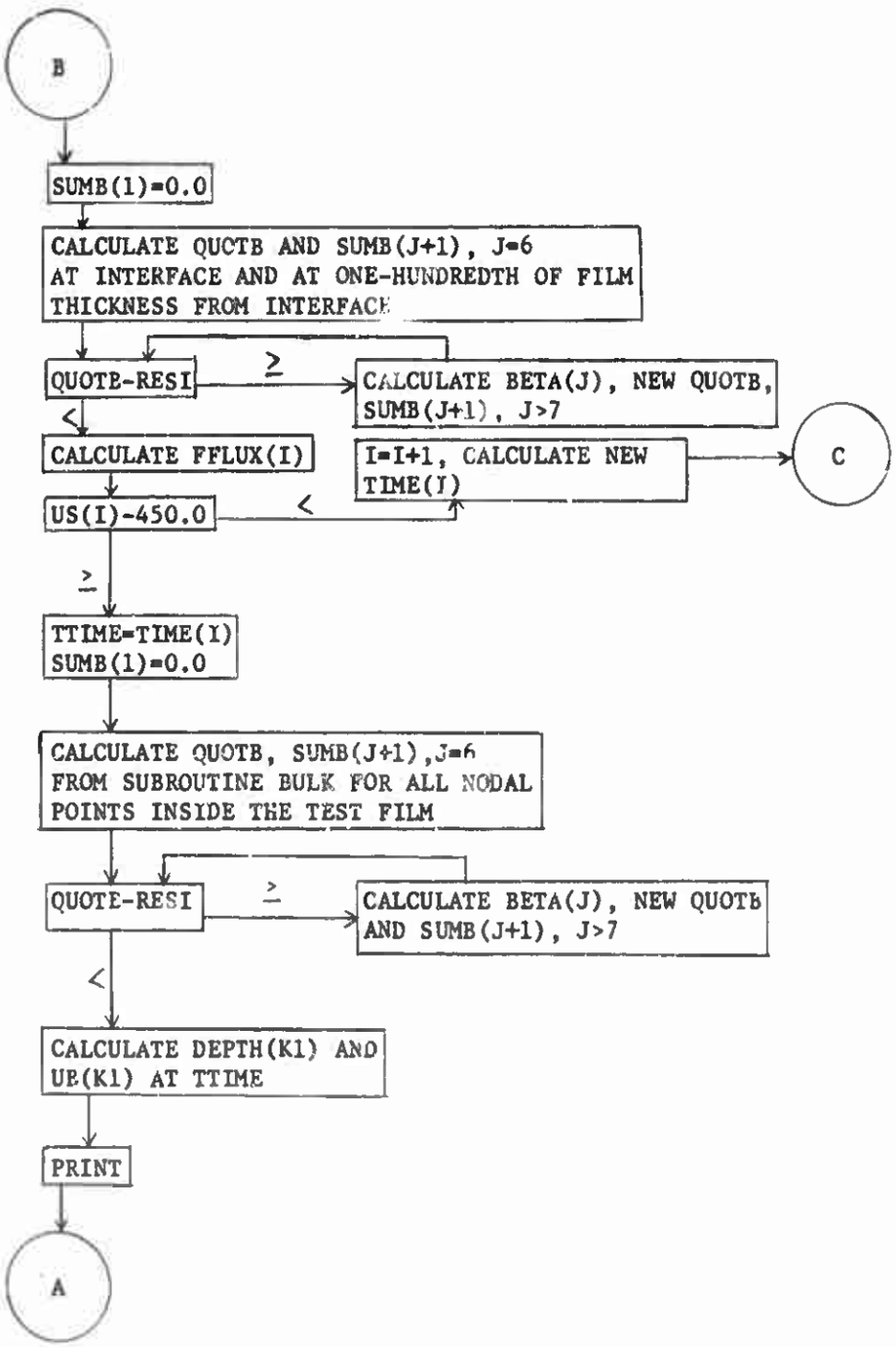

APPENDIX G

TABLE OF NOMENCLATURE

A	Pre-exponential conatant in the Arrhenius expression.
A_a	Aperture area of plane aluminum foil ahield for calorimeter cm^2.
a	Area of copper diak gage, cm^2.
a_e	Area of exposure in the radiation furnace test, cm^2.
a_r	Abaorptivity of calorimeter receiver.
a_w	Crosa aectional area of thermocouple wire, cm^2.
B	Pre-exponential conatant in the Arrheniua expression for aurface reaction # 1, cal/(aec)$(cm)^2$.
B_c	Defined aa $L\rho'c'$, cal/$(cm)^2$(°C)
C	Pre-exponantial conatant in the Arrhenius expression for aurface reaction # 2, cal/(sec)$(cm)^2$.
C_a	A conatant.
C_1, C_2	Two constanta in Eq. (VI-14), °K for C_1, C_2 haa no unit.
c, c_c, c'	Heat capacities of test sample, calorimeter and copper diak, cal/°C)(g).
c_1, c_2, c_3	Constanta.
D_1, D_2	Two integration constants.
E, E_a E_b, E_c	Activation energiea of reactiona, kcal/g-mole.
F	Defined as ϵf_s, cal/(sec)$(cm)^2$.
f	Heat flux meaaured by the calorimeter, cal/(aec)$(cm)^2$.

f_e Heat flux during exotherm measured at the test film-copper disk interface, cal/(sec)(cm)^2.

f_i Heat flux measured at the test film-copper disk interface before reaction, cal/(sec)(cm)^2.

f_s Incident radiation heat flux, cal/(sec)(cm)^2.

$G_{o,j}$ Total heat flux at the test film surface at jth time increment defined in Eq. (B-18), cal/(sec)(cm)^2.

G_c Convective heat flux at the surface of test film, cal/(sec)(cm)^2.

G_o A time-invariant constant.

h Surface heat transfer coefficient between the surface and agitated bath, cal/(sec)(°C)(cm)^2.

$\bar{h}$ Average natural heat transfer coefficient between the test film surface and the environmental gas, cal/(sec)(°C)(cm)^2.

k Reaction rate constant.

k_a Thermal conductivity of the continuous phase in a composite solid, cal/(°C)(sec)(cm).

k_c Thermal conductivity of calorimeter receiver, cal/(°C)(sec)(cm).

k_o Rate constant for initiation.

k_s Thermal conductivity of test sample, cal/(°C)(sec)(cm).

k_w Thermal conductivity of thermocouple wire, cal/(°C)(sec)(cm).

L Thickness of copper disk calorimeter, cm.

L_d, L_{rb}, L_v Conduction heat loss, radiation heat loss, and convection heat loss respectively from back face of copper disk calorimeter, cal/(sec).

L_{rs} Radiation heat loss at the surface of test film, cal/(sec)(cm)^2.

ℓ Thickness of test film, cm.

ℓ_c Half-cylinder height, cm.

$\ell_d, \ell_{rb}, \ell_v$ Coefficients of conduction heat loss, radiation heat loss, convection heat loss respectively from back face of copper disk calorimeter.

M_n Number average molecular weight of residue in monomer units.

M(s) One of pyrolysis fragments in solid state.

m The maximum chain length of volatile fragment.

m_o Total number of monomer units in the polymer sample.

m_r Mass of calorimeter copper receiver, g.

m_1 Monomer.

N have numerical values, 0, 1 and 2.

N_p, N_{p_o} Number of chains of length p and p_o.

N_o Original number of chains of length p_o.

$N^*_{p_o}$ Number of activated radicals.

N(s) One of pyrolysis fragments in condensed state.

N(g) Pyrolysis fragment in gaseous state.

N_1 Number of monomers.

n Reaction order with respect to oxygen pressure.

n_p Defined as N_p/N_o.

O_x Oxidizing species produced from ammonium perchlorate.

P Transform variable in the Laplace transformation.

P_e External pressure, atm.

P_{O_2} External oxygen pressure, atm.

P(s) Original polymer in solid state.

P'(s) Recombined polymer in solid state.

(P) Volume fraction of PBAA binder.

p_o, p Chain length of original polymer and intermediate polymer fragments.

PG Differentiation of $G_{0,j}$ with respect to temperature at the surface of test film, cal/(sec)(cm)^2(°C).

q Defined as square root of $\frac{\lambda}{\alpha}$

R Gas constant, 1.987 cal/(g-mole)(°C).

r_c Cylindrical radius, cm.

$\dot{r}$ Rate of oxidstive reaction.

s Reaction order with respect to volume fraction of PBAA binder.

T Temperature, °K.

T_f Furnace temperature, °K.

T_i Interfsce temperature, °K.

$T_{i,j}$ Temperature at ith space increment and jth time increment.

T_{i-1} Temperature at N=1, or one Δx from interfsce.

T_{i-2} Temperature at N=0, or two Δx from interface.

T_o Initial sample temperature, °K.

T_{ph} Surface tempersture of test film at the photocell signsl, °K.

T_s Surface tempersture of test film, °K.

t Time.

V_{pyr}, V_{25} V_{-80} Pyrolysis products volatile at the tempereture of pyrolysis, st 25°C snd at -80°C respectively.

v, v_o, v_b Center temperature, initisl temperature, bsth tempersture respectively in the measurement of thermal diffusivity, °C.

$\bar{v}$ A trsnsformed variable for temperature in the Laplace transformstion.

W Watt, a power rate unit.

w_{AP} Weight per cent ammonium perchlorate.

w_f Fraction of weight loss.

$\dot{w}_f$ Rate of loss-in-weight.

x Distsnce from the surface of test film, cm.

Greek

α Thermal diffusivity of test sample, cm^2/sec.

α_r Thermal diffusivity of calorimeter receiver, cm^2/sec.

β_s Roots of Eq. (C-18).

β_1 The smallest root of Eqs.(A-2) and (A-3).

γ_1 The smallest root of Eq. (A-2).

δ Thickness of calorimeter copper receiver, cm.

ΔH_λ Heat of vaporization, kcal/g-mole.

ΔT Temperature rise of calorimeter, °C.

Δt Time of exposure for calorimeter, sec.

Δx Space increment, cm.

ϵ Surface emissivity.

ϵ_c Emissivity of back face of copper disk calorimeter.

η Volume fraction of discontinuous phase.

θ Fraction of scissions followed by unzipping.

λ Defined as P and used as a dummy variable of integration.

μ Same as q, defined as square root of $\frac{\lambda}{\alpha}$.

ν Ratio of the thermal conductivities of the discontinuous phase to that of the continuous phase.

ξ Defined as $L\rho'c'/\rho c$, cm.

π A numerical constant (3,14159...).

ρ, ρ_c, ρ' Densities of test film. calorimeter receiver and copper disk, g/cm^3.

σ Stefan-Boltzmann constant, 1.3545×10^{-12} $cal/(cm)^2(°K)^4(sec)$.

LIST OF REFERENCES

1. Alvares, N. J., "The Effect of Pressure on Ignition by Thermal Radiation", Western States Sec. Combust. Inst. Paper 66-27, Denver, Colorado (April 1966).

2. Andersen, W. H., Bills, K. W., Mishuck, E., Moe, G. and Schultz, R. D., "A Model Describing Combustion of Solid Composite Propellants Containing Ammonium Nitrate," Combust. Flame, 3, 301-317 (1959).

3. Anderson, R., Brown, R. S., Thompson, G. T. and Ebeling, R. W., "Theory of Hypergolic Ignition of Solid Propellants," AIAA Preprint No. 63-514 (December 1963).

4. Baer, A. D., Ryan, N. W., "Ignition of Composite Propeallants by Low Radiant Fluxes," AIAA J. 3, 884-889 (1965).

5. Beyer R. B., McCulley, L. and Evans, M. W., "Measurement of Energy Flux Density Distribution in the Focus of an Arc Image Furnace," Appl. Opt. 3, 131-135 (1964).

6. Bouck, L. S., "An Arc Image Furnace for the Study of Solid Rocket Propellant Ignition," B. S. thesis, University of Utah, Department of Chemical Engineering, Salt Lake City, (1966).

7. Broida, T. R., "The Production of Intense Beams of Thermal Radiation by Meana of a High Current Carbon Arc and Relay-Condenser Optical System," U.S. Nav. Res. Dev. Lab.-TR-417 (November 1953).

8. Broido, A. ano Willoughby, A. B., "Measurement of Intense Beams of Thermal Radiation," J. Opt. Soc. Am. 48, 344-350 (1958).

9. Brown, D. W., and Wall, L. A., "Pyrolysis of Poly-α-methylstyrene," J. Phys. Chem., 62, 848-852 (1958).

10. Cantrell, R. H., "Gas-Film Effecta in the Linear Pyrolysis of Solida," AIAA J. 1, 1544-1549 (1963).

11. Carslaw, H. S. and Jaeger, J. C., Conduction of Heat in Solids, 2nd Ed., Oxford University Press, London (1959).

12. Chaiken, R. F., Andersen, W. H., Barsh, M. K., Mishuck, E., Moe, C. and Schultz, R. D., "Kinetics of the Surface Degradation of Polymethylmethacrylate," J. Chem. Phsy. 32, 141-146 (1960).

13. Coates, R. L., "Linear Pyrolysis Rate Measurements of Propellant Constituents," AIAA Preprint No. 65-55 (January 1965).

14. Corring, R. L., and Churchill, S. W., "Thermal Conductivity of Heterogeneous Materials," Chem. Eng. Progr. 57, 53-59 (July 1961).

15. Grassie, N., Chemistry of High Polymer Degradation Processes, Butterworths Scientific Publications, London (1956).

16. Grassie, N. and Kerr, W. W., "The Thermal Depolymerization of Polystyrene, Pt 1.-The Reaction Mechanism," Trans. Faraday Soc., 53, 234-239 (1957).

17. Crassie, N. and Kerr, W. W., "The Thermal Depolymerization of Polystyrene, Pt. 2.-Formation of 'Weak Links'," Trans. Faraday Soc., 55, 1050-1055 (1959).

18. Crassie, N., and Melville, H. W., "The Thermal Degradation of Polyvinyl Compounds I. A New Type of Molecular Still," Proc. Roy. Soc., A199, 1-13 (1949).

19. Harms, D. L., "Identification of Complex Organic Materials by Infrared Spectra of Their Pyrolysis Products," Anal. Chem. 25 1140-1155 (1953).

20. Heath, G. A. and Hirst, R., "Some Characteristics of the High Pressure Combustion of Double-Base Propellant," Eighth Symposium (International) on Combustion, Williams and Wilkins Co., Baltimore, Md., (1962), pp. 711-720.

21. Hellums, J. O. and Chruchill, S. W., "Transient and Steady State, Free and Natural Convection, Numerical Solutions: Pt. 1. The Isothermal Vertical Plate," A.I.Ch.E.J. 8, 690-695 (1962).

22. Henkin, H., and McGill, R., "Rates of Explosive Decomposition of Explosives," Ind. Eng. Chem. 44, 1391-1395 (1952).

23. Hershkowitz, J., Schwartz, F. and Kaufman, J. V. R., "Combustion in Loose Granular Mixtures of Potassium Perchlorate and Aluminum," Eighth Symposium (International) on Combustion, Williams and Wilkins Co., Baltimore, Md. (1962), pp. 720-727.

24. Jellinek, H. H. G., "On the Degradation of Long Chain Molecules," Trans. Faraday Soc., 40, 266-279 (1944).

25. Jellinek, H. H. G., "Thermal Degradation of Polystyrene, Pt. I," J. Polymer Sci., 3, 850-865 (1948).

26. Jellinek, H. H. G., "Thermal Degradation of Polystyrene and Polyethylene Part III," J. Polymer Sci., 4, 13-35 (1949).

27. Jellinek, H. H. G., Degradation of Vinyl Polymers, Academic Press Inc., New York (1955).

28. Keller, J. A., "Studies on Ignition of Ammonium Perchlorate-Based Propellants by Convective Heating," Ph.D. thesis, University of Utah, Department of Chemicsl Engineering, Salt Lake City,(1965).

29. Keller, J. A., Baer, A D., and Ryan, N. W., "The Ignition of Composite Propellants by Hot Gases," Western States Sec. Combust. Inst. Paper 64-27 (October 1964).

30. Levy, J. B. and Friedman, R., "Further Studies of Pure Ammonium Perchlorate Deflagration," Eighth Symposium (International) on Combustion, Williams and Wilkins Co., Baltimore, Md., (1962), pp. 663-672.

31. Lewis, E. E. and Naylor, M. A., "Pyrolysis of Polytetrafluroethylene," J. Amer. Chem. Soc., 69, 1968-1970 (1947).

32. Madorsky, S. L., "Rates of Thermal Degradation of Polystyrene and Polyethylene in a Vacuum," J. Polymer Sci., 9, 133-156 (1952).

33. Madorsky, S. L., McIntyre, D., O'mara, J. H., and Straus, S., "Thermal Degradation of Polymers at Low Rates," J. Res. Nat. Bur. Std., 66A, 307-311 (1962).

34. Madorsky, S. L., and Straus, S., "Pyrolytic Fractionation of Polystyrene in a High Vacuum and Mass Spectrometer Analysis of Some of the Fractions," J. Res. Nat. Bur. Std., 40, 417-425 (1948).

35. Madorsky, S. L., Straus, S., Thompson, D., Williamson, L., "Pyrolysis of Polyisobutene (Vistanex), Polyisoprene, Polybutadiene, GR-S, and Polyethylene in a High Vacuum," J. Res. Nat. Bur. Std., 42, 499-514 (1949).

36. Martin, S. B., "Diffusion-Controlled Ignition of Organic Solids by Intense Radiant Energy," Western States Sec. Combust. Inst. Paper [illegible]-7, Stanford Univ. Calif., (April 1964).

37. McAlevy, R. F., III, Cowan, P. L. and Summerfield, M., "The Mechanism of Ignition of Composite Solid Propellants by Hot Gases," Progress in Astronautica and Rocketry: Vol. 1. Solid Propellant Rocket Research, Edited by M. Summerfield, Academic Press Inc., New York, (1960), pp. 623-652.

38. McAlevy, R. F., III and Hanoel, J. G., "The Linear pyrolysis of Thermoplastic in Chemically Reactive Environments," AIAA J. 3, 244-249 (1965).

39. Meek, R. L. and Thompson, R. L., "Thermal Degradation and Oxidation of Polybutadiene-Acrylic Acid," B. S. thesis, University of Utah, Department of Chemical Engineering, Salt Lake City, (1964).

40. Nachbar, W. and Williams, F. A., "On the Analysis of Linear Pyrolysis Experiments," Ninth Symposium (International) on Combustion, Williams and Wilkins Co., Baltimore, Md., (1963), pp. 345-357.

41. Nagler, R. G., "Degradation of Homogeneous Polymeric Materials Exposed to High Heat Fluxes," Jet Propulsion Lab. Technical Report No. 32-527 (February 1964).

42. Powling, J. and Smith, W. A. W., "The Surface Temperature of Burning Ammonium Perchlorate," Combust. Flame, 7, 269-275 (1963).

43. Powling, J. and Smith, W. A. W., "The Surface Temperature of Ammonium Perchlorate Burning at Elevated Pressures," Tenth Symposium (International) on Combustion, The Combustion Institute, Pittsburgh, (1965), pp. 1373-1380.

44. Rice, O. K. and Ginell, R., "The Theory of the Burning of Double-Base Rocket Powders," J. Phys. Chem. 54, 885-917 (1950).

45. Ryan, N. W., Baer, A. D., Keller, J. A., and Mitchell, R. C., "Ignition and Combustion of Solid Propellants," Department of Chemical Engineering, University of Utah, Technical Report under Air Force Grant 40-63, AFOSR 40-63 (September 1963).

46. Simha, R., "Kinetics of Degradation and Size Distribution of Long Chain Polymers," J. Appl. Phys. 12, 569-578 (1941).

47. Straus, S. and Madorsky, S. L., "Thermal Degradation of Polyacrylonitrile, Polybutadiene, and Copolymers of Butadiene with Acrylonitrile and Styrene," J. Res. Nat. Bur. Std., 61, 77-81 (1958).

48. Straus, S. and Madorsky, S. L., "Pyrolysis of Some Polyvinyl Polymers at Temperatures up to 1200°C," J. Res. Nat. Bur. Std., 66A, 401-406 (1962).

49. Wsll, L. A., snd Florin, R. E., "Effect of Structure on the Thermal Decomposition of Polymers," J. Res. Nat. Bur. Std., 60, 451-458 (1958).

50. Wall, L. A., Madorsky, S. L., Brown, D. W., Straus, S. and Simha, R., "The Depolymerizstion of Polymethylene and Polyethylene," J. Am. Chem. Soc., 76, 3430-3437 (1954).

51. Whitworth, C. R., "Design and Construction of a High Vacuum System," B. S. thesis, University of Utah, Department of Chemical Engineering, Salt Lake City, (1963).

52. Wilfong, R. E., Penner, S. S., and Daniels, F., "An Hypothesis for Propellant Burning," J. Phys. Chem. 54, 863-872 (1950).

BLANK PAGE

UNCLASSIFIED
Security Classification

DOCUMENT CONTROL DATA - R&D

(Security classification of title, body of abstract and indexing annotation must be entered when the overall report is classified)

1. ORIGINATING ACTIVITY (Corporate author)
University of Utah
Chemical Engineering Department
Salt Lake City, Utah 84112

2a. REPORT SECURITY CLASSIFICATION
UNCLASSIFIED

2b. GROUP

3. REPORT TITLE
THERMAL EFFECTS OF COMPOSITE-PROPELLANT REACTIONS

4. DESCRIPTIVE NOTES (Type of report and inclusive dates)
Scientific Interim

5. AUTHOR(S) (Last name, first name, initial)
J. T. Cheng
Alva D. Baer
Norman W. Ryan

6. REPORT DATE
1 August 1967

7a. TOTAL NO. OF PAGES
260

7b. NO. OF REFS
52

8a. CONTRACT OR GRANT NO.
AF-AFOSR-40-67

b. PROJECT NO.
9711-01

c. 61445014

d. 681308

9a. ORIGINATOR'S REPORT NUMBER(S)

9b. OTHER REPORT NO(S) (Any other numbers that may be assigned this report)
AFOSR 68-0243

10. AVAILABILITY/LIMITATION NOTICES
2. This document is subject to special export controls and each transmittal to foreign governments or foreign nationals may be made only with prior approval of AFOSR (SRGO).

11. SUPPLEMENTARY NOTES
TECH. OTHER

12. SPONSORING MILITARY ACTIVITY
AF Office of Scientific Research (SREP)
1400 Wilson Boulevard
Arlington, Virginia 22209

13. ABSTRACT
This report covers the investigation of the decomposition reactions of epoxy-cured polybutadiene-acrylic acid copolymer (PBAA). Relevant research performed by previous workers and current theories concerning the mechanisms of polymer decomposition in inert and chemically reactive gases are discussed. Results are presented of the pyrolysis experiments carried out in this investigation, utilizing thin-film samples of both the simple polymer and the polymer mixed with burning rate catalysts, ammonium perchlorate and glass beads, and obtained under various conditions of temperature, gaseous environment and pressure. The data obtained is analyzed and conclusions are drawn pertaining to the events occurring at the heated surface of the thin-film polymer or propellant-like material.

DD FORM 1 JAN 64 1473

UNCLASSIFIED
Security Classification

UNCLASSIFIED
Security Classification

14. KEY WORDS	LINK A ROLE	LINK A WT	LINK B ROLE	LINK B WT	LINK C ROLE	LINK C WT
Composite Solid Propellant Decomposition						
Solid Propellant Ignition						
Solid Propellant Combustion						
Polymer Decomposition Reactions						
Polymer Pyrolysis Mechanisms						
Solid Polymer Degradation						

INSTRUCTIONS

1. ORIGINATING ACTIVITY: Enter the name and address of the contractor, subcontractor, grantee, Department of Defense activity or other organization (*corporate author*) issuing the report.

2a. REPORT SECURITY CLASSIFICATION: Enter the overall security classification of the report. Indicate whether "Restricted Data" is included. Marking is to be in accordance with appropriate security regulations.

2b. GROUP: Automatic downgrading is specified in DoD Directive 5200.10 and Armed Forces Industrial Manual. Enter the group number. Also, when applicable, show that optional markings have been used for Group 3 and Group 4 as authorized.

3. REPORT TITLE: Enter the complete report title in all capital letters. Titles in all cases should be unclassified. If a meaningful title cannot be selected without classification, show title classification in all capitals in parenthesis immediately following the title.

4. DESCRIPTIVE NOTES: If appropriate, enter the type of report, e.g., interim, progress, summary, annual, or final. Give the inclusive dates when a specific reporting period is covered.

5. AUTHOR(S): Enter the name(s) of author(s) as shown on or in the report. Enter last name, first name, middle initial. If military, show rank and branch of service. The name of the principal author is an absolute minimum requirement.

6. REPORT DATE: Enter the date of the report as day, month, year; or month, year. If more than one date appears on the report, use date of publication.

7a. TOTAL NUMBER OF PAGES: The total page count should follow normal pagination procedures, i.e., enter the number of pages containing information.

7b. NUMBER OF REFERENCES: Enter the total number of references cited in the report.

8a. CONTRACT OR GRANT NUMBER: If appropriate, enter the applicable number of the contract or grant under which the report was written.

8b, 8c, & 8d. PROJECT NUMBER: Enter the appropriate military department identification, such as project number, subproject number, system numbers, task number, etc.

9a. ORIGINATOR'S REPORT NUMBER(S): Enter the official report number by which the document will be identified and controlled by the originating activity. This number must be unique to this report.

9b. OTHER REPORT NUMBER(S): If the report has been assigned any other report numbers (*either by the originator or by the sponsor*), also enter this number(s).

10. AVAILABILITY/LIMITATION NOTICES: Enter any limitations on further dissemination of the report, other than those imposed by security classification, using standard statements such as:

(1) "Qualified requesters may obtain copies of this report from DDC."

(2) "Foreign announcement and dissemination of this report by DDC is not authorized."

(3) "U. S. Government agencies may obtain copies of this report directly from DDC. Other qualified DDC users shall request through _____."

(4) "U. S. military agencies may obtain copies of this report directly from DDC. Other qualified users shall request through _____."

(5) "All distribution of this report is controlled. Qualified DDC users shall request through _____."

If the report has been furnished to the Office of Technical Services, Department of Commerce, for sale to the public, indicate this fact and enter the price, if known.

11. SUPPLEMENTARY NOTES: Use for additional explanatory notes.

12. SPONSORING MILITARY ACTIVITY: Enter the name of the departmental project office or laboratory sponsoring (*paying for*) the research and development. Include address.

13. ABSTRACT: Enter an abstract giving a brief and factual summary of the document indicative of the report, even though it may also appear elsewhere in the body of the technical report. If additional space is required, a continuation sheet shall be attached.

It is highly desirable that the abstract of classified reports be unclassified. Each paragraph of the abstract shall end with an indication of the military security classification of the information in the paragraph, represented as (*TS*), (*S*), (*C*), or (*U*).

There is no limitation on the length of the abstract. However, the suggested length is from 150 to 225 words.

14. KEY WORDS: Key words are technically meaningful terms or short phrases that characterize a report and may be used as index entries for cataloging the report. Key words must be selected so that no security classification is required. Identifiers, such as equipment model designation, trade name, military project code name, geographic location, may be used as key words but will be followed by an indication of technical context. The assignment of links, rules, and weights is optional.

GPO 886-551

UNCLASSIFIED
Security Classification